S CUOLA N ORMALE S UPERIORE

T ESI DI P ERFEZIONAMENTO IN F ISICA

On String Vacua without Supersymmetry

BRANE DYNAMICS, BUBBLES AND HOLOGRAPHY

Candidato:

Ivano B ASILE

Relatore:

Prof. Augusto S AGNOTTI

Corso di Perfezionamento in Fisica

Classe di Scienze

XXXIII Ciclo

Anno Accademico 2019-2020

Abstract

In this thesis we investigate some aspects of the dramatic consequences of super-symmetry breaking on string vacua. In particular, we focus on the issue of vacuum stability in ten-dimensional string models with broken, or without, supersymmetry, whose perturbative spectra are free of tachyons. After introducing the models at stake in Chapter 2, we introduce their low-energy effective description in Chapter 3, presenting a number of vacuum solutions to the classical equations of motion. In Chapter 4 we analyze their classical stability, studying linearized field fluctuations, and in Chapter 5 we turn to the issue of quantum stability. In Chapter 6 we frame the resulting instabilities in terms brane dynamics, studying brane interactions and back-reacted geometries. In Chapter 7 we propose a holographic correspondence connecting bulk instabilities with dual renormalization group flows, and we explore a potential concrete scenario involving world-volume gauge theories. Finally, in Chapter 8 we turn to cosmology, deriving generalized no-go results for warped flux compactifications and building a brane-world scenario along the lines of a recent proposal, providing a string embedding of constructions of this type. In Chapter 9 we provide a summary and collect some concluding remarks.

Acknowledgements

Contents

Contents

Introduction

The issue of supersymmetry breaking in string theory is of vital importance, on both a technical and conceptual level. On a foundational level, many of the richest and most illuminating lessons appear obscured by a lack of solid, comprehensive formulations and of befitting means to explore these issues in depth. As a result, unifying guiding principles to oversee our efforts have been elusive, albeit a variety of successful complementary frameworks [1–5] hint at a unique, if tantalizing, consistent structure [6]. Despite these shortcomings, string theory has surely provided a remarkable breadth of new ideas and perspectives to theoretical physics, and one can argue that its relevance as a framework has thus been established to a large extent, notwithstanding its eventual vindication as a realistic description of our universe. On a more phenomenological level, the absence of low-energy supersymmetry and the extensive variety of mechanisms to break it, an consequently the wide range of relevant energy scales, points to a deeper conundrum, whose resolution would conceivably involve qualitatively novel insights. However, the paradigm of spontaneous symmetry breaking in gauge theories has proven pivotal in model building, both in particle physics and condensed matter physics, and thus it is natural to envision spontaneous supersymmetry breaking as an elegant resolution of these bewildering issues. Yet, in the context of string theory this phenomenon could in principle occur around the string scale, perhaps even naturally so, and while the resulting dramatic consequences have been investigated for a long time, the ultimate fate of these settings appears still largely not under control.

All in all, a deeper understanding of the subtle issues of supersymmetry breaking in string theory is paramount to progress toward a more complete picture of its underlying foundational principles and more realistic phenomenological models. While approaches based on string world-sheets would appear to offer a more fundamental perspective, the resulting analyses are typically met by gravitational tadpoles,

which signal an incongruous starting point of the perturbative expansion and whose resummation entails a number of technical and conceptual subtleties [7–10]. On the other hand, low-energy effective theories appear more tractable in this respect, but connecting the resulting lessons to the underlying microscopic physics tends to be more intricate. In this respect, a tempting analogy would compare current knowledge to the coastline of an unexplored island, whose internal regions remain unscathed by any attempt to further explore them.

Nevertheless, this thesis is motivated by an attempt to shed some light on these remarkably subtle issues. Indeed, as we shall discuss, low-energy effective theories, accompanied by some intuition drawn from well-understood supersymmetric settings, appears to provide the tools necessary to elucidate matters, at least to some extent. A detailed analysis of the resulting models, and in particular of their classical solutions and the corresponding instabilities, suggests that fundamental branes play a crucial rôle in unveiling the microscopic physics at stake. Both the relevant space-time field configurations and their (classical and quantum) instabilities dovetail with a brane-based interpretation, whereby controlled flux compactifications arise as near-horizon limits within back-reacted geometries, strongly-warped regions arise as confines of the space-time "carved out" by the branes in the presence of runaway tendencies, and instabilities arise from brane interactions. In addition to provide a vantage point to build intuition from, the rich dynamics of fundamental branes offers potentially fruitful avenues of quantitative investigation via world-volume gauge theories and holographic approaches. Furthermore, settings of this type naturally accomodate cosmological brane-world scenarios alongside the simpler bulk cosmologies that have been analyzed, and the resulting models offer a novel and intriguing perspective on the long-standing problem of dark energy in string theory. Indeed, many of the controversies regarding the ideas that have been put forth in this respect [11–15] point to a common origin, namely an attempt to impose static configurations on systems naturally driven toward dynamics. As a result, uncontrolled back-reactions and instabilities can arise, and elucidating the aftermath of their manifestation has proven challenging.

While in supersymmetric settings the lack of a selection principle generates

seemingly unfathomable "landscapes" of available models, in the absence of super-symmetry the requirement for their very consistency has been questioned, leading to the formulation of a number of criteria and proposals collectively dubbed "swamp-land conjectures" [16, 17]. Among the most ubiquitous stands the weak gravity conjecture [18], which appears to entail far-reaching implications concerning the nature of quantum-gravitational theories in general. In this thesis we shall approach matters from a complementary viewpoint, but, as we shall discuss, the emerging lessons resonate with the results of "bottom-up" programs of this type. Altogether, the indications that we have garnered appear to portray an enticing, if still embryonic, picture of dynamics as a fruitful as a selection mechanism for more realistic models and as a rich area of to investigate on a more foundational level, and to this end a deeper understanding of high-energy supersymmetry breaking would constitute an invaluable asset to string theory insofar as we grasp it at present.

SYNOPSIS

The material presented in this thesis is organized as follows.

We shall begin in Chapter 2 with an overview of the formalism of vacuum amplitudes in string theory, and the construction of three ten-dimensional string models with broken supersymmetry. These comprise two orientifold models, the $USp(32)$ model of [19] and the $U(32)$ model of [20, 21], and the $SO(16) \times SO(16)$ heterotic model of [22, 23], and their perturbative spectra feature no tachyons. Despite this remarkable property, these models also exhibit gravitational tadpoles, whose low-energy imprint includes an exponential potential which entails runaway tendencies. The remainder of this thesis is focused on investigating the consequences of this feature, and whether interesting phenomenological scenarios can arise as a result.

In Chapter 3 we shall describe a family of effective theories which describes the low-energy physics of the string models that we have introduced in Chapter 2, and we present a number of solutions to the corresponding equations of motion. In order to balance the runaway effects of the dilaton potential, the resulting field profiles can be warped [24, 25] or involve large fluxes [26]. In particular, we shall present in

detail the Dudas-Mourad solutions of [24], which comprise static solutions that are dynamically compactified on a warped interval, and ten-dimensional cosmological solutions. We shall also present general Freund-Rubin flux compactifications, among which the AdS $\times$ S solutions found in [26] and their generalizations [25]. While dS solutions of this type are not allowed in the actual string models at stake, whenever the model parameters allow them they are always unstable. On the other hand, AdS solutions of this type are always parametrically under control for large fluxes.

In Chapter 4 we shall present a detailed analysis of the classical stability of the Dudas-Mourad solutions of [24] and of the AdS $\times$ S solutions of [26]. To this end, we shall derive the linearized equations of motion for field perturbations, and obtain criteria for the stability of modes. In the case of the Dudas-Mourad solutions, we shall recast the equations of motion in terms of Schrödinger-like problems, and writing the corresponding Hamiltonians in terms of ladder operators. In this fashion, we shall prove that these solutions are stable at the classical level, but in the cosmological case an intriguing instability of the homogeneous tensor mode emerges [27], and we offer as an enticing, if speculative, explanation a potential tendency of space-time toward spontaneous compactification. On the other hand, perturbations of the AdS $\times$ S solutions can be analyzed according to Kaluza-Klein theory, and the scalar sector contains unstable modes. [27] for a finite number of internal angular momenta. We shall conclude discussing how to remove them with suitable freely-acting projections on the internal spheres, or by modifying the internal manifold.

In Chapter 5 we shall turn to the non-perturbative instabilities of the AdS compactifications discussed in Chapter 3, in which a charged membranes nucleate [25] reducing the flux in the space-time inside of them. We shall compute the decay rate associated to this process, and frame it in terms of fundamental branes via consistency conditions that we shall derive and discuss. In the actual string models that we shall consider, there ought to nucleate D1-branes in the orientifold models and NS5-branes in the heterotic model, but more general models can accomodate "exotic" branes [28–32] whose tensions scales differently with the string coupling.

In Chapter 6 we shall further develop the brane picture presented in Chapter 5, starting from the Lorentzian expansion that bubbles undergo after nucleation. The potential that drives the expansion encodes a renormalization charge-to-tension ratio

that is consistent with the weak gravity conjecture. Moreover, as we shall discuss, the same renormalized ratio affects the dispersion relation of world-volume deformations. Then we shall turn to the gravitational back-reaction of the branes, studying the resulting near-horizon and asymptotic geometries. In the near-horizon limit we shall recover AdS × S throats, while the asymptotic region features a "pinch-off" singularity at a finite distance, mirroring the considerations of [24]. Our findings support a picture of instabilities as the result of brane interactions, and in order to shed light on the non-extremal case we shall discuss their gravitational back-reaction and derive interaction potentials in some controlled regimes. The case of N_1 D1-branes interacting with uncharged N_8 8-branes in the orientifold models is particularly noteworthy in this respect, since it appears calculable in three complementary regimes: $N_1 \gg N_8$, $N_1 \ll N_8$ and $N_1, N_8 = \mathcal{O}(1)$. We shall compare the respective results finding qualitative agreement, despite the absence of supersymmetry.

In Chapter 7 we shall motivate a holographic correspondence between meta-stable AdS (false) vacua and dual (renormalization group) RG flows. Specifically, the correspondence relates the nucleation of vacuum bubbles in the bulk to a relevant deformation in the dual CFT, and the resulting RG flow mirrors the irreversible expansion of bubbles. In order to provide evidence for our proposal, we shall compute the holographic entanglement entropy in the case of a three-dimensional bulk, and we shall discuss a variety of *c*-functions whose behavior appears to agree with our expectations. Then, in order to address more complicated bubble configurations, we shall describe and apply the framework of holographic integral geometry [33]. To conclude, we shall discuss some potential "top-down" scenarios in which our construction could potentially be verified quantitatively from both sides of the correspondence.

In Chapter 8 we shall return to the issue of dS cosmology, considering warped flux compactifications and extending the no-go result discussed in Chapter 2. In particular, we shall obtain an expression for the space-time cosmological constant in terms of the model parameters, and derive from it a no-go result that generalizes that of [34]. We shall also include the contribution of localized sources and discuss how our findings connect with recent swampland conjectures [17]. Finally, we shall propose a string-theoretic embedding of the brane-world scenarios recently revisited in [35–37],

studying the effective gravitational dynamics on the world-volume of nucleated branes. The resulting models describe dS cosmologies coupled to matter and (non-)Abelian gauge fields, and we shall discuss a mechanism to generate stochastically massive particles of arbitrarily small masses via open strings stretching between expanding branes.

PUBLICATIONS

The material that I shall present in this thesis is based on the following three published articles:

- R. Antonelli, I. Basile,

  "**Brane annihilation in non-supersymmetric strings**", In: *Journal of High Energy Physics*, 1911 (2019): 021.

- R. Antonelli, I. Basile, A. Bombini,

  "**AdS Vacuum Bubbles, Holography and Dual RG flows**", In: *Classical and Quantum Gravity*, 36.4 (2019): 045004.

- I. Basile, J. Mourad, A. Sagnotti,

  "**On Classical Stability with Broken Supersymmetry**", In: *Journal of High Energy Physics*, 1901 (2019): 174.

In addition, I have published an article in collaboration with R. Antonelli and E. Hatefi:

- R. Antonelli, I. Basile, E. Hatefi,

  "**On All-Order Higher-Point** $\mathrm{D}p - \overline{\mathrm{D}p}$ **Effective Actions.**", *Journal of Cosmology and Astroparticle Physics*, 2019.10 (2019): 041–041.

In this article we have presented a novel computation of a scattering amplitude in type II superstrings, and we have derived a technique to systematically build expansions in powers of α' to the effect of connecting them to their respective effective couplings.

Some of the material presented in this thesis has not been published before, and in particular Chapter 8 is based on a collaboration with S. Lanza, and a preprint is currently in preparation. Finally, some unrelated results that I shall outline in Chapter 9 are based on a collaboration with A. Platania, and a preprint is currently in preparation.

String models with broken supersymmetry

In this chapter we introduce the string models with broken supersymmetry that we shall investigate in the remainder of this thesis. To this end, we begin in Section 1 with a review of one-loop vacuum amplitudes in string theory, starting from the supersymmetric ten-dimensional models. Then, in Section 2 we introduce orientifold models, or "open descendants", within the formalism of vacuum amplitudes, focusing on the $USp(32)$ model [19] and the $U(32)$ model [20, 21]. While the latter features a non-supersymmetric perturbative spectrum without tachyons, the former is particularly intriguing, since it realizes supersymmetry non-linearly in the open sector [38–41]. Finally, in Section 3 we move on to heterotic models, constructing the non-supersymmetric $SO(16) \times SO(16)$ projection [22, 23]. The material presented in this chapter is largely based on [42]. For a more recent review, see [43].

1 VACUUM AMPLITUDES

Vacuum amplitudes probe some of the most basic aspects of quantum systems. In the functional formulation, they can be computed evaluating the effective action Γ on vacuum configurations. While in the absence of supersymmetry or integrability exact results are generally out of reach, their one-loop approximation only depends on the perturbative excitations around a classical vacuum. In terms of the corresponding mass operator M^2, one can write integrals over Schwinger parameters of the form

$$\Gamma = -\frac{\text{Vol}}{2\,(4\pi)^{\frac{D}{2}}} \int_{\Lambda^{-2}}^{\infty} \frac{dt}{t^{\frac{D}{2}+1}}\, \text{STr}\left(e^{-tM^2}\right), \tag{2.1}$$

where Vol is the volume of (Euclidean) D-dimensional space-time, and the supertrace Str sums over *signed* polarizations, *i.e.* with a minus sign for fermions. The UV divergence associated to small values of the world-line proper time t is regularized by

the cut-off scale Λ.

Due to modular invariance[1], one-loop vacuum amplitudes in string theory can be recast as integrals over the moduli space of Riemann surfaces with vanishing Euler characteristic, and the corresponding integrands can be interpreted as partition functions of the world-sheet conformal field theory. Specifically, in the case of a torus with modular parameter $q \equiv e^{2\pi i \tau}$, in the RNS light-cone formalism one ought to consider[2] (combinations of) the four basic traces

$$
\begin{aligned}
Z_{(--)}(\tau) &\equiv \mathrm{Tr}_{\mathrm{NS}}\, q^{L_0} = \frac{\prod_{m=1}^{\infty}\left(1 + q^{m-\frac{1}{2}}\right)^8}{q^{\frac{1}{2}} \prod_{n=1}^{\infty}\left(1 - q^n\right)^8}\,, \\
Z_{(+-)}(\tau) &\equiv \mathrm{Tr}_{\mathrm{R}}\, q^{L_0} = 16\, \frac{\prod_{m=1}^{\infty}\left(1 + q^m\right)^8}{\prod_{n=1}^{\infty}\left(1 - q^n\right)^8}\,, \\
Z_{(-+)}(\tau) &\equiv \mathrm{Tr}_{\mathrm{NS}}\left((-1)^F q^{L_0}\right) = \frac{\prod_{m=1}^{\infty}\left(1 - q^{m-\frac{1}{2}}\right)^8}{q^{\frac{1}{2}} \prod_{n=1}^{\infty}\left(1 - q^n\right)^8}\,, \\
Z_{(++)}(\tau) &\equiv \mathrm{Tr}_{\mathrm{R}}\left((-1)^F q^{L_0}\right) = 0\,,
\end{aligned}
\tag{2.2}
$$

which arise from the four spin structures depicted in figure 2.1. The latter two correspond to "twisted" boundary conditions for the world-sheet fermions, and are implemented inserting the fermion parity operator $(-1)^F$. While $Z_{(++)}$ vanishes, its structure contains non-trivial information about perturbative states, and its modular properties are needed in order to build consistent models.

The modular properties of the traces in eq. (2.2) can be highlighted recasting them in terms of the *Dedekind η function*

$$
\eta(\tau) \equiv q^{\frac{1}{24}} \prod_{n=1}^{\infty}\left(1 - q^n\right),
\tag{2.3}
$$

which transforms according to

$$
\eta(\tau + 1) = e^{\frac{i\pi}{12}}\, \eta(\tau), \qquad \eta\left(-\frac{1}{\tau}\right) = (-i\tau)^{\frac{1}{2}}\, \eta(\tau)
\tag{2.4}
$$

---

[1]We remark that, in this context, modular invariance arises as the residual gauge invariance left after fixing world-sheet diffeomorphisms and Weyl rescalings. Hence, violations of modular invariance would result in gauge anomalies.

[2]We work in ten space-time dimensions, since non-critical string perturbation theory entails a number of challenges.
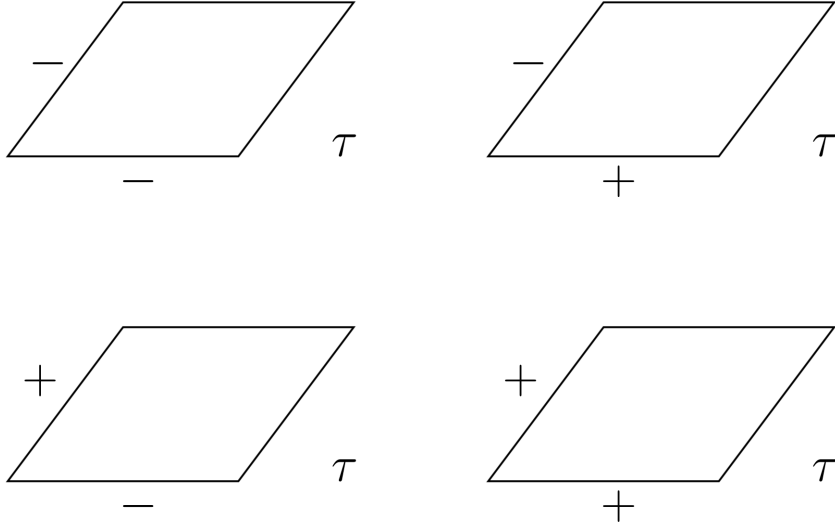
FIGURE 2.1: inequivalent spin structures on the torus, specified by a choice of periodic (−) or anti-periodic (+) conditions along each independent cycle.

under the action of the generators

$$T : \tau \rightarrow \tau + 1, \qquad S : \tau \rightarrow -\frac{1}{\tau} \tag{2.5}$$

of the modular group on the torus, and the Jacobi ϑ functions. The latter afford both the series representation [44]

$$\vartheta \begin{bmatrix} \alpha \\ \beta \end{bmatrix} (z|\tau) \equiv \sum_{n \in \mathbb{Z}} q^{\frac{1}{2}(n+\alpha)^2} e^{2\pi i (n+\alpha)(z-\beta)} \tag{2.6}$$

and the infinite product representation

$$\vartheta \begin{bmatrix} \alpha \\ \beta \end{bmatrix} (z|\tau) = e^{2\pi i \alpha (z-\beta)} q^{\frac{\alpha^2}{2}} \prod_{n=1}^{\infty} (1-q^n)$$
$$\times \left(1 + q^{n+\alpha-\frac{1}{2}} e^{2\pi i (z-\beta)} \right) \left(1 + q^{n-\alpha-\frac{1}{2}} e^{-2\pi i (z-\beta)} \right), \tag{2.7}$$

and they transform under the action of T and S according to

$$\vartheta \begin{bmatrix} \alpha \\ \beta \end{bmatrix} (z|\tau+1) = e^{-i\pi\alpha(\alpha+1)} \vartheta \begin{bmatrix} \alpha \\ \beta - \alpha - \frac{1}{2} \end{bmatrix} (z|\tau),$$
$$\vartheta \begin{bmatrix} \alpha \\ \beta \end{bmatrix} \left(\frac{z}{\tau} \middle| -\frac{1}{\tau} \right) = (-i\tau)^{\frac{1}{2}} e^{-2\pi i \alpha \beta + \frac{i\pi z^2}{\tau}} \vartheta \begin{bmatrix} -\beta \\ \alpha \end{bmatrix} (z|\tau). \tag{2.8}$$

Therefore, both the Dedekind η function and the Jacobi ϑ functions are modular forms of weight $\frac{1}{2}$. In particular, we shall make use of ϑ functions evaluated at $z = 0$ and $\alpha, \beta \in \{0, \frac{1}{2}\}$, which are commonly termed Jacobi constants[3]. Using these ingredients, one can recast the traces in eq. (2.2) in the form

$$
Z_{(--)}(\tau) = \frac{\vartheta^4 \begin{bmatrix} 0 \\ 0 \end{bmatrix}(0|\tau)}{\eta^{12}(\tau)}, \qquad Z_{(+-)}(\tau) = \frac{\vartheta^4 \begin{bmatrix} 0 \\ \frac{1}{2} \end{bmatrix}(0|\tau)}{\eta^{12}(\tau)},
$$
$$
Z_{(-+)}(\tau) = \frac{\vartheta^4 \begin{bmatrix} \frac{1}{2} \\ 0 \end{bmatrix}(0|\tau)}{\eta^{12}(\tau)}, \qquad Z_{(++)}(\tau) = \frac{\vartheta^4 \begin{bmatrix} \frac{1}{2} \\ \frac{1}{2} \end{bmatrix}(0|\tau)}{\eta^{12}(\tau)},
$$

(2.9)

and, in order to obtain the corresponding (level-matched) torus amplitudes, one is to integrate products of left-moving holomorphic and right-moving anti-holomorphic contributions over the fundamental domain $\mathcal{F}$ with respect to the modular invariant measure $\frac{d^2\tau}{\text{Im}(\tau)^2}$. The absence of the UV region from the fundamental domain betrays a striking departure from standard field-theoretic results, and arises from the gauge-fixing procedure in the Polyakov functional integral.

All in all, modular invariance is required by consistency, and the resulting amplitudes are constrained to the extent that the perturbative spectra of consistent models are fully determined. In order to elucidate their properties, it is quite convenient to introduce the characters of the level-one affine $\mathfrak{so}(2n)$ algebra

$$
O_{2n} \equiv \frac{\vartheta^n \begin{bmatrix} 0 \\ 0 \end{bmatrix}(0|\tau) + \vartheta^n \begin{bmatrix} 0 \\ \frac{1}{2} \end{bmatrix}(0|\tau)}{2\eta^n(\tau)},
$$
$$
V_{2n} \equiv \frac{\vartheta^n \begin{bmatrix} 0 \\ 0 \end{bmatrix}(0|\tau) - \vartheta^n \begin{bmatrix} 0 \\ \frac{1}{2} \end{bmatrix}(0|\tau)}{2\eta^n(\tau)},
$$
$$
S_{2n} \equiv \frac{\vartheta^n \begin{bmatrix} \frac{1}{2} \\ 0 \end{bmatrix}(0|\tau) + i^{-n}\, \vartheta^n \begin{bmatrix} \frac{1}{2} \\ \frac{1}{2} \end{bmatrix}(0|\tau)}{2\eta^n(\tau)},
$$
$$
C_{2n} \equiv \frac{\vartheta^n \begin{bmatrix} \frac{1}{2} \\ 0 \end{bmatrix}(0|\tau) - i^{-n}\, \vartheta^n \begin{bmatrix} \frac{1}{2} \\ \frac{1}{2} \end{bmatrix}(0|\tau)}{2\eta^n(\tau)},
$$

(2.10)

which comprise contributions from states pertaining to the four conjugacy classes of $SO(2n)$. Furthermore, they also inherit the modular properties from ϑ and η functions,

---

[3]Non-vanishing values of the argument z of Jacobi ϑ functions are nonetheless useful in string theory. They are involved, for instance, in the study of string perturbation theory on more general backgrounds and D-brane scattering.

reducing the problem of building consistent models to matters of linear algebra[4].
While $n = 4$ in the present case, the general expressions can also encompass heterotic
models, whose right-moving sector is built from 26-dimensional bosonic strings. As
we have anticipated, these expressions ought to be taken in a formal sense: if one were
to consider their actual value, one would find for instance the *numerical* equivalence
$S_8 = C_8$, while the two corresponding sectors of the Hilbert space are distinguished
by the chirality of space-time fermionic excitations. Moreover, a remarkable identity
proved by Jacobi [44] implies that

$$V_8 = S_8 = C_8 \,. \tag{2.11}$$

This peculiar identity was referred to by Jacobi as *aequatio identica satis abstrusa*, but in
the context of superstrings its meaning becomes apparent: it states that string models
built using an $SO(8)$ vector and a $SO(8)$ Majorana-Weyl spinor, which constitute
the degrees of freedom of a ten-dimensional supersymmetric Yang-Mills multiplet,
contain equal numbers of bosonic and fermionic excited states at all levels. In other
words, it is a manifestation of space-time supersymmetry in these models.

1.1 *Modular invariant closed-string models*

Altogether, only four torus amplitudes built out of the $\mathfrak{so}(8)$ characters of eq. (2.10)
satisfy the constraints of modular invariance and spin-statistics[5]. They correspond to
type IIA and type IIB superstrings,

$$\begin{aligned} \mathcal{T}_{\text{IIA}} &: \ (V_8 - C_8)\,\overline{(V_8 - S_8)}\,, \\ \mathcal{T}_{\text{IIB}} &: \ (V_8 - S_8)\,\overline{(V_8 - S_8)}\,, \end{aligned} \tag{2.12}$$

---

[4]We remark that different combinations of characters reflect different projections at the level of the
Hilbert space.

[5]In the present context, spin-statistics amounts to positive (resp. negative) contributions from
space-time bosons (resp. fermions).

which are supersymmetric, and to two non-supersymmetric models, termed type 0A and type 0B,

$$\mathcal{T}_{0\mathrm{A}} \ : \ O_8\,\overline{O_8} + V_8\,\overline{V_8} + S_8\,\overline{C_8} + C_8\,\overline{S_8}\,,$$

$$\mathcal{T}_{0\mathrm{B}} \ : \ O_8\,\overline{O_8} + V_8\,\overline{V_8} + S_8\,\overline{S_8} + C_8\,\overline{C_8}\,, \tag{2.13}$$

where we have refrained from writing the volume prefactor and the integration measure

$$\int_{\mathcal{F}} \frac{d^2\tau}{\tau_2^6}\,\frac{1}{|\eta(\tau)|^{16}}\,, \qquad \tau_2 \equiv \mathrm{Im}(\tau) \tag{2.14}$$

for clarity. We shall henceforth use this convenient notation. Let us remark that the form of (2.12) translates the chiral nature of the type IIB superstring into its world-sheet left-right symmetry[6].

2   ORIENTIFOLD MODELS

The approach that we have outlined in the preceding section can be extended to open strings, albeit with one proviso. Namely, one ought to include all Riemann surfaces with vanishing Euler characteristic, including the Klein bottle, the annulus and the Möbius strip.

To begin with, the orientifold projection dictates that the contribution of the torus amplitude be halved and added to (half of) the Klein bottle amplitude $\mathcal{K}$. Since the resulting amplitude would entail gauge anomalies due to the Ramond-Ramond (R-R) tadpole, one ought to include the annulus amplitude $\mathcal{A}$ and Möbius strip amplitude $\mathcal{M}$, which comprise the contributions of the open sector and signal the presence of D-branes. The corresponding modular parameters are built from the covering tori of the fundamental polygons, depicted in fig. 2.2, while the Möbius strip amplitude involves "hatted" characters that differ from the ordinary one by a phase[7]. so that in

---

[6]Despite this fact the type IIB superstring, as well as all five supersymmetric models, is actually anomaly-free owing to the Green-Schwarz mechanism [45]. This remarkable result was a considerable step forward in the development of string theory.

[7]The "hatted" characters appear since the modular paramater of the covering torus of the Möbius strip is not real, and they ensure that states contribute with integer degeneracies.
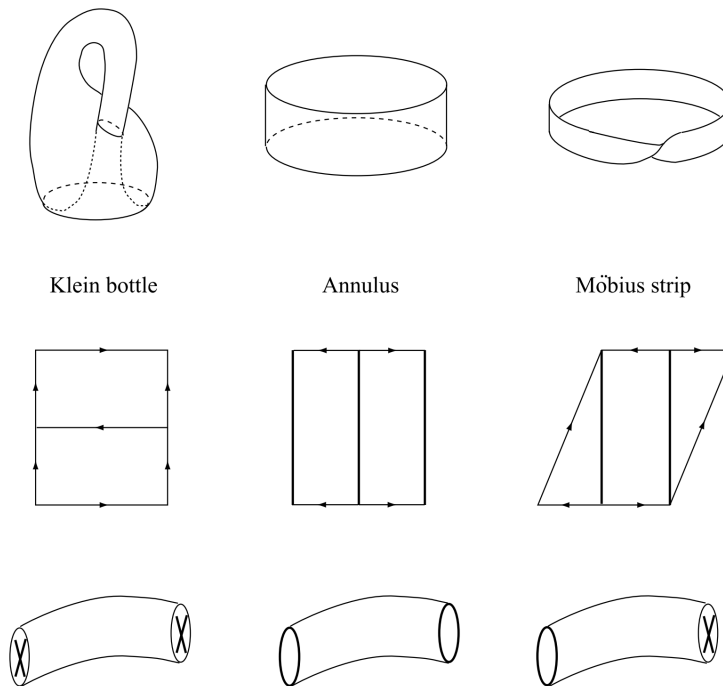
FIGURE 2.2: The string world-sheet topologies (excluding the torus) which contribute to the one-loop vacuum amplitude, and the corresponding fundamental polygons. From the point of view of open strings, they can be associated to boundary conditions with boundaries or cross-caps. The corresponding space-time picture involves D-branes or orientifold planes. Taken from [42].

the case of the type I superstring

$$
\mathcal{K} = \frac{1}{2} \int_0^\infty \frac{d\tau_2}{\tau_2^6} \frac{(V_8 - S_8)(2i\tau_2)}{\eta^8(2i\tau_2)} \, ,
$$

$$
\mathcal{A} = \frac{N^2}{2} \int_0^\infty \frac{d\tau_2}{\tau_2^6} \frac{(V_8 - S_8)\left(\frac{i\tau_2}{2}\right)}{\eta^8\left(\frac{i\tau_2}{2}\right)} \, , \qquad (2.15)
$$

$$
\mathcal{M} = \frac{\varepsilon N}{2} \int_0^\infty \frac{d\tau_2}{\tau_2^6} \frac{\left(\widehat{V}_8 - \widehat{S}_8\right)\left(\frac{i\tau_2}{2} + \frac{1}{2}\right)}{\widehat{\eta}^8\left(\frac{i\tau_2}{2} + \frac{1}{2}\right)} \, ,
$$

where the sign ϵ is a reflection coefficient and N is the number of Chan-Paton factors. At the level of the closed spectrum, the projection symmetrizes the NS-NS sector, so that the massless closed spectrum rearranges into the minimal ten-dimensional $\mathcal{N} = (1,0)$ supergravity multiplet, but anti-symmetrizes the R-R sector, while the massless open spectrum comprises a super Yang-Mills multiplet. It is instructive to recast the "loop channel" amplitudes of eq. (2.15) in the "tree-channel" using a modular transformation. The resulting amplitudes describe tree-level exchange of

closed-string states, and read

$$\widetilde{\mathcal{K}} = \frac{2^5}{2} \int_0^\infty d\ell \, \frac{(V_8 - S_8)(i\ell)}{\eta^8(i\ell)} \,,$$

$$\widetilde{\mathcal{A}} = \frac{2^{-5} N^2}{2} \int_0^\infty d\ell \, \frac{(V_8 - S_8)(i\ell)}{\eta^8(i\ell)} \,, \qquad (2.16)$$

$$\widetilde{\mathcal{M}} = \frac{2 \, \varepsilon \, N}{2} \int_0^\infty d\ell \, \frac{\left(\widehat{V}_8 - \widehat{S}_8\right)\left(i\ell + \frac{1}{2}\right)}{\widehat{\eta}^8\left(i\ell + \frac{1}{2}\right)} \,.$$

The UV divergences of the loop-channel amplitudes are translated into IR divergences, which are associated to the $\ell \to \infty$ regime of the integration region. Physically they describe the exchange of zero-momentum massless modes, either in the NS-NS sector or in the R-R sector, and the corresponding coefficients can vanish on account of the tadpole cancellation condition

$$\frac{2^5}{2} + \frac{2^{-5} N^2}{2} + \frac{2 \, \varepsilon \, N}{2} = \frac{2^{-5}}{2} \left(N + 32 \, \varepsilon\right) = 0 \,. \qquad (2.17)$$

Let us stress that these conditions apply both to the NS–NS sector, where they grant the absence of a dilaton tadpole, and to the R-R sector, where they grant R-charge neutrality and thus anomaly cancellation via the Green-Schwarz mechanism. The unique solution to eq. (2.17) is $N = 32$ and $\varepsilon = -1$, *i.e.* the $SO(32)$ type I superstring. The corresponding space-time interpretation involves 32 D9-branes[8] and an O9$_-$-plane, which has *negative* tension and charge.

2.1 *The Sugimoto model: brane supersymmetry breaking*

On the other hand, introducing an O9$_+$-plane with positive tension and charge one can preserve the R-R tadpole cancellation while generating a non-vanishing dilaton tadpole, thus breaking supersymmetry at the string scale. At the level of vacuum amplitudes, this is reflected in a sign change in the Möbius strip amplitude, so that now

---

[8]Since the D9-branes are on top of the O9$_-$-plane, counting conventions can differ based on whether one includes "image" branes.

$$\mathcal{M}_{\text{BSB}} = \frac{\varepsilon N}{2} \int_0^\infty \frac{d\tau_2}{\tau_2^6} \frac{\left(\widehat{V}_8 + \widehat{S}_8\right)\left(\frac{i\tau_2}{2} + \frac{1}{2}\right)}{\widehat{\eta}^8\left(\frac{i\tau_2}{2} + \frac{1}{2}\right)} . \tag{2.18}$$

The resulting tree-channel amplitudes are given by

$$\widetilde{\mathcal{M}}_{\text{BSB}} = \frac{2\,\varepsilon\,N}{2} \int_0^\infty d\ell \, \frac{\left(\widehat{V}_8 + \widehat{S}_8\right)\left(i\ell + \frac{1}{2}\right)}{\widehat{\eta}^8\left(i\ell + \frac{1}{2}\right)} , \tag{2.19}$$

from which the R-R tadpole condition now requires that $\varepsilon = 1$ and $N = 32$, *i.e.* a $USp(32)$ gauge group. However, one is now left with a NS-NS tadpole, and thus at low energies runaway exponential potential of the type

$$T \int d^{10}x \, \sqrt{-g_S} \, e^{-\phi} \tag{2.20}$$

emerges in the string frame, while its Einstein-frame counterpart is

$$T \int d^{10}x \, \sqrt{-g} \, e^{\gamma\phi} , \qquad \gamma = \frac{3}{2} . \tag{2.21}$$

Exponential potentials of the type of eq. (2.21) are smoking guns of string-scale supersymmetry breaking, and we shall address their effect on the resulting low-energy physics in following chapters. Notice also that the fermions are in the anti-symmetric representation of $USp(32)$, which is reducible. The corresponding singlet is a very important ingredient: it is the Goldstino that is to accompany the breaking of supersymmetry, while the closed spectrum is supersymmetric to lowest order and contains a ten-dimensional gravitino. The relevant low-energy interactions manifest an expected structure *à la* Volkov-Akulov [46], but a complete understanding of the super-Higgs mechanism in this ten-dimensional context remains elusive.

All in all, a supersymmetric closed sector is coupled to a non-supersymmmetric open sector, which lives on 32 $\overline{\text{D9}}$-branes where supersymmetry is non-linearly realized[9] [46, 56, 57] in a manner reminiscent of the Volkov-Akulov model, and due to the runaway potential of eq. (2.20) the effective space-time equations of motion do not

---

[9] The original works can be found in [47–54]. For reviews, see [42, 43, 55].

admit Minkowski solutions. The resulting model is a special case of more general D9-$\overline{\text{D9}}$ branes systems, which were studied in [19], and the aforementioned phenomenon of "brane supersymmetry breaking" (BSB) was investigated in detail in [38–41]. On the phenomenological side, the peculiar behavior of BSB also appears to provide a rationale for the low-ℓ lack of power in the Cosmic Microwave Background [43, 58–60].

While the presence of a dilaton tadpole is instrumental in breaking supersymmetry in a natural fashion, in its presence string theory back-reacts dramatically[10] on the original Minkowski vacuum, whose detailed fate appears, at present, largely out of computational control. Let us remark that these difficulties are not restricted to this type of scenarios. Indeed, while a variety of supersymmetry-breaking mechanisms have been investigated, they are all fraught with conceptual and technical obstacles, and primarily with the generic presence of instabilities, which we shall address in detail in Chapter 4 and Chapter 5.

2.2 *The type $0'B$ string*

Let us now describe another instance of orientifold projection which leads to non-tachyonic perturbative spectra. Starting from the type 0B model[11], described by (2.13). There are a number of available projections, encoded in different choices of the Klein bottle amplitude. Here we focus on

$$\mathcal{K}_{0'\text{B}} : \frac{1}{2}\left(-O_8 + V_8 + S_8 - C_8\right) , \tag{2.22}$$

which, in contrast to the more standard projection defined by the combination $O_8 + V_8 - S_8 - C_8$, implements anti-symmetrization in the O_8 and C_8 sectors. This purges tachyons from the spectrum, and thus the resulting model, termed type "$0'B$", is particularly intriguing. The corresponding tree-channel amplitude is given by

$$\widetilde{K}_{0'\text{B}} : -\frac{2^6}{2}\,C_8 . \tag{2.23}$$

---

[10]In principle, one could address these phenomena by systematic vacuum redefinitions [7–10], but carrying out the program at high orders appears prohibitive.

[11]The corresponding orientifold projections of the type 0A model were also investigated. See [42], and references therein.

In order to complete the projection one is to specify the contributions of the open sector, consistently with anomaly cancellation. Let us consider a family of solution that involves two Chan-Paton charges, and is described by [21]

$$
\begin{aligned}
\mathcal{A}_{0'B} &: n\,\bar{n}\,V_8 - \frac{n^2 + \bar{n}^2}{2}\,C_8\,, \\
\mathcal{M}_{0'B} &: \frac{n + \bar{n}}{2}\,\widehat{C}_8\,.
\end{aligned}
\tag{2.24}
$$

This construction is a special case of a more general four-charge solution [21], and involves *complex* "eigencharges" $n\,,\bar{n}$ with corresponding unitary gauge groups. Moreover, while we kept the two charges formally distinct, consistency demands $n = \bar{n}$, while the tadpole conditions fix $n = 32$, and the resulting model has a $U(32)$ gauge group[12]. As in the case of the $USp(32)$ model, this model admits a space-time description in terms of orientifold planes, now with vanishing tension, and the low-energy physics of both non-supersymmetric orientifold models can be captured by effective actions that we shall discuss in Chapter 3. In addition to orientifold models, the low-energy description can also encompass the non-supersymmetric heterotic model, which we shall now discuss in detail, with a simple replacement of numerical coefficients in the action.

3 HETEROTIC STRINGS

Heterotic strings are remarkable hybrids of the bosonic string and superstrings, whose existence rests on the fact that the right-moving sector and the left-moving sector are decoupled. Indeed, their right-moving sector can be built using the 26-dimensional bosonic string[13], while their left-moving sector is built using the ten-dimensional superstring. In order for these costructions to admit a sensible space-time interpretation, 16 of the 26 dimensions pertaining to the right-moving sector are compactified on a torus defined by a lattice Λ, of which there are only two consistent choices, namely the weight lattices of $SO(32)$ and $E_8 \times E_8$. These groups play the

---

[12]Strictly speaking, the anomalous $U(1)$ factor carried by the corresponding gauge vector disappears from the low-lying spectrum, thus effectively reducing the group to $SU(32)$.

[13]One can alternatively build heterotic right-moving sectors using ten-dimensional strings with auxiliary fermions.

rôle of gauge groups of the two corresponding supersymmetric heterotic models, aptly dubbed "HO" and "HE" respectively. Their perturbative spectra are concisely captured by the torus amplitudes

$$
\begin{aligned}
\mathcal{T}_{\text{HO}} &: (V_8 - S_8)\,\overline{(O_{32} + S_{32})}\,, \\
\mathcal{T}_{\text{HE}} &: (V_8 - S_8)\,\overline{(O_{16} + S_{16})}^2\,,
\end{aligned}
\tag{2.25}
$$

which feature $\mathfrak{so}(16)$ and $\mathfrak{so}(32)$ characters in the right-moving sector. As in the case of type II superstrings, these two models can be related by T-duality, which in this context acts as a projection onto states with even fermion number in the right-moving ("internal") sector. However, a slightly different projection yields the non-supersymmetric heterotic string of [22, 23], which we shall now describe.

3.1 *The non-supersymmetric heterotic model*

Let us consider a projection of the HE theory onto the states with even *total* fermion number. At the level of one-loop amplitudes, one is to halve the original torus amplitude and add terms obtained changing the signs in front of the S characters, yielding the two "untwisted" contributions

$$
\begin{aligned}
\mathcal{T}_{(++)} &: \frac{1}{2}\,(V_8 - S_8)\,\overline{(O_{16} + S_{16})}^2\,, \\
\mathcal{T}_{(+-)} &: \frac{1}{2}\,(V_8 + S_8)\,\overline{(O_{16} - S_{16})}^2\,.
\end{aligned}
\tag{2.26}
$$

The constraint of modular invariance under S, which is lacking at this stage, further leads to the addition of the image of $\mathcal{T}_{+-}$ under S, namely

$$
\mathcal{T}_{(-+)} : \frac{1}{2}\,(O_8 - C_8)\,\overline{(V_{16} + C_{16})}^2\,.
\tag{2.27}
$$

The addition of $\mathcal{T}_{-+}$ now spoils invariance under T transformations, which is restored adding

$$
\mathcal{T}_{(--)} : -\frac{1}{2}\,(O_8 + C_8)\,\overline{(V_{16} - C_{16})}^2\,.
\tag{2.28}
$$

All in all, the torus amplitude arising from this projection of the HE theory yields a theory with a manifest $SO(16) \times SO(16)$ gauge group, and whose torus amplitude

finally reads

$$
\begin{aligned}
\mathcal{T}_{SO(16)\times SO(16)} \; : \; O_8 \, & \overline{\left(V_{16}\, C_{16} + C_{16}\, V_{16}\right)} \\
+ \, V_8 \, & \overline{\left(O_{16}\, O_{16} + S_{16}\, S_{16}\right)} \\
- \, S_8 \, & \overline{\left(O_{16}\, S_{16} + S_{16}\, O_{16}\right)} \\
- \, C_8 \, & \overline{\left(V_{16}\, V_{16} + C_{16}\, C_{16}\right)} \, .
\end{aligned}
\tag{2.29}
$$

The massless states originating from the V_8 terms comprise the gravitational sector, constructed out of the bosonic oscillators, as well as a $(\mathbf{120}, \mathbf{1}) \oplus (\mathbf{1}, \mathbf{120})$ multiplet of $SO(16) \times SO(16)$, *i.e.* in the adjoint representation of its Lie algebra, while the S_8 terms provide spinors in the $(\mathbf{1}, \mathbf{128}) \oplus (\mathbf{128}, \mathbf{1})$ representation. Furthermore, the C_8 terms correspond to right-handed $(\mathbf{16}, \mathbf{16})$ spinors. The terms in the first line of eq. (2.29) do not contribute at the massless level, due to level matching and the absence of massless states in the corresponding right-moving sector. In particular, this entails the absence of tachyons from this string model, but the vacuum energy does not vanish[14], since it is not protected by supersymmetry. Indeed, its value can be computed integrating eq. (2.29), and, since the resulting string-scale vacuum energy couples with the gravitational sector in a universal fashion[15], its presence also entails a dilaton tadpole, and thus a runaway exponential potential for the dilaton. In the Einstein frame, it takes the form

$$
T \int d^{10}x \, \sqrt{-g} \, e^{\gamma\phi} \, , \qquad \gamma = \frac{5}{2} \, ,
\tag{2.30}
$$

and thus the effect of the dilaton tadpoles on the low-energy physics of both the orientifold models of Section 2 and the $SO(16) \times SO(16)$ heterotic model can be accounted for with the same type of exponential dilaton potential. In Chapter 3 we shall investigate in detail the consequences of dilaton tadpoles on space-time.

---

[14] In some orbifold models, it is possible to obtain suppressed or vanishing leading contributions to the cosmological constant [61–63].

[15] At the level of the space-time effective action, the vacuum energy contributes to the string-frame cosmological constant. In the Einstein frame, it corresponds to a runaway exponential potential for the dilaton.

Non-supersymmetric vacuum solutions

In this chapter we investigate the low-energy physics of the string models that we have described in Chapter 2, namely the non-supersymmetric $SO(16) \times SO(16)$ heterotic model [22, 23], whose first quantum correction generates a dilaton potential, and two orientifold models, the non-supersymmetric $U(32)$ type $0'$B model [20, 21] and the $USp(32)$ model [19] with "Brane Supersymmetry Breaking" (BSB) [38–41], where a similar potential reflects the tension unbalance present in the vacuum. To begin with, in Section 1 we discuss the low-energy effective action that we shall consider. Then we proceed to discuss some classes of solutions of the equations of motion. Specifically, in Section 2 we present the Dudas-Mourad solutions of [24], which comprise nine-dimensional static compactifications on warped intervals and ten-dimensional cosmological solutions. In Section 3 we introduce fluxes, which lead to parametrically controlled Freund-Rubin [64] compactifications [25, 26], and we show that, while the string models at stake admit only AdS solutions of this type, in a more general class of effective theories dS solutions always feature an instability of the radion mode. Furthermore, compactifications with multiple internal factors yield multi-flux landscapes, and we show that a two-flux example can accomodate scale separation, albeit not in the desired sense.

1 THE LOW-ENERGY DESCRIPTION

Let us now present the effective (super)gravity theories related to the string models at stake. For the sake of generality, we shall often work with a family of D-dimensional effective gravitational theories, where the bosonic fields include a dilaton ϕ and a $(p+2)$-form field strength $H_{p+2} = dB_{p+1}$. Using the "mostly-plus" metric signature, the (Einstein-frame) effective actions

$$S = \frac{1}{2\kappa_D^2} \int d^D x \sqrt{-g} \left(R - \frac{4}{D-2} (\partial\phi)^2 - V(\phi) - \frac{f(\phi)}{2(p+2)!} H_{p+2}^2 \right) \qquad (3.1)$$

encompass all relevant cases[1], and whenever needed we specialize them according to

$$V(\phi) = T\, e^{\gamma\phi}\,, \qquad f(\phi) = e^{\alpha\phi}\,, \qquad (3.2)$$

which capture the lowest-order contributions in the string coupling for positive[2] γ and T. In the orientifold models, the dilaton potential arises from the non-vanishing NS-NS tadpole at (projective-)disk level, while in the heterotic model it arises from the torus amplitude. The massless spectrum of the corresponding string models also includes Yang-Mills fields, whose contribution to the action takes the form

$$S_{\text{gauge}} = -\frac{1}{2\kappa_D^2} \int d^D x \sqrt{-g} \left(\frac{w(\phi)}{4} \operatorname{Tr} \mathcal{F}_{MN}\, \mathcal{F}^{MN} \right) \qquad (3.3)$$

with $w(\phi)$ an exponential, but we shall not consider them. Although AdS compactifications supported by non-abelian gauge fields, akin to those discussed in Section 3, were studied in [26], their perturbative corners appear to forego the dependence on the non-abelian gauge flux. On the other hand, an $\text{AdS}_3 \times \text{S}^7$ solution of the heterotic model with no counterpart without non-abelian gauge flux was also found [26], but it is also available in the supersymmetric case.

The (bosonic) low-energy dynamics of both the $USp(32)$ BSB model and the $U(32)$ type $0'$B model is encoded in the Einstein-frame parameters

$$D = 10\,, \quad p = 1\,, \quad \gamma = \frac{3}{2}\,, \quad \alpha = 1\,, \qquad (3.4)$$

---

[1]This effective field theory can also describe non-critical strings [65, 66], since the Weyl anomaly can be saturated by the contribution of an exponential dilaton potential.

[2]The case $\gamma = 0$, which at any rate does not arise in string perturbation theory, would not complicate matters further.

whose string-frame counterpart stems from the effective action[3] [46]

$$S_{\text{orientifold}} = \frac{1}{2\kappa_{10}^2} \int d^{10}x \sqrt{-g_S} \left(e^{-2\phi} \left[R + 4 (\partial\phi)^2 \right] - T e^{-\phi} - \frac{1}{12} F_3^2 \right). \qquad (3.5)$$

The $e^{-\phi}$ factor echoes the (projective-)disk origin of the exponential potential for the dilaton, and the coefficient T is given by

$$T = 2\kappa_{10}^2 \times 64 \, T_{\text{D9}} = \frac{16}{\pi^2 \, \alpha'} \qquad (3.6)$$

in the BSB model, reflecting the cumulative contribution of 16 $\overline{\text{D9}}$-branes and the orientifold plane [19], while in the type $0'$B model T is half of this value.

On the other hand, the $SO(16) \times SO(16)$ heterotic model of [22] is described by

$$D = 10, \quad p = 1, \quad \gamma = \frac{5}{2}, \quad \alpha = -1, \qquad (3.7)$$

corresponding to the string-frame effective action

$$S_{\text{heterotic}} = \frac{1}{2\kappa_{10}^2} \int d^{10}x \sqrt{-g_S} \left(e^{-2\phi} \left[R + 4 (\partial\phi)^2 - \frac{1}{12} H_3^2 \right] - T \right), \qquad (3.8)$$

which contains the Kalb-Ramond field strength H_3 and the one-loop cosmological constant T, which was estimated in [22]. One can equivalently dualize the Kalb-Ramond form and work with the Einstein-frame parameters

$$D = 10, \quad p = 5, \quad \gamma = \frac{5}{2}, \quad \alpha = 1. \qquad (3.9)$$

One may wonder whether the effective actions of eq. (3.1) can be reliable, since the dilaton potential contains one less power of α' with respect to the other terms. The AdS landscapes that we shall present in Section 3 contain weakly coupled regimes, where curvature corrections and string loop corrections are expected to be under control, but their existence rests on large fluxes. While in the orientifold models the vacua are supported by R-R fluxes, and thus a world-sheet formulation appears subtle, the simpler nature of the NS-NS fluxes in the heterotic model is balanced by

---

[3]In eq. (3.5) we have used the notation $F_3 = dC_2$ in order to stress the Ramond-Ramond (RR) origin of the field strength.

the quantum origin of the dilaton tadpole[4]. On the other hand, the solutions discussed in Section 2 do not involve fluxes, but their perturbative corners do not extend to the whole space-time.

The equations of motion stemming from the action in eq. (3.1) are

$$R_{MN} = \widetilde{T}_{MN} \, ,$$

$$\Box \phi - V'(\phi) - \frac{f'(\phi)}{2(p+2)!} H_{p+2}^2 = 0 \, , \qquad (3.10)$$

$$d \star (f(\phi) H_{p+2}) = 0 \, ,$$

where the trace-reversed stress-energy tensor

$$\widetilde{T}_{MN} \equiv T_{MN} - \frac{1}{D-2} T^A{}_A \, g_{MN} \qquad (3.11)$$

is defined in terms of the standard stress-energy tensor T_{MN}, and with our conventions

$$T_{MN} \equiv - \frac{\delta S_{\text{matter}}}{\delta g^{MN}} \, . \qquad (3.12)$$

From the effective action of eq. (3.1), one obtains

$$
\begin{aligned}
\widetilde{T}_{MN} = {}& \frac{4}{D-2} \partial_M \phi \, \partial_N \phi + \frac{f(\phi)}{2(p+1)!} \left(H_{p+2}^2 \right)_{MN} \\
& + \frac{g_{MN}}{D-2} \left(V - \frac{p+1}{2(p+2)!} f(\phi) H_{p+2}^2 \right) \, ,
\end{aligned}
\qquad (3.13)
$$

where $\left(H_{p+2}^2 \right)_{MN} \equiv H_{M A_1 \dots A_{p+1}} H_N{}^{A_1 \dots A_{p+1}}$. In the following sections, we shall make use of eqs. (3.10) and (3.13) to obtain a number of solutions, both with and without fluxes.

2   SOLUTIONS WITHOUT FLUX

Let us now describe in detail the Dudas-Mourad solutions of [24]. They comprise static solutions with nine-dimensional Poincaré symmetry[5], where one dimension is

---

[4]At any rate, it is worth noting that world-sheet conformal field theories on AdS$_3$ backgrounds have been related to WZW models, which can afford α'-exact algebraic descriptions [67].

[5]For a similar analysis of a T-dual version of the $USp(32)$ model, see [68].

compactified on an interval, and ten-dimensional cosmological solutions.

2.1 *Static Dudas-Mourad solutions*

Due to the presence of the dilaton potential, the maximal possible symmetry available to static solutions is nine-dimensional Poincaré symmetry, and therefore the most general solution of this type is a warped product of nine-dimensional Minkowski space-time, parametrized by coordinates x^μ, and a one-dimensional internal space, parametrized by a coordinate y. As we shall discuss in Chapter 6, in the absence of fluxes the resulting equations of motion can be recast in terms of an integrable Toda-like dynamical system, and the resulting Einstein-frame solution reads

$$
\begin{aligned}
ds^2_{\text{orientifold}} &= \left|\alpha_O\, y^2\right|^{\frac{1}{18}} e^{-\frac{\alpha_O y^2}{8}}\, dx^2_{1,8} + e^{-\frac{3}{2}\Phi_0}\left|\alpha_O\, y^2\right|^{-\frac{1}{2}} e^{-\frac{9\alpha_O y^2}{8}}\, dy^2\,,\\
\phi &= \frac{3}{4}\,\alpha_O\, y^2 + \frac{1}{3}\,\log\left|\alpha_O\, y^2\right| + \Phi_0
\end{aligned}
\tag{3.14}
$$

for the orientifold models, where here and in the remainder of this thesis

$$
dx^2_{1,p} \equiv \eta_{\mu\nu}\, dx^\mu\, dx^\nu
\tag{3.15}
$$

is the $(p+1)$-dimensional Minkowski metric. The absolute values in eq. (3.14) imply that the geometry is described by the coordinate patch in which $y \in (0,\infty)$. The corresponding Einstein-frame solution of the heterotic model reads

$$
\begin{aligned}
ds^2_{\text{heterotic}} &= \left(\sinh\left|\sqrt{\alpha_H}\, y\right|\right)^{\frac{1}{12}}\left(\cosh\left|\sqrt{\alpha_H}\, y\right|\right)^{-\frac{1}{3}} dx^2_{1,8}\\
&\quad + e^{-\frac{5}{2}\Phi_0}\left(\sinh\left|\sqrt{\alpha_H}\, y\right|\right)^{-\frac{5}{4}}\left(\cosh\left|\sqrt{\alpha_H}\, y\right|\right)^{-5} dy^2\,,\\
\phi &= \frac{1}{2}\,\log\sinh\left|\sqrt{\alpha_H}\, y\right| + 2\,\log\cosh\left|\sqrt{\alpha_H}\, y\right| + \Phi_0\,.
\end{aligned}
\tag{3.16}
$$

In eqs. (3.14) and (3.16) the scales $\alpha_{O,H} \equiv \frac{T}{2}$, while Φ_0 is an arbitrary integration constant. As we shall explain in Chapter 6, the internal spaces parametrized by y are actually intervals of finite length, and the geometry contains a weakly coupled region in the middle of the parametrically wide interval for $g_s \equiv e^{\Phi_0} \ll 1$. Moreover, the isometry group appears to be connected to the presence of uncharged 8-branes [25].

It is convenient to recast the two solutions in terms of conformally flat metrics, so that one is led to consider expressions of the type

$$
\begin{aligned}
ds^2 &= e^{2\Omega(z)} \left(dx_{1,8}^2 + dz^2 \right), \\
\phi &= \phi(z),
\end{aligned}
\tag{3.17}
$$

In detail, for the orientifold models the coordinate z is obtained integrating the relation

$$
dz = \left| \alpha_{\mathrm{O}} \, y^2 \right|^{-\frac{5}{18}} e^{-\frac{3}{4}\Phi_0} \, e^{-\frac{\alpha_{\mathrm{O}} y^2}{2}} \, dy,
\tag{3.18}
$$

while

$$
e^{2\Omega(z)} = \left| \alpha_{\mathrm{O}} \, y^2 \right|^{\frac{1}{18}} e^{-\frac{\alpha_{\mathrm{O}} y^2}{8}}.
\tag{3.19}
$$

On the other hand, for the heterotic model

$$
dz = e^{-\frac{5}{4}\Phi_0} \left(\sinh \left| \sqrt{\alpha_{\mathrm{H}}} \, y \right| \right)^{-\frac{2}{3}} \left(\cosh \left| \sqrt{\alpha_{\mathrm{H}}} \, y \right| \right)^{-\frac{7}{3}} dy,
\tag{3.20}
$$

and the corresponding conformal factor reads

$$
e^{2\Omega(z)} = \left(\sinh \left| \sqrt{\alpha_{\mathrm{H}}} \, y \right| \right)^{\frac{1}{12}} \left(\cosh \left| \sqrt{\alpha_{\mathrm{H}}} \, y \right| \right)^{-\frac{1}{3}}.
\tag{3.21}
$$

Notice that one is confronted with an interval whose finite length is proportional to $\frac{1}{\sqrt{g_s \, \alpha_{\mathrm{O,H}}}}$ in the two cases, but which hosts a pair of curvature singularities at its two ends, with a local string coupling e^{ϕ} that is weak at the former and strong at the latter. Moreover, the parameters $\alpha_{\mathrm{O,H}}$ are proportional to the dilaton tadpoles, and therefore as one approaches the supersymmetric case the internal length diverges[6].

2.2 *Cosmological Dudas-Mourad solutions*

The cosmological counterparts of the static solutions of eqs. (3.14) and (3.16) can be obtained via the analytic continuation $y \to it$, and consequently under $z \to i\eta$ in

---

[6]The supersymmetry-breaking tadpoles cannot be sent to zero in a smooth fashion. However, it is instructive to treat them as parameters, in order to highlight their rôle.

conformally flat coordinates. For the orientifold models, one thus finds

$$ds^2_{\text{orientifold}} = \left|\alpha_O\, t^2\right|^{\frac{1}{18}} e^{\frac{\alpha_O t^2}{8}}\, d\mathbf{x}^2 - e^{-\frac{3}{2}\Phi_0}\left|\alpha_O\, t^2\right|^{-\frac{1}{2}} e^{\frac{9\alpha_O t^2}{8}}\, dt^2\,,$$

$$\phi = -\frac{3}{4}\,\alpha_O\, t^2 + \frac{1}{3}\,\log\left|\alpha_O\, t^2\right| + \Phi_0\,,$$

(3.22)

where the parametric time t takes values in $(0,\infty)$, as usual for a decelerating cosmology with an initial singularity. The corresponding solution of the heterotic model reads

$$ds^2_{\text{heterotic}} = \left(\sin\left|\sqrt{\alpha_H}\, t\right|\right)^{\frac{1}{12}}\left(\cos\left|\sqrt{\alpha_H}\, t\right|\right)^{-\frac{1}{3}} d\mathbf{x}^2$$

$$- e^{-\frac{5}{2}\Phi_0}\left(\sin\left|\sqrt{\alpha_H}\, t\right|\right)^{-\frac{5}{4}}\left(\cos\left|\sqrt{\alpha_H}\, t\right|\right)^{-5} dt^2\,,$$

(3.23)

$$\phi = \frac{1}{2}\,\log\sin\left|\sqrt{\alpha_H}\, t\right| + 2\,\log\cos\left|\sqrt{\alpha_H}\, t\right| + \Phi_0\,,$$

where now $0 < \sqrt{\alpha_H}\, t < \frac{\pi}{2}$. Both cosmologies have a nine-dimensional Euclidean symmetry, and in both cases, as shown in [69], the dilaton is forced to emerge from the initial singularity climbing up the potential. In this fashion it reaches an upper bound before it begins its descent, and thus the local string coupling is bounded and parametrically suppressed for $g_s \ll 1$.

As in the preceding section, it is convenient to recast these expressions in conformal time according to

$$ds^2 = e^{2\Omega(\eta)}\left(d\mathbf{x}^2 - d\eta^2\right)\,,$$

$$\phi = \phi(\eta)\,,$$

(3.24)

and for the orientifold models the conformal time η is obtained integrating the relation

$$d\eta = \left|\alpha_O\, t^2\right|^{-\frac{5}{18}} e^{-\frac{3}{4}\Phi_0}\, e^{\frac{\alpha_O t^2}{2}}\, dt\,,$$

(3.25)

while the conformal factor reads

$$e^{2\Omega(\eta)} = \left|\alpha_O\, t^2\right|^{\frac{1}{18}} e^{\frac{\alpha_O t^2}{8}}\,.$$

(3.26)

On the other hand, for the heterotic model

$$d\eta = \left(\sin\left|\sqrt{\alpha_H}\, t\right|\right)^{-\frac{2}{3}}\left(\cos\left|\sqrt{\alpha_H}\, t\right|\right)^{-\frac{7}{3}} e^{-\frac{5}{4}\Phi_0}\, dt\,,$$

(3.27)

and

$$e^{2\Omega(\eta)} = (\sin|\sqrt{\alpha_{\mathrm{H}}}\,t|)^{\frac{1}{12}}\,(\cos|\sqrt{\alpha_{\mathrm{H}}}\,t|)^{-\frac{1}{3}} \,. \tag{3.28}$$

In both models one can choose the range of η to be $(0, \infty)$, with the initial singularity at the origin, but in this case the future singularity is not reached in a finite proper time. Moreover, while string loops are in principle under control for $g_s \ll 1$, curvature corrections are expected to be relevant at the initial singularity [70].

3   FLUX COMPACTIFICATIONS

While the Dudas-Mourad solutions that we have discussed in the preceding section feature the maximal amount of symmetry available in the string models at stake, they are fraught with regions where the low-energy effective theory of eq. (3.1) is expected to be unreliable. In order to address this issue, in this section we turn on form fluxes, and study Freund-Rubin compactifications. While the parameters of eq. (3.4) and (3.9) allow only for AdS solutions, it is instructive to investigate the general case in detail. To this effect, we remark that the results presented in the following sections apply to general $V(\phi)$ and $f(\phi)$, up to the replacement

$$\gamma \;\to\; \frac{V'(\phi_0)}{V(\phi_0)}\,, \qquad \alpha \;\to\; \frac{f'(\phi_0)}{f(\phi_0)}\,, \tag{3.29}$$

since the dilaton is stabilized to a constant value ϕ_0.

3.1 *Freund-Rubin solutions*

Since *a priori* both electric and magnetic fluxes may be turned on, let us fix the convention that $\alpha > 0$ in the frame where the field strength H_{p+2} is a $(p+2)$-form. With this convention, the dilaton equation of motion implies that a Freund-Rubin solution[7] of the form $X_{p+2} \times \mathcal{M}_q$ can only exist with an electric flux. Here X_{p+2} is Lorentzian and maximally symmetric with curvature radius L, while $\mathcal{M}_q$ is a compact

---

[7]The Laplacian spectrum of the internal space $\mathcal{M}_q$ can have some bearing on perturbative stability.

Einstein space with curvature radius R. The corresponding ansatz takes the form

$$
\begin{aligned}
ds^2 &= L^2 \, ds^2_{X_{p+2}} + R^2 \, ds^2_{\mathcal{M}_q}, \\
H_{p+2} &= c \, \mathrm{Vol}_{X_{p+2}}, \\
\phi &= \phi_0,
\end{aligned}
\tag{3.30}
$$

where $ds^2_{X_{p+2}}$ is the unit-radius space-time metric and $\mathrm{Vol}_{X_{p+2}}$ denotes the canonical volume form on X_{p+2} with radius L. The dilaton is stabilized to a *constant* value by the electric form flux on internal space[8],

$$
n = \frac{1}{\Omega_q} \int_{\mathcal{M}_q} f \star H_{p+2} = c f R^q,
\tag{3.31}
$$

whose presence balances the runaway tendency of the dilaton potential. Here Ω_q denotes the volume of the unit-radius internal manifold. Writing the Ricci tensor

$$
\begin{aligned}
R_{\mu\nu} &= \sigma_X \frac{p+1}{L^2} g_{\mu\nu}, \\
R_{ij} &= \sigma_{\mathcal{M}} \frac{q-1}{R^2} g_{ij}
\end{aligned}
\tag{3.32}
$$

in terms of $\sigma_X, \sigma_{\mathcal{M}} \in \{-1, 0, 1\}$, the geometry exists if and only if

$$
\sigma_{\mathcal{M}} = 1, \qquad \alpha > 0, \qquad q > 1, \qquad \sigma_X \left((q-1)\frac{\gamma}{\alpha} - 1 \right) < 0,
\tag{3.33}
$$

and using eq. (3.2) the values of the string coupling $g_s = e^{\phi_0}$ and the curvature radii L, R are given by

$$
\begin{aligned}
c &= \frac{n}{g_s^\alpha R^q}, \\
g_s^{(q-1)\gamma - \alpha} &= \left(\frac{(q-1)(D-2)}{(1 + \frac{\gamma}{\alpha}(p+1))T} \right)^q \frac{2\gamma T}{\alpha n^2}, \\
R^{2\frac{(q-1)\gamma - \alpha}{\gamma}} &= \left(\frac{\alpha + (p+1)\gamma}{(q-1)(D-2)} \right)^{\frac{\alpha+\gamma}{\gamma}} \left(\frac{T}{\alpha} \right)^{\frac{\alpha}{\gamma}} \frac{n^2}{2\gamma}, \\
L^2 &= -\sigma_X R^2 \left(\frac{p+1}{q-1} \cdot \frac{(p+1)\gamma + \alpha}{(q-1)\gamma - \alpha} \right) \equiv \frac{R^2}{A}.
\end{aligned}
\tag{3.34}
$$

---

[8]The flux n in eq. (3.31) is normalized for later convenience, albeit it is not dimensionless nor an integer.

From eq. (3.34) one can observe that the ratio of the curvature radii is a constant independent on n but is not necessarily unity, in contrast with the case of the supersymmetric $AdS_5 \times S^5$ solution of type IIB supergravity. Furthermore, in the actual string models the existence conditions imply $\sigma_X = -1$, i.e. an $AdS_{p+2} \times \mathcal{M}_q$ solution.

These solutions exhibit a number of interesting features. To begin with, they only exist in the presence of the dilaton potential, and indeed they have no counterpart in the supersymmetric case for $p \neq 3$. Moreover, the dilaton is constant, but in contrast to the supersymmetric $AdS_5 \times S^5$ solution its value is not a free parameter. Instead, the solution is entirely fixed by the flux parameter n. Finally, in the case of AdS the large-n limit always corresponds to a perturbative regime where both the string coupling and the curvatures are parametrically small, thus suggesting that the solution reliably captures the dynamics of string theory for its special values of p and q. As a final remark, let us stress that only one sign of α can support a vacuum with *electric* flux threading the internal manifold. However, models with the opposite sign admit vacua with *magnetic* flux, which can be included in our general solution dualizing the form field, and thus also inverting the sign of α. No solutions of this type exist if $\alpha = 0$, which is the case relevant to the back-reaction of D3-branes in the type $0'B$ model. Indeed, earlier attempts in this respect [71–73] were met by non-homogeneous deviations from AdS_5, which are suppressed, but not uniformly so, in large-n limit[9].

3.2 *No-go for de Sitter compactifications: first hints*

From the general Freund-Rubin solution one can observe that dS Freund-Rubin compactifications exist only whenever[10]

$$(q - 1)\frac{\gamma}{\alpha} - 1 < 0.$$ (3.35)

However, this requirement also implies the existence of perturbative instabilities. This can be verified studying fluctuations of the $(p + 2)$-dimensional metric, denoted

---

[9]Analogous results in tachyonic type 0 strings were obtained in [74].
[10]The same result was derived in [75].

by $\widetilde{ds}^2_{p+2}(x)$, and of the radion $\psi(x)$, writing

$$ds^2 = e^{-\frac{2q}{p}\psi(x)} \widetilde{ds}^2_{p+2}(x) + R_0^2 e^{2\psi(x)} ds^2_{\mathcal{M}_q} \tag{3.36}$$

with R_0 an arbitrary reference radius, thus selecting the $(p+2)$-dimensional Einstein frame. The corresponding effective potential for the dilaton and radion fields

$$\mathcal{V}(\phi, \psi) = V(\phi)\, e^{-\frac{2q}{p}\psi} - \frac{q(q-1)}{R_0^2}\, e^{-\frac{2(D-2)}{p}\psi} + \frac{n^2}{2R_0^{2q}}\, \frac{e^{-\frac{q(p+1)}{p}\psi}}{f(\phi)} \tag{3.37}$$

$$\equiv \mathcal{V}_T + \mathcal{V}_{\mathcal{M}} + \mathcal{V}_n$$

reproduces the Freund-Rubin solution when extremized[11], and identifies three contributions: the first arises from the dilaton tadpole, the second arises from the curvature of the internal space, and the third arises from the flux. Since each contribution is exponential in both ϕ and ψ, extremizing $\mathcal{V}$ one can express $\mathcal{V}_{\mathcal{M}}$ and $\mathcal{V}_n$ in terms of $\mathcal{V}_T$, so that

$$\mathcal{V} = \frac{p}{D-2}\left(1 - (q-1)\frac{\gamma}{\alpha}\right)\mathcal{V}_T, \tag{3.38}$$

which is indeed positive whenever eq. (3.35) holds. Moreover, the same procedure also shows that the determinant of the corresponding Hessian matrix is proportional to $(q-1)\frac{\gamma}{\alpha} - 1$, so that de Sitter solutions always entail an instability. This constitutes a special case of the general no-go results that we shall present in Chapter 8.

3.3 *In orientifold models:* $\text{AdS}_3 \times \mathcal{M}_7$ *solutions*

For later convenience, let us present the explicit solution in the case of the two orientifold models. Since $\alpha = 1$ in this case, they admit $\text{AdS}_3 \times \mathcal{M}_7$ solutions with electric flux, and in particular $\mathcal{M}_7 = \mathbb{S}^7$ ought to correspond to near-horizon geometries of D1-brane stacks, according to the microscopic picture that we shall discuss in Chapter 5 and Chapter 6. On the other hand, while D5-branes are also present in the perturbative spectra of these models [76], they appear to behave

---

[11]Notice that, in order to derive eq. (3.37) substituting the ansatz of eq. (3.36) in the action, the flux contribution is to be expressed in the magnetic frame, since the correct equations of motion arise varying ϕ and B_{p+1} independently, while the electric-frame ansatz relates them.

differently in this respect, since no corresponding $AdS_7 \times S_3$ vacuum exists[12]. Using the values in eq. (3.4), one finds

$$
\begin{aligned}
g_s &= 3 \times 2^{\frac{7}{4}}\, T^{-\frac{3}{4}} n^{-\frac{1}{4}}\,, \\
R &= 3^{-\frac{1}{4}} \times 2^{-\frac{5}{16}}\, T^{\frac{1}{16}}\, n^{\frac{3}{16}}\,, \\
L^2 &= \frac{R^2}{6}\,.
\end{aligned}
\tag{3.39}
$$

Since every parameter in this $AdS_3 \times \mathcal{M}_7$ solution is proportional to a power of n, one can use the scalings

$$
g_s \propto n^{-\frac{1}{4}}\,, \qquad R \propto n^{\frac{3}{16}}
\tag{3.40}
$$

to quickly derive some of the results that we shall present in Chapter 5.

3.4 *In the heterotic model:* $AdS_7 \times \mathcal{M}_3$ *solutions*

The case of the heterotic model is somewhat subtler, since the physical parameters of eq. (3.7) only allow for solutions with *magnetic flux*,

$$
n = \frac{1}{\Omega_3} \int_{\mathcal{M}_3} H_3\,.
\tag{3.41}
$$

The corresponding microscopic picture, which we shall discuss in Chapter 5 and Chapter 6, would involve NS5-branes, while the dual electric solution, which would be associated to fundamental heterotic strings, is absent. Dualities of the strong/weak type could possibly shed light on the fate of these fundamental strings, but their current understanding in the non-supersymmetric context is limited[13].

In the present case the Kalb-Ramond form lives on the internal space, so that dualizing it one can recast the solution in the form of eq. (3.34), using the values in

---

[12]This is easily seen dualizing the three-form in the orientifold action (3.4), which inverts the sign of α, in turn violating the condition of eq. (3.33).

[13]Despite conceptual and technical issues, non-supersymmetric dualities connecting the heterotic model to open strings have been explored in [77, 78].

eq. (3.9) for the parameters. The resulting $\text{AdS}_7 \times \mathcal{M}_3$ solution is described by

$$
\begin{aligned}
g_s &= 5^{\frac{1}{4}}\, T^{-\frac{1}{2}} n^{-\frac{1}{2}}\,, \\
R &= 5^{-\frac{5}{16}}\, T^{\frac{1}{8}}\, n^{\frac{5}{8}}\,, \\
L^2 &= 12\, R^2\,,
\end{aligned}
\tag{3.42}
$$

so that the relevant scalings are

$$
g_s \propto n^{-\frac{1}{2}}\,, \qquad R \propto n^{\frac{5}{8}}\,.
\tag{3.43}
$$

3.5 *Compactifications with more factors*

As a natural generalization of the Freund-Rubin solutions that we have described in the preceding section, one can consider flux compactifications on products of Einstein spaces. The resulting multi-flux landscapes appear considerably more complicated to approach analytically, but can feature regimes where some of the internal curvatures are parametrically smaller than the other factors, including space-time [79].

Heterotic $\text{AdS}_4 \times \mathcal{M}_3 \times \mathcal{N}_3$ *solutions*

As a minimal example of a multi-flux landscape, let us consider a product of two internal Einstein manifolds of equal dimensions, so that there are only two cycles that can be threaded by a flux. Specifically we focus on the heterotic model, since multi-flux landscape of this type involve equations of motion that cannot be solved in closed form for generic values of the parameters. Letting L, R_1, R_2 be the curvature radii of the AdS_4 and of the internal spaces $\mathcal{M}_3$, $\mathcal{N}_3$ respectively, $\text{Vol}_{\mathcal{M}_3}$, $\text{Vol}_{\mathcal{N}_3}$ the corresponding volume forms, and letting

$$
H_3 = \frac{n_1}{R_1^3}\, \text{Vol}_{\mathcal{M}_3} + \frac{n_2}{R_2^3}\, \text{Vol}_{\mathcal{N}_3}
\tag{3.44}
$$

in the magnetic frame, the equations of motion simplify to

$$
\begin{aligned}
5\,V &= \left(\frac{n_1^2}{R_1^6} + \frac{n_2^2}{R_2^6} \right) f\,, \\
\frac{6}{L^2} &= V\,, \\
\frac{4}{R_1^2} &= -V + \frac{n_1^2}{R_1^6}\,f\,, \\
\frac{4}{R_2^2} &= -V + \frac{n_2^2}{R_2^6}\,f\,,
\end{aligned}
\tag{3.45}
$$

and imply that space-time is indeed AdS$_4$. Moreover, letting $n_1 \ll n_2$ achieves the partial scale separation $\sqrt{\alpha'} \ll L$, $R_1 \ll R_2$. Indeed, solving the first equation with respect to ϕ and substituting the result in the other equations, the resulting system can be solved asymptotically. To this end, taking the ratio of the last two equation gives

$$
\frac{R_2^2}{R_1^2} = \frac{4\,\frac{n_1^2}{n_2^2}\,\frac{R_2^6}{R_1^6} - 1}{4 - \frac{n_1^2}{n_2^2}\,\frac{R_2^6}{R_1^6}}\,,
\tag{3.46}
$$

so that

$$
\frac{R_2^2}{R_1^2} \sim 4^{\frac{1}{3}} \left(\frac{n_2}{n_1} \right)^{\frac{2}{3}} - \frac{5}{4}\,,
\tag{3.47}
$$

where we retained the subleading term in order to substitute the result in eq. (3.45). Doing so finally yields

$$
\begin{aligned}
g_s &\sim 4 \times 3^{-\frac{3}{4}}\,n_1^{-\frac{1}{2}}\,, \\
L &\sim 3^{\frac{7}{8}} \times 2^{-\frac{1}{2}}\,n_1^{\frac{5}{8}}\,, \\
R_1 &\sim 3^{\frac{7}{16}} \times 4^{-\frac{3}{4}}\,n_1^{\frac{5}{8}}\,, \\
R_2 &\sim 3^{\frac{7}{16}} \times 4^{-\frac{7}{12}}\,n_1^{\frac{7}{24}}\,n_2^{\frac{1}{3}}\,,
\end{aligned}
\tag{3.48}
$$

where we have expressed the results in units of T for clarity. However, the resulting scale separation does not reduce the effective space-time dimension at low energies, which appears to resonate with the results of [79] and with recent conjectures regarding scale separation in the absence of supersymmetry [80, 81][14].

As a final remark, it is worth noting that the stability properties of multi-flux landscapes appear qualitatively different from the those of single-flux landscapes. This issue has been addressed in [83] in the context of models with no exponential

---

[14]For recent results on the issue of scale separation in supersymmetric AdS compactifications, see [82].

dilaton potentials.

Heterotic $AdS_5 \times \mathbb{H}^2 \times \mathcal{M}_3$ **solutions**

To conclude let us observe that the single-flux Freund-Rubin solutions that we have described in Section 3.1 apply to any product of Einstein manifolds, provided that the curvature radii be suitably tuned. As an example, the AdS_7 factor in the heterotic solution can be interchanged with $AdS_5 \times \mathbb{H}^2$, where $\mathbb{H}^2$ is a compact Einstein hyperbolic manifold, *e.g.* a torus with positive genus, or more generally a quotient of the hyperbolic plane by a suitable discrete group. The solution exists provided the curvature radii L_5, L_2 of the two spaces satisfy

$$\frac{4}{L_5^2} = \frac{1}{L_2^2},$$
(3.49)

so that the $AdS_5 \times \mathbb{H}^2$ factor retains the Einstein property.

Classical stability: perturbative analysis

In this chapter we investigate in detail the classical stability of the solutions that we have described in the preceding chapter, presenting the results of [27]. To this end, we derive the linearized equations of motion for field fluctuations around each background, and we study the resulting conditions for stability. In Section 1 we study fluctuations around the Dudas-Mourad solutions, starting from the static case, and subsequently applying our results to the cosmological case in Section 2. Intriguingly, in this case a logarithmic instability of the homogeneous tensor mode suggests a tendency toward dynamical compactification[1]. Then, in Section 3 we proceed to the AdS $\times$ $\mathbb{S}$ solutions[2], deriving the linearized equations of motion and comparing the resulting masses to the Breitenlohner-Freedman bounds. While the AdS compactifications that we have obtained in the preceding chapter allow for general Einstein internal spaces, choosing the sphere simplifies the analysis of tensor and vector perturbations. Moreover, as we shall argue in Chapter 6, the case of AdS $\times$ $\mathbb{S}$ appears to relate to near-horizon geometries sourced by brane stacks.

1 STABILITY OF STATIC DUDAS-MOURAD SOLUTIONS

Let us begin deriving the linearized equations of motion for the static Dudas-Mourad solutions that we have presented in the preceding chapter. The equations of interest are now

$$\Box \phi - V'(\phi) = 0 \,,$$

$$R_{MN} + \frac{1}{2} \partial_M \phi \, \partial_N \phi + \frac{1}{8} g_{MN} \, V = 0 \,,$$

(4.1)

---

[1]An analogous idea in the context of higher-dimensional dS space-times was put forth in [84].

[2]A family of non-supersymmetric AdS$_7$ solutions of the type IIA superstring was recently studied in [85], and its stability properties were investigated in [86].

and the corresponding perturbed fields take the form

$$ds^2 = e^{2\Omega(z)} \left(\eta_{MN} + h_{MN}(x,z) \right) dx^M dx^N \,,$$

$$\phi = \phi(z) + \varphi(x,z) \,. \tag{4.2}$$

As a result, the perturbed Ricci curvature can be extracted from

$$
\begin{aligned}
R^{(1)}_{MN} = {}& 8 \, \nabla_M \nabla_N \Omega + \left(\eta_{MN} + h_{MN} \right) \nabla^A \nabla_A \Omega \\
& - 8 \left(\nabla_M \Omega \, \nabla_N \Omega - \left(\eta_{MN} + h_{MN} \right) \nabla^A \Omega \, \nabla_A \Omega \right) \\
& + \frac{1}{2} \left(\left(\Box_9 + \partial_z^2 \right) h_{MN} - \nabla_M \left(\nabla \cdot h \right)_N - \nabla_N \left(\nabla \cdot h \right)_M + \nabla_M \nabla_N h^A{}_A \right) \,,
\end{aligned}
\tag{4.3}
$$

an expression valid up to first order in the perturbations. Here and henceforth $\Box_9$ denotes the d'Alembert operator pertaining to Minkowski slices, while in the following we shall denote derivatives ∂_z with respect to z by $f' \equiv \partial_z f$ (except for the dilaton potential V). In addition, covariant derivatives do not involve Ω, and thus refer to $\eta_{MN} + h_{MN}$, which is also used to raise and lower indices. Up to first order the metric equations of motion thus read

$$
\begin{aligned}
& R^{(1)}_{MN} + \frac{1}{2} \partial_M \phi \, \partial_N \phi + \frac{1}{2} \partial_M \phi \, \partial_N \varphi + \frac{1}{2} \partial_M \varphi \, \partial_N \phi \\
& + \frac{1}{8} e^{2\Omega} \left(\left(\eta_{MN} + h_{MN} \right) V + \eta_{MN} V' \varphi \right) = 0 \,,
\end{aligned}
\tag{4.4}
$$

and combining this result with the dilaton equation of motion in eq. (4.1) yields the unperturbed equations of motion

$$
\begin{aligned}
\Omega'' + 8 \left(\Omega' \right)^2 + \frac{1}{8} e^{2\Omega} V &= 0 \,, \\
9 \, \Omega'' + \frac{1}{8} e^{2\Omega} V + \frac{1}{2} \left(\phi' \right)^2 &= 0 \,, \\
\phi'' + 8 \, \Omega' \, \phi' - e^{2\Omega} V' &= 0 \,,
\end{aligned}
\tag{4.5}
$$

where V and V' shall henceforth denote the potential and its derivative computed on the classical vacuum. Notice that the first two equations can be equivalently recast in the form

$$
\begin{aligned}
72 \left(\Omega' \right)^2 - \frac{1}{2} \left(\phi' \right)^2 + e^{2\Omega} V &= 0 \,, \\
8 \left(\Omega'' - \left(\Omega' \right)^2 \right) + \frac{1}{2} \left(\phi' \right)^2 &= 0 \,,
\end{aligned}
\tag{4.6}
$$

and that the equation of motion for ϕ is a consequence of these.

All in all, eq. (4.3) finally leads to

$$
\begin{aligned}
-\frac{1}{8}\,e^{2\Omega}\,\eta_{\mu\nu}\,V'\,\varphi = {}& -\,4\,\Omega'\left(\partial_\mu h_{\nu 9}+\partial_\nu h_{\mu 9}-h'_{\mu\nu}\right) \\
& -\,\eta_{\mu\nu}\Bigg[\left(\Omega''+8\left(\Omega'\right)^2\right)h_{99} \\
& \quad +\,\Omega'\left(\partial_\alpha h^{\alpha 9}-\frac{1}{2}\left(h'^\alpha{}_\alpha-h'_{99}\right)\right)\Bigg] \\
& +\,\frac{1}{2}\Bigg[\Box_9\,h_{\mu\nu}+h''_{\mu\nu}-\partial_\mu\left(\partial_\alpha h^\alpha{}_\nu+h'_{\nu 9}\right) \\
& \quad -\,\partial_\nu\left(\partial_\alpha h^\alpha{}_\mu+h'_{\mu 9}\right)\Bigg]-\frac{1}{2}\,\partial_\mu\partial_\nu\left(h^\alpha{}_\alpha+h_{99}\right)\,, \quad (4.7)\\
-\frac{1}{2}\,\phi'\,\partial_\mu\varphi = {}& -\,4\,\Omega'\,\partial_\mu h_{99} \\
& +\,\frac{1}{2}\left(\Box_9\,h_{\mu 9}-\partial_\mu\partial_\alpha h^\alpha{}_9-\partial_\alpha h'^\alpha{}_\mu+\partial_\mu h'^\alpha{}_\alpha\right)\,, \\
-\phi'\,\varphi'-\frac{1}{8}\,e^{2\Omega}\left(V\,h_{99}+V'\,\varphi\right) = {}& -\,4\,\Omega'\,h'_{99}-\Omega'\left(\partial_\alpha h^\alpha{}_9-\frac{1}{2}\left(h'^\alpha{}_\alpha-h'_{99}\right)\right) \\
& +\,\frac{1}{2}\left(\Box_9\,h_{99}-2\,\partial_\alpha h'^\alpha{}_9+h''^\alpha{}_\alpha\right)\,,
\end{aligned}
$$

while the perturbed dilaton equation of motion reads

$$
\begin{aligned}
& \Box_9\,\varphi+\varphi''+8\,\Omega'\,\varphi'+\phi'\left(\frac{1}{2}\,h'^\alpha{}_\alpha-\frac{1}{2}\,h'_{99}-\partial_\alpha h^\alpha{}_9-8\,\Omega'\,h_{99}\right) \\
& \quad -\phi''\,h_{99}-e^{2\Omega}\,V''\,\varphi=0\,.
\end{aligned}
\quad (4.8)
$$

Starting from eqs. (4.7) and (4.8) we shall now proceed separating perturbations into tensor, vector and scalar modes.

1.1 *Tensor and vector perturbations*

Tensor perturbations are simpler to study, and to this end one only allows a transverse trace-less $h_{\mu\nu}$. After a Fourier transform with respect to x one is thus led to

$$
h''_{\mu\nu}+8\,\Omega'\,h'_{\mu\nu}+m^2\,h_{\mu\nu}=0\,, \quad (4.9)
$$

where $m^2\equiv-\,p^\mu\,p^\nu\,\eta_{\mu\nu}$, which defines a Schrödinger-like problem along the lines of eq. (4.25), with $b=0$ and $a=8\,\Omega'$. Hence, with Dirichlet or Neumann boundary

conditions the argument of Section 1.2 applies, and one obtains a discrete spectrum of masses. Moreover, one can verify that there is a normalizable mode with $h_{\mu\nu}$ independent of z, which signals that at low energies gravity is effectively nine-dimensional[3].

Vector perturbations entail some mixings, since in this case they originate from transverse $h_{\mu 9}$ and from the trace-less combination

$$h_{\mu\nu} = \partial_\mu \Lambda_\nu + \partial_\nu \Lambda_\mu \,, \tag{4.10}$$

so that

$$\partial^\mu \Lambda_\mu = 0 \,. \tag{4.11}$$

The relevant vector combination

$$C_\mu = h_{\mu 9} - \Lambda'_\mu \tag{4.12}$$

satisfies the two equations

$$\begin{aligned} \left(p_\mu \, C_\nu + p_\nu \, C_\mu \right)' + 8\,\Omega' \left(p_\mu \, C_\nu + p_\nu \, C_\mu \right) &= 0 \,, \\ m^2 \, C_\mu &= 0 \,, \end{aligned} \tag{4.13}$$

the first of which is clearly solved by

$$C_\mu = C_\mu^{(0)} \, e^{-8\Omega} \,, \tag{4.14}$$

with a constant $C_\mu^{(0)}$. In analogy with the preceding discussion, one might be tempted to identify a massless vector. However, one can verify that, contrary to the case of tensors, this is not associated to a normalizable zero mode. The result is consistent with standard expectations from Kaluza-Klein theory, since the internal manifold has no translational isometry.

---

[3]The same conclusion can be reached computing the effective nine-dimensional Newton constant [24].

1.2 *Scalar perturbations*

The scalar perturbations are defined by[4]

$$h_{\mu\nu} = \eta_{\mu\nu}\, e^{ip \cdot x}\, A(z)\,, \qquad h_{\mu 9} = ip_\mu\, D(z)\, e^{ip \cdot x}\,, \qquad h_{99} = e^{ip \cdot x}\, C(z)\,, \qquad (4.15)$$

with $p \cdot x \equiv p^\mu\, x^\nu\, \eta_{\mu\nu}$, so that the Einstein equations become altogether the four scalars A, C, D and ϕ obey the linearized equations

$$
\begin{aligned}
-\frac{1}{8}\, e^{2\Omega}\, V'\, \varphi &= -\Omega' \left(m^2\, D - \frac{1}{2}\, (17\, A' - C') \right) \\
&\quad + \frac{1}{2}\, (m^2\, A + A'') - C \left(\Omega'' + 8\, (\Omega')^2 \right)\,, \\
-\phi'\, \varphi' - \frac{1}{8}\, e^{2\Omega}\, (V\, C + V'\, \varphi) &= -\Omega' \left(m^2\, D - \frac{9}{2}\, (A' - C') \right) \\
&\quad + \frac{1}{2}\, (m^2\, (C - 2\, D') + 9\, A'')\,, \\
7\, A + C - 2\, D' - 16\, \Omega'\, D &= 0\,, \\
4\, \Omega'\, C - 4\, A' - \frac{1}{2}\, \phi'\, \varphi &= 0\,.
\end{aligned}
\qquad (4.16)
$$

Notice that some of the metric equations, the third one and the fourth one above, are constraints, and that there is actually another constraint that obtains combining the first and the last so as to remove A''. Moreover, the dilaton equation of motion is a consequence of these.

The system, however, has a residual local gauge invariance, a diffeomorphism of the type

$$z' = z + \epsilon(x, z)\,, \qquad (4.17)$$

which is available in the presence of a single internal dimension and implies

$$dz = dz' \left(1 - \frac{d\epsilon}{dz'} \right) - dx^\mu\, \partial_\mu \epsilon\,. \qquad (4.18)$$

---

[4]We reserve the symbol B to scalar perturbations of the form field, which we shall introduce in Section 3.

Taking into account the original form of the metric, which in terms of the scalar perturbations of eq. (4.15) reads

$$ds^2 = e^{2\Omega} \left((1+A)\, dx_{1,8}^2 + 2\, dz\, dx^\mu\, \partial_\mu D + (1+C)\, dz^2 \right), \tag{4.19}$$

one can thus identify the transformations

$$
\begin{aligned}
A &\to A - 2\,\Omega'\,\epsilon, \\
C &\to C - 2\,\Omega'\,\epsilon - 2\,\epsilon', \\
D &\to D - \epsilon, \\
\varphi &\to -\phi'\,\epsilon.
\end{aligned}
\tag{4.20}
$$

Notice that D behaves as a Stückelberg field, and can be gauged away, leaving only one scalar degree of freedom after taking into account the constraints, as expected from Kaluza-Klein theory. After gauging away D the third equation of eq. (4.16) implies that

$$C = -7\,A, \tag{4.21}$$

while the third equation of eq. (4.16) implies that

$$\varphi = -\frac{8}{\phi'} \left(A' + 7\,\Omega'\,A \right). \tag{4.22}$$

Substituting these expressions in the first equation of eq. (4.16) finally leads to a second–order eigenvalue equation for m^2:

$$A'' + \left(24\,\Omega' - \frac{2}{\phi'}\, e^{2\Omega}\, V' \right) A' + \left(m^2 - \frac{7}{4}\, e^{2\Omega}\, V - 14\, e^{2\Omega}\, \Omega'\, \frac{V'}{\phi'} \right) A = 0. \tag{4.23}$$

There is nothing else, since differentiating the fourth equation of eq. (4.16) and using eq. (4.6) gives

$$-\phi'\,\varphi' = -8\,A'' - 120\,\Omega'\,A' + 8\,e^{2\Omega}\, \frac{V'}{\phi'}\, A' + 7\,e^{2\Omega} \left(V + 8\,\Omega'\, \frac{V'}{\phi'} \right) A. \tag{4.24}$$

Taking this result into account, one can verify that the second equation of eq. (4.16) also leads to eq. (4.23), whose properties we now turn to discuss.

The issue at stake is the stability of the solution, which in this case reflects itself in the sign of m^2: a negative value would signal a tachyonic instability in the nine-dimensional Minkowski space, and one can show that the solution corresponding the lowest-order level potentials is stable, in both the orientifold and heterotic models. To this end, let us recall that a generic second-order equation of the type

$$f''(z) + a(z) f'(z) + \left(m^2 - b(z) \right) f(z) = 0 \qquad (4.25)$$

can be turned into a Schrödinger-like form via the transformation

$$f(z) = \Psi(z) \, e^{-\frac{1}{2} \int a \, dz} . \qquad (4.26)$$

One is thus led to

$$\Psi'' + \left(m^2 - b - \frac{a'}{2} - \frac{a^2}{4} \right) \Psi = 0 , \qquad (4.27)$$

and tracing the preceding steps one can see that $\Psi \in L^2$. Eq. (4.27) can be conveniently discussed connecting it to a more familiar problem of the type

$$\widehat{H} \, \Psi = m^2 \, \Psi , \qquad \widehat{H} \equiv b + \mathcal{A}^\dagger \mathcal{A} , \qquad (4.28)$$

with

$$\mathcal{A} \equiv -\frac{d}{dz} + \frac{a}{2} , \qquad \mathcal{A}^\dagger \equiv \frac{d}{dz} + \frac{a}{2} . \qquad (4.29)$$

Once these relations are supplemented with Dirichlet or Neumann conditions at each end in z, one can conclude that in all these cases the operator

$$\mathcal{A}^\dagger \mathcal{A} \geq 0 . \qquad (4.30)$$

All in all, positive b then implies positive values of m^2, and this condition is indeed realized for the static Dudas-Mourad solutions, since

$$b = \frac{7}{4} \, e^{2\Omega} \left(V + 8 \, \Omega' \, \frac{V'}{\phi'} \right) , \qquad (4.31)$$

and the corresponding $V \propto e^{\frac{3}{2}\phi}$, so that

$$b = \frac{7}{4} e^{2\Omega} V \left(1 + 12\frac{\Omega'}{\phi'}\right). \tag{4.32}$$

The ratio of derivatives can be computed in terms of the y coordinate using the expressions that we have presented in the preceding chapter, yielding

$$b = \frac{7 e^{2\Omega} V}{1 + \frac{9}{4}\alpha_O y^2} \geq 0. \tag{4.33}$$

For the heterotic model $V \propto e^{\frac{5}{2}\phi}$, so that

$$b = \frac{7}{4} e^{2\Omega} V \left(1 + 20\frac{\Omega'}{\phi'}\right). \tag{4.34}$$

Making use of the explicit solutions that we have presented in the preceding chapter, one thus finds

$$b = \frac{8}{3} e^{2\Omega} V \frac{1 - \frac{1}{2}\tanh^2\left(\sqrt{\alpha_H}\, y\right)}{1 + 4\tanh^2\left(\sqrt{\alpha_H}\, y\right)} \geq 0, \tag{4.35}$$

which is again non negative, so that both nine-dimensional Dudas-Mourad solutions are perturbatively stable solutions of the respective Einstein-dilaton systems for all allowed choices of boundary conditions at the ends of the interval. The presence of regions where curvature or string loop corrections are expected to be relevant, however, makes the lessons of these results less evident for String Theory.

As a final comment, let us mention that one can repeat the calculations that we have presented in D dimensions without further difficulties, and one finds

$$b = 2\,(D-3)\,e^{2\Omega}\left(\frac{V}{D-2} + \frac{D-2}{8}\Omega'\frac{V'}{\phi'}\right) \geq 0, \tag{4.36}$$

so that the resulting solutions are perturbatively stable in any dimension.

2 STABILITY OF COSMOLOGICAL DUDAS-MOURAD SO-LUTIONS

Let us now turn to the issue of perturbative stability of the Dudas-Mourad cosmological solutions that we have presented in the preceding chapter. The following analysis is largely analogous to the one of the preceding section, and we shall begin discussing tensor perturbations, which reveal an interesting feature in the homogeneous case.

2.1 *Tensor perturbations: an intriguing instability*

The issue at stake, here and in the following sections, is whether solutions determined by arbitrary initial conditions provided some time after the initial singularity can grow in the future evolution of the universe. This can be ascertained rather simply at large times, which translate into large values of the conformal time η, where many expressions simplify. Moreover, for finite values of η the geometry is regular, and the coefficients in eq. (4.37) are bounded, so that the solutions are also not singular. However, a growth of order $\mathcal{O}(1)$ is relevant for perturbations, and therefore we shall begin with the late-time asymptotics and then, at the end of the section, we shall also approach the problem globally.

In the ten-dimensional orientifold and heterotic models of interest, performing spatial Fourier transforms and proceeding as in the preceding section, one can show that tensor perturbations evolve according to

$$h_{ij}'' + 8\,\Omega'\,h_{ij}' + \mathbf{k}^2\,h_{ij} = 0\,, \tag{4.37}$$

where "primes" denote derivatives with respect to the conformal time η. Let us begin observing that, for all exponential potentials

$$V = T\,e^{\gamma\phi} \tag{4.38}$$

with $\gamma \geq \frac{3}{2}$, and therefore for the potentials pertaining to the orientifold models, which have $\gamma = \frac{3}{2}$ and are "critical" in the sense of [69], but also for the heterotic

model, which has $\gamma_E = \frac{5}{2}$ and is "super-critical" in the sense of [69], the solutions of the background equations

$$\Omega'' + 8\left(\Omega'\right)^2 - \frac{1}{8} e^{2\Omega} V = 0,$$
$$9\,\Omega'' - \frac{1}{8} e^{2\Omega} V + \frac{1}{2} \left(\phi'\right)^2 = 0, \tag{4.39}$$
$$\phi'' + 8\,\Omega'\,\phi' + \gamma\,e^{2\Omega}\,V = 0$$

are dominated, for large values of η, by

$$\phi \sim -\frac{3}{2}\,\log\left(\sqrt{\alpha_H}\,\eta\right), \qquad \Omega \sim \frac{1}{8}\,\log\left(\sqrt{\alpha_H}\,\eta\right). \tag{4.40}$$

In the picture of [69], in this region the scalar field has overcome the turning point and is descending the potential, so that the supergravity approximation is expected to be reliable, but the potential contribution is manifestly negligible only in the "super-critical" case, where $e^{2\Omega}\,V$ decays faster than $\frac{1}{\eta^2}$ for large η. However, the result also applies for $\gamma = \frac{3}{2}$, which marks the onset of the "climbing behavior". This can be appreciated retaining subleading terms, which results in

$$\phi \sim -\frac{3}{2}\,\log\left(\sqrt{\alpha_O}\,\eta\right) - \frac{5}{6}\,\log\log\left(\sqrt{\alpha_O}\,\eta\right),$$
$$\Omega \sim \frac{1}{8}\,\log\left(\sqrt{\alpha_O}\,\eta\right) + \frac{1}{8}\,\log\log\left(\sqrt{\alpha_O}\,\eta\right), \tag{4.41}$$

so that the potential decays as

$$e^{2\Omega}\,V \sim \frac{T}{2\,\alpha_O\,\eta^2\,\log\left(\sqrt{\alpha_O}\,\eta\right)}, \tag{4.42}$$

which is faster than $\frac{1}{\eta^2}$. Notice that a similar behavior, but with the scalar climbing up the potential, also emerges for small values of η, for which

$$\phi \sim \frac{3}{2}\,\log\left(\sqrt{\alpha_{O,H}}\,\eta\right), \qquad \Omega \sim \frac{1}{8}\,\log\left(\sqrt{\alpha_{O,H}}\,\eta\right) \tag{4.43}$$

for all $\gamma \geq \frac{3}{2}$, and thus in all orientifold and heterotic models of interest. However, these expressions are less compelling, since they concern the onset of the climbing phase. The potential is manifestly subleading for small values of η, but curvature corrections, which are expected to be relevant in this region, are not taken into account.

In conclusion, for $\gamma \geq \frac{3}{2}$ and for large values of η eq. (4.40) holds and eq. (4.37), which describes tensor perturbations, therefore approaches

$$h_{ij}'' + \frac{1}{\eta} h_{ij}' \sim -\mathbf{k}^2 h_{ij} . \tag{4.44}$$

Consequently, for $\mathbf{k} \neq 0$

$$h_{ij} \sim A_{ij} J_0 (k\eta) + B_{ij} Y_0 (k\eta) , \tag{4.45}$$

and the oscillations are damped for large times, so that no instabilities arise.

On the other hand, an intriguing behavior emerges for $\mathbf{k} = 0$. In this case the solution of eq. (4.44) implies that

$$h_{ij} \sim A_{ij} + B_{ij} \log \left(\frac{\eta}{\eta_0} \right) , \tag{4.46}$$

and therefore spatially homogeneous tensor perturbations experience in general a logarithmic growth. This result indicates that homogeneity is preserved while isotropy is generally violated in the ten-dimensional "climbing-scalar" cosmologies [69] that emerge in string theory with broken supersymmetry. One can actually get a global picture of the phenomenon: the linearized equation of motion for $\mathbf{k} = 0$ can be solved in terms of the parametric time t, and one finds

$$h_{ij} = A_{ij} + B_{ij} \log \left(\sqrt{\alpha_O}\, t \right) \tag{4.47}$$

for the orientifold models, while

$$h_{ij} = A_{ij} + B_{ij} \log \tan \left(\sqrt{\alpha_H}\, t \right) \tag{4.48}$$

for the heterotic model. These results are qualitatively similar, if one takes into account the limited range of t in the heterotic model, and typical behaviors are displayed in fig. 4.1.

The general lesson is that perturbations acquire $\mathcal{O}(1)$ variations toward the end of the climbing phase, where curvature corrections do not dominate the scene anymore, thus providing support to the present analysis. This result points naturally to an
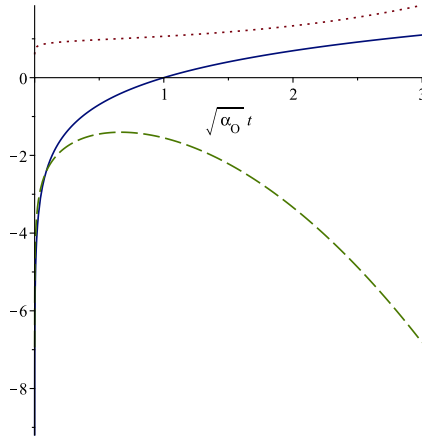
FIGURE 4.1: the scale factor e^{Ω} (red, dotted), the unstable homogeneous tensor mode (blue) and the dilaton ϕ (green, dashed) as functions of the parametric time $\sqrt{\alpha_O}\, t$.

awaited tendency toward lower-dimensional space-times, albeit without a selection criterion for the resulting dimension[5]. While perturbation theory is at most a clue to this effect, the resulting picture appears enticing, and moreover the dynamics becomes potentially richer and more stable in lower dimensions, where other branes that become space-filling can inject an inflationary phase devoid of this type of instability [27].

2.2 Scalar perturbations

Scalar perturbations exhibit a very different behavior in the presence of the exponential potentials of eq. (4.38) with $\gamma \geq \frac{3}{2}$. Our starting point is now the analytic continuation of eq. (4.23) with respect to $z \to i\,\eta$, which reads

$$A'' + \left(24\,\Omega' + 2\,e^{2\Omega}\,\frac{V'}{\phi'} \right) A' + \left(\mathbf{k}^2 + \frac{7}{4}\,e^{2\Omega}\,V + 14\,e^{2\Omega}\,\Omega'\,\frac{V'}{\phi'} \right) A = 0\,. \tag{4.49}$$

---

[5]This result resonates at least with some previous investigations [87, 88] of matrix models related to the type IIB superstring [89].

As in eq. (4.37), we have also replaced m^2 with $-\mathbf{k}^2$, which originates from a spatial Fourier transform, and "primes" denote again derivatives with respect to the conformal time η. As we have stressed in the preceding section, the potential is subdominant in eq. (4.49) for $\gamma \geq \frac{3}{2}$, which leads to the asymptotic behaviors of eq. (4.43) during the climbing phase, and of eq. (4.40) during the descending phase. As a result, during the latter eq. (4.49) reduces to

$$A'' + \frac{3}{\eta} A + \mathbf{k}^2 A = 0 \,, \tag{4.50}$$

whose general solution takes the form

$$A = A_1 \frac{J_1\left(k\eta\right)}{\eta} + A_2 \frac{Y_1\left(k\eta\right)}{\eta} \,, \tag{4.51}$$

with A_1, A_2 constants. For $\mathbf{k} \neq 0$ the amplitude always decays proportionally to $\eta^{-\frac{3}{2}}$, while for $\mathbf{k} = 0$ the two independent solutions of eq. (4.49) are dominated by

$$A = A_3 + \frac{A_4}{\eta^2} \,, \tag{4.52}$$

with A_3, A_4 constants. Therefore, scalar perturbations do not grow in time, even for the homogeneous mode with $\mathbf{k} = 0$, for $\gamma \geq \frac{3}{2}$, and thus, in particular, for the orientifold models and for the heterotic model. Similar results can be obtained studying the perturbative stability of linear dilaton backgrounds, both in the static case and in the cosmological case [27].

3 STABILITY OF AdS FLUX COMPACTIFICATIONS

In this section we discuss the perturbative stability of the AdS flux compatifications that we have presented in the preceding chapter. In order to simplify the analysis of tensor and vector perturbations, we shall work with internal spheres, but the results regarding scalar perturbations are independent of this choice[6], insofar as the internal space is Einstein. In the following we shall work in the duality frames where $p = 1$,

---

[6]The stability analysis of scalar perturbations can also be carried out in general dimensions and for general parameters without additional difficulties, but we have not found such generalizations particularly instructive in the context of this thesis.

which is the electric frame in the orientifold models, for which $\alpha = 1$, and the magnetic frame in the heterotic model, for which $\alpha = -1$. Let us begin from the orientifold models, writing the perturbations

$$g_{MN} = g_{MN}^{(0)} + h_{MN}, \qquad \phi = \phi_0 + \varphi, \qquad B_{MN} = B_{MN}^{(0)} + \frac{e^{-\alpha\phi_0}}{c} b_{MN}, \qquad (4.53)$$

where the background metric is split as

$$ds_{(0)}^2 = L^2 \lambda_{\mu\nu} dx^\mu dx^\nu + R^2 \gamma_{ij} dy^i dy^j, \qquad (4.54)$$

and linearizing the resulting equations of motion. We shall also make use of the convenient relations

$$\begin{aligned}
[\nabla_\mu, \nabla_\nu] V_\rho &= \frac{1}{L^2} \left(\lambda_{\nu\rho} V_\mu - \lambda_{\mu\rho} V_\nu \right), \\
[\nabla_i, \nabla_j] V_k &= -\frac{1}{R^2} \left(\gamma_{jk} V_i - \gamma_{ik} V_j \right),
\end{aligned} \qquad (4.55)$$

valid for maximally symmetric spaces. The linearized equations of motion for the form field are[7]

$$\begin{aligned}
&\Box_{10}\, b_{\mu\nu} - \nabla_\mu \nabla^M b_{M\nu} - \nabla_\nu \nabla^M b_{\mu M} + \frac{2}{L^2}\, b_{\mu\nu} \\
&\quad + 4\, \mathcal{R}_O^+\, \epsilon_{\mu\nu\rho} \left(\alpha\, \nabla^\rho \phi - \nabla^i h_i{}^\rho - \frac{1}{2} \nabla^\rho \lambda \cdot h + \frac{1}{2} \nabla^\rho \gamma \cdot h \right) = 0, \\
&\Box_{10}\, b_{\mu i} - \nabla_\mu \nabla^M b_{Mi} - \nabla_i \nabla^M b_{\mu M} + 2\, \mathcal{R}_O^-\, b_{\mu i} + 4\, \mathcal{R}_O^+\, \epsilon_{\alpha\beta\mu} \nabla^\alpha h^\beta{}_i = 0, \\
&\Box_{10}\, b_{ij} - \nabla_i \nabla^M b_{Mj} - \nabla_j \nabla^M b_{iM} - \frac{10}{R^2}\, b_{ij} = 0,
\end{aligned} \qquad (4.56)$$

where, here and in the following, the ten-dimensional d'Alembert operator

$$\Box_{10} = \Box + \nabla^2 \qquad (4.57)$$

is split in terms of the AdS and sphere contributions, and we have defined

$$\mathcal{R}_O^\pm \equiv \frac{1}{L^2} \pm \frac{3}{R^2} \qquad (4.58)$$

---

[7]Here and in the following ϵ denotes the Levi-Civita tensor, which includes the metric determinant prefactor.

for convenience. Similarly, the linearized equation of motion for the dilaton is

$$\Box_{10}\,\varphi - V_0''\,\varphi + 2\,\mathcal{R}_O^+\left(\alpha^2\,\varphi - \alpha\,\lambda\cdot h\right) - \frac{\alpha}{2}\,\epsilon^{\mu\nu\rho}\,\nabla_\mu b_{\nu\rho} = 0\,. \tag{4.59}$$

Finally, the linearized Einstein equations rest on the linearized Ricci tensor

$$
\begin{aligned}
R_{MN}^{(1)} &= R_{MN}^{(0)} + \frac{1}{2}\left(\Box\,h_{MN} - \nabla_M\left(\nabla\cdot h\right)_N - \nabla_N\left(\nabla\cdot h\right)_M + \nabla_M\nabla_N h^A{}_A\right) \\
&\quad + \frac{1}{2}\,R^{(0)\,A}{}_M\,h_{AN} + \frac{1}{2}\,R^{(0)\,A}{}_N\,h_{AM} - R^{(0)\,A}{}_M{}^B{}_N\,h_{AB}\,,
\end{aligned} \tag{4.60}
$$

and read

$$
\begin{aligned}
&\Box_{10}\,h_{\mu\nu} + \frac{2}{L^2}\,h_{\mu\nu} - \nabla_\mu\left(\nabla\cdot h\right)_\nu - \nabla_\nu\left(\nabla\cdot h\right)_\mu + \nabla_\mu\nabla_\nu\left(\lambda\cdot h + \gamma\cdot h\right) \\
&\quad + \lambda_{\mu\nu}\left(-\frac{5\alpha}{2}\,\mathcal{R}_O^+\,\varphi - 3\,\mathcal{R}_O^-\,\lambda\cdot h - \frac{3}{4}\,\epsilon^{\alpha\beta\gamma}\,\nabla_\alpha b_{\beta\gamma}\right) = 0\,, \\
&\Box_{10}\,h_{\mu i} + 2\,\mathcal{R}_O^+\,h_{\mu i} - \nabla_\mu\left(\nabla\cdot h\right)_i - \nabla_i\left(\nabla\cdot h\right)_\mu + \nabla_\mu\nabla_i\left(\lambda\cdot h + \gamma\cdot h\right) \\
&\quad + \frac{1}{2}\,\epsilon^{\alpha\beta}{}_\mu\left(\nabla_i b_{\alpha\beta} + \nabla_\alpha b_{\beta i} + \nabla_\beta b_{i\alpha}\right) = 0\,, \\
&\Box_{10}\,h_{ij} - \frac{2}{R^2}\,h_{ij} - \nabla_i\left(\nabla\cdot h\right)_j - \nabla_j\left(\nabla\cdot h\right)_i + \nabla_i\nabla_j\left(\lambda\cdot h + \gamma\cdot h\right) \\
&\quad + \gamma_{ij}\left(\frac{2}{R^2}\,\gamma\cdot h + \mathcal{R}_O^+\left(\frac{3\alpha}{2}\,\varphi - \lambda\cdot h\right) - \frac{1}{4}\,\epsilon^{\alpha\beta\gamma}\,\nabla_\alpha b_{\beta\gamma}\right) = 0\,,
\end{aligned} \tag{4.61}
$$

where $\lambda\cdot h$ and $\gamma\cdot h$ denote the partial traces of the metric perturbation with respect to AdS and the internal sphere. In all cases and models, the perturbations depend on the AdS coordinates x^μ and on the sphere coordinates y^i, and they will be expanded in terms of the corresponding spherical harmonics[8], whose structure is briefly reviewed in Appendix A. For instance, expanding internal scalars with respect to $\mathbb{S}^n$ spherical harmonics will always result in expressions of the type

$$h_{\mu\nu}(x,y) = \sum_\ell h_{\mu\nu,\,I_1\dots I_\ell}(x)\,\mathcal{Y}_{(n)}^{I_1\dots I_\ell}(y)\,, \tag{4.62}$$

where $I_i = 1,\dots,n$ and $h_{\mu\nu,\,I_1\dots I_\ell}(x)$ is totally symmetric and trace-less in the Euclidean I_i labels. However, the eigenvalues of the internal Laplace operator ∇^2 will only depend on ℓ. Hence, for the sake of brevity, we shall leave the internal labels implicit, although in some cases we shall refer to their ranges when counting multiplicities. For tensors in internal space there are some additional complications. For example,

---

[8]Choosing a different internal space would require knowledge of its (tensor) Laplacian spectrum.

expanding mixed metric components one obtains expressions of the type

$$h_{\mu i}(x, y) = \sum_{\ell} h_{\mu J, I_1 \ldots I_\ell}(x) \, \mathcal{Y}_{(n)\,i}^{I_1 \ldots I_\ell, J}(y) \,, \tag{4.63}$$

where $h_{\mu J, I_1 \ldots I_\ell}(x)$ corresponds to a "hooked" Young tableau of mixed symmetry and $\ell \geq 1$, as explained in Appendix A. Here the $\mathcal{Y}_{(n)\,i}$ are vector spherical harmonics, and we shall drop all internal labels, for brevity, also for the internal tensors that we shall consider.

In the heterotic model the linearized equations of motion for the form field read

$$\Box_{10} \, b_{ij} - \nabla_i \nabla^M b_{Mj} - \nabla_j \nabla^M b_{iM} - \frac{2}{R^2} \, b_{ij}$$
$$+ 4 \, \mathcal{R}_{\mathrm{H}}^+ \, \epsilon_{ijk} \left(\alpha \, \nabla^k \phi - \nabla^\alpha h_\alpha{}^k - \frac{1}{2} \nabla^k \gamma \cdot h + \frac{1}{2} \nabla^k \lambda \cdot h \right) = 0 \,,$$

$$\Box_{10} \, b_{i\mu} - \nabla_i \nabla^M b_{M\mu} - \nabla_\mu \nabla^M b_{iM} + 2 \, \mathcal{R}_{\mathrm{H}}^- \, b_{i\mu} + 4 \, \mathcal{R}_{\mathrm{H}}^+ \, \epsilon_{kli} \, \nabla^k h^l{}_\mu = 0 \,, \tag{4.64}$$

$$\Box_{10} \, b_{\mu\nu} - \nabla_\mu \nabla^M b_{M\nu} - \nabla_\nu \nabla^M b_{\mu M} + \frac{10}{L^2} \, b_{\mu\nu} = 0 \,,$$

where now

$$\mathcal{R}_{\mathrm{H}}^\pm \equiv \frac{3}{L^2} \pm \frac{1}{R^2} \,, \tag{4.65}$$

while the linearized equation of motion for the dilaton is

$$\Box_{10} \, \varphi - V_0'' \, \varphi - 2 \, \mathcal{R}_{\mathrm{H}}^+ \left(\alpha^2 \, \varphi - \alpha \, \gamma \cdot h \right) - \frac{\alpha}{2} \, \epsilon^{ijk} \, \nabla_i b_{jk} = 0 \,. \tag{4.66}$$

Finally, the linearized Einstein equations rest on eq. (4.60) and read

$$\Box_{10} \, h_{ij} - \frac{2}{R^2} \, h_{ij} - \nabla_i \left(\nabla \cdot h \right)_j - \nabla_j \left(\nabla \cdot h \right)_i + \nabla_i \nabla_j \left(\lambda \cdot h + \gamma \cdot h \right)$$
$$+ \gamma_{ij} \left(\frac{5\alpha}{2} \, \mathcal{R}_{\mathrm{H}}^+ \, \varphi - 3 \, \mathcal{R}_{\mathrm{H}}^- \, \gamma \cdot h - \frac{1}{4} \, \epsilon^{klm} \, \nabla_k b_{lm} \right)$$
$$+ \frac{1}{2} \, \epsilon^{kl}{}_i \left(\nabla_j b_{kl} + \nabla_k b_{lj} + \nabla_l b_{jk} \right) + (i \leftrightarrow j) = 0 \,,$$

$$\Box_{10} \, h_{i\mu} - 2 \, \mathcal{R}_{\mathrm{H}}^+ \, h_{i\mu} - \nabla_i \left(\nabla \cdot h \right)_\mu - \nabla_\mu \left(\nabla \cdot h \right)_i + \nabla_i \nabla_\mu \left(\lambda \cdot h + \gamma \cdot h \right) \tag{4.67}$$
$$+ \frac{1}{2} \, \epsilon^{kl}{}_i \left(\nabla_\mu b_{kl} + \nabla_k b_{l\mu} + \nabla_l b_{\mu k} \right) = 0 \,,$$

$$\Box_{10} \, h_{\mu\nu} + \frac{2}{L^2} \, h_{\mu\nu} - \nabla_\mu \left(\nabla \cdot h \right)_\nu - \nabla_\nu \left(\nabla \cdot h \right)_\mu + \nabla_\mu \nabla_\nu \left(\lambda \cdot h + \gamma \cdot h \right)$$
$$+ \lambda_{\mu\nu} \left(- \frac{2}{L^2} \, \lambda \cdot h - \mathcal{R}_{\mathrm{H}}^+ \left(\frac{3\alpha}{2} \, \varphi - \gamma \cdot h \right) - \frac{1}{4} \, \epsilon^{ijk} \, \nabla_i b_{jk} \right) = 0 \,.$$

In order to simplify the linearized equations of motion for tensor, vector and scalar perturbations it is convenient to introduce (minus) the eigenvalues of the scalar Laplacian on the unit $\mathbb{S}^n$,

$$\Lambda_n \equiv \ell \left(\ell + n - 1 \right) , \qquad \ell \in \{0,1,2,\ldots\} , \tag{4.68}$$

as well as the two parameters

$$\sigma_3 \equiv 1 + 3 \, \frac{L^2}{R^2} = \frac{3}{2} \, , \qquad \tau_3 \equiv L^2 \, V_0'' = \frac{9}{2} \tag{4.69}$$

for the orientifold models, and

$$\sigma_7 \equiv 3 + \frac{L^2}{R^2} = 15 \, , \qquad \tau_7 \equiv L^2 \, V_0'' = 75 \tag{4.70}$$

for the heterotic model. These parameters are related to the first and second derivatives of the dilaton tadpole potential evaluated on the background solutions, and thus we shall explore the stability of these solutions varying their values. While in principle including curvature corrections or string loop corrections would modify the values in eqs. (4.69) and (4.70), one could expect that the differences would be subleading in the regime of validity of the present analysis, which corresponds to large fluxes.

3.1 *An aside: an equation relevant for scalar perturbations*

Before proceeding to study tensor, vector and scalar perturbations, let us derive a useful result. Let us consider an equation of the form

$$\lambda_{\mu\nu} \, A + \nabla_\mu \nabla_\nu B = 0 \, , \tag{4.71}$$

or similarly

$$\gamma_{ij} \, A + \nabla_i \nabla_j B = 0 \, , \tag{4.72}$$

which will appear recurrently in the analysis of scalar perturbations. Referring for definiteness to the first form, we shall prove that this type of equation implies that A

and B must both vanish, provided that A and B satisfy suitable boundary conditions[9]. To begin with, one can take the trace, and if the AdS space is of dimension d this gives

$$d\,A + \Box\,B = 0\,. \tag{4.73}$$

Then one can take the divergence, obtaining finally

$$A + \Box\,B + \frac{1-d}{L^2}\,B = 0\,. \tag{4.74}$$

Subtracting from this eq. (4.73) one finds

$$A + \frac{1}{L^2}\,B = 0\,, \tag{4.75}$$

and consequently eq. (4.71) can be recast in the form

$$\nabla_\mu \nabla_\nu B = \frac{1}{L^2}\,\lambda_{\mu\nu}\,B\,. \tag{4.76}$$

If B vanishes A has to vanish as well, and thus we shall assume that $B > 0$ without loss of generality, since eq. (4.76) is linear in B. Then, letting $C = \log B$ results in

$$\nabla_\mu \nabla_\nu C + \nabla_\mu C\, \nabla_\nu C = \frac{1}{L^2}\,\lambda_{\mu\nu}\,. \tag{4.77}$$

Redefining the background metric by a coordinate transformation, one can remove the first term, but the resulting equation is inconsistent, since $\nabla_\mu C\,\nabla_\nu C$ defines a matrix that is clearly of lower rank than the metric $\lambda_{\mu\nu}$. Hence $B = 0$ and therefore, *a fortiori*, $A = 0$.

3.2 *Tensor and vector perturbations in* AdS

Let us now move on to study tensor and vector perturbations, starting from the orientifold models. Following standard practice, we classify them referring to their behavior under the isometry group $SO(2,2) \times SO(8)$ of the AdS$_3 \times$ S^7 background. In this fashion, the possible unstable modes violate the Breitenlohner-Freedman

---

[9]For instance, both A and B must decay at infinity.

(BF) bounds, which depend on the nature of the fields involved and correspond, in general, to finite negative values of (properly defined) squared AdS masses. Indeed, as reviewed in Appendix B, care must be exercised in order to identify the proper masses to which the bounds apply, since in general they differ from the eigenvalues of the corresponding AdS d'Alembert operator. In particular, aside from the case of scalars, massless field equations always exhibit gauge invariance.

Tensor perturbations

Let us begin considering tensor perturbations, which result from transverse trace-less $h_{\mu\nu}$, with all other perturbations vanishing. The corresponding equations of motion

$$\left(\Box - \frac{\Lambda_7 \left(\sigma_3 - 1\right)}{3L^2}\right) h_{\mu\nu} + \frac{2}{L^2}\, h_{\mu\nu} = 0\,, \tag{4.78}$$

where we have replaced the internal radius R with the AdS radius L using eq. (4.69), is obtained expanding the perturbations in spherical harmonics using the results summarized in Appendix A. These harmonics are eigenfunctions of the internal Laplacian in eq. (4.57). In order to properly interpret this result, however, it is crucial to observe that the massless tensor equation in AdS is the one determined by gauge invariance. In fact, the linearized Ricci tensor determined by eq. (4.60) is not invariant under linearized diffeomorphisms of the *AdS* background, since

$$\delta_\xi R_{\mu\nu} = \frac{2}{L^2} \left(\nabla_\mu \xi_\nu + \nabla_\nu \xi_\mu\right)\,. \tag{4.79}$$

However, the fluxes that are present endow, consistently, the stress-energy tensor with a similar behavior, and $\ell = 0$ in eq. (4.78) corresponds precisely to massless modes. Thus, as expected from Kaluza-Klein theory, eq. (4.78) describes a massless field for $\ell = 0$, and an infinite tower of massive ones for $\ell > 0$. These perturbations are all consistent with the BF bound, and therefore no instabilities are present in this sector.

There are also (space-time) scalar excitations resulting from the trace-less part of h_{ij} that is also divergence-less, which is a tensor with respect to the internal rotation

group and thus $\ell \geq 2$. According to the results in Appendix A, they satisfy

$$\left(L^2 \,\square - \frac{\Lambda_7 \,(\sigma_3 - 1)}{3}\right) h_{ij} = 0\,, \tag{4.80}$$

so that their squared masses are all positive. Finally, there are massive b_{ij} perturbations, which are divergence-less and satisfy

$$\left(L^2 \,\square - \frac{(\Lambda_7 + 8)\,(\sigma_3 - 1)}{3}\right) b_{ij} = 0\,, \tag{4.81}$$

where again $\ell \geq 2$.

The corresponding tensor perturbations in the heterotic model, satisfy

$$\left(L^2 \,\square - \Lambda_3 \,(\sigma_7 - 3)\right) h_{\mu\nu} + \frac{2}{L^2}\, h_{\mu\nu} = 0\,, \tag{4.82}$$

which, for $\ell = 0$, describes a massless field, accompanied by a tower of Kaluza-Klein fields for higher ℓ. Hence, once again there are no instabilities in this sector.

Analogously to the case of the orientifold models, there are massive (space-time) scalar excitations resulting from the trace-less part of h_{ij} that is also divergence-less, which satisfy

$$\left(L^2 \,\square - \Lambda_3 \,(\sigma_7 - 3)\right) h_{ij} = 0\,, \tag{4.83}$$

so that the results in Appendix A imply that again no instabilities are present. There are also no instabilities arising from transverse $b_{\mu\nu}$ excitations, which satisfy

$$\left(L^2 \,\square - \Lambda_3 \,(\sigma_7 - 3) + 10\right) b_{\mu\nu} = 0\,, \tag{4.84}$$

so that the lowest ones, corresponding to $\ell = 0$, are massless.

Vector perturbations

The analysis of vector perturbations is slightly more involved, due to mixings between $h_{\mu i}$ and $b_{\mu i}$ induced by fluxes. The relevant equations are

$$\Box_{10} \, b_{\mu i} + 2 \, \mathcal{R}_{\mathrm{O}}^{-} \, b_{\mu i} + 4 \, \mathcal{R}_{\mathrm{O}}^{+} \, \epsilon_{\alpha\beta\mu} \, \nabla^{\alpha} h^{\beta}{}_{i} = 0 \,,$$
$$\Box_{10} \, h_{\mu i} + 2 \, \mathcal{R}_{\mathrm{O}}^{+} \, h_{\mu i} + \frac{1}{2} \, \epsilon^{\alpha\beta}{}_{\mu} \left(\nabla_{\alpha} b_{\beta i} + \nabla_{\beta} b_{i\alpha} \right) = 0 \,, \tag{4.85}$$

where $h_{\mu i}$ and $b_{\mu i}$ are divergence-less in both indices. It is now possible to write

$$b_{\mu i} = \epsilon_{\alpha\beta\mu} \, \nabla^{\alpha} F^{\beta}{}_{i} \,, \tag{4.86}$$

but this does not determine F^{β}_{i} uniquely, since the redefinitions

$$F^{\beta}{}_{i} \;\rightarrow\; F^{\beta}{}_{i} + \nabla^{\beta} w_i \tag{4.87}$$

do not affect $b_{\mu i}$. The divergence-less $b_{\mu i}$ of interest, in particular, corresponds to a F^{β}_{i} that is divergence-less in its internal index i, and divergence-less Λ_i do not affect this condition. One is thus led to the system[10]

$$\left(L^2 \Box - \frac{\Lambda_7 + 5}{3} \left(\sigma_3 - 1 \right) + 2 \right) F_i{}^{\mu} + 4 \, \sigma_3 \, h_i{}^{\mu} = 0 \,,$$
$$\left(L^2 \Box - \frac{\Lambda_7 + 5}{3} \left(\sigma_3 - 1 \right) - 2 \right) h_i{}^{\mu} + \frac{\Lambda_7 + 5}{3} \left(\sigma_3 - 1 \right) F_i{}^{\mu} = 0 \,. \tag{4.88}$$

Due to the redundancy expressed by eq. (4.87), the system in eq. (4.88) could in principle accommodate a source term of the type $\nabla^{\mu} \, \widetilde{\Lambda}_i$. However, its contribution can be absorbed by a redefinition according to eq. (4.87), and thus we shall henceforth neglect it. Similar arguments apply to the ensuing analysis of scalar perturbations. The eigenvalues of the resulting mass matrix[11], here and henceforth expressed in

---

[10]In all these expressions that refer to vector perturbations $\ell \geq 1$, as described in Appendix A.

[11]We use the convention in which the mass matrix $\mathcal{M}^2$ appears alongside the d'Alembert operator in the combination $\Box - \mathcal{M}^2$.

units of $\frac{1}{L^2}$, are thus

$$\frac{\Lambda_7 + 5}{3}\,(\sigma_3 - 1) \pm 2\sqrt{\frac{\Lambda_7 + 5}{3}\,(\sigma_3 - 1)\,\sigma_3 + 1}\,. \tag{4.89}$$

In order to refer to the BF bound discussed in Appendix B, one should add 2 to these expressions and compare the result with zero. All in all, there are no modes below the BF bound in this sector, and thus no instabilities. The vector modes lie above it for $\ell > 1$ for $\sigma_3 > 1$, while they are massless for $\ell = 1$ and all allowed values of $\sigma_3 > 1$, and also, for all ℓ, in the singular case where $\sigma_3 = 1$, which would translate into a seven-sphere of infinite radius. For $\ell = 1$ there are 28 massless vectors corresponding to one of the eigenvalues above. Indeed, according to the results in Appendix A they build up a second-rank anti-symmetric tensor in the internal vector indices, and therefore an adjoint multiplet of $SO(8)$ vectors. This counting is consistent with Kaluza-Klein theory and reflects the internal symmetry of S^7, although the massless vectors originate from mixed contributions of the metric and the two-form field in the present case.

The above considerations extend to the heterotic model, for which we let

$$b_{i\mu} = \epsilon_{ijk}\,\nabla^j F_\mu{}^k\,, \tag{4.90}$$

which is transverse in internal space. The resulting system reads

$$\left(L^2\,\square - (\ell+1)^2\,(\sigma_7 - 3) + 6\right) F_\mu{}^i + 4\,\sigma_7\,h_\mu{}^i = 0\,,$$
$$\left(L^2\,\square - (\ell+1)^2\,(\sigma_7 - 3) - 6\right) h_\mu{}^i + (\ell+1)^2\,(\sigma_7 - 3)\,F_\mu{}^i = 0\,, \tag{4.91}$$

and the eigenvalues of the corresponding mass matrix are given by

$$(\ell+1)^2\,(\sigma_7 - 3) \pm 2\sqrt{(\ell+1)^2\,(\sigma_7 - 3)\,\sigma_7 + 9}\,. \tag{4.92}$$

In order to refer to the BF bound in Appendix B one should add 6 to these expressions and compare the result with -4. Hence, there are no modes below the BF bound in this sector. The vector modes are massive for $\ell > 1$ in the region $\sigma_7 > 3$, while they become massless for $\ell = 1$ and all allowed values of $\sigma_7 > 3$, and for all values of ℓ

in the singular limit $\sigma_7 = 3$, which would correspond to a three-sphere of infinite radius. All in all, for $\ell = 1$ there are 6 massless vectors arising from one of the two eigenvalues above, and according to the results in Appendix A they build up an second-rank anti-symmetric tensor in the internal vector indices, and therefore an adjoint multiplet of $SO(4)$ vectors. The counting is consistent with Kaluza-Klein theory and with the internal symmetry of S^3, although the massless vectors originate once again from mixed contributions of the metric and the two-form field. In light of these results, one could expect that choosing a different internal space with non-trivial isometries would not result in instabilities of tensor or vector modes, since tensors are decoupled and the gauge invariance arising from Kaluza-Klein arguments underpins massless modes.

3.3 *Scalar perturbations in* AdS

Let us now discuss scalar perturbations. Since there are seven independent such perturbations in the present cases, the analysis of the resulting systems is more involved with respect to the case of tensor and vector perturbations. While the results in this section can be obtained using a suitable gauge fixing of the metric, we shall proceed along the lines of [27], where algebraic constraints arise from the Einstein equations.

Scalar perturbations in the orientifold models

Let us now focus on scalar perturbations in the orientifold models. To begin with, $b_{\mu\nu}$ contributes to scalar perturbations, as one can verify letting

$$b_{\mu\nu} = \epsilon_{\mu\nu\rho} \nabla^\rho B \,, \tag{4.93}$$

an expression that satisfies identically

$$\nabla^\mu b_{\mu\nu} = 0 \,. \tag{4.94}$$

On the other hand, they do not arise from $b_{\mu i}$ and b_{ij}, since the corresponding contributions would be pure gauge. On the other hand, scalar metric perturbations can be parametrized as

$$h_{\mu\nu} = \lambda_{\mu\nu}\, A\,,$$
$$h_{\mu i} = R^2\, \nabla_\mu \nabla_i D\,, \tag{4.95}$$
$$h_{ij} = \gamma_{ij}\, C\,,$$

up to a diffemorphism with independent parameters along AdS$_3$ and S^7 directions. The linearized equations of motion for $b_{\mu\nu}$ yield

$$\Box_{10}\, B + 4\,\mathcal{R}_O^+ \left(\alpha\,\varphi - R^2\,\nabla^2 D - \frac{3}{2}\,A + \frac{7}{2}\,C\right) = 0\,, \tag{4.96}$$

where ∇^2 denotes the internal background Laplacian, according to the decomposition of eq. (4.57). Expanding with respect to spherical harmonics, so that $\nabla^2 \to -\frac{\Lambda_7}{R^2}$, eq. (4.96) becomes (an AdS derivative of[12])

$$\left(\Box - \frac{\Lambda_7}{R^2}\right) B + 4\,\mathcal{R}_O^+ \left(\alpha\,\varphi + \Lambda_7\, D - \frac{3}{2}\,A + \frac{7}{2}\,C\right) = 0\,. \tag{4.97}$$

Notice that a redefinition $B \to B + \delta B(y)$, where $\delta B(y)$ depends only on internal coordinates, would not affect $b_{\mu\nu}$ in eq. (4.93). As a result, while eqs. (4.96) and (4.97) could in principle contain a source term, this can be eliminated taking this redundancy into account. Similar considerations apply for the heterotic model.

In a similar fashion, the linearized equation of motion for the dilaton becomes

$$\left(\Box - \frac{\Lambda_7}{R^2} - V_0''\right)\varphi + 2\,\mathcal{R}_O^+ \left(\alpha^2\,\varphi - 3\,\alpha\,A\right) + \alpha\,\Box\, B = 0\,, \tag{4.98}$$

---

[12]The overall derivative can be removed on account of suitable boundary conditions.

where the last term can be eliminated using eq. (4.97). Analogously, the linearized Einstein equations take the form

$$
\lambda_{\mu\nu} \left[\left(\Box - \frac{\Lambda_7}{R^2} - \frac{4}{L^2} \right) A + \mathcal{R}_{\mathrm{O}}^+ \left(\frac{7\alpha}{2} \varphi + 21\,C + 6\,\Lambda_7\,D \right) - \frac{3\,\Lambda_7}{2\,R^2}\,B \right]
$$

$$
+ \nabla_\mu \nabla_\nu \left(A + 7\,C + 2\,\Lambda_7\,D \right) = 0\,,
$$

$$
\nabla_\mu \nabla_i \left(12\,D - B + 2\,A + 6\,C \right) = 0\,, \qquad (4.99)
$$

$$
\gamma_{ij} \left[\left(\Box - \frac{\Lambda_7 + 9}{R^2} - \frac{7}{L^2} \right) C - \frac{\Lambda_7}{2} \left(4\,\mathcal{R}_{\mathrm{O}}^+\,D - \frac{1}{R^2}\,B \right) - \frac{\alpha}{2}\,\mathcal{R}_{\mathrm{O}}^+\,\varphi \right]
$$

$$
+ \nabla_i \nabla_j \left(3\,A + 5\,C - 2\,R^2\,\Box\,D \right) = 0\,.
$$

Although these equations have an unfamiliar form, we have shown in Section 3.1 that the terms involving gradients must vanish separately. For $\ell = 0$ nothing depends on internal coordinates, the terms involving $\nabla_\mu \nabla_i$ and $\nabla_i \nabla_j$ become empty and D also disappears. In this case one is thus led to the simplified system

$$
\left(L^2\,\Box - 4 - 3\,\sigma_3 \right) A + \frac{7\alpha}{2}\,\sigma_3\,\varphi = 0\,,
$$

$$
\left(L^2\,\Box - \tau_3 - 2\,\alpha^2\,\sigma_3 \right) \varphi + 2\,\alpha\,\sigma_3\,A = 0\,, \qquad (4.100)
$$

$$
L^2\,\Box\,B - 8\,\sigma_3\,A + 4\,\alpha\,\sigma_3\,\varphi = 0\,,
$$

to be supplemented by the linear relation

$$
A = -7\,C\,, \qquad (4.101)
$$

and the last column of the resulting mass matrix vanishes, so that there is a vanishing eigenvalue whose eigenvector is proportional to B. This perturbation is however pure gauge, since eq. (4.93) implies that the corresponding field strength vanishes identically. Leaving it aside, one can work with the reduced mass matrix determined by the other two equations, whose eigenvalues are

$$
\left(\alpha^2 + \frac{3}{2} \right) \sigma_3 + \frac{\tau_3}{2} + 2 \pm \frac{1}{2}\,\sqrt{\Delta}\,, \qquad (4.102)
$$

where the discriminant

$$
\Delta \equiv 4\alpha^4\,\sigma_3^2 + 16\,\alpha^2 \left(\sigma_3 + \frac{\tau_3}{4} - 1 \right) \sigma_3 + \left(3\,\sigma_3 - \tau_3 + 4 \right)^2\,. \qquad (4.103)
$$

There are regions of instability as one varies the parameters σ_3, τ_3 of eq. (4.69), but for the actual orientifold models, where $(\beta, \sigma_3, \tau_3) = \left(1, \frac{3}{2}, \frac{9}{2}\right)$, the two eigenvalues evaluate to 12 and 4, and thus lie well above the BF bound. To reiterate, there are no unstable scalar modes for the orientifold models in the $\ell = 0$ sector for the internal S^7. In view of the ensuing discussion, let us add that the stability persists for convex potentials, with $\tau_3 > 0$, independently of σ_3.

For $\ell \neq 0$ the system becomes more complicated, since it now includes the two algebraic constraints

$$A + 7C + 2\Lambda_7 D = 0,$$
$$2A - B + 6C + 12D = 0,$$

(4.104)

and the five dynamical equations

$$\left(\Box - \frac{\Lambda_7}{R^2} - \frac{4}{L^2}\right) A + \mathcal{R}_O^+ \left(\frac{7\alpha}{2}\varphi - 3A\right) - \frac{3\Lambda_7}{2R^2}B = 0,$$

$$\left(\Box - \frac{\Lambda_7}{R^2}\right) B + 4\mathcal{R}_O^+(\alpha\varphi - 2A) = 0,$$

$$\left(\Box - \frac{\Lambda_7 + 9}{R^2} - \frac{7}{L^2}\right) C - \frac{\Lambda_7}{2}\left(4\mathcal{R}_O^+ D - \frac{1}{R^2}B\right) - \frac{\alpha}{2}\mathcal{R}_O^+\varphi = 0,$$ (4.105)

$$\Box D - \frac{3}{2R^2}A - \frac{5}{2R^2}C = 0,$$

$$\left(\Box - \frac{\Lambda_7}{R^2} - V_0''\right)\varphi + \frac{\alpha\Lambda_7}{R^2}B - 2\mathcal{R}_O^+(\alpha^2\varphi - \alpha A) = 0.$$

Let us first observe that this set of seven equations for the five unknowns (A, B, C, D, φ) is consistent: one can indeed verify that the algebraic constraints of eq. (4.104) are identically satisfied by the system in eq. (4.105). One can thus concentrate on the equations relating A, φ and B, which do not involve the other fields and read

$$\left(L^2\Box - \frac{\Lambda_7}{3}(\sigma_3 - 1) - 4 - 3\sigma_3\right) A + \frac{7\alpha}{2}\sigma_3\varphi - \frac{\Lambda_7}{2}(\sigma_3 - 1)B = 0,$$

$$\left(L^2\Box - \frac{\Lambda_7}{3}(\sigma_3 - 1) - \tau_3 - 2\alpha^2\sigma_3\right)\varphi + 2\alpha\sigma_3 A - \frac{\alpha\Lambda_7}{3}(\sigma_3 - 1)B = 0,$$ (4.106)

$$\left(L^2\Box - \frac{\Lambda_7}{3}(\sigma_3 - 1)\right) B - 8\sigma_3 A + 4\alpha\sigma_3\varphi = 0,$$

to then determine C and D via the algebraic constraints. The mass matrix of interest is

now 3×3, and in all cases one is to compare its eigenvalues with the Breitenlohner–Freedman (BF) bound for scalar perturbations, which in this $\text{AdS}_3 \times \mathbb{S}^7$ case

$$m^2 L^2 \geq -1\,. \tag{4.107}$$

One is thus led, in agreement with [90][13], to the simple results

$$\left(\frac{\ell\,(\ell+6)}{6} + 4\,, \ \frac{(\ell+6)\,(\ell+12)}{6}\,, \ \frac{\ell\,(\ell-6)}{6} \right) \tag{4.108}$$

for the seven-sphere, and thus the BF bound is violated by the third eigenvalue for $\ell = 2\,, 3\,, 4$, as displayed in fig. 4.2. Decreasing the value of α could remove the problem for $\ell = 4$, but the instability would still be present for $\ell = 2\,, 3$. On the other hand, increasing the value of α instabilities would appear also for higher values[14] of ℓ.
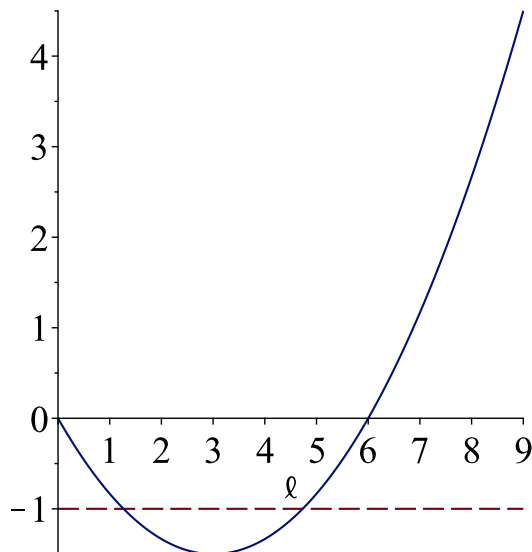
FIGURE 4.2: violations of the scalar BF bound in the orientifold models. The dangerous eigenvalue is displayed in units of $\frac{1}{L^2}$, and the BF bound is -1 in this case. Notice the peculiar behavior, already spotted in [90], whereby the squared masses decrease initially, rather than increasing, as ℓ increases between 1 and 3.

One could now wonder whether there exist regions within the parameter space spanned by σ_3 and τ_3 where the violation does not occur. We did find them, for all

---

[13]For an earlier analysis in general dimensions, see [91]. A subsequent analysis for two internal sphere factors was performed in [92].

[14]For recent results on unstable modes of non-vanishing angular momentum in AdS compactifications, see [93].

dangerous values of ℓ, for values of σ_3 that are close to one, and therefore for negative V_0, and for positive τ_3, *i.e.* for potentials that are convex close to the background configuration. These results are displayed in figs. 4.3 and 4.4.
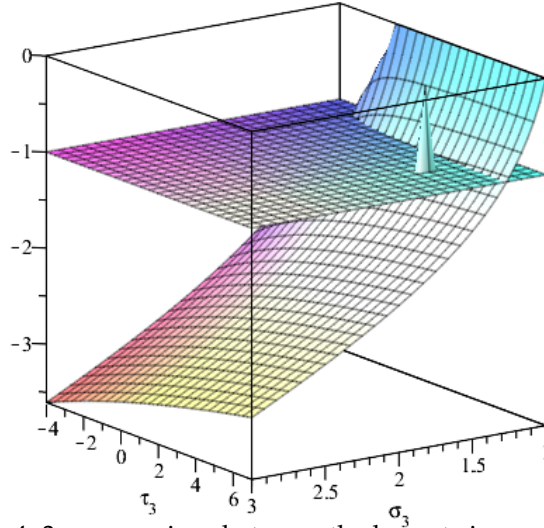
FIGURE 4.3: comparison between the lowest eigenvalue $m^2 L^2$ and the BF bound, which is -1 in this case. There are regions of stability for values of σ_3 close to 1, which correspond to $\frac{R^2}{L^2} > 9$ and negative values of V_0. The example displayed here refers to $\ell = 3$, which corresponds to the minimum in fig. 4.2, and the peak identifies the tree-level values $\sigma_3 = \frac{3}{2}$, $\tau_3 = \frac{9}{2}$.

Scalar perturbations in the heterotic model

Let us now move on to the stability analysis of scalar perturbations the heterotic model. Proceeding as in the preceding section, we let

$$b_{ij} = \epsilon_{ijk} \nabla^k B \,, \tag{4.109}$$

a choice that also identically satisfies

$$\nabla^i b_{ij} = 0 \,. \tag{4.110}$$
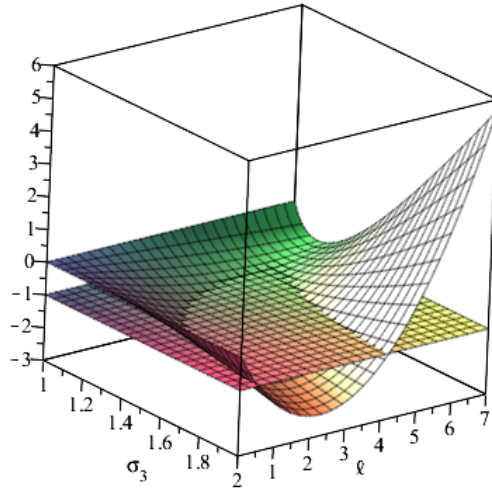
FIGURE 4.4: a different view. Comparison between the lowest eigenvalue of $m^2 L^2$ and the BF bound, which is -1 in this case, as functions of ℓ and σ_3, for $\tau_3 = \frac{9}{2}$. There are regions of stability for values of σ_3 close to 1, which correspond to large values for the ratio $\frac{R^2}{L^2}$ and to negative values of V_0.

In addition, let us parametrize scalar metric perturbations as

$$h_{\mu\nu} = \lambda_{\mu\nu} A,$$

$$h_{\mu i} = L^2 \nabla_\mu \nabla_i D,$$

$$(4.111)$$

$$h_{ij} = \gamma_{ij} C,$$

along the lines of the preceding section. For scalar perturbations one arrives again at seven equations for five unknowns, and one can verify that the system is consistent. All in all, one can thus work with C, φ and B, restricting the attention to

$$\left(L^2 \Box - \Lambda_3 (\sigma_7 - 3) - 5\sigma_7 - 12\right) C + \frac{5\alpha}{2} \sigma_7 \varphi - \frac{3\Lambda_3}{2} (\sigma_7 - 3) B = 0,$$

$$\left(L^2 \Box - \Lambda_3 (\sigma_7 - 3) - \tau_7 - 2\alpha^2 \sigma_7\right) \varphi + 6\alpha \sigma_7 C + \alpha \Lambda_3 (\sigma_7 - 3) B = 0, \quad (4.112)$$

$$\left(L^2 \Box - \Lambda_3 (\sigma_7 - 3)\right) B - 8\sigma_7 C + 4\alpha \sigma_7 \varphi = 0,$$

here expressed in terms of the two variables σ_7 and τ_7 of eq. (4.70), to then determine A and D algebraically. For $\ell = 0$ B again decouples, and the eigenvalues of the corresponding reduced mass matrix are

$$\left(\alpha^2 + \frac{5}{2}\right)\sigma_7 + \frac{\tau_7}{2} + 6 \pm \frac{1}{2}\sqrt{\Delta}, \tag{4.113}$$

with

$$\Delta \equiv \left(4\alpha^4 + 40\alpha^2 + 25\right)\sigma_7^2 + 4\left(\alpha^2 - \frac{5}{2}\right)(\tau_7 - 12)\,\sigma_7 + (\tau_7 - 12)^2. \tag{4.114}$$

In particular, in the heterotic model they read $24\left(4 \pm \sqrt{6}\right) > 0$. We can now move on to the $\ell \neq 0$ case, where the three scalars (C, ϕ, B) all contribute, so that one is led to a 3×3 mass matrix. In most of the parameter space, two eigenvalues are not problematic, but there is one dangerous eigenvalue, depicted in fig. 4.5, which corresponds to $\ell = 1$ and $k = 0$ in the expression

$$64 + 12\,\Lambda_3 - 16\sqrt{34 + 15\,\Lambda_3}\,\cos\left(\frac{\delta - 2\pi k}{3}\right), \tag{4.115}$$

where

$$\delta \equiv \arg\left(152 - 45\,\Lambda_3 + 3i\sqrt{3\left(5\,\Lambda_3 + 3\right)\left(\left(5\,\Lambda_3 + 14\right)^2 + 4\right)}\right). \tag{4.116}$$

Still, there is again a stability region for values of σ_7 that are close to 12, for negative V_0, and typically for positive τ_7, *i.e.* for potentials that are convex close to the background configuration. These results are displayed in figs. 4.6 and 4.7.

3.4 *Removing the unstable modes*

Since the number of unstable modes is finite, one can try to eliminate the unstable modes present, in the orientifold models, for $\ell = 2, 3, 4$ by projections in the internal $\mathbb{S}^7$, which can be embedded in $\mathbb{C}^4$ constraining its four complex coordinates Z^i to
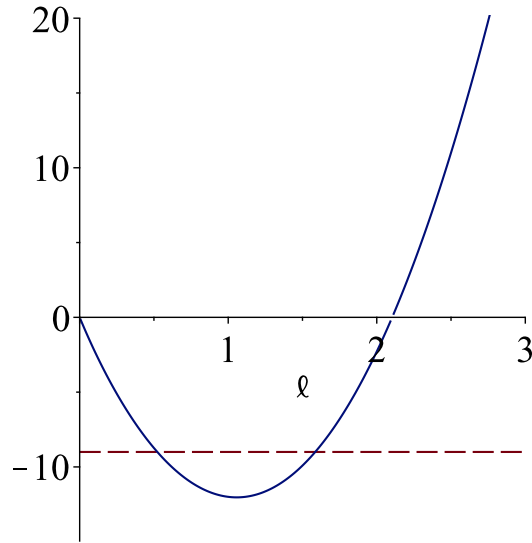
FIGURE 4.5: violations of the BF bound in the heterotic model. The dangerous eigenvalue is displayed in units of $\frac{1}{L^2}$, and the BF bound is -9 in this case.

satisfy

$$\sum_{i=1}^{4} Z^i \, \overline{Z^i} = R^2 \,. \tag{4.117}$$

According to the results in Appendix A, scalar spherical harmonics of order ℓ correspond to harmonic polynomials of degree ℓ in the Z^i and their complex conjugates, so that the issue is how to project out the dangerous ones. The three-sphere, which can be embedded in $\mathbb{C}^2$ demanding that

$$\sum_{i=1}^{2} Z^i \, \overline{Z^i} = R^2 \,, \tag{4.118}$$

provides an instructive simpler case. Indeed, one can associate each point on $\mathbb{S}^3$ to a unit quaternion, represented by the matrix

$$Q = \begin{pmatrix} Z_1 & i \, Z_2 \\ i \, \overline{Z_2} & \overline{Z_1} \end{pmatrix} \tag{4.119}$$

on which the $SU(2)$ rotations

$$R_k = e^{\frac{i\pi}{4} \sigma_k} \,, \qquad R_k^8 = I \tag{4.120}$$
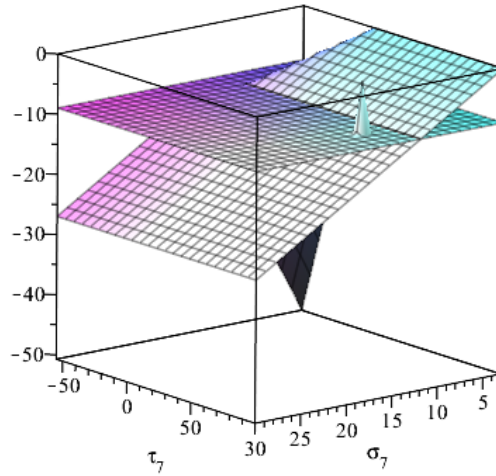
FIGURE 4.6: comparison between the lowest eigenvalue $m^2 L^2$ and
the BF bound, which is -9 in this case. There are regions of stability
for values of σ_7 close to 3, which correspond to $\frac{R^2}{L^2} > 9$, and to negative
values of V_0. The example displayed here refers to $\ell = 1$, which
corresponds to the minimum in fig. 4.5, and the peak identifies the
tree-level values $\sigma_7 = 15$, $\tau_7 = 75$.

act freely. One can verify that these rotations, when composed in all possible ways,
build the symmetry group of the cube in the three-dimensional Euclidean space
associated to the three generators $\frac{\sigma_i}{2}$. One can also show that these operations suffice
to eliminate all harmonic polynomials of degrees $\ell \leq 4$, while leaving no fixed
sub-varieties[15] on account of their free action on quaternions by left multiplication.
One would naturally expect octonions of unit norm to play a similar rôle for $\mathbb{S}^7$, but
we have just taken a cursory look at this more complicated construction. Alternatively,
and more simply, one could consider the transformations generated by the R_i in
eq. (4.120) acting simultaneously on complementary pairs of (Z^i, Z^j) coordinates.
This would suffice to eliminate all unwanted spherical harmonics, but unfortunately
it would also generate fixed sub-varieties. In the heterotic case one could eliminate
the bad eigenvalue by a $\mathbb{Z}_2$ antipodal projection in the internal sphere S^3, which can
be identified with the $SU(2)$ group manifold. This operation has no fixed points,
and reduces the internal space to the $SO(3)$ group manifold, without affecting the

---

[15]Projections that leave a sub-variety fixed could entail subtleties related to twisted states that become
massless.
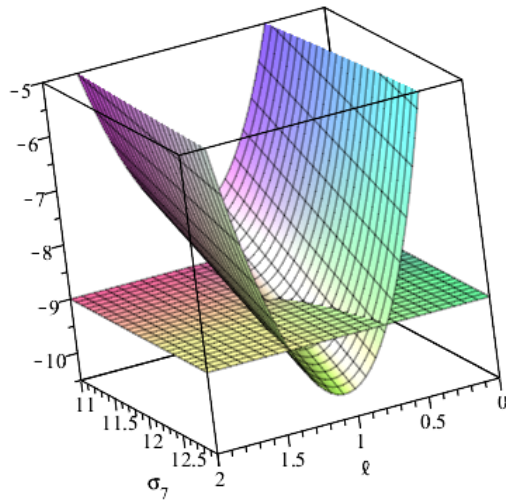
FIGURE 4.7: a different view. Comparison between the lowest eigenvalue $m^2 L^2$ and the BF bound, which is -9 in this case, as functions of ℓ and σ_7, for $\tau_7 = 75$. There are regions of stability for values of σ_3 below 12, which correspond to relatively large values for the ratio $\frac{R^2}{L^2}$ and to negative values of V_0.

massless vectors with $\ell = 1$ that we have identified. Alternatively, one could resort to the symmetry group of the sphere related to the action on unit quaternions that we have described for the orientifold vacua. However, non–perturbative instabilities would be in principle relevant to the story in this case, and we shall analyze them in detail in Chapter 5. Curvature corrections and string loop corrections would also deserve a closer look, since they could drive the potential to a nearby stability domain, providing an interesting alternative for these AdS $\times$ S solutions.

Let us conclude with a few remarks. To begin with, a suitable choice of internal manifold could rid the AdS flux compactifications of perturbative instabilities altogether, but in general the study of tensor and vector perturbations would become more involved. Moreover, in case the instabilities that we have discusses were not present, one would need to take into account the fluctuations of the remaining degrees of freedom of the low-energy effective theory, which include non-abelian gauge fields that couple to the gravitational sector. At any rate, one would eventually also have to exclude non-perturbative instabilities, the analysis of which is the subject of the following chapter.

4 ASYMMETRY OF THE MASS MATRICES

To conclude this chapter, let us briefly address the issue of (a)symmetry for the mass matrices that we have discussed in the preceding sections. It is apparent that the mass matrices that we have obtained from the linearized equations of motions is not symmetric, but they should be diagonalizable and have real eigenvalues nonetheless, since they arise from the fluctuations of a dissipation-less system. Indeed, one can show that

1. The asymmetry in the mass matrices is due to the non-canonical normalization of kinetic terms.

2. Despite their asymmetry, the mass matrices are in fact similar to a symmetric matrix and is therefore diagonalizable, with real eigenvalues.

To this end, let us consider a quadratic theory of scalar fields $\{\phi_i\}_i$, described by a generic action of the form

$$S = \frac{1}{2} \int d^D x \sqrt{-g} \left(\sum_i A_i \, (\partial \phi_i)^2 + \sum_{i,j} M_{ij} \, \phi_i \, \phi_j \right) \tag{4.121}$$

where the positive coefficients A_i encode non-canonical normalizations. The mass matrix $\mathcal{M}^{\text{EOM}}$ resulting from the equations of motion

$$\Box \, \phi_i + \sum_j \left(\frac{M_{ij}}{A_i} \right) \phi_j = 0 \tag{4.122}$$

is not symmetric in general. On the other hand, writing the action in terms of the canonically normalized fields

$$\chi_i \equiv \sqrt{A_i} \, \phi_i \tag{4.123}$$

yields the symmetric mass matrix

$$\mathcal{M}_{ij}^{\text{sym}} \equiv \frac{M_{ij}}{\sqrt{A_i A_j}} \, , \tag{4.124}$$

since M itself can be taken to be symmetric without loss of generality. The two matrices are related by

$$\mathcal{M}_{ij}^{\text{sym}} = \sqrt{\frac{A_i}{A_j}} \, \mathcal{M}_{ij}^{\text{EOM}} \,, \tag{4.125}$$

which is indeed a similarity transformation, since

$$\mathcal{M}^{\text{sym}} = P \, \mathcal{M}^{\text{EOM}} \, P^{-1} \,, \qquad P_{ij} \equiv \sqrt{A_i} \, \delta_{ij} \,. \tag{4.126}$$

Therefore, computing $\mathcal{M}^{\text{sym}}$ directly from the quadratic action leads to identical results, although numerical diagonalization algorithms are typically more suited to symmetric matrices.

4.1 *Constraints in the quadratic Lagrangian*

As we have discussed, the case of scalar metric perturbations leads to linear algebraic constraints, which appear in the linearized equations of motion but would be absent from the quadratic Lagrangian. Since linear algebraic constraints that can be solved projecting the scalars $\{\phi_i\}_i$ onto independent scalars $\{\chi_a\}_a$ according to an expression of the form

$$\phi_i = Q_i^a \chi_a \,, \tag{4.127}$$

one obtains in general different mass matrices depending on the order in which kinetic normalization, the above projection and the Euler-Lagrange equations are derived. Specifically, in the preceding sections we did not normalize the fields canonically, and thus we divided by the A_i factors before the projection, resulting in

$$\mathcal{M} = (Q^T Q)^{-1} (Q^T A^{-1} M Q) \,, \tag{4.128}$$

where $A \equiv \text{diag}(\{A_i\}_i)$.

Quantum stability: bubbles and flux tunneling

In this chapter we carry on the analysis of instabilities of the $AdS \times S$ flux compactifications that we have introduced in Chapter 3, presenting the results of [25]. Specifically, we address in detail their non-perturbative instabilities, which manifest themselves as (charged) vacuum bubbles at the semi-classical level, and we compute the corresponding decay rates. We find that this tunneling process reduces the flux number n, thus driving the vacua toward stronger couplings and higher curvatures, albeit at a rate that is exponentially suppressed in n. We also recast these effects in terms of branes[1], drawing upon the analogy with the supersymmetric case where BPS brane stacks generate supersymmetric near-horizon AdS throats. While NS5-branes in the heterotic model appear more difficult to deal with in this respect, in the orientifold models D1-brane stacks provide a natural canditate for a microscopic description of these flux vacua and of their instabilities. Indeed, non-supersymmetric analogues of $AdS_5 \times S^5$ vacua in type 0 strings, where tachyon condensation breaks conformal invariance of the dual gauge theory, were described in terms of D3-branes in [74]. In the non-tachyonic type 0′B orientifold model this rôle is played by the dilaton potential, which generates a running of the gauge coupling [71–73]. As a result, the near-horizon geometry is modified, and one recovers $AdS_5 \times S^5$ only in the limit[2] of infinitely many D3-branes, when the supersymmetry-breaking dilaton potential ought to become negligible. In contrast, D1-branes and NS5-branes should underlie the $AdS_3 \times S_7$ and $AdS_7 \times S_3$ solutions found in [26][3]. This might appear somewhat surprising, since Dp-brane stacks in type II superstrings do not exhibit near-horizon geometries of this type for $p \neq 3$, but dress them instead with singular warp factors.

---

[1]For a recent investigation along these lines in the context of the (massive) type IIA superstring, see [86].

[2]It is worth noting that this large-N limit is not uniform, since factors of $\frac{1}{N}$ are accompanied by factors that diverge in the near-horizon limit. In principle, a resummation of $\frac{1}{N}$ corrections could cure this problem.

[3]One could expect that solutions with different internal spaces, discussed in Chapter 3, arise from near-horizon throats of brane stacks placed on conical singularities [94].

Correspondingly, the dual gauge theory is non-conformal [95]. While the emergence of a conformal dual involving D1-branes and NS5-branes in non-supersymmetric cases would be an enticing scenario, it is first necessary to establish whether brane descriptions of the AdS × S solutions hold ground in these models. In this chapter we provide some evidence to this effect, and in Chapter 6 we address this issue in more detail. In particular, matching the gravitational decay rates that we shall compute in Section 2.2 to the results of the respective brane instanton computations, in Section 2.4 we find consistency conditions that single out fundamental branes as the localized sources that mediate flux tunneling in the settings at stake.

We begin in Section 1 with brief overview of flux tunneling. Then, in Section 2 we study it in the context of the AdS × S solutions that we have described in Chapter 3, and we present the computation of the resulting semi-classical decay rate within their low-energy description. In Section 2.3 we introduce the microscopic picture, studying probe D1-branes and NS5-branes in the AdS throat, which we develop in Section 2.4 deriving consistency conditions from decay rates. We conclude in Section 2.5 presenting explicit expressions for the decay rates in the orientifold models and in the heterotic model.

1   FLUX TUNNELING

Introducing charged localized sources of codimension one ("membranes") in gravitational systems with Abelian gauge (form) fields, a novel decay mechanism arises for meta-stable flux vacua [96, 97], whereby charged membranes nucleate in space-time, sourcing vacuum bubbles that expand carrying away flux. In the semi-classical limit, the resulting process can be analyzed via instanton computations [98–100], albeit the resulting (Euclidean) equations of motion are modified by the contribution due to membranes[4] [101], which arises from actions of the form

$$S_{\text{membrane}} = -\int_{\mathcal{W}} d^{p+1}x \sqrt{-j^*g}\, \tau_p + \mu_p \int_{\mathcal{W}} B_{p+1} \qquad (5.1)$$

---

[4]We shall not discuss the Gibbons-Hawking-York boundary term, which is to be included at any rate to consistently formulate the variational problem.

for $(p+2)$-dimensional space-times supported by flux configurations of a $(p+1)$-form field B_{p+1}, where j describes the embedding of the world-volume $\mathcal{W}$ in space-time and, in general, the tension τ_p can depend on the bulk scalar fields, if any. Typically one expects that maximally symmetric instanton configurations dominate the decay rate associated to processes of this type, and in practical terms one is thus faced with a shooting problem where, in addition to the initial conditions of the (Euclidean) fields, one is to determine the nucleation radius of the bubble[5].

1.1 *Small steps and giant leaps: the thin-wall approximation*

Since flux numbers are typically quantized, even simple toy models result in rather rich landscapes of geometries supported by fluxes [103], and it has been argued [83, 102, 104] that flux tunneling in multi-flux landscapes is dominated by "giant leaps", where a sizable fraction of the initial flux is discharged, while in single-flux landscape "small steps" dominate, and thus the thin-wall approximation is expected to capture the correct leading-order physics. Therefore, we shall focus on the latter case, since the AdS $\times$ S solutions discussed in Chapter 3 are supported by a single flux parameter n, and we shall consider thin-wall bubbles with charge $\delta n \ll n$. Within this approximation, one can neglect the back-reaction of the membrane and the resulting space-time geometry is obtained gluing the initial and final states along the bubble wall, which expands at the speed of light[6].

1.2 *Bubbles of nothing*

In addition to flux tunneling, bubbles of nothing [105] provide oft-controlled decay channels, whose existence in the absence of supersymmetry appears quite generic [106, 107][7]. Although one expects that extreme "giant leaps", which discharge almost all of the initial flux, lie outside of the semi-classical regime, it is conceivable that the limit in which all of the initial flux is discharged corresponds to a bubble of nothing. Indeed, some evidence to this effect was presented in [108], and, at least in the case of AdS

---

[5]For a detailed exposition of the resulting (distributional) differential equations, see [102].

[6]In Chapter 7 we shall discuss the geometrical perspective in more detail.

[7]We shall further elaborate on these matters in Chapter 8, framing them in a cosmological context.

landscapes, holographic arguments also provide some hints in this direction [109], as we shall discuss in more detail in Chapter 7.

2   BUBBLES AND BRANES IN AdS COMPACTIFICATIONS

Let us now move on to study flux tunneling in the AdS $\times$ S solutions that we have described in Chapter 3. These solutions feature perturbative instabilities carrying internal angular momenta [27, 90], but we shall not concern ourselves with their effects, since we shall impose unbroken spherical symmetry at the outset. Alternatively, as we have mentioned, one could replace the internal sphere with an Einstein manifold, if any, whose Laplacian spectrum does not contain unstable modes, or with an orbifold that projects them out. This can be simply achieved with an antipodal $\mathbb{Z}_2$ projection in the heterotic model, while an analogous operation in the orientifold models appears more elusive [27], albeit a microscopic interpretation in terms of fundamental branes appears more subtle in this case. However, as we shall see in the following, even in the absence of classical instabilities the AdS $\times$ S solutions would be at best meta-stable, since they undergo flux tunneling.

2.1 *Vacuum energy within dimensional reduction*

In order to appreciate this, it is instructive to perform a dimensional reduction over the sphere following [101], retaining the dependence on a dynamical radion field ψ in a similar vein to our analysis of dS instabilities in Chapter 3. The ansatz

$$ds^2 = e^{-\frac{2q}{p}\psi(x)}\, \widetilde{ds}^2_{p+2}(x) + e^{2\psi(x)}\, R_0^2\, d\Omega_q^2\,, \tag{5.2}$$

where R_0 is an arbitrary reference radius, is warped in order to select the $(p+2)$-dimensional Einstein frame, described by $\widetilde{ds}^2_{p+2}$. Indeed, placing the dilaton and the form field on shell results in the dimensionally reduced action

$$S_{p+2} = \frac{1}{2\kappa_{p+2}^2} \int d^{p+2}x\, \sqrt{-\widetilde{g}}\, \left(\widetilde{R} - 2\widetilde{\Lambda} \right)\,, \tag{5.3}$$

where the $(p+2)$-dimensional Newton's constant is

$$\frac{1}{\kappa_{p+2}^2} = \frac{\Omega_q R_0^q}{\kappa_D^2} \, , \tag{5.4}$$

while the "physical" cosmological constant $\Lambda = -\frac{p(p+1)}{2L^2}$, associated to the frame used in the preceding section, is related to $\widetilde{\Lambda}$ according to

$$\widetilde{\Lambda} = \Lambda \, e^{-\frac{2q}{p}\psi} \, , \tag{5.5}$$

which is a constant when the radion is on-shell, and

$$e^{\psi} = \frac{R}{R_0} \propto n^{\frac{\gamma}{(q-1)\gamma - \alpha}} \, . \tag{5.6}$$

 Let us remark that the dimensionally reduced action of eq. (5.3) does not necessarily capture a sensible low-energy regime, since in the present settings there is no scale separation between space-time and the internal sphere. Moreover, as we have discussed in Chapter 4, in general one cannot neglect the instabilities arising from fluctuations with non-vanishing angular momentum. On the other hand, the resulting vacuum energy (density)

$$\widetilde{E}_0 = \frac{2\widetilde{\Lambda}}{2\kappa_{p+2}^2} = -\frac{p(p+1)\,\Omega_q R_0^q}{2\kappa_D^2 \, L^2} \left(\frac{R}{R_0} \right)^{-\frac{2q}{p}}$$
$$\propto -\, n^{-\frac{2(D-2)}{p(q-1-\frac{\alpha}{\gamma})}} \tag{5.7}$$

 is actually sufficient to dictate whether n increases or decreases upon flux tunneling. In particular, the two signs present in eq. (5.7) and the requirement that flux tunneling decreases the vacuum energy imply that this process drives the (false) vacua to lower values of n, eventually reaching outside of the perturbative regime where the semi-classical analysis is expected to be reliable.

2.2 *Decay rates: gravitational computation*

Let us now compute the decay rate associated to flux tunneling in the semi-classical regime. To this end, standard instanton methods [98–100] provide most needed tools,

but in the present case one is confined to the thin-wall approximation, which entails a flux variation[8] $\delta n \ll n$, and the tension τ of the resulting bubble, which cannot be computed within the formalism, rests on the tension of the corresponding membrane and on its back-reaction[9]. However, the probe limit, in which the membrane does not affect the radion potential due to changing n, identifies the tension of the bubble with that of the membrane, and it can be systematically improved upon [83] adding corrections to this equality.

In order to proceed, we work within the dimensionally-reduced theory in AdS_{p+2}, using coordinates such that the relevant instanton is described by the Euclidean metric

$$ds_E^2 = d\xi^2 + \rho^2(\xi)\, d\Omega_{p+1}^2 \,, \tag{5.8}$$

so that the Euclidean on-shell (bulk) action takes the form

$$S_E = 2\,\Omega_{p+1} \int d\xi\, \rho(\xi)^{p+1} \left(\widetilde{E}_0 - \frac{p(p+1)}{2\kappa_{p+2}^2\, \rho(\xi)^2} \right) \,, \tag{5.9}$$

with the vacuum energy $\widetilde{E}_0$, along with the associated curvature radius $\widetilde{L}$, defined piece-wise by its values inside and outside of the bubble. Then, the energy constraint

$$(\rho')^2 = 1 - \frac{2\kappa_{p+2}^2}{p(p+1)}\, \widetilde{E}_0\, \rho^2 = 1 + \frac{\rho^2}{\widetilde{L}^2} \,, \tag{5.10}$$

which stems from the Euclidean equations of motion, allows one to change variables in eq. (5.9), obtaining

$$S_E = -\frac{2p(p+1)\,\Omega_{p+1}}{2\kappa_{p+2}^2} \int d\rho\, \rho^{p-1} \sqrt{1 + \frac{\rho^2}{\widetilde{L}^2}} \,. \tag{5.11}$$

This expression defines the (volume term of the) exponent $B \equiv S_{\text{inst}} - S_{\text{vac}}$ in the semi-classical formula for the decay rate (per unit volume),

$$\frac{\Gamma}{\text{Vol}} \sim (\det) \times e^{-B} \,, \qquad B = B_{\text{area}} + B_{\text{vol}} \,, \tag{5.12}$$

---

[8]On the other hand, as we have mentioned, the extreme case $\delta n = n$ would correspond to the production of a bubble of nothing [105].

[9]It is common to identify the tension of the bubble with the ADM tension of a brane soliton solution [101]. In our case this presents some challenges, as we shall discuss in Chapter 6.

in the standard fashion [98, 99]. The thin-wall bubble is a $(p+1)$-sphere of radius $\widetilde{\rho}$, over which the action has to be extremized, and therefore the area term of the exponent B reads

$$B_{\text{area}} \sim \widetilde{\tau} \, \Omega_{p+1} \, \widetilde{\rho}^{\, p+1} \, , \tag{5.13}$$

where the tension $\widetilde{\tau} = \tau \, e^{-(p+1)\frac{q}{p}\psi}$ is measured in the $(p+2)$-dimensional Einstein frame. On the other hand, in the thin-wall approximation the volume term becomes

$$
\begin{aligned}
B_{\text{vol}} &= \frac{2p(p+1)\,\Omega_{p+1}}{2\kappa_{p+2}^2} \int_0^{\widetilde{\rho}} d\rho \, \rho^{p-1} \left[\sqrt{1 + \frac{\rho^2}{\widetilde{L}_{\text{vac}}^2}} - \sqrt{1 + \frac{\rho^2}{\widetilde{L}_{\text{inst}}^2}} \right] \\
&\sim -\epsilon \, \widetilde{\text{Vol}}(\widetilde{\rho}) \, ,
\end{aligned}
\tag{5.14}
$$

where the energy spacing

$$\epsilon \sim \frac{d\widetilde{E}_0}{dn} \, \delta n \propto n^{-\frac{2(D-2)}{p(q-1-\frac{\alpha}{\gamma})}-1} \, \delta n \tag{5.15}$$

and the volume $\widetilde{\text{Vol}}(\widetilde{\rho})$ enclosed by the bubble is computed in the $(p+2)$-dimensional Einstein frame,

$$
\begin{aligned}
\widetilde{\text{Vol}}(\widetilde{\rho}) &= \widetilde{L}^{p+2} \, \Omega_{p+1} \, \mathcal{V}\left(\frac{\widetilde{\rho}}{\widetilde{L}}\right) \, , \\
\mathcal{V}(x) &\equiv \frac{x^{p+2}}{p+2} \, {}_2F_1\left(\frac{1}{2}, \frac{p+2}{2}; \frac{p+4}{2}; -x^2\right) \, , \\
x &\equiv \frac{\widetilde{\rho}}{\widetilde{L}} \, .
\end{aligned}
\tag{5.16}
$$

All in all, the thin-wall exponent[10]

$$B \sim \tau \, \Omega_{p+1} \, L^{p+1} \left(x^{p+1} - (p+1)\beta \, \mathcal{V}(x) \right) \, , \qquad \beta \equiv \frac{\epsilon \, \widetilde{L}}{(p+1)\widetilde{\tau}} \tag{5.17}$$

attains a local maximum at $x = \frac{1}{\sqrt{\beta^2-1}}$ for $\beta > 1$. On the other hand, for $\beta \leq 1$ the exponent is unbounded, since $B \to \infty$ as $x \to \infty$, and thus the decay rate is completely suppressed. Hence, it is crucial to study the large-flux scaling of β, which plays a role akin to an extremality parameter for the bubble. In particular, if β scales with a negative power of n nucleation is suppressed, whereas if it scales with a positive power of n the extremized exponent B approaches zero, thus invalidating the semi-classical computation. Therefore, the only scenario in which nucleation is

---

[10]Notice that eq. (5.17) takes the form of an effective action for a $(p+1)$-brane in AdS electrically coupled to H_{p+2}. This observation is the basis for the microscopic picture that we shall present shortly.

both allowed and semi-classical at large n is when $\beta > 1$ and is flux-independent. Physically, the bubble is super-extremal and has an n-independent charge-to-tension ratio. Since

$$\beta = v_0 \frac{\Omega_q \, \delta n}{2\kappa_D^2 \tau} g_s^{-\frac{\alpha}{2}} \, , \tag{5.18}$$

where the flux-independent constant

$$v_0 \equiv \sqrt{\frac{2(D-2)\gamma}{(p+1)((q-1)\gamma - \alpha)}} \, , \tag{5.19}$$

this implies the scaling[11]

$$\tau = T \, g_s^{-\frac{\alpha}{2}} \, , \tag{5.20}$$

where T is flux-independent and α denotes the coupling between the dilaton and the form field in the notation introduced in Chapter 3. In Section 2.4 we shall verify that this is precisely the scaling expected from Dp-branes and NS5-branes.

2.3 *Bubbles as branes*

Let us now proceed to describe a microscopic picture, studying probe branes in the AdS $\times$ S geometry and matching the semi-classical decay rate of eq. 5.17 to a (Euclidean) world-volume action. While a more complete description to this effect would involve non-Abelian world-volume actions coupled to the complicated dynamics driven by the dilaton potential, one can start from the simpler setting of brane instantons and probe branes moving in the AdS $\times$ S geometry. This allows one to retain computational control in the large-n limit, while partially capturing the unstable dynamics at play. When framed in this fashion, instabilities suggest that the non-supersymmetric models at stake are typically driven to time-dependent configurations[12], in the spirit of the considerations of [27].

We begin our analysis considering the dynamics of a p-brane moving in the AdS$_{p+2} \times$ S^q geometry of eq. (3.34). In order to make contact with D-branes in the

---

[11]Notice that in the gravitational picture the charge of the membrane does not appear. Indeed, its contribution arises from the volume term of eq. (5.14) in the thin-wall approximation.

[12]Indeed, as we have discussed in Chapter 2, cosmological solutions of non-supersymmetric models display interesting features [27, 43, 58–60].

orientifold models and NS5-branes in the heterotic model, let us consider a generic string-frame world-volume action of the form

$$S_p = -T_p \int d^{p+1}\zeta \sqrt{-j^* g_s} \, e^{-\sigma \phi} + \mu_p \int B_{p+1} \,, \tag{5.21}$$

specified by an embedding j of the brane in space-time, which translates into the D-dimensional and $(p+2)$-dimensional Einstein-frame expressions

$$\begin{aligned}
S_p &= -T_p \int d^{p+1}\zeta \sqrt{-j^* g} \, e^{\left(\frac{2(p+1)}{D-2} - \sigma\right)\phi} + \mu_p \int B_{p+1} \\
&= -T_p \int d^{p+1}\zeta \sqrt{-j^* \widetilde{g}} \, e^{\left(\frac{2(p+1)}{D-2} - \sigma\right)\phi - (p+1)\frac{q}{p}\psi} + \mu_p \int B_{p+1} \,.
\end{aligned} \tag{5.22}$$

Since the dilaton is constant in the AdS $\times$ S backgrounds that we consider, from eq. (5.22) one can read off the effective tension

$$\tau_p = T_p \, g_s^{\frac{2(p+1)}{D-2} - \sigma} \,. \tag{5.23}$$

While in this action T_p and μ_p are independent of the background, for the sake of generality we shall not assume that in non-supersymmetric models $T_p = \mu_p$, albeit this equality is supported by the results of [76].

2.4 *Microscopic branes from semi-classical consistency*

In this section we reproduce the decay rate that we have obtained in Section 2.2 with a brane instanton computation[13]. Since flux tunneling preserves the symmetry of the internal manifold, the Euclidean branes are uniformly distributed over it, and are spherical in the Wick-rotated AdS geometry. The Euclidean p-brane action of eq. (5.22), written in the D-dimensional Einstein frame, then reads

$$\begin{aligned}
S_p^E &= \tau_p \, \text{Area} - \mu_p \, c \, \text{Vol} \\
&= \tau_p \, \Omega_{p+1} \, L^{p+1} \left(x^{p+1} - (p+1) \, \beta_p \, \mathcal{V}(x) \right) \,,
\end{aligned} \tag{5.24}$$

---

[13]For more details, we refer the reader to [96, 97, 110, 111].

where v_0 is defined in eq. (5.19), and

$$\beta_p \equiv v_0 \, \frac{\mu_p}{T_p} \, g_s^{\sigma - \frac{2(p+1)}{D-2} - \frac{\alpha}{2}} \, .$$

(5.25)

This result matches in form the thin-wall expression in eq. (5.17), up to the identifica-tions of the tensions τ, τ_p and the parameters β, β_p. As we have argued in Section 2.2, the former is expected to be justified in the thin-wall approximation. Furthermore, according to the considerations that have led us to eq. (5.20), it is again reasonable to assume that β_p does not scale with the flux, which fixes the exponent σ to

$$\sigma = \frac{2(p+1)}{D-2} + \frac{\alpha}{2} \, .$$

(5.26)

This is the value that we shall use in the following. Notice that for Dp-branes in ten dimensions, where $\alpha = \frac{3-p}{2}$, this choice gives the correct result $\sigma = 1$, in particular for D1-branes in the orientifold models. Similarly, for NS5-branes in ten dimensions, eq. (5.26) also gives the correct result $\sigma = 2$. This pattern persists even for the more "exotic" branes of [28–32], and it would be interesting to explore this direction further. Notice that in terms of the string-frame value α_S, eq. (5.26) takes the simple form

$$\sigma = 1 + \frac{\alpha_S}{2} \, .$$

(5.27)

Moreover, from eqs. (5.23) and (5.26) one finds that

$$\tau_p = T_p \, g_s^{-\frac{\alpha}{2}}$$

(5.28)

scales with the flux with the same power as τ, as can be seen from eq. (5.20). Since the flux dependence of the decay rates computed extremizing eqs. (5.17) and (5.24) is determined by the respective tensions τ and τ_p, they also scale with the same power of n. Together with eq. (5.27), this provides evidence for the fact that, in the present setting, vacuum bubbles can be identified with fundamental branes, namely Dp-branes in the orientifold models and NS5-branes in the heterotic model.

Requiring furthermore that the decay rates computed extremizing eqs. (5.17) and (5.24) coincide, one is led to $\beta = \beta_p$, which implies

$$\mu_p = \frac{\Omega_q \, \delta n}{2\kappa_D^2} = \delta \left(\frac{1}{2\kappa_D^2} \int_{S^q} f \star H_{p+2} \right) , \tag{5.29}$$

where δ denotes the variation across the bubble wall, as expected for electrically coupled objects.

2.5 *Decay rates: extremization*

Extremizing the Euclidean action of eq. (5.24) over the nucleation radius, one obtains the final result for the semi-classical tunneling exponent

$$S_p^E = T_p \, L^{p+1} \, g_s^{-\frac{\alpha}{2}} \, \Omega_{p+1} \, \mathcal{B}_p \left(v_0 \frac{\mu_p}{T_p} \right)$$
$$\propto n^{\frac{(p+1)\gamma + \alpha}{(q-1)\gamma - \alpha}} , \tag{5.30}$$

where we have introduced

$$\mathcal{B}_p(\beta) \equiv \frac{1}{(\beta^2 - 1)^{\frac{p+1}{2}}} - \frac{p+1}{2} \beta \int_0^{\frac{1}{\beta^2 - 1}} \frac{u^{\frac{p}{2}}}{\sqrt{1+u}} \, du . \tag{5.31}$$

This expression includes a complicated flux-independent pre-factor, but it always scales with a positive power of n, consistently with the semi-classical limit. For the sake of completeness, let us provide the explicit result for non-supersymmetric string models, where the microscopic picture goes beyond the world-volume actions of eq. (5.21). Notice that we do not assume that $\mu_p = T_p$ in the non-supersymmetric setting, for the sake of generality. However, as we have already remarked in eq. (5.17), the tunneling process is allowed also in this case. This occurs because $v_0 > 1$, and thus also $\beta > 1$, in the supersymmetry-breaking backgrounds that we consider, since using eq. (5.19) one finds

$$(v_0)_{\text{orientifold}} = \sqrt{\frac{3}{2}} \tag{5.32}$$

for the orientifold models, while

$$(v_0)_{\text{heterotic}} = \sqrt{\frac{5}{3}} \qquad (5.33)$$

for the heterotic model. For D1-branes in the orientifold models, eq. (5.30) yields

$$
\begin{aligned}
S_1^E &= \frac{T_1 L^2}{\sqrt{g_s}} \, \Omega_2 \, \mathcal{B}_1 \left(\sqrt{\frac{3}{2}} \frac{\mu_1}{T_1} \right) \\
&= \frac{\pi}{9\sqrt{2}} \, \mathcal{B}_1 \left(\sqrt{\frac{3}{2}} \frac{\mu_1}{T_1} \right) T_1 \, \sqrt{T} \, \sqrt{n} \, ,
\end{aligned}
\qquad (5.34)
$$

and $S_1^E \approx 0.1 \, T_1 \, \sqrt{T} \, \sqrt{n}$ if $\mu_1 = T_1$. For the heterotic model, using eq. (5.30) the Euclidean action of NS5-branes evaluates to

$$
\begin{aligned}
S_5^E &= \frac{T_5 L^6}{\sqrt{g_s}} \, \Omega_6 \, \mathcal{B}_5 \left(\sqrt{\frac{5}{3}} \frac{\mu_5}{T_5} \right) \\
&= \frac{9216 \, \pi^3}{125} \, \mathcal{B}_5 \left(\sqrt{\frac{5}{3}} \frac{\mu_5}{T_5} \right) T_5 \, T \, n^4 \, ,
\end{aligned}
\qquad (5.35)
$$

and $S_5^E \approx 565.5 \, T_5 \, T \, n^4$ if $\mu_5 = T_5$. In the presence of large fluxes the tunneling instability is thus far milder in the heterotic model.

To conclude, the results in this chapter provide evidence to the effect that the non-supersymmetric AdS flux compactifications that we have described in Chapter 3 are non-perturbatively unstable, and the flux tunneling process that they undergo can be described in terms of (stacks of) fundamental branes, namely D1-branes for the $\text{AdS}_3 \times \mathbb{S}^7$ solutions of the orientifold models, and NS5-branes for the $\text{AdS}_7 \times \mathbb{S}^3$ solutions of the heterotic model. In the following chapter we shall expand upon this picture, studying the Lorentzian evolution of the branes after a tunneling event occurs and relating the resulting dynamics to interactions between branes and to the weak gravity conjecture [18]. In addition, we shall recover the relevant $\text{AdS} \times \mathbb{S}$ solutions as near-horizon geometries of the full the gravitational back-reaction of the branes, thus further supporting the idea that these solutions are built up from stacks of parallel fundamental branes.

Brane dynamics: probes and back-reaction

In this chapter we elaborate in detail on the microscopic picture of non-perturbative instabilities of the AdS $\times$ S solutions that we have introduced in the preceding chapter. The results that we have described hitherto suggest that the *adsts* geometries at stake can be built up from stacks of parallel fundamental branes, an enticing picture that could, at least in principle, shed light on the high-energy regime of the settings at hand. In particular, our proposal can potentially open a computational window beyond the semi-classical regime, perhaps providing also a simpler realization of AdS$_3$/CFT$_2$ duality[1]. Moreover, in principle one could investigate these non-perturbative instabilities recasting them as holographic RG flows in a putative dual gauge theory [109]. In order to further ground this proposal, in Section 1 we study the Lorentzian evolution of the expanding branes after a nucleation event takes place, identifying the relevant dynamics and comparing it to the supersymmetric case, and the resulting interaction potentials imply a version of the weak gravity conjecture for extended objects [16]. Then, in Section 2 we investigate the gravitational back-reaction of stacks of parallel branes within the low-energy effective theory described in Chapter 3, deriving a reduced dynamical system that captures the relevant dynamics and recovering an attractive near-horizon AdS $\times$ S throat. In order to provide a more intuitive understanding of this result, we compare the asymptotic behavior of the fields to the corresponding ones for D3-branes in the type IIB superstring and for the four-dimensional Reissner-Nordström black hole. The latter represents a particularly instructive model, where one can identify the physical origin of singular perturbations. However, away from the stack the resulting space-time exhibits a space-like singularity at a finite transverse geodesic distance [25], as in[2] [24], which hints at the idea that, in the presence of dilaton tadpoles, any breaking of ten-dimensional Poincaré invariance is accompanied by a finite-distance "pinch-off" singularity determined by the residual

---

[1]The alternative case of AdS$_7$ could be studied, in principle, via M5-brane stacks.
[2]Indeed, our results suggest that the solutions of [24], which are not fluxed, correspond to 8-branes.

symmetry. Physically, this corresponds to the fact that branes are not isolated objects in these settings, since in the case of the orientifold models non-supersymmetric projections bring along additional (anti-)D-branes that interact with them. In the heterotic model, this rôle is played at leading order by the one-loop vacuum energy. Finally, in Section 2.4 and Section 3 we extend our considerations to the case of non-extremal branes, focusing on the uncharged of D8-branes in the orientifold models in order to compare probe-brane computations with the corresponding string amplitudes.

1   THE AFTERMATH OF TUNNELING

After a nucleation event takes place, the dynamics is encoded in the Lorentzian evolution of the bubble. Its counterpart in the microscopic brane picture is the separation of pairs of branes and anti-branes, which should then lead to brane-flux annihilation[3], with negatively charged branes absorbed by the stack and positively charged ones expelled out of the AdS $\times$ S near-horizon throat. In order to explore this perspective, we now study probe (anti-)branes moving in the AdS $\times$ S geometry. To this end, it is convenient to work in Poincaré coordinates, where the D-dimensional Einstein-frame metric reads

$$ds^2 = \frac{L^2}{z^2}\left(dz^2 + dx_{1,p}^2\right) + R^2\, d\Omega_q^2\,, \qquad dx_{1,p}^2 \equiv \eta_{\mu\nu}\, dx^\mu dx^\nu\,, \tag{6.1}$$

embedding the world-volume of the brane according to the parametrization

$$j: \quad x^\mu = \zeta^\mu\,, \qquad z = Z(\zeta)\,, \qquad \theta^i = \Theta^i(\zeta)\,. \tag{6.2}$$

Furthermore, when the brane is placed at a specific point in the internal sphere[4], $\Theta^i(\zeta) = \theta_0^i$, the Wess-Zumino term gives the volume enclosed by the brane in AdS. As a result, the action that we have introduced in the preceding chapter evaluates to

$$S_p = -\tau_p \int d^{p+1}\zeta \left(\frac{L}{Z}\right)^{p+1} \left[\sqrt{1 + \eta^{\mu\nu}\,\partial_\mu Z\,\partial_\nu Z} - \frac{c\,L}{p+1}\,\frac{\mu_p}{\tau_p}\right] \tag{6.3}$$

---

[3]For a discussion of this type of phenomenon in Calabi-Yau compactifications, see [11].

[4]One can verify that this ansatz is consistent with the equations of motion for linearized perturbations.

in the notation of Chapter 3, so that rigid, static branes are subject to the potential

$$
\begin{aligned}
V_{\text{probe}}(Z) &= \tau_p \left(\frac{L}{Z}\right)^{p+1} \left[1 - \frac{c\, L\, g_s^{\frac{\alpha}{2}}}{p+1} \frac{\mu_p}{T_p}\right] \\
&= \tau_p \left(\frac{L}{Z}\right)^{p+1} \left[1 - v_0 \frac{\mu_p}{T_p}\right].
\end{aligned}
\tag{6.4}
$$

The potential in eq. (6.4) indicates how rigid probe branes are affected by the AdS $\times$ S geometry, depending on the value of v_0. In particular, if $v_0 \frac{|\mu_p|}{T_p} > 1$ positively charged branes are driven towards small Z and thus exit the throat, while negatively charged ones are driven in the opposite direction.

Small deformations δZ of the brane around the rigid configuration at constant Z satisfy the linearized equations of motion

$$
-\partial_\mu \partial^\mu \delta Z \sim \frac{p+1}{Z}\left(1 - v_0 \frac{\mu_p}{T_p}\right) - \frac{(p+1)(p+2)}{Z^2}\left(1 - v_0 \frac{\mu_p}{T_p}\right)\delta Z,
\tag{6.5}
$$

where the constant first term on the right-hand side originates from the potential of eq. (6.4) and affects rigid displacements, which behave as

$$
\frac{\delta Z}{Z} \sim \frac{p+1}{2}\left(1 - v_0 \frac{\mu_p}{T_p}\right)\left(\frac{t}{Z}\right)^2
\tag{6.6}
$$

for small times $\frac{t}{Z} \ll 1$. On the other hand, for non-zero modes $\delta Z \propto e^{i\mathbf{k}_0 \cdot \mathbf{x} - i\omega_0 t}$ one finds the approximate dispersion relation

$$
\omega_0^2 = \mathbf{k}_0^2 + \frac{(p+1)(p+2)}{Z^2}\left(1 - v_0 \frac{\mu_p}{T_p}\right),
\tag{6.7}
$$

which holds in the same limit, so that Z remains approximately constant. In terms of the proper, red-shifted frequency $\omega_z = \sqrt{g^{tt}}\,\omega_0$ and wave-vector $\mathbf{k}_z = \sqrt{g^{tt}}\,\mathbf{k}_0$ for deformations of Z in AdS, eq. (6.7) becomes

$$
\omega_z^2 = \mathbf{k}_z^2 + \frac{(p+1)(p+2)}{L^2}\left(1 - v_0 \frac{\mu_p}{T_p}\right).
\tag{6.8}
$$

The dispersion relation of eq. (6.8) displays a potential long-wavelength instability

toward deformations of positively charged branes, which can drive them to grow in time, depending on the values of v_0 and the charge-to-tension ratio $\frac{\mu_p}{T_p}$. Comparing with eqs. (6.4) and (6.6), one can see that this instability toward "corrugation" is present if and only if the branes are also repelled by the stack.

To conclude our analysis of probe-brane dynamics in the AdS $\times$ S throat, let us also consider small deformations $\delta\Theta$ in the internal sphere. They evolve according to the linearized equations of motion

$$- \partial_\mu \partial^\mu \delta\Theta = 0 \,, \tag{6.9}$$

 so that these modes are stable at the linearized level.

1.1 *Weak gravity from supersymmetry breaking*

In the ten-dimensional orientifold models, in which the corresponding branes are D1-branes, $v_0 = \sqrt{\frac{3}{2}}$, so that even extremal D1-branes with[5] $\mu_p = T_p$ are crucially repelled by the stack, and are driven to exit the throat toward $Z \to 0$. On the other hand $\overline{D1}$-branes, which have negative μ_p, are always driven towards $Z \to +\infty$, leading to annihilation with the stack. This dynamics is the counterpart of flux tunneling in the probe-brane framework, and eq. (5.19) suggests that while the supersymmetry-breaking dilaton potential allows for AdS vacua of this type, it is also the ingredient that allows BPS branes to be repelled. Physically, D1-branes are mutually BPS, but they interact with the $\overline{D9}$-branes that fill space-time. This resonates with the fact that, as we have argued in Section 2.2, the large-n limit ought to suppress instabilities, since in this regime the interaction with $\overline{D9}$-branes is expected to be negligible [71, 72]. Furthermore, the dispersion relation of eq. (6.8) highlights an additional instability toward long-wavelength deformations of the branes, of the order of the AdS curvature radius. Similarly, in the heterotic model $v_0 = \sqrt{\frac{5}{3}}$, so that negatively charged NS5-branes are also attracted by the stack, while positively charged ones are repelled and unstable towards sufficiently long-wavelength deformations,

---

[5]As we have anticipated, verifying the charge-tension equality in the non-supersymmetric case presents some challenges. We shall elaborate upon this issue in Section 2.3.

and the corresponding physical interpretation would involve interactions mediated by the quantum-corrected vacuum energy.

Moreover, the appearance of $v_0 > 1$ in front of the charge-to-tension ratio $\frac{\mu_p}{T_p}$ is suggestive of a dressed extremality parameter, which can be thought of, *e.g.,* as an effective enhancement of the charge-to-tension ratio due to both dimensional reduction and supersymmetry breaking. This behavior resonates with considerations stemming from the weak gravity conjecture [18], since the presence of branes which are (effectively) lighter than their charge would usually imply a decay channel for extremal or near-extremal objects. While non-perturbative instabilities of non-supersymmetric AdS due to brane nucleation have been thoroughly discussed in the literature [16, 110, 111], we stress that in the present case this phenomenon arises from fundamental branes interacting in the absence of supersymmetry. Therefore, one may envision reproducing this result from a string amplitude computation, at least for D1-branes in the orientifold models, but since the relevant annulus amplitude vanishes [76] the leading contribution would involve "pants" amplitudes and is considerably more complicated[6]. On the other hand, in the non-extremal case one has access to both a probe-brane setting, which involves the gravitational back-reaction of D8-branes, and to a string amplitude computation, and we shall pursue this direction in Section 2.4.

As a final comment, let us observe that in the heterotic model one can also compute the potential for probe fundamental strings, extended along one of the directions longitudinal to the world-volume of the NS5-branes[7]. However, since the Kalb-Ramond form B_2 pull-backs to zero on the string world-sheet, the result is determined solely by the Nambu-Goto action, leading to an attractive potential.

2 GRAVITATIONAL BACK-REACTION

In this section we study the background geometry sourced by a stack of branes in the class of low-energy effective theories that we have described in Chapter 3. The dilaton potential brings along considerable challenges in this respect, both conceptual and

---

[6]The systematics of computations of this type in the bosonic case were developed in [112].

[7]The corresponding objects in the orientifold models would be probe D5-branes, which however would wrap vanishing cycles in the internal spheres, leading to an uncontrolled computation.

technical. To begin with, there is no maximally symmetric vacuum that could act as a background, and thus in the presence of branes there is no asymptotic infinity of this type[8]. We find, instead, that the geometry away from the branes "pinches off" at a finite geodesic distance, and exhibits a curvature singularity where $\phi \to +\infty$. This resonates with the findings of [24], and indeed we do reconstruct the solutions therein in the case $p = 8$. These results suggest that, due to their interactions with the dilaton potential, branes cannot be described as isolated objects in these models, reflecting the probe-brane analysis of Section 1. Consequently, identifying a sensible background string coupling or sensible asymptotic charges, such as the brane tension, appears considerably more difficult with respect to the supersymmetric case.

Despite these challenges, one can gain some insight studying the asymptotic geometry near the branes, where an AdS $\times$ S throat develops, and near the outer singularity, where the geometry pinches off. In Section 2.2 we shall argue that the AdS $\times$ S solutions discussed in Chapter 3 can arise as near-horizon "cores" of the full geometry, investigating an attractor-like behavior of radial perturbations which is characteristic of extremal objects and arises after a partial fine-tuning, reminiscent of the BPS conditions on asymptotic charges in supersymmetric cases. This feature is reflected by the presence of free parameters in the asymptotic geometry away from the branes, which we construct in Section 2.3.

2.1 *Reduced dynamical system: extremal case*

Let us begin imposing $SO(1, p) \times SO(q)$ symmetry, so that the metric is characterized by two dynamical functions $v(r) , b(r)$ of a transverse radial coordinate r. Specifically, without loss of generality we shall consider the ansatz

$$ds^2 = e^{\frac{2}{p+1}v - \frac{2q}{p}b} dx_{1,p}^2 + e^{2v - \frac{2q}{p}b} dr^2 + e^{2b} R_0^2 d\Omega_q^2 ,$$

$$\phi = \phi(r) , \tag{6.10}$$

$$H_{p+2} = \frac{n}{f(\phi)(R_0 e^b)^q} \, \text{Vol}_{p+2} , \qquad \text{Vol}_{p+2} = e^{2v - \frac{q}{p}(p+2)b} d^{p+1}x \wedge dr ,$$

---

[8]Even if one were to envision a pathological Minkowski solution with "$\phi = -\infty$" as a degenerate background (for instance, by introducing a cutoff), no asymptotically flat solution with $\phi \to -\infty$ can be found.

where R_0 is an arbitrary reference radius and the form field automatically solves its field equations. This gauge choice simplifies the equations of motion, which can be recast in terms of a constrained Toda-like system [73, 74]. Indeed, substituting the ansatz of eq. (6.10) in the field equations and taking suitable linear combinations, the resulting system can be derived by the "reduced" action

$$S_{\text{red}} = \int dr \left[\frac{4}{D-2} \left(\phi'\right)^2 - \frac{p}{p+1} \left(v'\right)^2 + \frac{q(D-2)}{p} \left(b'\right)^2 - U \right], \qquad (6.11)$$

where the potential is given by

$$U = - T e^{\gamma\phi + 2v - \frac{2q}{p}b} - \frac{n^2}{2R_0^{2q}} e^{-\alpha\phi + 2v - \frac{2q(p+1)}{p}b} + \frac{q(q-1)}{R_0^2} e^{2v - \frac{2(D-2)}{p}b}, \qquad (6.12)$$

and the equations of motion are supplemented by the zero-energy constraint

$$\frac{4}{D-2} \left(\phi'\right)^2 - \frac{p}{p+1} \left(v'\right)^2 + \frac{q(D-2)}{p} \left(b'\right)^2 + U = 0. \qquad (6.13)$$

For the reader's convenience, let us present collect general results concerning warped products. Let us consider a multiple warped product described by a metric of the type

$$ds^2 = \widetilde{ds}^2(x) + \sum_I e^{2a_I(x)} \widehat{ds}^2_{(I)}, \qquad (6.14)$$

where the dimensions of the I-th internal space is denoted by q_I. The Ricci tensor is then block-diagonal, and its space-time components read

$$R_{\mu\nu} = \widetilde{R}_{\mu\nu} - \sum_I q_I \left(\nabla_\mu \nabla_\mu a_I + (\nabla_\mu a_I)(\nabla_\mu a_I) \right), \qquad (6.15)$$

while its internal components in the I-th internal space read

$$R^{(I)}_{ij} = \widehat{R}^{(I)}_{ij} - e^{2a_I(x)} \left(\Delta a_I + \sum_J q_J \left(\partial^\mu a_J\right) \left(\partial_\mu a_I\right) \right) \widehat{g}^{(I)}_{ij}, \qquad (6.16)$$

where Δ denotes the Laplacian operator associated to space-time and we have kept the notation signature-independent for the sake of generality. Using eqs. (6.15) and (6.16)

we have derived the field equations that led to the Toda-like system of eqs. (6.11) and (6.13), and we have also used them to derive some results in Chapter 8 concerning warped flux compactifications.

2.2 AdS $\times$ S throat as a near-horizon geometry

Let us now apply the results in the preceding section to recast the AdS $\times$ S solutions discussed in Chapter 3 as a near-horizon limit of the geometry described by eqs. (6.11) and (6.13). To begin with, one can verify that the AdS $\times$ S solution now takes the form[9]

$$\phi = \phi_0 \, ,$$
$$e^v = \frac{L}{p+1} \left(\frac{R}{R_0} \right)^{-\frac{q}{p}} \frac{1}{-r} \, , \tag{6.17}$$
$$e^b = \frac{R}{R_0} \, ,$$

where we have chosen negative values $r < 0$. This choice places the core at $r \to -\infty$, with the horizon infinitely far away, while the outer singularity lies either at some finite $r = r_0$ or emerges as[10] $r \to +\infty$. The metric of eq. (6.10) can then be recast as AdS $\times$ S in Poincaré coordinates rescaling x by a constant and substituting

$$r \mapsto -\frac{z^{p+1}}{p+1} \, . \tag{6.18}$$

In supersymmetric cases, infinitely long AdS throats behave as attractors going toward the horizon from infinity, under the condition on asymptotic parameters that specifies extremality. Therefore we proceed by analogy, studying linearized radial perturbations $\delta\phi, \delta v, \delta b$ around eq. (6.17) and comparing them to cases where the full geometry is known. To this end, notice that the potential of eq. (6.12) is factorized,

$$U(\phi, v, b) \equiv e^{2v} \widehat{U}(\phi, b) \, , \tag{6.19}$$

so that perturbations δv of v do not mix with perturbations $\delta\phi, \delta b$ of ϕ and b at the linearized level. In addition, since the background values of ϕ and b are constant in r,

---

[9]Up to the sign of r and rescalings of R_0, this realization of AdS $\times$ S with given L and R is unique.
[10]In either case we shall find that the geodesic distance is finite.

the constraint obtained linearizing eq. (6.13) involves only v, and reads

$$\frac{2p}{p+1}\, v'\, \delta v' = \partial_v U \Big|_{\text{AdS}\times\text{S}} \delta v = 2\, U \Big|_{\text{AdS}\times\text{S}} \delta v = \frac{2p}{(p+1)r^2}\, \delta v\,, \tag{6.20}$$

so that

$$\delta v \sim \text{const.} \times (-r)^{-1}\,. \tag{6.21}$$

Thus, the constraint of eq. (6.21) retains only one mode $\sim (-r)^{\lambda_0}$ with respect to the linearized equation of motion for δv, with exponent $\lambda_0 = -1$.

On the other hand, ϕ and b perturbations can be studied using the canonically normalized fields

$$\chi \equiv \left(\sqrt{\frac{8}{D-2}}\, \delta\phi\,, \ \sqrt{\frac{2q(D-2)}{p}}\, \delta b \right)\,, \tag{6.22}$$

in terms of which one finds

$$\chi'' \sim -\frac{1}{r^2}\, H_0\, \chi\,, \tag{6.23}$$

where the Hessian

$$H_{ab} \equiv \frac{\partial^2 U}{\partial\chi_a \partial\chi_b} \Big|_{\text{AdS}\times\text{S}} \equiv \frac{1}{r^2}\, (H_0)_{ab}\,, \qquad (H_0)_{ab} = \mathcal{O}(r^0)\,. \tag{6.24}$$

The substitution $t = \log(-r)$ then results in the autonomous system

$$\left(\frac{d^2}{dt^2} - \frac{d}{dt} \right) \chi = -\, H_0\, \chi\,, \tag{6.25}$$

so that the modes scale as $\chi \propto (-r)^{\lambda_i}$, where the λ_i are the eigenvalues of the block matrix

$$\begin{pmatrix} 1 & -H_0 \\ 1 & 0 \end{pmatrix}\,. \tag{6.26}$$

In turn, these are given by

$$\begin{aligned} \lambda_{1,2}^{(\pm)} &= \frac{1 \pm \sqrt{1 - 4\, h_{1,2}}}{2}\,, \\ h_{1,2} &\equiv \frac{\text{tr}(H_0) \pm \sqrt{\text{tr}(H_0) - 4\det(H_0)}}{2}\,, \end{aligned} \tag{6.27}$$

where the trace and determinant of H_0 are given by

$$\text{tr}(H_0) = -\frac{\alpha\left(\gamma\left(\alpha+\gamma\right)(D-2)^2-16\right)+16\,\gamma\,(p+1)\,(q-1)}{8\,(p+1)\left((q-1)\,\gamma-\alpha\right)},$$

$$\det(H_0) = \frac{\alpha\,\gamma\,(D-2)^2\left((p+1)\,\gamma+\alpha\right)}{4\,(p+1)^2\left((q-1)\,\gamma-\alpha\right)}.$$

(6.28)

In the case of the orientifold models, one obtains the eigenvalues

$$\frac{1\pm\sqrt{13}}{2}\,,\qquad\frac{1\pm\sqrt{5}}{2}\,,$$

(6.29)

while in the heterotic model one obtains the eigenvalues

$$\pm\,2\,\sqrt{\frac{2}{3}}\,,\qquad 1\pm 2\,\sqrt{\frac{2}{3}}\,.$$

(6.30)

All in all, in both cases one finds three negative eigenvalues and two positive ones, signaling the presence of three attractive directions as $r \to -\infty$. The remaining unstable modes should physically correspond to deformations that break extremality, resulting in a truncation of the AdS $\times$ S throat and in the emergence of an event horizon at a finite distance, and it should be possible to remove them with a suitable tuning of the boundary conditions at the outer singularity. In the following section we shall argue for this interpretation of unstable modes in the throat.

Comparison with known solutions

In order to highlight the physical origin of the unstable modes, let us consider the Reissner-Nordström black hole in four dimensions, whose metric in isotropic coordinates takes the form

$$ds_{\text{RN}}^2 = -\frac{g(\rho)^2}{f(\rho)^2}\,dt^2 + f(\rho)^2\left(d\rho^2 + \rho^2\,d\Omega_2^2\right),$$

(6.31)

where

$$f(\rho) \equiv 1 + \frac{m}{\rho} + \frac{m^2}{4\rho^2} - \frac{e^2}{4\rho^2}\,,$$

$$g(\rho) \equiv 1 - \frac{m^2}{4\rho^2} + \frac{e^2}{4\rho^2}\,.$$

(6.32)

The extremal solution, for which $m = e$, develops an infinitely long $\text{AdS}_2 \times \text{S}^2$ throat in the near-horizon limit $\rho \to 0$, and radial perturbations of the type

$$ds^2_{\text{pert}} = -\frac{4\rho^2}{m^2} e^{2\,\delta a(\rho)}\, dt^2 + \frac{m^2}{4\rho^2}\, e^{2\,\delta b(\rho)}\left(d\rho^2 + \rho^2\, d\Omega_2^2\right) \tag{6.33}$$

solve the linearized equations of motion with power-law modes $\sim \rho^{\lambda_{\text{RN}}}$, with eigenvalues

$$\lambda_{\text{RN}} = -2\,,\,1\,,\,0\,. \tag{6.34}$$

The zero-mode reflects invariance under shifts of δa, while the unstable mode reflects a breaking of extremality. Indeed, writing $m \equiv e\,(1 + \epsilon)$ the $\frac{\rho}{m} \ll 1\,,\epsilon \ll 1$ asymptotics of the red-shift g_{tt} take the schematic form

$$\frac{(g_{tt})_{\text{RN}}}{(g_{tt})_{\text{AdS}_2 \times \text{S}^2}} \sim \text{regular} + \epsilon\left(-\frac{1}{\rho^2} + \frac{3}{m\rho} + \text{regular}\right) + o(\epsilon)\,, \tag{6.35}$$

so that for $\epsilon = 0$ only a regular series in positive powers of ρ remains. Geometrically, near extremality an approximate $\text{AdS} \times \text{S}$ throat exists for some finite length, after which it is truncated by a singularity corresponding to the event horizon. As ϵ decreases, this horizon recedes and the throat lengthens, with the length in $\log \rho$ growing as $-\log \epsilon$. This is highlighted numerically in the plot of fig. 6.1.

A similar analysis for BPS D3-branes in type IIB supergravity [113] yields the eigenvalues $-8\,,\,-4\,,\,-2\,,\,4\,,\,0\,,0$, suggesting again that breaking extremality generates unstable directions, and that a fine-tuning at infinity removes them leaving only the attractive ones. Notice that the zero-modes correspond to constant rescalings of x^μ, which is pure gauge, and to shifts of the asymptotic value of the dilaton.

2.3 *The pinch-off singularity*

Let us now proceed to address the asymptotic geometry away from the core. Since the dynamical system at hand is not integrable in general[11], we lack a complete solution of the equations of motion stemming from eq. (6.11), and therefore we shall assume that

---

[11]In the supersymmetric case the contribution arising from the dilaton tadpole is absent, and the resulting system is integrable. Moreover, for $p = 8\,,q = 0$ the system is also integrable, since only the dilaton tadpole contributes.
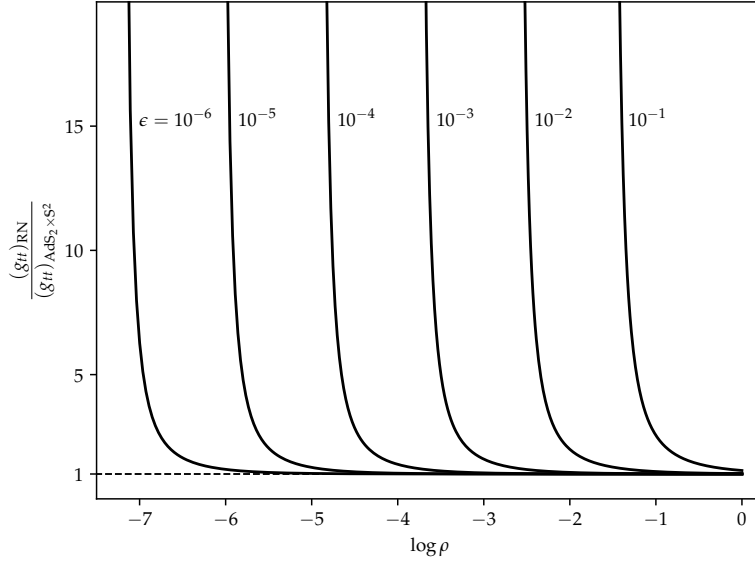
FIGURE 6.1: a plot of the ratio of the Reissner-Nordström red-shift factor to the one of the corresponding $AdS_2 \times S^2$, for various values of the extremality parameter $\epsilon \equiv \frac{m}{e} - 1$. Only values outside of the event horizon are depicted. As extremality is approached, the horizon recedes to infinity and the geometry develops an approximate $AdS \times S$ throat, marked by $(g_{tt})_{RN} \approx (g_{tt})_{AdS_2 \times S^2}$, whose length in units of $\log \rho$ grows asymptotically linearly in $-\log \epsilon$.

the dilaton potential overwhelms the other terms of eq. (6.12) for large (positive) r, to then verify it *a posteriori*. In this fashion, one can identify the asymptotic equations of motion

$$
\begin{aligned}
\phi'' &\sim \frac{\gamma(D-2)}{8}\, T\, e^{\gamma\phi + 2v - \frac{2q}{p} b}\,, \\
v'' &\sim -\frac{p+1}{p}\, T\, e^{\gamma\phi + 2v - \frac{2q}{p} b}\,, \\
b'' &\sim -\frac{1}{D-2}\, T\, e^{\gamma\phi + 2v - \frac{2q}{p} b}\,,
\end{aligned}
\tag{6.36}
$$

whose solutions

$$
\begin{aligned}
\phi &\sim \frac{\gamma(D-2)}{8}\, y + \phi_1 r + \phi_0\,, \\
v &\sim -\frac{p+1}{p}\, y + v_1 r + v_0\,, \\
b &\sim -\frac{1}{D-2}\, y + b_1 r + b_0
\end{aligned}
\tag{6.37}
$$

are parametrized by the constants $\phi_{1,0}, v_{1,0}, b_{1,0}$ and a function $y(r)$ which is not asymptotically linear (without loss of generality, up to shifts in ϕ_1, v_1, b_1). Rescaling x and redefining R_0 in eq. (6.10) one can set *e.g.* $b_0 = v_0 = 0$. The equations of motion

and the constraint then reduce to

$$y'' \sim \widehat{T} \, e^{\Omega y + L r} \, ,$$

$$\frac{1}{2} \, \Omega \, (y')^2 + L \, y' \sim \widehat{T} \, e^{\Omega y + L r} - M \, ,$$

(6.38)

where[12]

$$\widehat{T} \equiv T \, e^{\gamma \phi_0 + 2 v_0 - \frac{2q}{p} \, b_0} \, ,$$

$$\Omega \equiv \frac{D-2}{8} \, \gamma^2 - \frac{2(D-1)}{D-2} \, ,$$

$$L \equiv \gamma \, \phi_1 + 2 \, v_1 - \frac{2q}{p} \, b_1 \, ,$$

$$M \equiv \frac{4}{D-2} \, \phi_1^2 - \frac{p}{p+1} \, v_1^2 + \frac{q(D-2)}{p} \, b_1^2 \, .$$

(6.39)

The two additional exponentials in eq. (6.12), associated to flux and internal curvature contributions, are both asymptotically $\sim \exp\left(\Omega_{n,c} \, y + L_{n,c} \, r\right)$, with corresponding constant coefficients $\Omega_{n,c}$ and $L_{n,c}$. Thus, if y grows super-linearly the differences $\Omega - \Omega_{n,c}$ determine whether the dilaton potential dominates the asymptotics. On the other hand, if y is sub-linear the dominant balance is controlled by the differences $L - L_{n,c}$. In the ensuing discussion we shall consider the former case[13], since it is consistent with earlier results [24], and, in order to study the system in eq. (6.38), it is convenient to distinguish the two cases $\Omega = 0$ and $\Omega \neq 0$. Moreover, we have convinced ourselves that the tadpole-dominated system of eq. (6.36) is actually integrable, and its solutions behave indeed in this fashion. As a final remark, us observe that, on account of eq. (6.37), the warp exponents of the longitudinal sector dx_{p+1}^2 and the sphere sector $R_0 \, d\Omega_q^2$ are asymptotically equal,

$$\frac{2}{p+1} v - \frac{2q}{p} b \sim 2b \, .$$

(6.40)

This is to be expected, since if one takes a solution with $q = 0$ and replaces

$$dx_{p+1}^2 \; \to \; dx_{p'+1}^2 + R_0^2 \, d\Omega_{p-p'}^2$$

(6.41)

---

[12]Notice that $\Omega = \frac{D-2}{8} \left(\gamma^2 - \gamma_c^2\right)$, where the critical value γ_c defined in [27] marks the onset of the "climbing" phenomenon described in [69, 70, 114, 115] use different notations.

[13]The sub-linear case is controlled by the parameters ϕ_1 , v_1 , b_1, which can be tuned as long as the constraint is satisfied. In particular, the differences $L - L_{n,c}$ do not contain v_1.

for some $p' < p$ and large R_0, and then makes use of the freedom to rescale R_0 shifting b by a constant (which does not affect the leading asymptotics), one obtains another asymptotic solution with lower $p' < p$, whose warp factors are both equal to the one of the original solution.

Pinch-off in the orientifold models

In the orientifold models $\Omega = 0$, since the exponent $\gamma = \gamma_c$ attains its "critical" value [27] in the sense of [69]. The system in eq. (6.38) then yields

$$
\begin{aligned}
y &\sim \frac{\widehat{T}}{L^2}\, e^{L r}, \quad M = 0, \qquad L > 0, \\
y &\sim \frac{\widehat{T}}{2}\, r^2, \quad M = \widehat{T}, \qquad L = 0.
\end{aligned}
\tag{6.42}
$$

These conditions are compatible, since the quadratic form M has signature $(+, -, +)$ and thus the equation $M = \widehat{T} > 0$ defines a one-sheeted hyperboloid that intersects any plane, including $\{L = 0\}$. The same is also true for the cone $\{M = 0\}$.

In both solutions the singularity arises at finite geodesic distance

$$
R_c \equiv \int^{\infty} dr\, e^{v - \frac{q}{p} b} < \infty,
\tag{6.43}
$$

since at large r the warp factor

$$
v - \frac{q}{p}\, b \sim -\frac{D-1}{D-2}\, y.
\tag{6.44}
$$

In the limiting case $L = 0$, where the solution is quadratic in r, due to the discussion in the preceding section this asymptotic behavior is consistent, up to the replacement of dx_9^2 with $dx_2^2 + R_0^2\, d\Omega_7^2$, with the full solution found in [24], whose singular structure is also reconstructed in our analysis for $p = 8$, $q = 0$, $L = 0$. The existence of a closed-form solution in this case rests on the integrability of the corresponding Toda-like system, since neither the flux nor the internal curvature are present.

Pinch-off in the heterotic model

In the heterotic model $\Omega = 4$, and therefore one can define

$$Y \equiv y + \frac{L}{\Omega} r , \tag{6.45}$$

removing the $L r$ terms from the equations. One is then left with the first-order equation

$$\frac{1}{2} Y'^2 - \frac{\widehat{T}}{\Omega} e^{\Omega Y} = E , \tag{6.46}$$

which implies the second-order equation of motion, where the "energy"

$$E \equiv \frac{M}{2\Omega} - \frac{L^2}{2\Omega^3} . \tag{6.47}$$

The solutions of eq. (6.46) depend on the sign of E, and one can verify that, if $r \to +\infty$, Y grows at most linearly. On the other hand, super-linear solutions develop a singularity at a finite radius $r = r_0$, and they all take the form

$$Y \sim -\frac{2}{\Omega} \log (r_0 - r) , \tag{6.48}$$

which is actually the exact solution of eq. (6.46) for $E = 0$. The geodesic distance to the singularity

$$R_c \equiv \int^{r_0} dr \, e^{v - \frac{q}{p} b} < \infty \tag{6.49}$$

is again finite, since from eqs. (6.44) and (6.48)

$$v - \frac{q}{p} b \sim \frac{2}{\Omega} \frac{D-1}{D-2} \log (r_0 - r) = \frac{9}{16} \log (r_0 - r) . \tag{6.50}$$

In terms of the geodesic radial coordinate $\rho_c < R_c$, the asymptotics[14] are

$$\phi \sim -\frac{4}{5} \log (R_c - \rho_c) ,$$
$$ds^2 \sim (R_c - \rho_c)^{\frac{2}{25}} \left(dx_6^2 + R_0^2 \, d\Omega_3^2 \right) + d\rho^2 . \tag{6.51}$$

---

[14]More precisely, the asymptotics for the metric in eq. (6.51) refer to the exponents in the warp factors, which are related to v and b. Subleading terms could lead to additional prefactors in the metric.

While these results are at most qualitative in this asymptotic region, since curvature corrections and string loop corrections are expected to be relevant, they again hint at a physical picture whereby space-time pinches off at finite distance in the presence of (exponential) dilaton potentals, while branes dictate the symmetries of the geometry, as depicted in Figure 6.2. In this context, the nine-dimensional Dudas-Mourad solutions correspond to (necessarily uncharged) 8-branes[15]. This picture highlights the difficulties encountered in defining tension and flux as asymptotic charges, but analogous quantities might appear as parameters in the sub-leading portion of the solution, of which there are indeed two. They ought to be matched with the $AdS \times S$ core, and we are currently pursuing this direction, which however appears to entail complicated non-linear numerics. We shall elaborate on this issue in Section 2.4. For the time being let us recall that the results of [76] suggest that a that an analysis based on string perturbation theory [76] suggests that at least the D1-branes that we consider are extremal, albeit the presence of dilaton tadpoles makes this lesson less clear.

As a final comment, let us add that cosmological counterparts, if any, of these solutions, whose behavior appears milder, can be expected to play a rôle when the dynamics of pinch-off singularities are taken into account, and they could be connected to the hints of spontaneous compactification discussed in Chapter 4. Indeed, as already stressed in [27], the general lesson is that non-supersymmetric settings are dynamically driven towards time-dependent configurations, and this additional potential instability might be mitigated to an arbitrarily large extent studying the dynamics deep inside the AdS throat, the deeper the more any effect of an asymptotic collapse is red-shifted.

2.4 *Black branes: back-reaction*

Let us conclude our discussion on back-reactions extending machinery that we have developed in Section 2.1 to the case of non-extremal branes. Including a "blackening" factor entails the presence of an additional dynamical function, and thus after gauge-fixing radial diffeomorphisms one is left with four dynamical functions (including the

---

[15]In particular, on account of the analysis that we described in the preceding chapter, it is reasonable to expect that in the orientifold models the Dudas-Mourad solution corresponds to D8-branes.
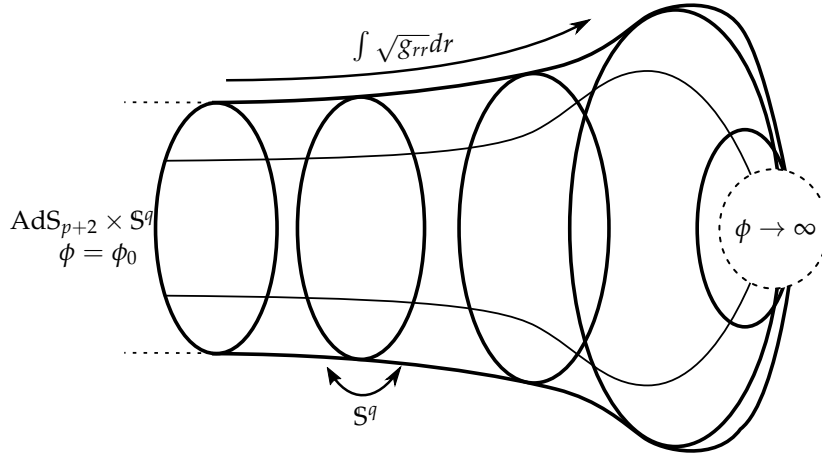
FIGURE 6.2: a schematic depiction of the expected structure of the complete geometry sourced by the branes, displaying only geodesic radial distance and the S^q radius. The geometry interpolates between the AdS × S throat and the pinch-off singularity (dashed circle).

dilaton). Specifically, in order to arrive at a generalization of the Toda-like system of eqs. (6.11) and (6.13), the correct ansatz takes the form

$$ds_D^2 = e^{2(a(r)+pb(r)+qc(r))} \, dr^2 - e^{2a(r)} \, dt^2 + e^{2b(r)} \, d\mathbf{x}_p^2 + e^{2c(r)} \, R_0^2 \, d\Omega_q^2 \,,$$

$$\phi = \phi(r) \,, \tag{6.52}$$

$$H_{p+2} = \frac{n}{f(\phi)(R_0 \, e^c)^q} \, \mathrm{Vol}_{p+2} \,, \qquad \mathrm{Vol}_{p+2} = e^{2a+2pb+qc} \, dr \wedge dt \wedge d^p x \,.$$

Then, one can verify that the resulting reduced equations of motion can be derived from the Toda-like action

$$S_{\mathrm{red}} = \int dr \left[\frac{4}{D-2} \, (\phi')^2 + q(q-1) \, (a'^2 - b'^2) + \frac{p(D-2)}{q} \, (c')^2 - U \right] \tag{6.53}$$

where the effective potential now reads

$$U = - T \, e^{\gamma\phi + 2a + 2qb - \frac{2p}{q}c} - \frac{n^2}{2R_0^{2q}} \, e^{-\alpha\phi - 2(q-1)a + \frac{2p(q-1)}{q}c} + \frac{q(q-1)}{R_0^2} \, e^{2(q-1)b} \,, \tag{6.54}$$

and the equations of motion are to be supplemented by the zero-energy constraint

$$\frac{4}{D-2} \, (\phi')^2 + q(q-1) \, (a')^2 - q(q-1) \, (b')^2 + \frac{p(D-2)}{q} \, (c')^2 + U = 0 \,. \tag{6.55}$$

Changing variables in eq. 6.52 in order to match the ansatz of eq. 6.10, and substituting
the resulting expressions in eqs. (6.53) and (6.55), one recovers the Toda-like system
that describes extremal branes. Hence, the generalized system that we have derived
can in principle describe the back-reaction of non-extremal branes, which ought to
exhibit Rindler geometries in the near-horizon limit. On the other hand, one can verify
that the tadpole-dominated asymptotic system reproduces the behavior of eq. (6.37),
thus suggesting that the pinch-off singularities described in the preceding sections are
generic and do not depend on the gravitational imprint of the sources that are present
in space-time, rather only on the residual symmetry left unbroken.

3   BLACK BRANES: DYNAMICS

Let us now extend the considerations of Section 1 to the non-extremal case, studying
potentials between non-extremal brane stacks and between stacks of different types
and dimensions. While probe-brane computations are rather simple to perform using
the back-reacted geometries that we described in the preceding section, they pertain
to regimes in which the number of p-branes N_p in one stack is much larger than the
number of q-branes N_q in the other stack. However, with respect to the extremal case,
the leading contribution to the string amplitude for brane scattering corresponds to
the annulus, which is non-vanishing and does not entail the complications due to
orientifold projections, anti-branes and Riemann surfaces of higher Euler characteristic.
This setting therefore offers the opportunity to compare probe computations with
string amplitude computations. Specifically, we shall consider the uncharged 8-
branes in the orientifold models, since their back-reacted geometry is described
by the static Dudas-Mourad solution[16] [24] that we have described in Chapter 3.
Furthermore, the other globally known back-reacted geometry in this setting pertains
to extremal D1-branes, and 8-branes are the only probes (of different dimension)
whose potential can be reliably computed in this case, since they can wrap the
internal S^7 in the near-horizon $AdS_3 \times S^7$ throat. On the other hand, while probe

---

[16]The generalization to non-extremal p-branes of different dimensions would entail solving non-
integrable systems, whose correct boundary conditions are not well-understood hitherto. Moreover, a
reliable probe-brane regime would exclude the pinch-off asymptotic region, thereby requiring numerical
computations.

computations in the heterotic model can be performed with no further difficulties, their stringy interpretation appears more subtle, since it would involve NS5-branes or non-supersymmetric dualities. Nevertheless, probe-brane calculations in this setting yield attractive potentials for 8-branes and fundamental strings, as in the orientifold models, while NS5-branes are repelled. In addition, in some cases the potential scales with a positive power of g_s. Otherwise, the instability appears to be still under control, since probes would reach the strong-coupling regions in a parametrically large time for $g_s \ll 1$.

3.1 *Brane probes in the Dudas-Mourad geometry*

Let us consider a stack of N_p probe Dp-branes, with $p \leq 8$, embedded in the Dudas-Mourad geometry parallel to the 8-branes[17], at a position y in the notation of Chapter 3. We work in units where $\alpha_O = 1$ for clarity. This setting appears to be under control as long as the geodesic coordinate

$$r \equiv \frac{1}{\sqrt{g_s}} \int_0^y \frac{du}{u^{\frac{1}{3}}}\, e^{-\frac{3}{8} u^2} \tag{6.56}$$

is far away from its endpoints $r = 0$, $r = R_c$. Such an overlap regime exists provided that $g_s \equiv e^{\Phi_0} \ll 1$, and thus both curvature corrections and string loop corrections are expected to be under control.

Writing the metric as

$$ds_{10}^2 = e^{2A(y)}\, dx_9^2 + e^{2B(y)}\, dy^2 \tag{6.57}$$

the DBI action evaluates to

$$S_p = - N_p\, T_p \int d^{p+1}x\, e^{(p+1)A(y) - \Phi(y)}$$
$$\equiv - N_p\, T_p \int d^{p+1}x\, V_{p8}\,, \tag{6.58}$$

where the probe potential per unit tension

---

[17]While the number N_8 of 8-branes does not appear explicit in the solution, there is a single free parameter $g_s \equiv e^{\Phi_0}$, which one could expect to be determined by N_8 analogously to the extremal case, with $g_s \ll 1$ for $N_8 \gg 1$.

$$V_{p8} = g_s^{\frac{p-3}{4}} \, y^{\frac{2}{9}(p-2)} \, e^{\frac{p-5}{8} y^2} \qquad\qquad (6.59)$$

displays a non-trivial dependence on p, and is depicted in figs. 6.3 and 6.4. In particular, if the potential drives probes toward $y \to \infty$ it is repulsive, since the corresponding pinch-off singularity derived in the preceding sections agrees with the Dudas-Mourad geometry in this regime. All in all, for $p < 3$ probes are repelled by the 8-branes, while for $p > 4$ they are attracted to the 8-branes. The cases $p = 3$, 4 feature unstable equilibria[18] which appear to be within the controlled regime, but the large-separation behavior, to be compared to a string amplitude computation, appears repulsive. As we have anticipated, the analogous computation for branes probing the back-reacted geometry sourced by other non-extremal branes appears considerably more challenging. This is due to the fact that even if the reduced dynamical system derived in the preceding sections were solved numerically in a reliable regime, the asymptotic boundary conditions corresponding to uncharged branes are not yet understood. While this is the case also for extremal branes, one can make progress observing that in the probe regime the scale of the dimensions transverse to the extremal stack should be large enough to ensure that the near-horizon limit is reliable. The exponential term in eq. (6.59) is actually universal, since repeating the above probe-brane computation for the generic pinch-off singularity of eq. (6.42) in the orientifold models[19] yields the same result, with the potential at large separation repulsive for $p < 5$ and attractive for $p > 5$, while the case $p = 5$ requires subleading, presumably power-like, terms in the metric. However, we do not expect these cases to provide reliable insights, since the pinch-off singularity lies beyond the controlled regime.

In order to verify that this construction is at least parametrically under control, one ought to verify that the probe-brane stack remains in the controlled region for parametrically large times. To this end, let us consider the reduced dynamical system that describes motion along y, with the initial conditions $y(0) = y_0$, $\dot{y}(0) = 0$. The

---

[18]Notice that, in the absence of fluxes, brane polarization [11, 116] would not suffice to stabilize these equilibria.

[19]As we have discussed in Section 2.4, the leading-order behavior of the pinch-off singularity is expected to be applicable to the non-extremal case, since it is dominated by the dilaton potential.

corresponding Lagrangian reads

$$\mathcal{L}_{\text{red}} = -T_p \, N_p \, V_{p8} \, \sqrt{1 - e^{2(B-A)} \dot{y}^2} \,, \qquad (6.60)$$

and, since the corresponding Hamiltonian

$$H_{\text{red}} = \frac{T_p \, N_p \, V_{p8}}{\sqrt{1 - e^{2(B-A)} \dot{y}^2}} = T_p \, N_p \, V_{p8}(y_0) \qquad (6.61)$$

is conserved, solving the equation of motion by quadrature gives

$$t = \int_{y_0}^{y} \frac{e^{B(u)-A(u)}}{\sqrt{1 - \left(\frac{V_{p8}(u)}{V_{p8}(y_0)}\right)^2}} \, du = g_s^{-\frac{3}{4}} \int_{y_0}^{y} \frac{e^{-\frac{u^2}{2}}}{u^{\frac{5}{9}} \sqrt{1 - \left(\frac{u}{y0}\right)^{\frac{4}{9}(p-2)} e^{\frac{p-5}{4}\left(u^2-y_0^2\right)}}} \,, \qquad (6.62)$$

which is indeed parametrically large in string units.

3.2 *String amplitude computation*

Let us now compare the probe-brane result of eq. (6.59) with a string amplitude computation. As we have anticipated, in the non-extremal case the relevant amplitude for the leading-order interaction between stacks of N_p Dp-branes and N_q Dq-branes[20], with $p < q$ for definiteness, is provided by the annulus amplitude, whose transverse-channel integrand in the present cases takes the form [76]

$$\widetilde{A}_{pq} \propto N_p \, N_q \left(V_{8-q+p} \, O_{q-p} - O_{8-q+p} \, V_{q-p} \right) \,, \qquad (6.63)$$

where the characters are evaluated at $\mathfrak{q} = e^{-2\pi\ell}$ and we have omitted the overall unimportant positive normalization, which encodes the tensions and depends on whether both stacks consist of non-extremal branes or one stack consists of extremal branes. In suitable units for the transverse separation r bewtween the two stacks, the potential V_{pq} takes the form

$$V_{pq} \propto - N_p \, N_q \int_0^{\infty} \frac{d\ell}{\ell^{\frac{9-q}{2}}} \, \frac{\widetilde{A}_{pq}}{\eta^{8-q+p}} \left(\frac{2\eta}{\vartheta_2} \right)^{\frac{q-p}{2}} e^{-\frac{r^2}{\ell}} \,. \qquad (6.64)$$

---

[20]The ensuing string amplitude computation is expected to be reliable as long as N_p and N_q are $\mathcal{O}(1)$, complementary to the probe regimes $N_p \gg N_q$ and $N_p \ll N_q$.

For large r, the integral is dominated by the large ℓ region, where the integrand asymptotes to $\mathfrak{q}^{-\frac{1}{3}} \, \tilde{A}_{pq}$, where

$$
\begin{aligned}
\tilde{A}_{pq} &\propto V_{8-q+p} \, O_{q-p} - O_{8-q+p} \, V_{q-p} \\
&\sim 2 \, (4 - q + p) \, \mathfrak{q}^{\frac{1}{3}} \, ,
\end{aligned}
\tag{6.65}
$$

so that the overall sign of the potential is the sign of $q - p - 4$. Thus, for large r and $q < 7$ one finds

$$
V_{pq} \propto (q - p - 4) \, \frac{N_p \, N_q}{r^{7-q}} \, ,
\tag{6.66}
$$

which is repulsive for $p < q - 4$ and attractive for $p > q - 4$. While the integral of eq. (6.64) diverges for $q \geq 7$, a distributional computation for $q = 7, 8$ yields a finite force stemming from potentials that behave as $(p - 3) \log(r)$ and $(p - 4) \, r$ respectively. Therefore, the only case that can be compared with a reliable probe-brane computation is $q = 8$, where the potential behaves as $(p - 4) \, r$ and is thus repulsive for $p < 4$ and attractive for $p > 4$, consistently with the results in the preceding section.

3.3 *Probe 8-branes in* $\mathrm{AdS} \times S$ *throats*

To conclude, let us thus consider N_8 8-branes embedded in the near-horizon $\mathrm{AdS}_3 \times \mathbb{S}^7$ geometries sourced by $N_1 \gg N_8$ extremal D1-branes in the orientifold models and, for the sake of completeness, by $N_5 \gg N_8$ NS5-branes in the heterotic model. Other than the interaction potential bewteen two extremal stacks, which we have computed in Section 1, this is the only case where a probe-brane potential can be reliably computed, since the 8-branes can wrap the internal spheres without collapsing in a vanishing cycle, leaving only one dimension across which to separate from the stack. Moreover, this is the only case where computations can be performed in the opposite regime N_1 , $N_5 \ll N_8$, as we have described in Section 3.1. Since the 8-branes are uncharged,

the respective potentials V_{81}, V_{85} arise from the DBI contribution only, and one finds

$$
\begin{aligned}
V_{81} &= N_8 \, N_1 \, T_8 \, R^7 \left(\frac{L}{Z} \right)^2 , \\
V_{85} &= N_8 \, N_5 \, T_8 \, R^3 \left(\frac{L}{Z} \right)^6 ,
\end{aligned}
\tag{6.67}
$$

where we have omitted the *a priori* unknown (and unimportant) scaling with g_s. These potentials are thus attractive, which may appear in contradiction with the results in the preceding sections, where both D1-branes and NS5-branes are repelled by the 8-branes. However, let us observe that, since the 8-branes wrap the internal spheres, in the large-separation regime they ought to behave as uncharged 1-branes and 5-branes respectively, consistently with an attractive interaction. Furthermore, when expressed in terms of the geodesic coordinate $r = L \log \left(\frac{Z}{L} \right)$, the potentials of eq. (6.67) decay exponentially in r.

All in all, the results in this chapter further support the idea that brane dynamics plays a crucial rôle in elucidating the fate of string models with broken supersymmetry. Whenever available, microscopic information such as the scaling of the tensions of fundamental branes and the string amplitude computation of eq. (6.64) appear to be consistent with the low-energy effective theory introduced in Chapter 3. The resulting picture builds an intuitive understanding of the high-energy behavior of the settings at stake, and points to some avenues to more quantitative results in this respect. In particular, the interpretation of the AdS$_3$ × S^7 solution introduced in Chapter 3 as the near-horizon limit of the back-reacted geometry sourced by D1-branes, which subsequently nucleate and are repelled by each other, suggests that an holographic approach could expose some intriguing lessons. This shall be the focus of the following chapter, in which we propose a dual interpretation of non-perturbative instabilities in meta-stable AdS$_3$ (false) vacua.

Dudas–Mourad probe potentials

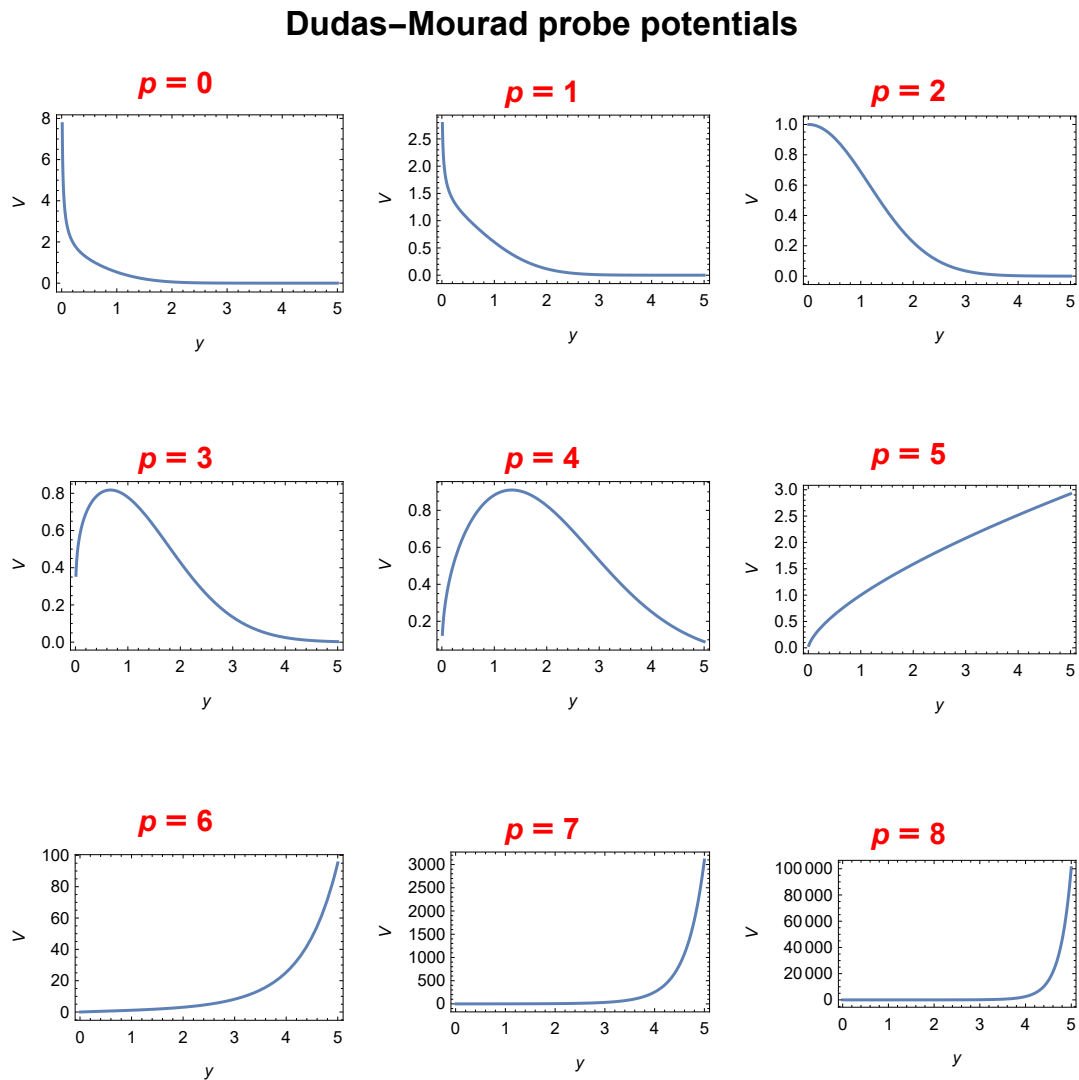FIGURE 6.3: probe potentials for $g_s = 1$ and $p \leq 8$. For $p < 3$ the probe stack is repelled by the 8-branes, while for $p > 4$ it is attracted to the 8-branes. A string amplitude computation yields a qualitatively similar behavior, despite the string-scale breaking of supersymmetry.
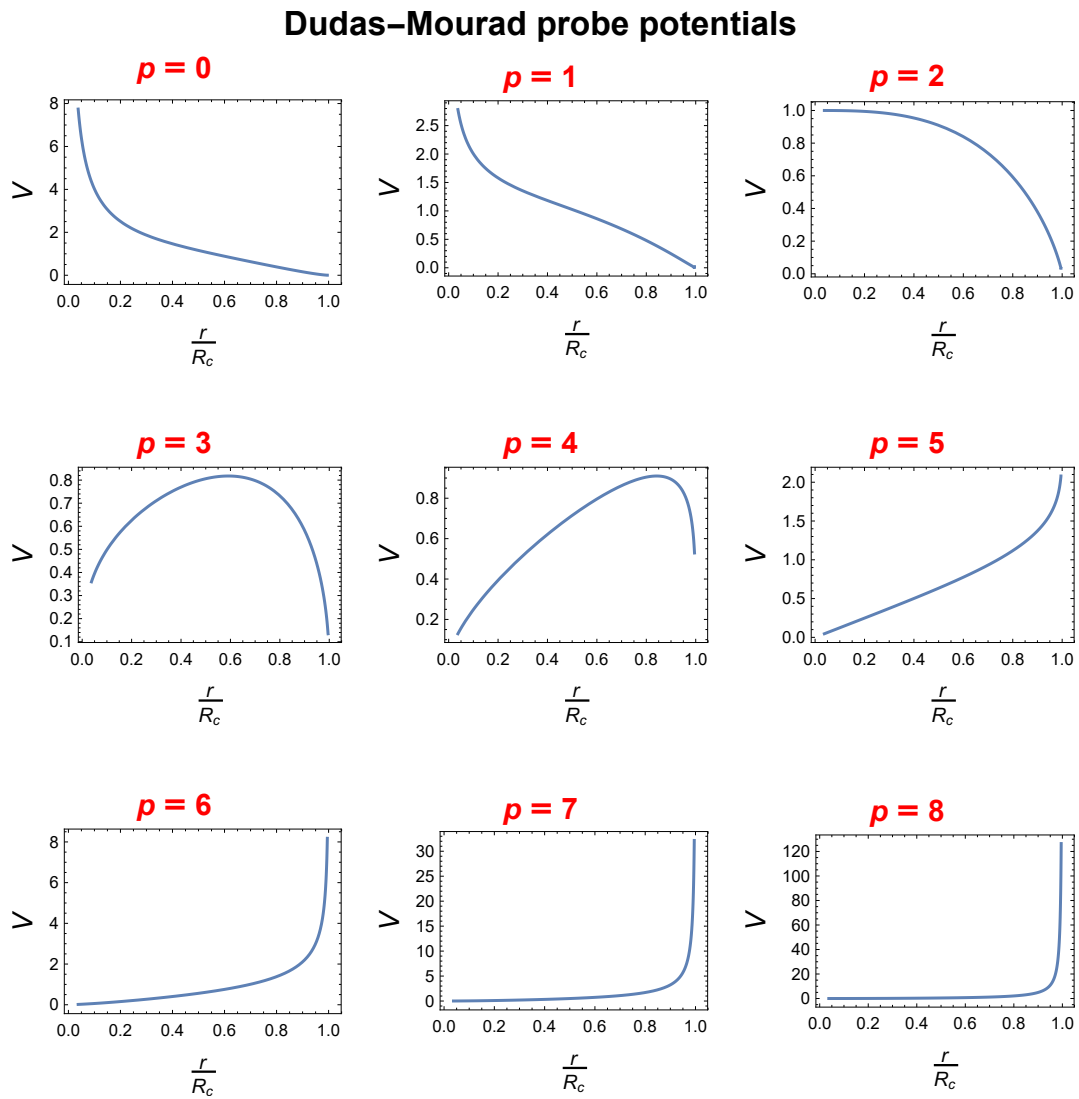
FIGURE 6.4: probe potentials for $g_s = 1$ and $p \leq 8$, plotted as functions of the geodesic coordinate along the compact direction.

Holography: bubbles and RG flows

7

In this chapter we describe in detail a holographic approach to non-perturbative instabilities of meta-stable AdS (false) vacua, presenting the results of [109] and connecting them to the discussions in the preceding chapters. Alongside (non-)perturbative dualities, which are best understood in supersymmetric scenarios, holography has established itself as one of the main available tools to obtain insights in quantum gravity, at least in (asymptotically) AdS geometries [4, 117, 118]. In particular, remarkable progress has been achieved in black-hole thermodynamics, which is amenable to both semi-classical [119] and holographic analyses [120–122]. The holographic properties of black holes are encoded in thermal states of the corresponding boundary theories, and (entanglement) entropy computations provide a useful tool to study them [123–125]. All in all, black holes constitute a prototypical example of a quantum-gravitational phenomenon. Similarly, vacuum decay processes [96, 97, 100] comprise a different class of scenarios where genuine quantum-gravitational effects drive the physics. Much as for black holes, the semi-classical description of vacuum decay has been thoroughly dissected in the literature [16, 126–128], and is currently an active topic of research, but its holographic properties have been only explored to a lesser extent[1]. The issue has been investigated in connection with the walls of vacuum bubbles [134–136], but in this chapter we would like to explore the links with the boundary of AdS, which suggests a qualitatively different picture. Moreover, since vacuum decay processes also play an important rôle in identifying a "swampland" and its relation to UV completions of gravity, it is conceivable that probing them beyond the semi-classical level could provide new gateways to the intricacies of the field [137].

Therefore, motivated also by the brane constructions that we have discussed

---

[1]For recent results, which have appeared during the development of [109], see [129, 130]. See also [131, 132] for other works on the structure of the vacuum in the presence of bubbles. For a field-theoretical discussion of instanton contributions to entanglement entropy, see [133].

in Chapter 5 and Chapter 6, in this chapter we propose a first step to bridge the gap between holographic methods, which typically address stable, often exclusively stationary states, and aspects of the standard semi-classical techniques used to study vacuum decay, focusing in particular on the development of vacuum bubbles that mediate transitions between classical vacua. Here we consider them in the simplest case of interest, namely AdS geometries in three space-time dimensions, which according to the results described in the preceding chapters arise, for instance, from D1-brane stacks in the $USp(32)$ and $U(32)$ orientifold models. For the sake of clarity we shall keep the ensuing discussion quite general, with few references to the string-theoretic settings that we have in mind.

Altogether, we shall present evidence that, holographically, vacuum bubbles behave much like RG flows of the boundary theory, and appear to provide, in some sense, a set of building blocks for such flows, as we shall discuss later on. The motivation for considering this interpretation relies on two facts:

- Vacuum decay has an irreversible direction, from AdS radius L_- to $L_+ < L_-$, *i.e.* the (negative) cosmological constant must increase in absolute value [96, 97].

- The (holographic) central charge, in an AdS$_3$ vacuum, is proportional to the AdS$_3$ radius, in particular

$$c = \frac{3L}{2G_3} \tag{7.1}$$

  in three dimensions [138], where G_3 is the three-dimensional Newton constant. This suggests that vacuum decay be accompanied by a *decrease* of the central charge c, along the lines of the Zamolodchikov c-theorem [139]. Our choice of working in three space-time dimensions is indeed motivated by the fact that, while gravity becomes more tractable [140, 141], the central charge encodes key information on the boundary theory [142–144].

In order to put this idea on firmer grounds, it will be useful to study the behavior of the entanglement entropy of any subregion of the deformed boundary theory, since this quantity provides a probe for its quantum-mechanical properties. If this framework gives a correct description of the problem, important lessons are potentially in store regarding the swampland program and the stability of non-supersymmetric

AdS "vacua". Moreover, powerful standard techniques that apply to the boundary description could conceivably shed light on the analysis of vacuum instabilities beyond the semi-classical regime. In particular, the world-volume gauge theories associated to the low-energy dynamics of D1-branes would provide a quantitative connection to the orientifold models that we have discussed in Chapter 2.

To begin with, in Section 1 we describe in detail the geometry that results from bubble nucleation, introducing the coordinate systems that we shall employ. In Section 2 we present the computation of the holographic entanglement entropy associated to a bubble, referring to the results in Appendix C, and in Section 3 we introduce a number of *c*-functions connected to the entanglement entropy, the null-energy condition and the trace anomaly. Then, in order to extend our results to the case of off-centered bubbles, in Section 4 we describe the powerful formalism o (holographic) integral geometry [33], and we apply it to the present setting. Finally, in Section 5 we collect some remarks on a holographic interpretation of non-supersymmetric brane dynamics, and we specialize our considerations to the case of D1-branes in the $USp(32)$ and $U(32)$ orientifold models, connecting the following results to the ones described in the preceding chapters. In particular, these settings could provide a firmer basis for further developments non-supersymmetric in brane dynamics and holography which are qualitatively different from orbifolds of their well-understood supersymmetric counterparts.

1 CONSTRUCTION OF THE BULK GEOMETRY

In this section we present the geometry which models the decay process that we shall consider. It describes, in the semi-classical limit, the expansion of a bubble of AdS geometry, nucleated by tunneling inside a meta-stable AdS of higher vacuum energy. Physically, such a situation can be realized, in the simplest setting, in a gravitational theory with a minimally coupled scalar Φ subject to an asymmetric double well potential [100, 127] of the form

$$\mathcal{L} = R - \frac{1}{2} (\partial \Phi)^2 - V_{\text{well}}(\Phi) \,, \tag{7.2}$$

but, as we have described in Chapter 5, settings of this type can be concretely realized by fundamental branes in non-supersymmetric string models. In the following we shall not need a precise construction, since we shall focus on model-independent features, but let us stress that more explicit "top-down" constructions should provide better control of the holographic dictionary in this context. In order to isolate the relevant physics in the most tractable scenario, we shall work in three space-time dimensions, while resorting to the thin-wall approximation. Furthermore, we shall focus on nucleation at vanishing initial radius[2], occurring at the center of a global chart of an original AdS_3^+ space-time. The generalization to arbitrary initial radius and dimension is straightforward and does not appear to affect our analysis qualitatively, while off-centered nucleation is discussed later. On the other hand, according to the discussions in Chapter 5 the thin-wall approximation ought to reliably describe the dominant decay channels in the settings that we have in mind [102].

Let us consider two AdS_3 (false) vacua, dubbed AdS_3^+ and AdS_3^-, of radii $L_+ > L_-$ respectively, connected by a tunneling process

$$AdS_3^+ \;\rightarrow\; AdS_3^- \tag{7.3}$$

mediated by the nucleation of a bubble. Working in the thin-wall approximation, we realize the metric corresponding to the decay process gluing the two AdS_3 geometries over a null surface, which represents the bubble trajectory as depicted in fig. 7.1.

It is most convenient to work in a coordinate chart[3] such that the metric reads

$$ds_\pm^2 = -\left(1 + \frac{r^2}{L_\pm^2}\right)\frac{d\eta^2}{\left(1 + \frac{\eta^2}{L_\pm^2}\right)^2} + \frac{dr^2}{1 + \frac{r^2}{L_\pm^2}} + r^2\,d\phi^2 \tag{7.4}$$

for both the initial and final AdS_3 geometries. In the thin-wall approximation the bubble is described, in the $AdS_3^\pm$ charts respectively, by the radial null surfaces

$$ds_\pm^2 = 0 \;\Rightarrow\; r = \eta\,. \tag{7.5}$$

---

[2]While our preceding results show that AdS-scale nucleation radii are favored, from a phenomenological perspective one may expect tunneling to favor microscopic initial radii [100], since bubble nucleation is a genuinely quantum-gravitational event. At any rate, the qualitative picture is not affected by this approximation, which we expect to be instructive.

[3]This chart is related to the (t, r, ϕ) global coordinates via the transformation $\eta = L_\pm \tan\left(\frac{t}{L_\pm}\right)$. It does not cover the full geometry, but it does cover the entirety of the collapse.
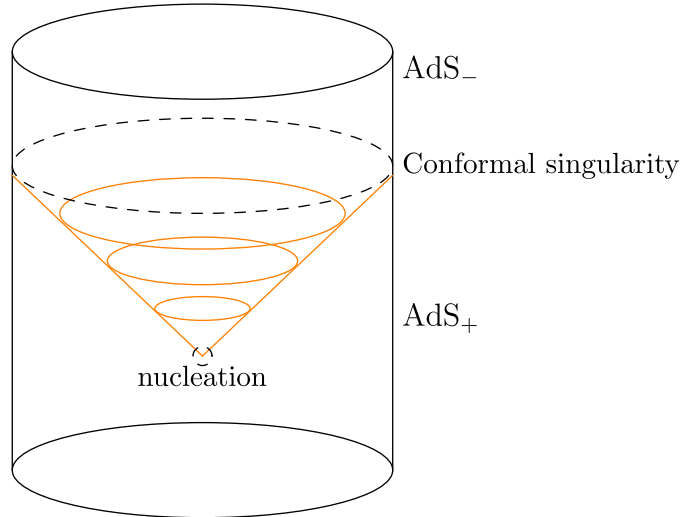
FIGURE 7.1: a Penrose-like diagram of the geometry describing the decay process.

Gluing along the bubble[4], the complete metric can be written in the compact form

$$ds^2 = -\left(1 + \frac{r^2}{L_{\text{eff}}^2}\right) \frac{d\eta^2}{\left(1 + \frac{\eta^2}{L_{\text{eff}}^2}\right)^2} + \frac{dr^2}{1 + \frac{r^2}{L_{\text{eff}}^2}} + r^2\, d\phi^2\,, \tag{7.6}$$

where L_{eff} denotes an "effective curvature radius", defined by

$$L_{\text{eff}}(\eta, r) \equiv \begin{cases} L_+\,, & r > \eta \\ L_-\,, & r < \eta \end{cases}. \tag{7.7}$$

It is worth noting that L_{eff} can be written as a step function with argument $r - \eta$. This may lead one to expect that doing away with the thin-wall approximation could amount to a "smoothing" of L_{eff}, perhaps as a function of an invariant quantity, which we shall indeed identify in the following section. This gluing procedure agrees with the standard Israel junction conditions for null hypersurfaces [145–147]. Indeed, the continuity condition for the (degenerate) induced metric h on the bubble reduces to eq. (7.13), while the transverse curvature exhibits a discontinuity proportional to h, which can be ascribed to the bubble stress-energy tensor [147]. In detail, following the notation of [147], in the global (η, r, ϕ) chart the bubble (where $\eta = r$) is described by ϕ, generated by the integral flow of the tangent space-like vector e_ϕ, and by the null

---

[4]We remark that this can be done with no issues, since the bubble is null. Equivalently, the equations for the bubble trajectory, seen from both sides, take the same form, which motivates this choice of time coordinate.

coordinate $\lambda \equiv \eta + r$, generated by the integral flow of the null vector e_λ. In addition, the transverse null vector N is chosen such that

$$e_\phi \cdot e_\lambda = e_\phi \cdot N = 0 , \quad N^2 = e_\lambda^2 = 0 , \quad N \cdot e_\lambda = -1 . \tag{7.8}$$

Explicitly,

$$e_\lambda \equiv \sqrt{\frac{f_\pm(r)}{2}} \left(\partial_\eta + \partial_r \right) , \qquad e_\phi \equiv \frac{1}{r} \partial_\phi , \qquad N \equiv \sqrt{\frac{f_\pm(r)}{2}} \left(\partial_\eta - \partial_r \right) \tag{7.9}$$

on either side of the bubble, where $f_\pm(r) \equiv 1 + \frac{r^2}{L_\pm^2}$. The resulting transverse curvature

$$C_{ab} \equiv - g_{\mu\nu} N^\mu e_a^\rho \nabla_\rho e_b^\nu , \quad a , b \in \{\lambda , \phi\} , \tag{7.10}$$

is then

$$C_{\lambda\lambda} = C_{\lambda\phi} = 0 , \quad C_{\phi\phi} = \frac{1}{r} \sqrt{\frac{f_\pm(r)}{2}} . \tag{7.11}$$

Hence, C_{ab} is indeed proportional to the (degenerate) induced metric $h_{ab} = g(e_a, e_b)$ on the bubble.

While this coordinate system is convenient to describe the geometry, due to the simplicity of the gluing conditions, the same results can be reproduced in another global coordinate system, denoted by (τ, ρ, ϕ), in which the AdS$_3^\pm$ metrics read

$$ds_\pm^2 = L_\pm^2 \left(- \cosh^2 \rho_\pm \, d\tau_\pm^2 + d\rho_\pm^2 + \sinh^2 \rho_\pm \, d\phi_\pm^2 \right) . \tag{7.12}$$

This turns the gluing condition into

$$L_+ \sinh \rho_+ = L_- \sinh \rho_- , \tag{7.13}$$

which induces a discontinuity ρ that must be taken into account. There is also a corresponding discontinuity in τ. We shall make use of this coordinate system to compute the entanglement entropy in Section 2.

Let us observe the $SO(2,2)$ isometry group of AdS$_3$ is broken by the metric of eq. (7.6) to the subgroup $SO(1,2)$ that keeps the nucleation event fixed, and under which the bubble wall and the two AdS$_3^\pm$ regions are all invariant.

1.1 *Thick walls and conformal structure*

The metric described in the preceding section has a boundary with a ill-formed conformal structure, since the two semi-infinite cylinders corresponding to the (conformal structures of the) boundaries of $\text{AdS}_3^{\pm}$ are separated by a ring-like "conformal singularity", which builds up when the bubble reaches infinity. While this might seem an artifact of the thin-wall approximation, we have reasons to believe that this is not the case. In general, a "thick-wall" bubble could be realized via a smooth metric with the same isometry group[5] as a thin-wall bubble, which is the $SO(1,2)$ subgroup of $SO(2,2)$ that keeps the nucleation center fixed. Up to diffeomorphisms, the only invariant of this subgroup is

$$\xi^2 \equiv \log |\cosh \rho \, \cos \tau| \,, \tag{7.14}$$

which generalizes the flat-space-time $r^2 - t^2$, so that any candidate "smoothed" L_{eff} can only depend on ξ^2 and, possibly, on a discrete choice of angular sectors[6] for τ. We have convinced ourselves that, independently of the smooth behavior of the effective radius, the boundary value of L_{eff} is still given by a step function, namely

$$\lim_{\rho \to \infty} L_{\text{eff}}(\tau, \rho) = \begin{cases} L_+, & \tau < \frac{\pi}{2} \\ L_-, & \tau > \frac{\pi}{2} \end{cases}. \tag{7.15}$$

In geometric terms, all "layers" of the thick bubble can reach the boundary at the same time, and thus produce again a conformal singularity, separating the two conformal structures. This is schematically depicted in the Penrose-like diagram of fig. 7.2. We remark that this structure is indeed imposed by symmetry, since it originates from a suitable Wick rotation of an $SO(3)$-invariant instanton. This is consistent with an intuitive picture in which each "layer" moves in a uniformly accelerated fashion, is asymptotically null and the slower ones start out closer to the boundary.

---

[5]Actually, the nucleation event cannot itself have such a symmetry, which can only hold for sufficiently large bubble well after nucleation. This is not an issue for what concerns the conformal structure of the boundary.

[6]For instance, single-bubble tunneling can be implemented letting $L_{\text{eff}} = L_+$ for $\tau < 0$, a smooth function of ξ^2 for $0 < \tau < \frac{\pi}{2}$, and L_- for $\tau > \frac{\pi}{2}$.
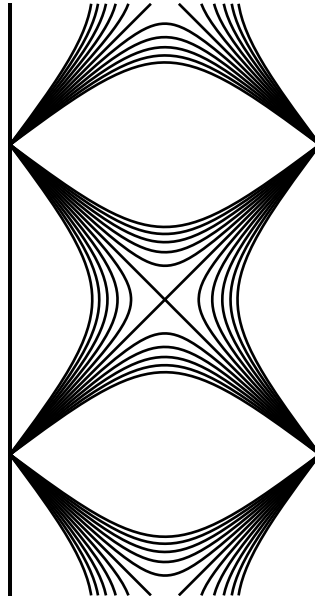
FIGURE 7.2: a cross-section of a Penrose-like diagram for AdS space-time with selected level sets of ξ^2, representing potential layers of a thick bubble. A choice of angular sector for τ eliminates the periodicity.

To conclude this section, let us briefly address the issue of gravitational collapse. It was shown [100, 148] that AdS thick-wall bubbles nucleating inside Minkowski false vacua induce a "big crunch" due to a singular evolution of the scalar field $\Phi(\xi)$. However, the issue is subtler in the present case, since the proof in [148] rests on the existence of global Cauchy surfaces, which AdS does not accommodate. To wit, the initial-value problem in global AdS is ill-defined unless it is supplemented with appropriate boundary conditions. However, the $SO(1, D-1)$ symmetry assumed in [100] and in the present discussion does not allow any plausible choice of boundary conditions. For instance, Dirichlet conditions for $\Phi(\xi)$ at the conformal singularity constrain it to be constant, since all slices of constant ξ converge there[7]. Regardless of how boundary conditions affect the issue at stake, we remark that the present discussion concerns primarily the expansion of the bubble, rather than the fate of AdS_3^-.

---

[7]An analogous constraint holds for boundary conditions involving a finite number of derivatives.

2 THE HOLOGRAPHIC ENTANGLEMENT ENTROPY

In general terms, holographic dualities relate a gravitational theory to a non-gravitational one, typically a quantum field theory in a fixed background space-time, in such a way that, whenever one side of the duality is strongly coupled, the other is weakly coupled and the two theories describe the same physics [4, 117, 118, 149]. The identification of the two theories then takes the form of a link between the bulk action and the boundary generating functional. This prescription for holography has been employed to derive a number of important checks. Some of these have led to the Ryu-Takayanagi formula [123–125], which relates entanglement entropy in the boundary theory and geometric quantities in the bulk, in a generalization of the Bekenstein-Hawking formula for black holes. In detail, the entanglement entropy of region $\mathscr{A}$ on the boundary is given by the extremal area of surfaces in (space-like slices of) the bulk whose boundary is $\partial \mathscr{A}$,

$$S_{\text{ent}}(\mathscr{A}) = \inf_{\partial \mathcal{A} = \partial \mathscr{A}} \frac{\text{Area}(\mathcal{A})}{4G_{\text{N}}} \,. \tag{7.16}$$

The Ryu-Takayanagi formula is decorated by various corrections, arising for instance from higher curvature terms in the effective action for the bulk theory. In light of its geometric simplicity, we shall take the Ryu-Takayanagi formula as a starting point and investigate the entanglement entropy of the boundary theory during the growth of the vacuum bubble. To this end, we shall study the variational problem of finding the geodesic between two boundary points in the bubble geometry described in Section 1.

2.1 *The entanglement entropy of the bubble geometry*

In accordance with the Ryu-Takayanagi formula, the entanglement entropy of a boundary interval $\mathscr{A} = A\overline{A}$ of size $2\theta_A$ is related to the (regularized) length of the shortest curve between its endpoints. The condition of extremality for a curve in the bubble geometry corresponds to it being composed, inside and outside the bubble,

of segments of hyperbolic lines (in the relevant hyperbolic plane $\mathbb{H}^2$), joining with no kink at the bubble wall. This no-kink condition is more precisely stated as the requirement that the slope $\frac{d\ell}{d\phi}$, where $d\ell \equiv (1 + \frac{r^2}{L_{\text{eff}}^2})^{-\frac{1}{2}} dr$ is the differential radial geodesic distance, be continuous across the bubble wall[8]. Explicitly, it follows from the (distributional) geodesic equation, which in the present case can be integrated to

$$\frac{dr}{ds} = \sqrt{\left(1 + \frac{r^2}{L_{\text{eff}}^2}\right)\left(E - \frac{J^2}{r^2}\right)}, \qquad (7.17)$$

where E and J are integration constants and s an affine parameter, so that

$$\frac{d\ell}{d\phi} = \left(1 + \frac{r^2}{L_{\text{eff}}^2}\right)^{-\frac{1}{2}} \frac{r^2}{J} \frac{dr}{ds} = \frac{r^2}{J} \sqrt{E - \frac{J^2}{r^2}} \qquad (7.18)$$

is indeed continuous at the bubble wall. To explain it in a more intuitive fashion, "zooming in" on the intersection of the geodesic with the bubble and sending $L_\pm \to \infty$, one recovers the regular Euclidean plane, consistently with the absence of a kink.

Let us distinguish two possible phases for the extremal curve:

- The **vacuum phase**, simply given by the hyperbolic line in $\mathbb{H}^2_-$ between two symmetric endpoints A and $\overline{A}$, which only exists if

$$\cos \theta_A > \cos \theta_A^{\text{par}} \equiv \tanh\left(\frac{r_{\text{bubble}}}{L_-}\right). \qquad (7.19)$$

- The **injection phase**, where the curve injects into the bubble at a point B at an angle θ_B from the center of the interval, follows a line in $\mathbb{H}^2_+$ until it reaches the symmetric point $\overline{B}$, then exits the bubble and follows a line to $\overline{A}$. The angle θ_B is fixed by the no-kink condition.

In Appendix C we shall derive both the no-kink condition, written as an equation suitable to analize numerically, and the length of the corresponding geodesics using hyperbolic geometry. Then, for each value of θ_A we have first solved the no-kink equation for the injection phase numerically, and use the results to compare the lengths

---

[8]The absence of a kink translates graphically into the condition that the geodesic segments be tangent in a conformal model, such as the "twofold Poincaré disk" that we have depicted in fig. 7.4. Equivalently, the angles formed with a ray of the circle, measured in the inner and outer hyperbolic planes, coincide.

of the two phases in order to determine the minimal one. The result is depicted in fig. 7.3.
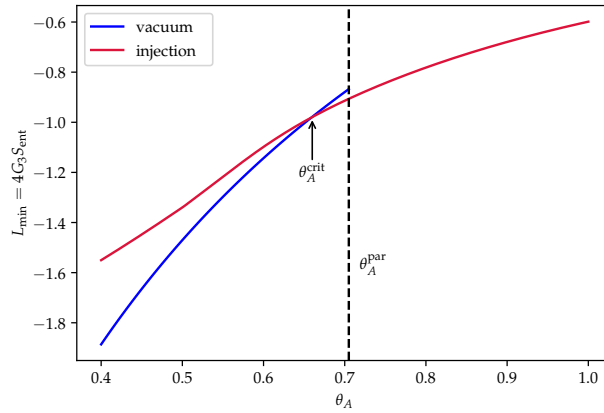
FIGURE 7.3: finite part of the geodesic length for the two phases plotted against boundary interval size. We have chosen a cosmological constant ratio of $\frac{1}{2}$ as an example.

We have found that the length of the injecting curve drops below that of the vacuum curve at a critical angle $\theta_A^{\mathrm{crit}} < \theta_A^{\mathrm{par}}$, marking a phase transition beyond which the penetrating geodesic is favored, as depicted in fig. 7.4.
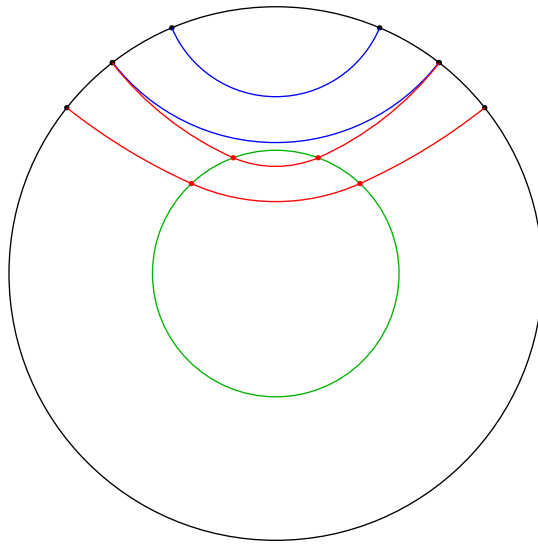
FIGURE 7.4: minimal curves for increasing θ_A in a twofold Poincaré disk model. The two equal-length geodesics at the injection phase transition are depicted. Notably, the transition occurs before the vacuum geodesic becomes tangent to the bubble.

In the following section we shall discuss how the resulting (finite part of the) entanglement entropy behaves as the bubble expands, and how the corresponding c-function provides a probe for the putative RG flow at place. One may wonder

whether our proposal conflicts with the dynamical nature of an expanding bubble, which would suggest a dual interpretation in terms of a time-dependent state in the boundary theory. However, let us remark that in the present setting time evolution affects only the radius of the bubble, and can therefore be traded for an AdS dilation. In turn, dilatons can be associated to coarse-graining in the dual theory, and indeed in the absence of bubbles the geometry would be invariant. In this sense, a more complete statement is that our proposal can co-exist with a time-dependent interpretation, which involves a single boundary theory instead of a flow connecting different boundary theories.

3   DUAL RG FLOWS AND c-FUNCTIONS

In this section we introduce our holographic picture of vacuum decay via bubble nucleation. As we have previously mentioned, the entanglement structure induced by the bubble via the Ryu-Takayanagi prescription hints at some process which reduces the effective number of degrees of freedom on the boundary. Moreover, this process is necessarily irreversible, since bubble nucleation only occurs in the direction of decreasing vacuum energy[9]. These features point to an holographic interpretation of non-perturbative[10] vacuum decay in terms of an RG flow. We can now follow a number of standard procedures to construct c-functions which appear to capture this type of scenario [150–155]. However, let us remark that in the present setting the resulting c-functions are evaluated on the RG flow directly, and we have no constructions of their "off-shell' counterparts, if any, at present, while in supersymmetric cases they are typically built from a superpotential for scalars dual to gauge couplings. In the following we shall work in global coordinates, since Poincaré coordinates, which do not cover the whole of AdS, are problematic in the presence of a centered, axially symmetric bubble. The holographic RG framework is usually described in Poincaré coordinates, a feature which impacts the nature of the dual RG flow in the boundary theory in a non-trivial fashion. We shall return to this issue in

---

[9]In contrast, dS false vacua can also undergo "up-tunneling", due to the finite total entropy (semi-classically) associated to dS.

[10]We emphasize that the original vacuum ought to be strictly meta-stable, namely stable against small fluctuations.

more detail in Section 4.1, explaining how our framework incorporates the Poincaré holographic RG picture as a limiting case. For the time being, we shall describe three types of holographic *c*-functions: one following from the entanglement entropy in the following section, one following from the null-energy condition in Section 3.2, and one from the holographic trace anomaly in Section 3.3.

3.1 *c-functions from entanglement entropy*

As we have outlined in the preceding discussion, one can use the entanglement entropy computed in Section 2.1 to construct a *c*-function. Given a fixed spatial slice, taken out of the preferred foliation induced by the isometries of the bubble, the dependence of the entanglement entropy on the interval length ℓ will be affected by the bubble only for sufficiently large ℓ, as we have explained in Section 2.1. This, along with the fact that we are working in global coordinates where the conformal boundary of a spatial slice has the topology of a circle, suggests that ℓ is not the most relevant quantity to construct a *c*-function. Indeed, our aim is to relate the bubble expansion to an RG flow, and the interval length at a fixed time does not appear suitable in this respect, since a canonical definition of a boundary length scale at infinity appears problematic in global coordinates. This is to be contrasted with the Poincaré holographic RG, where intervals result from a stereographic projection onto the line, and therefore the rescaling of interval lengths is reminiscent a coarse-graining procedure. Instead, the relevant scales in the bulk are, the coordinates r, η which are related via eq. (7.5). This means that, at fixed time $\eta = \eta^*$, the bubble radius $R \equiv \eta^*$ appears as the only relevant scale from the perspective of the boundary, and motivates the choice of fixing an interval $\mathscr{A}$ of half-angle θ_A, and considering

$$c_{\mathscr{A}}(R) \equiv 3\theta \left. \frac{dS_{\text{ent}}(\theta; R)}{d\theta} \right|_{\theta=\theta_A}. \tag{7.20}$$

The proposal of eq. (7.20) mirrors the standard Cardy-Calabrese formula [143, 144], and provides an example of a *c*-function constructed out of the entanglement pattern of the system, although not necessarily the only one. The aforementioned identification of the bubble radius with an RG scale is the first step toward the proposed framework

in which vacuum bubbles are associated to dual RG flows. Furthermore, one can recast the dependence on R of eq. (7.20) in terms of the interval half-angle θ in the following fashion: instead of fixing $\mathscr{A}$, given the bubble radius R one can take the critical interval size θ_A^{crit} which marks the onset of the injection phase. This defines a correspondence $\theta(R)$ which may be employed to recast the flow in terms of angular sizes. The most natural choices for $\mathscr{A}$ would be either half of the boundary, so that the corresponding entanglement entropy is immediately sensitive to the bubble upon nucleation in a smooth fashion, or the whole boundary[11], which interestingly yields a step function: before the bubble arrives at the boundary $c_{\text{bdry}} = c_+$, while afterwards its value jumps to $c_{\text{bdry}} = c_-$, where $c_\pm$ are the central charges associated to $L_\pm$. The presence of the bubble does not influence the boundary until the very instant it touches it, at the end of the expansion. Notably, this happens in a finite coordinate time $t_{\text{tot}} = L_+ \frac{\pi}{2}$ (or "$\eta = \infty$") in the AdS_3^+ patch outside the bubble, which conceivably leaves open the possibility of multi-bubble events that could modify the boundary theory in different ways.

3.2 *c-functions from the null energy condition*

When seeking holographic *c*-functions, another option is to apply the standard prescription [151–153, 156–161] in global coordinates. This involves a procedure analogous to the one typically carried out in the Poincaré patch, which defines *c*-functions in terms of the exponential warp factors that appear in asymptotically AdS metrics. Indeed, our choice of writing the metric as in eq. (7.6) conveniently defines a bulk *c*-function in terms of the effective radius $L_{\text{eff}}(\eta, r)$ given by eq. (7.7), extending the dictionary of eq. (7.1). An important difference with respect to the scenario outlined above, however, is that the resulting *c*-function is time-dependent. Physically, this can be ascribed to the dynamical nature of the geometry, although the actual functional dependence can be recast in terms of the combination $r - \eta$ only, consistently with the discussion in Section 2. Indeed, once again one obtains a step

---

[11]More precisely, one should take the limit as $\theta_A \to \frac{\pi}{2}^-$, since the full boundary has vanishing entanglement entropy.
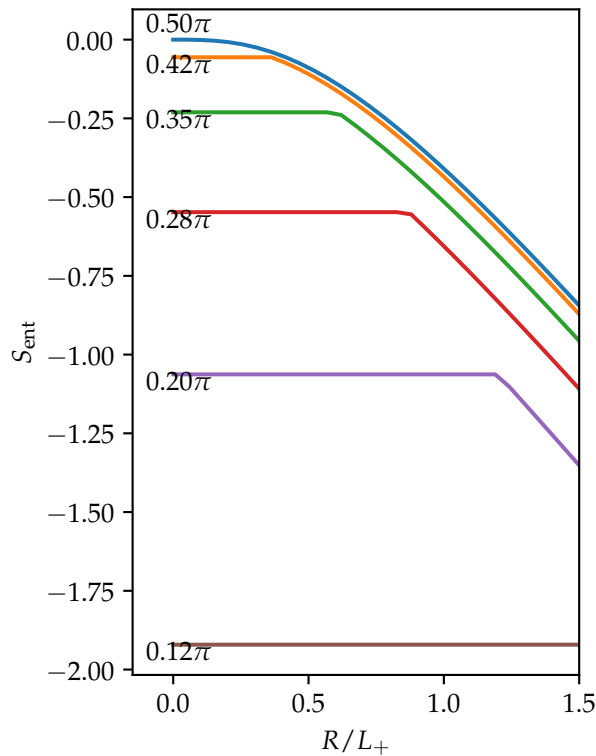
FIGURE 7.5: finite part of the entanglement entropy vs bubble radius, for various angular sizes θ_A. Notice the smooth behavior of the curve for $\theta_A = \frac{\pi}{2}$, which corresponds to half of the boundary. This would translate into a smooth interpolating description for the dual RG flow.

function

$$c_{\text{eff}}(\eta, r) \equiv \begin{cases} c_+, & r > \eta \\ c_-, & r < \eta \end{cases}.$$

(7.21)

One can readily verify that, when suitably extended beyond the collapse[12], these c-functions approach c_{bdry} as $r \to +\infty$, a reassuring consistency check, while their discontinuous nature can presumably be ascribed to the thin-wall approximation. The same cannot be said for the c-function defined by c_{bdry}, whose discontinuity is seemingly linked to the conformal singularity of the bubble geometry. Notice that the monotonic behavior of the c-function of eq. (7.21) may appear compromised by the discontinuous nature of the geometry that we consider. However, the thin-wall regime is only an ideal limit of a smooth function, which interpolates between $L_\pm$ and hence between $c_\pm$. The monotonic behavior of holographic c-functions reflects in general the null energy condition [151–153] and, as we shall explain in Section 4.1, the

---

[12]This can be done, for instance, gluing two coordinate charts, each of which would cover one of the AdS$_3^\pm$.

computation can be reproduced for horocyclic bubbles, since it reduces to the case of a domain wall in Poincaré coordinates. A similar computation can be carried out in global coordinates, employing a "smoothing" of the singular metric of eq. (7.6) of the form

$$ds^2 = -\left(1 + \frac{r^2}{L^2}\right) \frac{d\eta^2}{\left(1 + \frac{\eta^2}{L^2}\right)^2} + \frac{dr^2}{1 + \frac{r^2}{L^2}} + r^2 d\phi^2, \tag{7.22}$$

where now $L(\eta, r)$ is a smooth function of η and r. While this ansatz can be expected to have the correct form in the thin-wall regime, it would be interesting to investigate whether the exact Coleman-de Luccia instanton dictates a different one in more general cases.

On account of eq. (7.22), two null energy condition (NEC) bounds

$$T_{\mu\nu} k_\pm^\mu k_\pm^\nu \geq 0, \quad \text{with} \quad k_\pm \equiv \frac{1 + \frac{\eta^2}{L^2}}{\sqrt{1 + \frac{r^2}{L^2}}} \partial_\eta \pm \sqrt{1 + \frac{r^2}{L^2}} \partial_r, \tag{7.23}$$

yield, using the Einstein equations,

$$\frac{\eta^2}{1 + \frac{\eta^2}{L^2}} \partial_r L \geq \frac{r^2}{1 + \frac{r^2}{L^2}} |\partial_\eta L|. \tag{7.24}$$

These bounds further imply

$$\partial_r L \geq 0, \tag{7.25}$$

so that r can be interpreted as a holographic RG scale and

$$c \equiv \frac{3L}{2G_3} \tag{7.26}$$

is a *c*-function. Indeed, a constant L saturates both NEC bounds.

3.3 *The holographic trace anomaly*

As a final remark concerning other *c*-function constructions, and in order to provide further evidence for our proposal, let us briefly comment on an additional way to explore how the central charge of the boundary theory is affected by the bubble, namely via the (holographic) trace anomaly. Two-dimensional quantum field theories

on a curved space-time with Ricci scalar R_2 generally loose a classical conformal symmetry. In our case, this breaking reflects itself in an anomalous trace of the boundary stress-energy tensor,

$$\langle T^\mu{}_\mu \rangle = -\frac{c}{12} R_2 .$$ (7.27)

In Poincaré coordinates, the holographic computation of this anomaly has been carried out in [158]. Due to the dynamical nature of our setting, it is not clear *a priori* whether the same procedure applies, but one can expect that the time dependence would deform the anomaly in a manner compatible with replacing

$$c \rightarrow c_{\text{bdry}} .$$ (7.28)

However, the standard prescription to compute the (expectation value of the) stress-energy tensor should still apply insofar as holography is valid, since we are assuming the Ryu-Takayanagi conjecture to begin with. While the computation, which still presents some subtleties, can be simplified focusing on the trace directly, we would like to stress that the trace-less part of this vacuum expectation value should provide quantitative information on how an off-centered bubble affects the boundary theory. This issue will be the subject of a future investigation. In computing the trace anomaly, one can attempt to generalize the procedure followed in [162], whereby the boundary curvature in eq. (7.27) is recovered via the bulk extrinsic curvature. To this end, let us first emphasize that the general formula for the trace anomaly of the boundary theory,

$$\langle T^\mu{}_\mu \rangle = -\frac{1}{8\pi G} \left(\Theta + \Theta_{\text{c.t.}} \right) ,$$ (7.29)

derived in [162], will only hold in the present case if a term corresponding to the bubble stress-energy tensor is added to the classical action. This is needed in order that the bubble geometry and other field profiles satisfy the bulk equations of motion, and it also cancels the bulk contribution to the variation with respect to the boundary metric[13] $\gamma_{\mu\nu}$. Once this is done, it appears that the procedure can be extended to the present case. To begin with, one needs to modify the counterterm, which in AdS$_3$ is

---

[13]Specifically, only its conformal class matters.

$\frac{2}{L}$. If $\langle T_{\mu\nu} \rangle$ is to be finite when evaluated on all classical solutions, we expect that a correct counterterm, which in any case ought to reproduce $\frac{2}{L_{\mathrm{eff}}}$ in the bubble geometry, should be expressed as a suitable function of the scalar potential. Then, writing a generic metric deformation in the form

$$ds^2 = -f(\eta, r)\, \gamma_{\eta\eta}\, d\eta^2 + \frac{dr^2}{f(\eta, r)} + r^2\, \gamma_{\phi\phi}\, d\phi^2 + \frac{2r^2}{L_{\mathrm{eff}}}\, \gamma_{\eta\phi}\, d\eta\, d\phi\,, \qquad (7.30)$$

where $f(\eta, r) \equiv 1 + \frac{r^2}{L_{\mathrm{eff}}^2}$, one can verify that it coincides with the one derived in Fefferman-Graham [163, 164] coordinates[14], where the AdS radius jumps from L_+ to L_- after a finite time, provided that one extends the coordinate system to include times after the bubble has reached the boundary. In fact, letting n be the unit vector normal to the (regularized) boundary and h_{tr} be the associated transverse metric, the bulk expression for the extrinsic curvature,

$$\Theta = h_{\mathrm{tr}}^{\mu\nu}\, \Gamma_{\mu\nu}^{A}\, n_A = -\frac{1}{2}\, \sqrt{f(\eta, r)}\, g^{\mu\nu}\, \partial_r\, g_{\mu\nu}\,, \qquad (7.31)$$

gives the same result when evaluated in a Fefferman-Graham patch, since depending on whether the bubble has arrived at the boundary $f(\eta, r) \sim \frac{r^2}{L_{\pm}^2}$. This result also shows that the boundary deformation γ is the correct counterpart of the Fefferman-Graham one, as one may infer from the large-r asymptotics. Indeed, going back from η to the standard global time coordinate t, the transformed γ_{tt}, $\gamma_{t\phi}$ comprise, alongside $\gamma_{\phi\phi}$, the deformation parameters which correspond to the (conformal class of the) boundary metric

$$ds_{\mathrm{bdry}}^2 = -\gamma_{tt}\, dt^2 + \gamma_{\phi\phi}\, L_{\pm}^2\, d\phi^2 + 2\, L_{\pm}\, \gamma_{t\phi}\, dt\, d\phi\,, \qquad (7.32)$$

which dominates in eq. (7.30) for large r, since

$$ds^2 \sim \frac{r^2}{L_{\pm}^2}\, ds_{\mathrm{bdry}}^2\,, \qquad (7.33)$$

again depending on whether the bubble has arrived at the boundary.

Furthermore, one can verify that any smooth deviation from L_{eff}, which can

---

[14]The conventions used in Section 3.2 of [162] rescale γ by a factor r^2. In our convention, γ has a finite limiting value at the boundary.

also be defined for a thick bubble, does not contribute to the boundary asymptotics, consistently with the fact that, even outside the thin-wall approximation, the conformal structure of the boundary presents a singularity. To put it more simply, the boundary always sees the whole bubble arriving at the same instant. Hence, the trace anomaly

$$\langle T^{\mu}{}_{\mu} \rangle = - \frac{c_{\text{bdry}}}{12} R_2 \qquad (7.34)$$

indeed reflects the replacement of eq. (7.28) and the counterterm $\Theta_{\text{c.t.}} = \frac{2}{L_{\text{eff}}}$.

In summary, the above analysis shows that the deformation $\gamma_{\mu\nu}$ correctly corresponds to the Fefferman-Graham one, and the expectation of a step-like c-function from the trace anomaly is reproduced, alongside the absence of contributions due to deviations from a thin bubble. In addition, the framework that we employed can be readily extended to generic (multi-)bubble configurations. Thus one may conclude that, in some sense, the holographic entanglement entropy provides a better probe of the physics, since it can detect the arrival of the bubble in a smooth fashion.

4 INTEGRAL GEOMETRY AND OFF-CENTERED BUBBLES

A natural question concerns the holographic interpretation of the site of the nucleation event and, in particular, how off-centered bubbles modify the RG flow. For the purpose of performing $SO(1,2)$ hyperbolic translations to investigate this issue, we find it convenient to reformulate the correspondence in the formalism of holographic integral geometry [33][15], which we review in Appendix C, which in the three-dimensional case is particularly fruitful.

Let us begin with a brief review of integral geometry in the hyperbolic plane, since it concerns the specific case of $\text{AdS}_3/\text{CFT}_2$. A more comprehensive review can be found in [33]. In the present context the main object of interest is the topological space of "lines" in an asymptotically $\mathbb{H}^2$ bulk spatial slice, namely the set of extremal curves between two boundary points, which constitutes the kinematic space $\mathcal{K}_2$. It is a two-dimensional surface that has a natural symplectic (or equivalently Lorentzian) structure, the Crofton form, induced from the (finite part of the) length $\mathcal{L}$ of curves in

---

[15]For an earlier work on RG flows and integral geometry, albeit in a different setting, see [165].

$\mathcal{K}_2$ via

$$\omega(u,v) \equiv \frac{\partial^2 \mathcal{L}(u,v)}{\partial u \partial v}\, du \wedge dv = 4G_3 \frac{\partial^2 S_{\text{ent}}(u,v)}{\partial u \partial v}\, du \wedge dv\,, \tag{7.35}$$

where G_3 is the three-dimensional Newton constant and u, v are angular coordinates of the endpoints on the $\mathbb{S}^1$ boundary. The last equality holds assuming the Ryu-Takayanagi formula, and the Crofton form ω also affords an information-theoretic interpretation in terms of mutual conditional information [33]. In addition, one may define an induced Lorentzian metric

$$ds^2_{\mathcal{K}_2} \equiv \frac{\partial^2 \mathcal{L}}{\partial u \partial v}\, du\, dv\,. \tag{7.36}$$

In the case of an AdS$_3$ vacuum, indeed composed of $\mathbb{H}^2$ slices, the Crofton form reduces to

$$\omega_0(u,v) = \frac{L}{2\sin^2\left(\frac{u-v}{2}\right)}\, du \wedge dv\,, \tag{7.37}$$

which is actually the only $SO(1,2)$-invariant 2-form on kinematic space up to rescalings. Indeed, $\omega_0 = \text{vol}_{\text{dS}_2}$ is the volume form on two-dimensional de Sitter space-time[16], and $\mathcal{K}_2^{(0)}$ is naturally endowed with the Lorentzian structure of dS$_2$. For a general deformed metric that is still asymptotically $\mathbb{H}^2_+$ in any constant-time slice, one finds that the corresponding kinematic space is dS$_2^+$ asymptotically, in the limit of large (absolute) de Sitter time t, while the central region of small $|t|$ is modified. In the kinematic picture, which acts as an intermediary, vacuum bubbles translate into deviations of ω from vol_{dS_2}, which are localized around the throat and expand symmetrically in the dS$_2$ past and future as bulk time progresses, establishing in its interior the new dS$_2^-$, of different radius, associated to $\mathbb{H}^2_-$.

The relevance of the above construction comes from a classical theorem of Crofton, which states that the length $\mathcal{L}[\gamma]$ of any (not necessarily geodesic) bulk curve γ can be computed in terms of an area in $\mathcal{K}_2$, namely

---

[16]Some intuition on this stems from the embedding of $\mathbb{H}^2$ in $\mathbb{R}^{1,2}$ as a two-sheeted hyperboloid, where hyperbolic lines arise from intersections with time-like planes through the origin. Such planes are in a one-to-one correspondence with their unit space-like normal vectors, which lie in the dS$_2$ one-sheeted hyperboloid.

$$\mathcal{L}[\gamma] = \frac{1}{4} \int_{\mathcal{K}_2} \omega(\kappa) \, n_{\gamma,\kappa} \tag{7.38}$$

where $n_{\gamma,\kappa}$ is the (signed) intersection number of the curves γ and κ. Hence, excluding shadow effects [166, 167], which are absent in this case, the bulk geometry can be completely reconstructed from the Crofton form, which therefore provides an amount of information equivalent to the full entanglement entropy. Motivated by this remarkable result, we shall henceforth consider $\frac{\omega}{4G_3}$ instead of S_{ent}, since the former is insensitive to the cutoff and contains no divergent part. Indeed, an $SO(1,2)$ isometry translating the bubble behaves unwieldily in the presence of divergent terms: it deforms the cutoff surface which is then to be brought back to its original location. Equivalently, the finite part of S_{ent} is not an $SO(1,2)$ scalar, since the extraction of the finite part is not an invariant procedure. Instead, ω is a finite and covariant two-form. In particular, the ratio[17] to the vacuum dS_2^+ volume form, defined by

$$\omega(u,v) = \Omega(u,v) \, \text{vol}_{\text{dS}_2^+} \,, \tag{7.39}$$

is a finite scalar field on $\mathcal{K}_2$. Therefore, one may exploit this fact to study off-centered bubbles applying $SL(2,\mathbb{R}) \rightarrow SO(1,2)$ transformations to data and conclusions already obtained in the case of a centred bubble, which is displayed in fig. 7.6. In the present setting, these transformations appear in the triplicate role of asymptotic bulk isometries, kinematic symplectomorphisms, and conformal maps restricted to the boundary.

For centered bubbles, Ω only depends on the combination $\theta_A = \frac{u-v}{2}$, the boundary interval half-size[18], and not on the coordinate $\phi = \frac{u+v}{2}$ of the boundary center. $\Omega(\theta_A)$ displays an external δ-function wall corresponding to the injection phase transition that we have described in Section 2.1. Outside the wall $\Omega = 1$, the constant value pertaining to the original vacuum, while inside the wall one finds a smooth dependence approaching the constant value associated to the new vacuum, which is related to the ratio of the cosmological constants, as highlighted in fig. 7.6.

---

[17]This is possible only because ω is a form of top rank in the present case.

[18]In the language of dS_2 geometry, θ_A is diffeomorphic to dS_2 time in closed slicing, and ϕ is the coordinate on the slice.
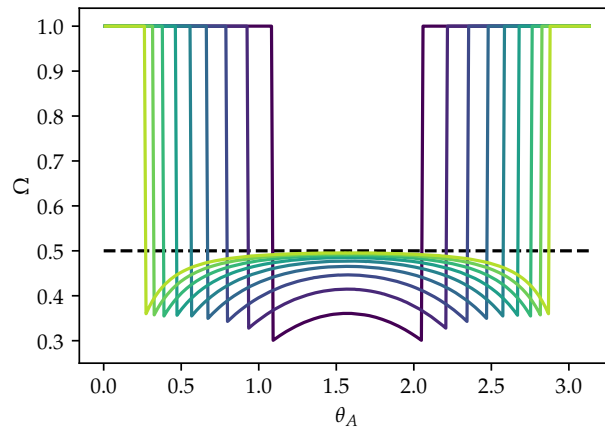
FIGURE 7.6: the relative Crofton factor Ω for a centered bubble as a function of interval size, for increasing values of the bubble radius (dark to light). A cosmological constant ratio of $\frac{1}{2}$ has been chosen as an example, which leads to the limiting values $\Omega_+ = 1, \Omega_- = \frac{1}{2}$. The δ-function wall at the injection phase transition is not depicted.

Shifting the bubble corresponds to a boost in dS_2, which induces a mixing between the θ_A and ϕ coordinates or, more suggestively, between boundary momenta and positions, a feature which we shall discuss in the following section. The δ-function wall in Ω is deformed into an ellipse in dS_2. Intuitively, when the bubble is off-centered, boundary intervals closer to it will begin to be affected at smaller sizes, as displayed fig. 7.8. Hence, the deformed entanglement pattern on the boundary ought to encode this effect in some spatial localization, and ought to evolve under the flow in a manner reminiscent of the corresponding bulk bubble expansion.

4.1 *Off-centered renormalization*

When the symmetries of the bubble geometry are taken into account, it becomes impossible to match the growth of a centered bubble to a standard holographic renormalization procedure, which is typically implemented as a sequence of decimations and rescalings within a Poincaré chart [151–153]. Poincaré rescalings do not map to an isometry of a centered bubble, which instead has an $SO(2)$ subgroup of rotational isometries. We propose that, instead, the precise prescription for a centered bubble is a renormalization procedure that respects this rotational symmetry, and is schematically implemented as a decimation and rescaling of the angular ϕ coordinate. Since the radius of the boundary circle shrinks under such an RG flow, and would naively

vanish in an infinite RG time, this ought to be counteracted by a preemptive blowup of the circle in the original, undeformed CFT$_+$. As a result, one should explore simultaneous limits of initial blowup and total RG flow time. We conjecture that theories with a holographic bulk dual do not degenerate under this limit and approach a non-trivial infrared CFT$_-$, which would reflect the existence of a stable final AdS$_-$ classical vacuum in the bulk. However, let us stress that in the string-theoretic settings that we have in mind no AdS is completely stable, except for the supersymmetric cases, but their instabilities are suppressed in a suitable large-N limit. At a result, the dual RG trajectories ought to approach the corresponding fixed points, enter a walking regime, and then flow away. In addition, if one imagines to extend the proposed "bubbleography" correspondence to cases in which tunneling to bubbles of nothing [105] can occur, the preceding discussion implies that such scenarios would conceivably lead to trivial endpoints of the dual RG flow: in this context, the expansion would leave behind an AdS geometry of vanishing radius. Indeed, as we have discussed in Chapter 5, within meta-stable flux landscapes bubbles of nothing can arise as limits in which all of the original flux is discharged [108]. For previous discussions on the holographic interpretation of bubbles of nothing, see [168–170].

At any rate, a "central" renormalization procedure respecting the rotational symmetry would allow one to define a renormalization step for off-centered bubbles simply as the "central" RG step conjugated by the $SO(1,2)$ isometry that shifts the bubble, as depicted in fig. 7.7. Analogously, bubble nucleation should again correspond to a relevant deformation, up to the same $SO(1,2)$ conjugation. Equivalently, there ought to be a boundary picture in which the deformation is space-dependent[19], and the RG flow proceeds also partially in position space. In addition, one may conceive multiple bubble nucleations occurring within the time frame of a single expansion. This should allow for the construction of a larger and diverse family of deformations and RG flows from CFT$_+$ to CFT$_-$, since the characteristic step-like behavior of c-functions provides a natural building block for a variety of scenarios.

---

[19]A simpler instance can be realized in a theory with a space-dependent running cutoff scale $\Lambda(x)$.
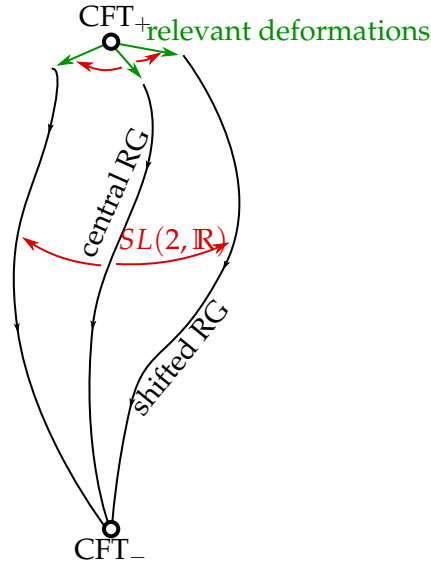
FIGURE 7.7: a schematic depiction of a family of relevant deformations followed by the respective RG flows, all connected by $SL(2, \mathbb{R})$ transformations.

Recovering Poincaré flows

A bubble translated infinitely far away from the origin, with its radius R suitably rescaled in such a way that the wall remains at a finite distance from the origin[20], is a limiting case of particular interest. This is actually, in a sense, the most likely scenario, since tunneling is favored by the exponentially large bulk volume fraction that lies far away from the origin for large cutoff. In the limit, the bubble wall becomes a traveling horocycle, and the corresponding dual RG flow reflects the standard holographic RG procedure in Poincaré coordinates. Indeed, the horocyclic bubble at each time is precisely a curve of constant z in a Poincaré chart.

   To conclude this discussion, let us present a computation of a holographic correlator in Poincaré coordinates, since the resulting expressions simplify to a large extent, using two patches glued along the Minkowski slices $\{z_\pm = z_\pm^*\}$, with $\frac{z_+^*}{L_+} = \frac{z_-^*}{L_-}$. Specifically, let us consider a spectator free scalar field ϕ of mass m, which ought to be dual to some scalar operator $\mathcal{O}$ in the boundary theory, probing a d-dimensional thin-wall bubble geometry, and let us compute the two-point correlator of $\mathcal{O}$ holographically. While the ensuing computation is Euclidean[21], and thus not qualitatively

---

[20]This limit is certainly sensible, since for bubbles in AdS the radius R becomes infinite in a finite coordinate time t, and can thus be made arbitrarily large with a small time translation. This is displayed in the bottom-right numerical plot of fig. 7.8.

[21]For a Lorentzian computation, and a discussion of its connection to eternal inflation, see [171].
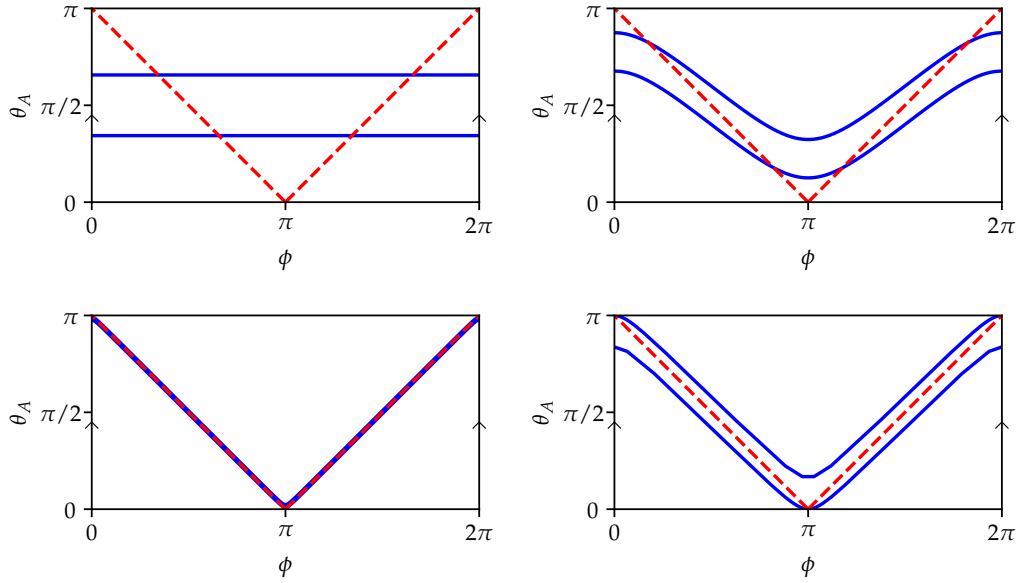
FIGURE 7.8: the δ-function wall in the Crofton factor Ω, the locus of the injection phase transition (blue), depicted in $\mathcal{K}_2$ using the (θ_A, ϕ) chart, which is conformal for dS$_2$. In all cases $\rho_+ = 0.5$, $L_+/L_- = 0.5$. Upper left: for a centered bubble. Upper right: after an $SO(1,2)$ boost with $\beta = 0.8$, which introduces a dependence on ϕ. Bottom left: after a $\beta = 0.999$ boost, the walls converge to the marked lightcone (red). Bottom right: again $\beta = 0.999$, but with a suitable rescaling of ρ_-.

different from standard holographic RG computations, the position $z_\pm^*$ of the thin-wall bubble is arbitrary on symmetry grounds, and therefore one can analyze how the resulting correlator flows varying it. Since the physical nucleation radius of the bubble is parametrically large in the semi-classical limit, this picture is expected to describe at least a sizeable fraction of the corresponding RG flow. To begin with, one can verify that matching the values and the derivatives

$$\phi_+(p, z_+^*) = \phi_-(p, z_-^*),$$

$$\left(\sqrt{g^{z_+ z_+}}\, \partial_{z_+} \phi_+\right)_{z_+ = z_+^*} = \left(\sqrt{g^{z_- z_-}}\, \partial_{z_-} \phi_-\right)_{z_- = z_-^*},$$

(7.40)

on account of the relevant gluing of tangent spaces, implies that the on-shell action is, as usual, given by the boundary term

$$S_E^{\text{on-shell}} = \frac{1}{2} \int \frac{d^{d-1}p}{(2\pi)^{d-1}} \left(\frac{L_+}{\epsilon}\right)^{d-2} \phi_+(-p, \epsilon)\, (\partial_{z_+} \phi_+(p, z_+))_{z_+ = \epsilon}.$$

(7.41)

The equation of motion can be solved in both patches in terms of modified Bessel functions. Imposing regularity at the center of AdS_{d+1}, the general solution

$$\phi_+(p,z_+) = a_p^+ \, z_+^{\frac{d-1}{2}} \, K_{\nu_+}(pz_+) + b_p^+ \, z_+^{\frac{d-1}{2}} \, I_{\nu_+}(pz_+),$$
$$\phi_-(p,z_-) = a_p^- \, z_-^{\frac{d-1}{2}} \, K_{\nu_-}(pz_-), \tag{7.42}$$

where $\nu_\pm \equiv \sqrt{m^2 L_\pm^2 + \frac{(d-1)^2}{4}}$, is fixed by the two matching conditions and the Dirichlet boundary condition

$$\phi_+(p,\epsilon) = \varphi_\epsilon(p) \tag{7.43}$$

imposed at the regularized boundary $z_+ = \epsilon$. These three conditions result in a linear system, and substituting the result in the on-shell action yields

$$S_E^{\text{on-shell}} = \frac{1}{2} \int \frac{d^{d-1}p}{(2\pi)^{d-1}} \frac{L_+^{d-2}}{\epsilon^{d-1}} \, \varphi_\epsilon(-p) \, \varphi_\epsilon(p) \, (p\epsilon) \, D_{K,+}(p\epsilon)$$
$$\times \frac{1 - \frac{D_{I,+}(p\epsilon) \, I_{\nu_+}(p\epsilon)}{D_{K,+}(p\epsilon) \, K_{\nu_+}(p\epsilon)} \mathcal{F}}{1 - \frac{I_{\nu_+}(p\epsilon)}{K_{\nu_+}(p\epsilon)} \mathcal{F}}, \tag{7.44}$$

where we have defined

$$D_{K,\pm}(z) \equiv \frac{d}{dz} \log \left(z^{\frac{d-1}{2}} \, K_{\nu_\pm}(z) \right),$$
$$D_{I,\pm}(z) \equiv \frac{d}{dz} \log \left(z^{\frac{d-1}{2}} \, I_{\nu_\pm}(z) \right), \tag{7.45}$$
$$\mathcal{F} \equiv \frac{K_{\nu_+}(pz_+^*)}{I_{\nu_+}(pz_+^*)} \frac{D_{K,+}(pz_+^*) - D_{K,-}(pz_-^*)}{D_{I,+}(pz_+^*) - D_{K,-}(pz_-^*)}$$

for convenience. Finally, we expect that using suitably normalized sources

$$\varphi(p) \equiv \epsilon^{\nu_+ - \frac{d-1}{2}} \, \varphi_\epsilon(p) \tag{7.46}$$

the continuum limit $p\epsilon \to 0$ exists[22], since the theory flows to a CFT. Indeed, the leading-order terms yield the standard result, corresponding to the UV CFT$_+$, accompanied by a finite correction, proportional to $\mathcal{F}$. For large $pz_\pm^*$ the correction is exponentially suppressed and corresponds to the bubble far away from the boundary,

---

[22]Apart from the usual divergent contact terms.

while for small $pz_\pm^*$ it produces the correlator of the IR CFT$_-$, with L_- replacing L_+ up to a finite wave-function renormalization.

In the fraction appearing in the second line of eq. (7.44) each coefficient of $\mathcal{F}$ tends to zero in the continuum limit, and thus making use of the expansions

$$I_\nu(z) \overset{z \to 0}{\sim} \frac{1}{\Gamma(1+\nu)} \left(\frac{z}{2}\right)^\nu ,$$

$$K_\nu(z) \overset{z \to 0}{\sim} \begin{cases} \frac{\Gamma(\nu)}{2} \left(\frac{z}{2}\right)^{-\nu} - \frac{\Gamma(1-\nu)}{2\nu} \left(\frac{z}{2}\right)^\nu , & \nu \notin \mathbb{N} \\ \frac{\Gamma(\nu)}{2} \left(\frac{z}{2}\right)^{-\nu} - \frac{(-1)^\nu}{\Gamma(1+\nu)} \left(\frac{z}{2}\right)^\nu \log \left(\frac{z}{2}\right) , & \nu \in \mathbb{N} \end{cases} , \qquad (7.47)$$

valid for $\nu > 0$, the correlator evaluated in the UV CFT$_+$ reads

$$\langle \mathcal{O}(p)\mathcal{O}(q) \rangle_+ = -L_+^{d-2} \left(pz_+^*\right)^{2\nu_+} \times \begin{cases} 2^{1-2\nu_+} \frac{\Gamma(1-\nu_+)}{\Gamma(\nu_+)} , & \nu_+ \notin \mathbb{N} \\ \frac{(-1)^{\nu_+} 2^{2(1-\nu_+)}}{\Gamma(\nu_+)^2} \log \left(pz_+^*\right) , & \nu_+ \in \mathbb{N} \end{cases} , \qquad (7.48)$$

in terms of the RG scale z_+^*, where we have suppressed the momentum-conserving δ-function $(2\pi)^{d-1} \delta^{(d-1)}(p+q)$ while evaluating the integrand of eq. (7.44) yields the correction

$$L_+^{d-2} \left(\frac{z_+^*}{\epsilon}\right)^{2\nu_+} \frac{I_{\nu_+}(p\epsilon)}{K_{\nu_+}(p\epsilon)} (p\epsilon) \left(D_{K,+}(p\epsilon) - D_{I,+}(p\epsilon)\right) \mathcal{F}$$
$$\overset{\epsilon \to 0}{\to} -L_+^{d-2} \left(pz_+^*\right)^{2\nu_+} \frac{2^{2(1-\nu_+)}}{\Gamma(\nu_+)^2} \mathcal{F} \qquad (7.49)$$

in both massless and massive cases, where we have suppressed the δ-function for clarity. All in all, one obtains the relative deviation

$$\frac{\delta \langle \mathcal{O}(p)\mathcal{O}(q) \rangle_{z_+^*}}{\langle \mathcal{O}(p)\mathcal{O}(q) \rangle_+} = \mathcal{F}\left(pz_+^* ; \frac{L_-}{L_+}\right) \times \begin{cases} \frac{2}{\pi} \sin \nu_+ \pi , & \nu_+ \notin \mathbb{N} \\ \frac{(-1)^{\nu_+}}{\log\left(pz_+^*\right)} , & \nu_+ \in \mathbb{N} \end{cases} , \qquad (7.50)$$

where we have once again suppressed the δ-functions and we have highlighted the dependence on the RG scale. Neglecting contact terms, for large pz_+^*, which corresponds to the bubble far away from the boundary, the correction decays exponentially, while for small pz_+^*, which corresponds to the bubble close to the boundary, the correlator reconstructs the one pertaining to the IR CFT$_-$, namely eq. (7.48) upon replacing L_+ with L_-, and in the massive case

5   B R A N E   D Y N A M I C S :   H O L O G R A P H I C   P E R S P E C T I V E

The identification of the relevant deformation of the original CFT_+ corresponding to the nucleation event remains an important open problem. Explicit "top-down" realizations of the scenario that we have discussed in this chapter should be relevant in order to address it, since they typically bring along a more transparent description of the corresponding holographic duals. This could also provide an additional handle to perform more in-depth analyses of the RG flow studying, for instance, the scaling of correlation functions in the spirit of the preceding section. In principle, one could expect that such a relevant deformation be related to the decay width (per unit volume) associated to the tunneling process, which can be computed via standard techniques in the semi-classical limit [98–100] as we have discussed in Chapter 5. Indeed, in the classical limit tunneling is completely suppressed, and the starting point of the flow ought to approach the original CFT_+, which remains fixed. In addition, the study of correlation functions and of the stress-energy tensor in the presence of off-centered and multi-bubble configurations could provide further insights: since bubbles entail deformations of the metric regardless of their origin, we are tempted to speculate that a sizeable contribution to the corresponding relevant deformation arises from the boundary stress-energy tensor. This picture resonates with recent results on $T\overline{T}$ deformations [172, 173] dual to hard-cutoff AdS_3 geometries [174–176], but in explicit "top-down" constructions involving non-supersymmetric string models, such as the ones described in Chapter 2, one expect additional contributions to arise from fluxes.

The emergence of an AdS geometry in models of this type suggests that a dual CFT description should in principle arise from non-supersymmetric brane dynamics, and that it ought to encode gravitational instabilities in a holographic fashion. In particular, the perturbative instabilities explored in [27, 90] and in Chapter 4 should correspond to operators with complex anomalous dimension [91, 177], so that a holographic description may be able to ascertain whether their presence persists for small values of n. On the other hand, the putative CFT deformations corresponding to non-perturbative instabilities should be "heavy", since their effect is suppressed in

the large-*n* limit. Starting from the brane picture that we have developed in the preceding chapters, one can expect that the CFT duals to the AdS flux compactifications described in Chapter 3 be related to a gauge theory living on the world-volume of the corresponding brane stacks. In particular, considering N parallel D1-branes in the orientifold models, so that the flux $n \propto N$, this would translate into a realization of the $\text{AdS}_3/\text{CFT}_2$ duality in a non-supersymmetric setting. The associated central charge, determined by the Brown-Henneaux formula [138], would be

$$c = \frac{3L}{2G_3} = \frac{12\pi\,\Omega_7}{\kappa_{10}^2}\,L\,R^7 \propto N^{\frac{3}{2}}\,. \tag{7.51}$$

This grows more slowly than N^2, the classical number of degrees of freedom present in the gauge theory[23]. This suggests that such a two-dimensional CFT arises as a non-trivial infra-red fixed point of a world-volume gauge theory which ought to be strongly-coupled, at least at large N, since the effective number of degrees of freedom is parametrically smaller with respect to the classical scaling. Indeed, the corresponding 't Hooft coupling $g_s\,N \propto N^{\frac{3}{4}} \gg 1$. Within this picture, perturbative instabilities can be expected to arise from world-volume deformations, described by world-volume scalar fields. Moreover, the brane-flux annihilation scenario described in the preceding chapters suggests that the non-perturbative instabilities should reflect the expulsion of branes from the point of view of the stack, so that in the language of the dual gauge theory the gauge group would break according to [111, 178]

$$\begin{aligned}
U(N) &\rightarrow U(N - \delta N) \times U(\delta N)\,, \\
USp(2N) &\rightarrow USp(2N - 2\delta N) \times USp(2\delta N)
\end{aligned} \tag{7.52}$$

in the two orientifold models[24]. However, this breaking would not arise from a Higgsing, since the initial expectation value attained by scalars would be driven to evolve by instabilities. Therefore, "Higgsing" via the separation of a small number of branes from the stack constitutes a natural candidate for the relevant deformation of the CFT, since it is not protected and may in principle grow in the infra-red. This

---

[23]More precisely, in general it is the order of the classical number of degrees of freedom for large N.

[24]Here we assume that the gauge group be unbroken in the vacuum. If not, the breaking pattern is modified accordingly.

is consistent with the considerations in [179], where the world-volume theory of a spherical brane contains a classically marginal coupling proportional to $\frac{1}{N}$, and it gives rise to a "Fubini instanton" that implements the mechanism. Characterizing precisely the relevant deformation, if any, dual to the flux tunneling process would in principle allow one to test the "bubble/RG" proposal of [109] that we shall describe in the following, and more importantly it would shed some light on the behavior of the system at small N, at least in the case of D1-branes where the dual gauge theory would be two-dimensional. In particular, the in $USp(32)$ orientifold model the relevant gauge theory would arise as a projection of a supersymmetric one, thereby potentially allowing it to retain some properties of the parent theory [180–186, 197]. We intend to pursue this possibility in a future work, but for the time being let us collect a few considerations about this gauge theory.

To begin with, the background in which the branes are placed ought to correspond to the flux-less limit of the back-reacted geometry that we have described in Chapter 6. However, in the absence of supersymmetry the resulting geometry appears out of reach, and in particular there is no Minkowski solution to take its place as in supersymmetric cases. On the other hand, introducing $N_8 \gg 1$ 8-branes sourcing the static Dudas-Mourad geometry discussed in Chapter 3, one can expect that placing $N \gg N_8$ D1-branes in the controlled region described in Chapter 6 would result in a back-reaction dominated by them, at least locally, and the force exerted by the branes should affect the system only on parametrically large time scales. If this construction is reliable, a decoupling argument along the lines of [4] should result in a two-dimensional world-volume gauge theory on flat space-time, whose perturbative spectrum has been described in [19]. At low energies, the corresponding effective action S_{D1} is expected to arise from a projection of the parent type IIB $U(2N)$ gauge theory, at least for large N [180] where the influence of the supersymmetry-breaking sources ought to be subleading in some respects. Thus schematically[25]

$$
\begin{aligned}
S_{\mathrm{D1}}^{E} = \frac{1}{g_{\mathrm{YM}}^2} \operatorname{Tr} \int d^2\zeta \bigg(& (\partial_+ A_-)^2 + \partial_+ X_i \left[\mathcal{D}_- , X_i \right] + \frac{1}{2} \left[X_i , X_j \right] \left[X_i , X_j \right] \\
& + \psi_+ \left[\mathcal{D}_- , \psi_+ \right] + \psi_- \partial_+ \psi_- + \psi_- \Gamma_i \left[X_i , \psi_+ \right] + \lambda_-^A \partial_+ \lambda_-^A \bigg)
\end{aligned}
\tag{7.53}
$$

---

[25]For analogous considerations on the type I superstring, see [187].

in the (Euclidean) light-cone gauge $A_+ = 0$. In contrast to the supersymmetric cases, the scalars X_i which comprise a vector of the transverse rotation group $SO(8)$ are in the anti-symmetric representation of $USp(2N)$, while the adjoint is symmetric and the world-volume fermion ψ_+ (resp. ψ_-) is in the symmetric (resp. anti-symmetric) representation and is a $SO(8)$ spinor. The λ_-^A are bifundamental fermions of $USp(2N) \times USp(2N_f)$ with $N_f = 16$ "flavors", and arise from (massless modes of) open strings stretching between the D1-branes and the $\overline{\text{D9}}$-branes. Conveniently, in the light-cone gauge ghosts are decoupled in two dimensions [188], and the gauge field can be integrated out exactly leading to a non-local effective action. At any rate, the theory is expected to flow to a strongly-coupled regime in the IR. Indeed, while in the absence of supersymmetry the couplings are expected to renormalize in a complicated fashion, the one-loop β function of the gauge coupling depends only on the (perturbative) matter content. In order to compute it, let us recall that the corresponding four-dimensional expression

$$\beta_{4d} = b_1 \frac{g_{\text{YM}}^3}{16\pi^2} \tag{7.54}$$

arises from the (dimension-independent) a_4 coefficient in the heat-kernel expansion of the one-loop functional determinant [189], which in the two-dimensional case would contribute to the bare coupling g_0 according to

$$\frac{1}{g_0^2} = \frac{1}{g_{\text{YM}}^2} - \frac{b_1}{4\pi} \frac{1}{2\Lambda_{\text{UV}}^2}. \tag{7.55}$$

The resulting two-dimensional one-loop β function of the dimensionless coupling $g_{\text{YM}} \equiv \widehat{g} \, \Lambda_{\text{UV}}$ is then

$$\widehat{\beta}_{2d} = -\widehat{g} + \frac{b_1}{4\pi} \widehat{g}^3, \tag{7.56}$$

with [190, 191]

$$b_1 = \frac{25 \, N + 2 \, N_f - 15}{3} \tag{7.57}$$

and therefore the gauge coupling eventually flows to a strongly-coupled region, which could exhibit confinement or screening [192]. On the other hand, the IR behavior of the gauge coupling should reflect the radial perturbations for the dilaton described in

Chapter 6, and in particular power-like perturbations $\phi \propto (-r)^{-\lambda}$ to the fixed point would translate into

$$\widehat{\beta}_{\text{IR}} = (2\lambda - 1)(\widehat{g} - \widehat{g}^*) \tag{7.58}$$

on account of the Poincaré scale-setting

$$-(p+1)\, r \;\mapsto\; z^{p+1} \;\mapsto\; \mu^{-(p+1)} \,. \tag{7.59}$$

While this scenario appears daunting, integrating out the gauge field yields an effective action with scalar and fermion couplings that are at most quartic, and thus potentially amenable to large-N Hubbard-Stratonovich techniques [193, 194] and non-Abelian bosonization [195][26]. At the one-loop level, choosing a "geometric" background in which $X_k = g_{\text{YM}} \frac{i\Omega}{\sqrt{2N}} x_k$ belongs to the (symplectic-trace) singlet, the resulting quadratic action for fluctuations $\delta X_i \equiv \delta X_i^a\, t_a$, decomposed in an orthogonal basis $\{t_a\}$ of the space of (imaginary) anti-symmetric matrices, takes the form

$$S_{\text{D1}}^{(2)} = \int d^2\zeta \left(\partial_+ \delta X_i^a\, \partial_- \delta X_i^a + \frac{1}{2}\, \delta X_i^a \left(M^2\right)_{ij}^{ab} \delta X_j^b \right) , \tag{7.60}$$

where the fermionic terms decouple because $\text{Tr}\,(\psi_-\,[\Omega, \psi_+]) = 0$ splits into (vanishing) inner products of the anti-symmetric matrix ψ_- and the symmetric matrices $\Omega\,\psi_+$, $\psi_+\,\Omega$. The (negative semidefinite) mass matrix

$$\left(M^2\right)_{ij}^{ab} = -\frac{g_{\text{YM}}^2}{N} \left(x_i\, x_j + x^2\, \delta_{ij}\right) \omega_{ab}\,, \qquad \omega_{ab} \equiv \text{Tr}\,([\Omega, t_a]\,[\Omega, t_b]) \tag{7.61}$$

arises from the quartic potential of eq. (7.53), and one is thus led to the one-loop effective potential

$$V_{\text{D1}}^{(1)} = \frac{1}{2}\, \text{Tr} \int \frac{d^2 p}{(2\pi)^2}\, \log(p^2 + M^2) \,. \tag{7.62}$$

Since ω has 4 and 0 as eigenvalues, letting μ_4 denote the multiplicity of the former, which scales at most as N^2, reflecting typical tree-level scalings, one obtains

$$V_{\text{D1}}^{(1)} = \frac{\mu_4}{8\pi} \int_{\Lambda_{\text{IR}}^2}^{\Lambda_{\text{UV}}^2} ds \left[\log\left(s - \frac{8\, g_{\text{YM}}^2 x^2}{N}\right) + 7 \log\left(s - \frac{4\, g_{\text{YM}}^2 x^2}{N}\right) \right] \tag{7.63}$$

---

[26]For recent results on bosonization in the three-dimensional case, see [196].

up to constant zero-mode contributions, and the Wick rotation prescribes a deformation of the integration contour. The perturbative regime translates into the condition $\widehat{g}^2 x^2 \ll N$, so that

$$V_{\text{D1}}^{(1)} \sim -\frac{9\mu_4}{\pi}\frac{g_{\text{YM}}^2 x^2}{N}\log\left(\frac{\Lambda_{\text{UV}}}{\Lambda_{\text{IR}}}\right) \tag{7.64}$$

shows a repulsive behavior. This result is consistent with our preceding considerations, according to which subleading $\frac{1}{N}$ corrections would then encode the relevant deformation that we seek, while, as expected, for $N = 1$ the (gauge singlet) scalars decouple, and thus their effective potential receives no corrections even beyond the one-loop level. As a final remark, let us mention that one could conceive compactifications on Einstein manifolds with non-trivial lower-dimensional cycles, which undergo semi-classically identical flux tunneling processes. In this case, wrapped branes could generate baryon-like Pfaffian operators [11, 178] in the gauge theory, which are additional candidates for relevant deformations dual to non-perturbative instabilities. However, one may anticipate that this setting could bring along subtleties due to the Myers effect [11, 116].

To conclude, we can comment on some potential implications. At present, vacuum stability in quantum gravity poses significant theoretical challenges, even at the semiclassical level. Hence, classifying criteria for stability appears of primary importance, and some properties that stable (classical) vacua should possess have already surfaced, a prime example being the weak gravity conjecture [18]. As explained in [16, 127, 128], it appears that if such a stability criterion holds, nucleation events should continue to occur at least until a supersymmetric AdS classical vacuum is reached. This is because, in the supersymmetric case, stability prevents tunneling, and only domain walls can be present [198–201]. In the RG picture that we have presented the stable IR endpoint of the flow would then be supersymmetric, which resonates with the phenomenon of emergent supersymmetry in some condensed matter systems[27]. It would be interesting to explore whether the framework that we have described in this chapter can be used as a tool to address vacuum stability in more intricate contexts from the perspective of better-understood RG flows, which can then be approached with powerful analytic and numerical techniques.

---

[27]See e.g. [202] or, for a modern review, [203], and references therein.

de Sitter cosmology: no-gos and brane-worlds

In this chapter we complete the discussion on dS flux compactifications that we have introduced in Chapter 3, where we have shown that Freund-Rubin de Sitter compactifications are either ruled out or unstable in low-energy effective theories with exponential potentials. While the results of our analysis resonate with the ones of [75], one could wonder whether similar conditions hold for more general dS settings, e.g. for fluxes threading cycles of complicated internal manifolds. To this end, in Section 1 we examine general warped flux compactifications, along the lines of [204], and we obtain conditions that fix the (sign of the) resulting cosmological constant in terms of the parameters of the model, generalizing the results of [34] to models with exponential potentials. Then, in Section 2 we include the contribution of localized sources, which leads to a generalized expression for the cosmological constant. The resulting sign cannot be fixed *a priori* in the entire space of parameters, but one can derive sufficient conditions that exclude dS solutions for certain ranges of parameters. In Section 3 we discuss how our results connect to recent swampland conjectures [17], showing that the ratio $\frac{|\nabla V|}{V}$ is bounded whenever $V > 0$. Finally, in Section 4 we review a recent proposal [35–37] which rests on the observation that branes nucleating amidst AdS $\rightarrow$ AdS transitions host dS geometries on their world-volume.

The issue of dS configurations in string theory has proven to be remarkably challenging, to the extent that the most well-studied constructions [12] have been subject to thorough scrutiny and discussion. We shall not attempt to provide a comprehensive account of this extensive subject and its state of affairs, since our focus in the present case lies in higher-dimensional approaches [13–15, 205–207] and, in particular, in the search for new solutions [208–211]. Specifically, the issue at stake is whether the ingredients provided by string-scale supersymmetry breaking can allow for dS compactifications. While a number of parallels between lower-dimensional anti-brane uplifts and the ten-dimensional BSB scenario discussed in Chapter 2

appear encouraging to this effect, as we shall see shortly the presence of exponential potentials does not ameliorate the situation, insofar as (warped) flux compactifications are concerned. On the other hand, as we shall explain in Section 4, the very presence of exponential potentials allows for intriguing brane-world scenarios within the AdS landscapes discussed in Chapter 3, whose non-perturbative instabilities, addressed in Chapter 5, play a crucial rôle in this respect.

1   WARPED FLUX COMPACTIFICATIONS: NO-GO RESULTS

In order to address the problem of dS solutions to low-energy effective theories with exponential potentials, let us consider a compactification of the D-dimensional theory discussed in Chapter 3 on a d_Y-dimensional closed manifold Y parametrized by coordinates y^i, while the d_X-dimensional space-time is parametrized by coordinates x^μ. Excluding the Freund-Rubin compactifications, which we have already described in 3, in the models of interest the space-time dimension does not match the rank of the form field strength, and thus there cannot be any electric flux. Since at any rate one can dualize the relevant forms, we shall henceforth work in the magnetic frame, which in our convention involves a q-form field strength with the coupling $f(\phi) = e^{-\alpha\phi}$ to the dilaton, and we shall seek configurations where H_q is supported on Y, and where each field only depends on the y^i. Writing the metric

$$ds^2 = e^{2bu(y)}\,\widehat{ds}^2(x) + e^{2u(y)}\,\widetilde{ds}^2(y)\,, \tag{8.1}$$

with $b = -\frac{d_Y}{d_X-2}$ in order to select the d_X-dimensional Einstein frame, one finds that sufficiently well-behaved functions $f(y)$ satisfy

$$\int_Y d^{d_Y}y\sqrt{\widetilde{g}}\,e^{2bu(y)}\,\Box_D f(y) = 0\,,$$
$$\int_Y d^{d_Y}y\sqrt{\widetilde{g}}\,\Delta_Y f(y) = 0\,, \tag{8.2}$$

where $\Box_D$ and Δ_Y denote the D-dimensional d'Alembert operator and the Laplacian operator on Y respectively. Furthermore, let us define

$$
\begin{aligned}
\mathcal{I}_V &\equiv \int_Y d^{d_Y} y \sqrt{\widetilde{g}}\, e^{2bu(y)}\, V > 0\,, \\
\mathcal{I}_H &\equiv \int_Y d^{d_Y} y \sqrt{\widetilde{g}}\, e^{2bu(y)}\, \frac{f}{q!}\, H_q^2 > 0
\end{aligned}
\tag{8.3}
$$

for convenience. Using these relations, integrating the equation of motion for the dilaton yields

$$
\mathcal{I}_H = \frac{2\gamma}{\alpha}\, \mathcal{I}_V\,,
\tag{8.4}
$$

while employing the formula for warped products discussed in Chapter 5, the space-time Ricci tensor takes the form

$$
\begin{aligned}
R_{\mu\nu} &= \widehat{R}_{\mu\nu} - b\, e^{-2u}\left(\Delta_Y u - \frac{2(D-2)}{d_X-2}\,|\nabla u|^2\right) g_{\mu\nu} \\
&= \widehat{R}_{\mu\nu} - \frac{d_Y}{2(D-2)}\, e^{-2bu}\, \Delta_Y\left(e^{-\frac{2(D-2)}{d_X-2}u}\right).
\end{aligned}
\tag{8.5}
$$

Hence, assuming a maximally symmetric space-time with $\widehat{R}_{\mu\nu} = \frac{2\Lambda}{d_X-2}\,\widehat{g}_{\mu\nu}$, integrating the space-time Einstein equations finally yields

$$
\begin{aligned}
\mathrm{vol}(Y)\,\Lambda &= \frac{d_X-2}{2(D-2)}\left(\mathcal{I}_V - \frac{q-1}{2}\,\mathcal{I}_H\right) \\
&= \frac{d_X-2}{2(D-2)}\left(1 - (q-1)\,\frac{\gamma}{\alpha}\right)\mathcal{I}_V\,,
\end{aligned}
\tag{8.6}
$$

where $\mathrm{vol}(Y) \equiv \int_Y \sqrt{\widetilde{g}}$ is the (unwarped) volume of Y. This result[1] shows that the existence condition for de Sitter Freund-Rubin compactifications actually extends to general warped flux compactifications as well, thus excluding this class of solutions for the string models that we have studied in the preceding chapters.

---

[1] As we have anticipated, eq. (8.6) can be thought of as a generalization of the no-go results of [34] to models with exponential potentials.

2 INCLUDING LOCALIZED SOURCES

Let us now add localized sources to the warped compactifications, in the spirit of [204]. For the sake of generality, let us consider a localized source with an $(m+1)$-dimensional world-volume. We shall describe its dynamics in terms of an effective action of the form

$$
\begin{aligned}
S_{\text{loc}} &= -\int_{\mathcal{W}} d^{m+1}\zeta \sqrt{-j^{*}g}\, \tau(\phi) \\
&= -\int d^{D}x \sqrt{-g}\, \tau(\phi)\, \delta_{\mathcal{W}},
\end{aligned}
\tag{8.7}
$$

where $j : \zeta \mapsto X(\zeta)$ denotes the space-time embedding of the $(m+1)$-dimensional world-volume $\mathcal{W}$ parametrized by coordinates ζ^{a},

$$
\delta_{\mathcal{W}} \equiv \int_{\mathcal{W}} d^{m+1}\zeta \left(\frac{\sqrt{-j^{*}g}}{\sqrt{-g}} \right) \delta^{(D)}\left(x - X(\zeta)\right),
\tag{8.8}
$$

and we have omitted Wess-Zumino terms, since they would not contribute to the relevant equations of motion[2]. In addition, we shall assume that the tension $\tau(\phi) = T_{m}\, e^{-\sigma\phi}$ is exponential in the dilaton. In terms of a projector Π, defined by

$$
(j^{*}g)_{ab}\, \delta(j^{*}g)^{ab} = \Pi_{MN}\, \delta g^{MN},
\tag{8.9}
$$

the associated (trace-reversed) stress-energy tensor reads

$$
\widetilde{T}^{\text{loc}}_{MN} = \left(-\frac{1}{2}\, \Pi_{MN} + \frac{m+1}{2(D-2)}\, g_{MN} \right) \tau(\phi)\, \delta_{\mathcal{W}}.
\tag{8.10}
$$

In the static gauge the coordinates $x^{M} = (x^{a}, x^{i})$ are divided in longitudinal and transverse directions relative to the world-volume, and the embedding is written as $X^{M}(\zeta) = (\zeta^{a}, x_{0}^{i})$, where x_{0} specifies the position of the source in the transverse space. In this gauge, $(j^{*}g)_{ab} = g_{ab}$ and thus $\Pi_{MN} = g_{ab}\, \delta^{a}_{M}\, \delta^{b}_{N}$.

In order for the theory to admit solutions where space-time is maximally symmetric, we shall further assume that $m+1 \geq d_{X}$, and that the localized source fills

---

[2]We have neglected the equation of motion of the form field, since it is not involved in the derivation of the no-go result.

space-time. Then, integrating the equation of motion for the dilaton then yields

$$\gamma \, \mathcal{I}_V - \frac{\alpha}{2} \, \mathcal{I}_H - \sigma \, T_m \, \mathcal{I}_{\mathrm{loc}} = 0 \,, \tag{8.11}$$

where

$$\mathcal{I}_{\mathrm{loc}} \equiv \frac{2\kappa_D^2}{T_m} \int d^{d_Y} y \sqrt{\widetilde{g}} \, e^{2bu(y)} \, \tau \, \delta_{\mathcal{W}} > 0 \,, \tag{8.12}$$

while integrating the space-time Einstein equations in the static gauge finally yields

$$
\begin{aligned}
\mathrm{vol}(Y) \, \Lambda &= \frac{d_X - 2}{2(D-2)} \left(\mathcal{I}_V - \frac{q-1}{2} \, \mathcal{I}_H - \frac{D-m-3}{2} \, T_m \, \mathcal{I}_{\mathrm{loc}} \right) \\
&= \frac{d_X - 2}{2(D-2)} \Bigg[\left(1 - (q-1) \, \frac{\gamma}{\alpha} \right) \mathcal{I}_V \\
&\quad + \left((q-1) \, \frac{\sigma}{\alpha} - \frac{D-m-3}{2} \right) T_m \, \mathcal{I}_{\mathrm{loc}} \Bigg] \,.
\end{aligned} \tag{8.13}
$$

Adding multiple localized sources amounts to summing their contributions[3], and the possible values of T_m and σ within a given model allow one to derive sufficient conditions that exclude de Sitter solutions. Namely, recasting eq. (8.13) in terms of any combination of the integrals $\mathcal{I}_V$, $\mathcal{I}_H$ and $\mathcal{I}_{\mathrm{loc}}$ and requiring that their coefficients be non-positive is sufficient to exclude dS solutions.

3 RELATIONS TO SWAMPLAND CONJECTURES

Let us now comment on whether our results support the recent conjectures concerning the existence of dS solutions in string theory [17]. Extending the arguments of Chapter 3 to the effect that dS Freund-Rubin compactifications are unstable in the dilaton-radion sector, let us recall the corresponding (magnetic-frame) effective potential, whose relevant features are highlighted in fig. 8.1 (resp. fig. 8.2) for the orientifold models (resp. for the heterotic model), reads

$$\mathcal{V}(\phi, \psi) = V(\phi) \, e^{-\frac{2q}{p}\psi} - \frac{q(q-1)}{R^2} \, e^{-\frac{2(D-2)}{p}\psi} + \frac{n^2}{2R^{2q}} \, f(\phi) \, e^{-\frac{q(p+1)}{p}\psi} \,, \tag{8.14}$$

---

[3]At any rate, since Y is compact, charged sources are to satisfy a tadpole condition, which one ought to take into account.

where we have shifted the radion in order to place its on-shell value to zero, and we have replaced $R_0 \to R$ accordingly. Then, introducing the canonically-normalized radion ρ, defined by

$$-\frac{q}{p}\,\psi \equiv \sqrt{\frac{q}{2\,p\,(D-2)}}\,\rho\,, \tag{8.15}$$

the ratio of interest takes the form

$$\frac{|\boldsymbol{\nabla}\mathcal{V}|}{\mathcal{V}} = \frac{\sqrt{(\partial_\phi\mathcal{V})^2 + (\partial_\rho\mathcal{V})^2}}{\mathcal{V}}\,, \tag{8.16}$$

while shifting ϕ one can also do away with the remaining parametric dependence on the dimensionless combination $\nu \equiv n\,T^{\frac{q-1}{2}}$. Altogether, the resulting ratios depend only on ϕ and ρ, and we have minimized them numerically imposing the constraint[4] $\mathcal{V} > 0$, finding approximately 2 (resp. 2.5) for the orientifold models (resp. the heterotic model). This result resonates with the dS swampland conjecture of [17], showing that in this case dS solutions are behind an $\mathcal{O}(1)$ "barrier" in the sense of eq. (8.16).

FIGURE 8.1: plots of the sign of the potential of eq. (8.14) in units of T, with its minimum marked, and of the signature of its Hessian matrix in the orientifold models. Left: regions where the potential is positive (orange) and negative (blue), for $n = 10^3$. Right: region where its Hessian matrix is positive-definite (green).

The above considerations can be extended to the more general warped flux compactifications that we have discussed in Section 1. In this case, in terms of the

---

[4]The constraint $\mathcal{V} > 0$ can also be recast in terms of ϕ and ρ only, with no parametric dependence left.
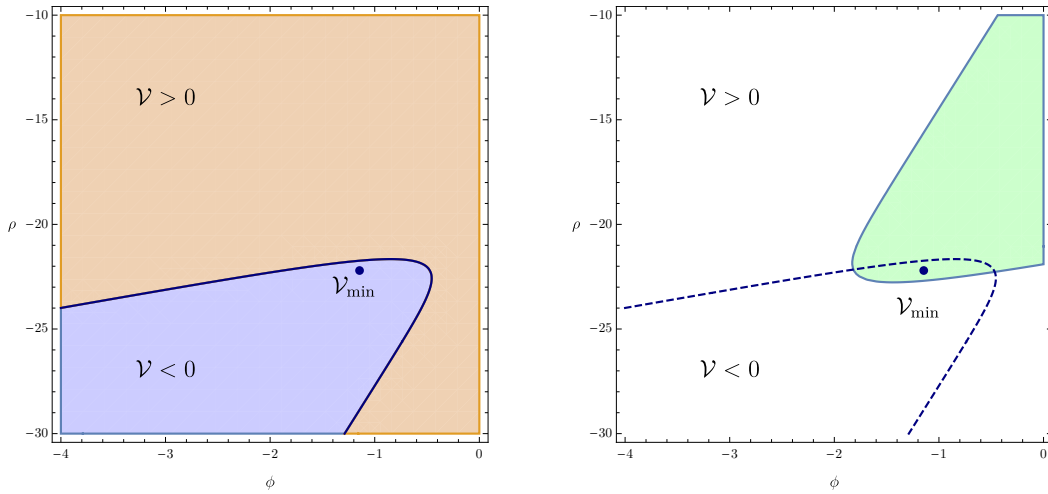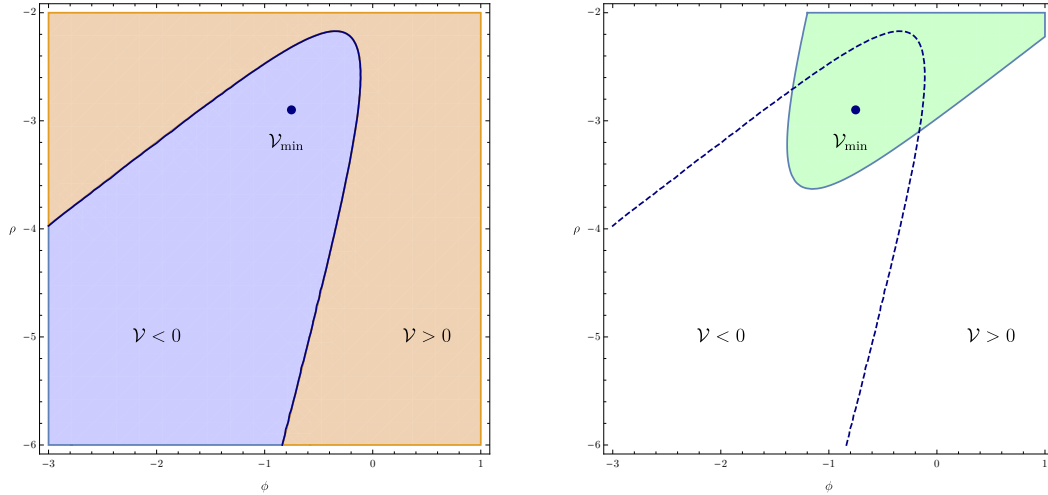
FIGURE 8.2: plots of the sign of the potential of eq. (8.14) in units of T, with its minimum marked, and of the signature of its Hessian matrix in the heterotic model. Left: regions where the potential is positive (orange) and negative (blue), for $n = 10$. Right: region where its Hessian matrix is positive-definite (green).

canonically-normalized dilaton and radion fields[5] ϕ, ρ, the effective potential is given by

$$\mathcal{V}(\phi, \rho) = \mathcal{I}_V \, e^{2k\rho} - \int_Y d^{d_Y} y \, \sqrt{-\tilde{g}} \, e^{2bu(y)} R_{\mathcal{M}_q} \, e^{\frac{2k(D-2)}{d_Y}\rho} + \frac{1}{2} \mathcal{I}_H \, e^{2k(d_X-1)\rho} \,, \qquad (8.17)$$

where we have introduced

$$k \equiv \sqrt{\frac{d_Y}{2\,(d_X - 2)\,(D-2)}} \qquad (8.18)$$

in order to canonically normalize ρ. Using the integrals defined in eq. (8.3), one can recast the potential of eq. (8.17) in terms of its derivatives according to

$$\mathcal{V} = \frac{d_Y(d_X - 1)}{\alpha(D-2)} \, \partial_\phi \mathcal{V} + \frac{d_Y}{2k(D-2)} \, \partial_\rho \mathcal{V} + \frac{d_X - 2}{D-2} \left(1 - (d_Y - 1)\frac{\gamma}{\alpha}\right) \mathcal{I}_V \, e^{2k\rho} \,, \quad (8.19)$$

and, since $d_Y \geq q$ in order to allow for magnetic fluxes, one finds that

$$\frac{d_Y(d_X - 1)}{\alpha(D-2)} \, \partial_\phi \mathcal{V} + \frac{d_Y}{2k(D-2)} \, \partial_\rho \mathcal{V} \geq \mathcal{V} \qquad (8.20)$$

---

[5]Notice that, in order to canonically normalize the radion, one needs to rescale the field $\psi(x)$ that we have introduced in Chapter 3.

holds off-shell whenever the no-go result discussed in Section 1 applies. Then, applying the Cauchy-Schwartz inequality one arrives at

$$\sqrt{(\partial_\phi \mathcal{V})^2 + (\partial_\rho \mathcal{V})^2} \geq \frac{\sqrt{2}\,\alpha\,(D-2)}{\sqrt{d_Y\left(2\,d_Y\,(d_X - 1)^2 + \alpha^2\,(D-2)\,(d_X - 2)\right)}}\,\mathcal{V}\,, \tag{8.21}$$

which whenever $\mathcal{V} > 0$ provides a lower bound for the ratio of eq. (8.16).

4   BRANE-WORLD DE SITTER COSMOLOGY

According to the proposal of [35–37], a thin-wall bubble nucleating between two AdS_{p+2} space-times hosts a dS_{p+1} geometry on its wall[6]. Here we make use of the results in Chapter 5 and Chapter 6 to propose an embedding of scenarios of this type in string theory. Specifically, nucleation of D1-branes in the $\mathrm{AdS}_3 \times \mathrm{S}^7$ solution and of NS5-branes in the $\mathrm{AdS}_7 \times \mathrm{S}^3$ solution lead to a dS_2 geometry and a dS_6 geometry respectively[7].

In the notation of Chapter 5, let us consider the landscape of AdS_{p+2} space-times with curvature radii $\widetilde{L}$, expressed in the $(p+2)$-dimensional Einstein frame, specified by large flux numbers n. The equations of motion for a spherical brane (stack) of charge $\delta n \ll n$ that describe its expansion after nucleation involve the extrinsic curvature Θ of the world-volume, and stem from the Israel junction conditions [145, 146]

$$\kappa_{p+2}^2\,\delta\left(\Theta\,(j^*g)_{ab} - \Theta_{ab}\right) = \widetilde{\tau}_p\,(j^*g)_{ab}\,, \tag{8.22}$$

where δ denotes the discontinuity across the brane and $\widetilde{\tau}_p$ is the (dressed) tension written in the $(p+2)$-dimensional Einstein frame. Writing the induced metric j^*g on the brane, which is continuous, according to

$$ds_{\mathrm{brane}}^2 = -dt^2 + a(t)^2\,d\Omega_p^2\,, \tag{8.23}$$

---

[6]For some earlier works along these lines, see [212–216].

[7]The analogous phenomenon in the case of D3-branes in the type 0′B model appears more elusive, since the corresponding bulk geometry is not $\mathrm{AdS}_5 \times \mathrm{S}^5$, and its large-flux behavior is not uniform [71–73].

the junctions conditions read

$$\delta \sqrt{\frac{1}{\widetilde{L}^2} + \frac{1 + \dot{a}^2}{a^2}} = \frac{\kappa_{p+2}^2 \, \widetilde{\tau}_p}{p} \, . \tag{8.24}$$

In the thin-wall limit $\delta n \ll n$ eq. (8.24) reduces to

$$\sqrt{\frac{1}{\widetilde{L}^2} + \frac{1 + \dot{a}^2}{a^2}} = \frac{p}{2\kappa_{p+2}^2 \, \widetilde{\tau}_p} \delta \left(\frac{1}{\widetilde{L}^2} \right)$$
$$= \frac{\epsilon}{(p+1) \, \widetilde{\tau}_p} = \frac{\beta}{\widetilde{L}} \, , \tag{8.25}$$

where ϵ is the energy (density) carried by the brane and $\beta > 1$ is the extremality parameter that we have discussed in Chapter 5. At the time of nucleation $\dot{a} = 0$, and $a(0) = \widetilde{\rho}$ gives the correct nucleation radius, while the time evolution of the scale factor a is described by the Friedmann equation

$$\left(\frac{\dot{a}}{a} \right)^2 = -\frac{1}{a^2} + \frac{\beta^2 - 1}{\widetilde{L}^2} \, , \tag{8.26}$$

whence $a = \frac{1}{H} \cosh(H t)$ identifies the Hubble parameter

$$H = \frac{1}{\widetilde{\rho}} = \frac{\sqrt{\beta^2 - 1}}{\widetilde{L}} \propto n^{-\frac{\gamma\left(1 + \frac{q}{p}\right)}{(q-1)\gamma - \alpha}} \, . \tag{8.27}$$

While the extremality parameter β in the string models at stake is not close to unity, as in the near-extremal cases studied in [35–37], the AdS curvature is nevertheless parametrically small for large n, and therefore the curvature of the dS wall is also parametrically small.

Furthermore, it has been shown that the Einstein gravity propagating in the bulk induces, at large distances, lower-dimensional Einstein equations on the brane [36], in a fashion reminiscent of Randall-Sundrum constructions [217–221][8]. In order to elucidate this issue in the present case, where the branes deviate from extremality by the $\mathcal{O}(1)$ factor v_0, let us compare the on-shell action for the expanding brane, which

---

[8]Despite some similarities, it is worth stressing that the present context is qualitatively different from scenarios of the Randall-Sundrum type.

takes the form

$$S_p = (\beta - 1)\, \widetilde{\tau} \int d^{p+1}\zeta \left(\frac{\widetilde{L}}{Z}\right)^{p+1} \tag{8.28}$$

in the Poincaré coordinates that we have employed in Chapter 6, with the corresponding Einstein-Hilbert action

$$S_p^{(\mathrm{EH})} = \frac{1}{2\kappa_{p+1}^2} \int d^{p+1}\zeta \left(\frac{\widetilde{L}}{Z}\right)^{p+1} \left(R_{p+1} - 2\Lambda_{p+1}\right), \tag{8.29}$$

since the resulting effective gravitational theory on the world-volume ought to reconstruct general covariance [213][9]. Since for dS_{p+1}

$$R_{p+1} - 2\Lambda_{p+1} = 2p\, H^2, \tag{8.30}$$

using eq. (8.27) and the defining relations

$$\beta \equiv \frac{\epsilon\, \widetilde{L}}{(p+1)\widetilde{\tau}}, \tag{8.31}$$
$$\epsilon \equiv \delta\widetilde{E}_0 = \frac{p(p+1)}{\kappa_{p+2}^2\, \widetilde{L}^3}\, \delta\widetilde{L},$$

introduced in Chapter 5, one finds the world-volume Newton constant

$$\kappa_{p+1}^2 = \beta\,(\beta + 1)\,\frac{\kappa_{p+2}^2}{\delta\widetilde{L}} \propto n^{1 - \frac{\gamma\left(1 + \frac{q}{p}\right)}{(q-1)\gamma - \alpha}}, \tag{8.32}$$

which indeed reproduces the results of [36, 215] in the near-extremal limit $\beta \to 1$. While for the orientifold models $p = 1$, and thus there would be no associated Planck mass $M_{\mathrm{Pl}}^{1-p} = \kappa_{p+1}^2$, in the heterotic model $p = 5$ and $\beta = \sqrt{\frac{5}{3}}$ for extremal NS5-branes, and thus the vacuum energy (density) in units of the $(p+1)$-dimensional Planck mass is given by

$$\left(\frac{E_{p+1}}{M_{\mathrm{Pl}}^{p+1}}\right)_{\mathrm{heterotic}} = \frac{25}{18\pi}\sqrt{\frac{5}{3}}\sqrt{1 + \sqrt{\frac{5}{3}}}\,\left(\kappa_{10}\, T^2\right)\frac{(T\, n)^2}{\sqrt{T\, \delta n}}, \tag{8.33}$$

which is parametrically small for large n.

---

[9]For a recent discussion in the context of entanglement islands, see [222].

4.1 *Massive particles*

It has been shown in [36, 37] that one can include radiation and matter densities in the Friedmann equation of eq. (8.26) introducing black holes and "string clouds" respectively. While the former case appears problematic [223–225], on account of the considerations of Chapter 6, one can nevertheless reproduce the effect of introducing string clouds using probe open strings stretching between branes in AdS. In order to compute the mass m_{str} of the point particle induced by an open string ending on a brane in more general settings, let us consider a bulk geometry with the symmetries corresponding to a flat (codimension-1) brane, with transverse geodesic coordinate ξ, and thus a metric of the type

$$ds^2 = d\xi^2 + \Omega(\xi)^2 \, \gamma_{\mu\nu}(x) \, dx^\mu \, dx^\nu \, . \tag{8.34}$$

Let us further consider a string with tension T stretched along ξ, attached to the brane at $\xi = \xi_b$, with longitudinal coordinates $x^\mu(\tau)$ in terms of the world-line of the induced particle. A suitable embedding with world-sheet coordinates (τ, σ) then takes the form

$$X^\mu = X^\mu(\tau, \sigma) \, , \qquad X^\mu(\tau, \sigma_b) \equiv x^\mu(\tau) \, ,$$
$$\xi = \xi(\sigma) \, , \qquad \xi(\sigma_b) \equiv \xi_b \, , \tag{8.35}$$

with Neumann boundary conditions on the X^μ, so that the induced metric determinant on the world-sheet yields the Nambu-Goto action

$$S_{\text{NG}} = -\, T \int d\tau \, d\sigma \, \Omega \, \sqrt{\Omega^2 \left(\dot{X} \cdot X' \right)^2 - (\xi'^2 + \Omega^2 \, X'^2) \, \dot{X}^2} \, , \tag{8.36}$$

where $\dot{X}^2 \equiv \gamma_{\mu\nu}(X) \, \dot{X}^\mu \, \dot{X}^\nu$ and we have assumed that $\Omega > 0$ and $\xi' > 0$, since both ξ and σ parametrize the string stretching in the transverse direction. In turn, this implies that $\sigma_b < \sigma_f$, where $\xi(\sigma_f) \equiv \xi_f$ corresponds to the (conformal) boundary where $\Omega(\sigma_f) = 0$. Then, varying the action and integrating by parts gives the boundary term

$$\delta S_{\text{NG}} = -\, T \int d\tau \, \Omega \, \delta\xi \, \sqrt{-\dot{X}^2} \, \Big|_{\sigma_b}^{\sigma_f} \, , \tag{8.37}$$

up to terms that vanish on shell[10]. Since the variation $\delta \xi_f = 0$, one can fix $X^\mu = X^\mu(\tau, \sigma_b) = x^\mu(\tau)$, and the resulting on-shell variation

$$\delta S_{\mathrm{NG}} = \delta \left(- T \int d\tau \int_{\xi_b}^{\xi_f} d\xi \, \Omega(\xi) \, \sqrt{-\dot{x}^2} \right) \tag{8.38}$$

ought to be identified with the variation of the particle action

$$S_{\mathrm{particle}} = - m_{\mathrm{string}} \int d\tau \, \Omega(\xi_b) \, \sqrt{-\dot{x}^2} \,, \tag{8.39}$$

which one can also obtain evaluating eq. (8.36) for a rigid string. Hence,

$$m_{\mathrm{string}} = \frac{T}{\Omega(\xi_b)} \int_{\xi_b}^{\xi_f} d\xi \, \Omega(\xi) \,, \tag{8.40}$$

and for AdS, for which $\Omega(\xi) \propto e^{-\frac{\xi}{L}}$, eq. (8.40) reduces to $m_{\mathrm{string}} = T L$, thus reproducing the results of [36, 37]. More generally, requiring that $\frac{\partial m_{\mathrm{string}}}{\partial \xi_b} = 0$ gives the condition $\Omega'(\xi_b) = - \frac{m_{\mathrm{string}}}{T} \Omega(\xi_b)$, i.e. the space-time is AdS if the mass remains constant as the brane expands. Moreover, if the string stretches between ξ_b and the position $\xi_{b'}$ of another brane, the endpoints of integration change, and if $\xi_b \sim \xi_{b'}$ one recovers the flat-space-time result $m_{\mathrm{string}} \sim T \delta\xi$. While for fundamental strings stretching between D1-branes the resulting masses would be large, and would thus bring one outside the regime of validity of the present analysis, successive nucleation events would allow for arbitrarily light strings stretched between nearby branes, although the probability of such events is highly suppressed in the semi-classical limit. The resulting probability distribution of particle masses is correspondingly heavily skewed toward large values.

4.2 *de Sitter foliations from nothing*

As a final comment, let us remark that the nucleation of bubbles of nothing [105] offers another enticing possibility to construct dS configurations [106]. While, to

---

[10]Let us remark that, as usual, initial and final configurations are fixed in order that the Euler-Lagrange equations hold.

our knowledge, realizations of this type of scenario in string theory have been investigated breaking supersymmetry in lower-dimensional settings [226][11], recent results indicate that within the relevant context the nucleation of bubbles of nothing is quite generic [107]. In particular, the supersymmetry-breaking $\mathbb{Z}_k$ orbifold of the type IIB $AdS_5 \times S^5$ solution, described in [226], appears to provide a calculable large-N regime and a dual interpretation in terms of the corresponding orbifold of $\mathcal{N} = 4$ supersymmetric Yang-Mills theory in four dimensions, which is a $U(N)^k$ gauge theory that is expected to retain some of the properties of the parent theory [71, 180–186]. For what concerns the $AdS \times S$ solutions discussed in Chapter 3, on the other hand, some evidence suggests that the decay rate per unit volume associated to the nucleation of bubble of nothing is subleading with respect to flux tunneling in single-flux landscapes [102], and thus in the $AdS \times S$ solutions of interest on account of the results presented in Chapter 5.

---

[11]Some lower-dimensional toy models offer flux landscapes where more explicit results can be obtained [102, 108, 227].

Conclusions

We can now summarize the main points that we have discussed in this thesis, collecting our considerations and results.

To begin with, in Chapter 2 we have presented a brief overview of three ten-dimensional string models with broken supersymmetry and their construction in terms of vacuum amplitudes. These comprise two orientifold models, the $USp(32)$ model of [19] and the $U(32)$ model of [20, 21], and the $SO(16) \times SO(16)$ heterotic model of [22, 23], and their perturbative spectra feature no tachyons. On the other hand, the perturbative expansion of these models around flat space-time involves gravitational tadpoles, whose back-reaction appears dramatic and is, at present, not completely under control.

In Chapter 3 we have described a family of effective theories which describes their low-energy physics. In particular, their actions contain exponential potentials for the dilaton, whose presence tends to drive the dynamics toward runaway. In order to counteract this behavior, the resulting classical solutions that have been found entail warped space-time geometries [24, 25] or compactifications supported by fluxes [26]. We have described in detail the Dudas-Mourad solutions of [24], which comprise nine-dimensional static solutions and ten-dimensional cosmological solutions, and general Freund-Rubin flux compactifications, which include the AdS $\times$ S solutions found in [26] and their generalizations studied in [25]. Whenever dS solutions of this type are allowed, they **always contain instabilities** in the dilaton-radion sector, but in the string models that we have introduced in Chapter 2 they **do not arise**.

In Chapter 4 we have studied in detail the classical stability of the solutions discussed in Chapter 3, deriving the linearized equations of motion for field perturbations. In particular, in the case of the Dudas-Mourad solutions we have recast the resulting equations as Schrödinger-like problems, whose Hamiltonians can be decomposed in terms of creation and annihilation operators. We have found that

these solutions are stable at the classical level, with the exception of an intriguing logarithmic **growth of the homogeneous tensor mode in the cosmological case** [27], which we are tempted to interpret as a **tendency of space-time toward spontaneous compactification**. However, let us remark that from the perspective of the underlying string models these solutions entail sizeable curvature corrections or string-loop corrections, thus potentially compromising some of these lessons. this issue does not appear to affect the $AdS \times S$ solutions, which for large fluxes are expected to be under control globally, but their Kaluza-Klein spectra contain **unstable modes in the (space-time) scalar sector** [27] for a finite number of internal angular momenta. One can then attempt to remove them with suitable freely-acting projections on the internal spheres, or choosing a different internal manifold altogether, and for the heterotic model one can achieve this with an antipodal $\mathbb{Z}_2$ projection on the internal S^3.

In Chapter 5 we have focused on some non-perturbative instabilities of the AdS compactifications discussed in Chapter 3, which undergo flux tunneling [25] gradually discharging space-time. This process is exponentially unlikely for large fluxes, and it entails the nucleation of charged bubbles which then expand, reaching the (conformal) boundary in a finite time. Motivated by the qualitative properties of these bubbles, we have developed a picture involving fundamental branes, matching bulk gravitational computations to brane instanton computations of decay rates and deriving consistency conditions. In particular, we have found that the (oppositely charged pairs of) branes that mediate flux tunneling ought to be **D1-branes in the orientifold models and NS5-branes in the heterotic model**, but our results apply also to "exotic" branes [28–32] whose tensions scales according to different powers of the string coupling.

In Chapter 6 we have kept developing the brane picture presented in Chapter 5, studying the Lorentzian evolution undergone by branes after nucleation. In the non-supersymmetric models described in Chapter 2, rigid fundamental branes are subject to a non-trivial potential which encodes an **enhanced charge-to-tension ratio** that is greater than its bare counterpart, thus **verifying the weak gravity conjecture in these settings**. In addition to their expansion, positively charged branes are driven toward **long-wavelength world-volume deformations**, while negatively charged branes are not affected by instabilities of this type. Moreover, in order to further develop the connection between the $AdS \times S$ solutions discussed in Chapter 3 and the

corresponding branes, we have investigated in detail the **full back-reacted geometries** sources by the latter, which feature AdS $\times$ S as **attractive near-horizon throats** and strongly-coupled regions where, classically, space-time **"pinches off" at a finite transverse geodesic distance**. This result generalizes the analogous behavior of the static solutions of [24], which is indeed reproduces for 8-branes and appears to depend only on the residual symmetry left unbroken by the branes. Therefore, the forces exerted on nucleated brane stacks afford an interpretation as the force between two stacks in the probe-brane regime in which one contains significantly more branes than the other. Finally, we turned to the non-extremal case, deriving a system of dynamical equations for the **back-reaction of non-extremal branes** and studying their dynamics in some probe-brane regimes, namely Dp-branes probing the static Dudas-Mourad geometry in the orientifold models and, in a complementary regime, 8-branes probing the AdS$_3 \times$ S^7 throat sourced by D1-branes. We have compared the resulting interaction potentials to a **string amplitude computation**, finding **qualitative agreement** whenever both results are reliable.

In Chapter 7 we have developed a holographic proposal that relates, in general terms, **non-perturbative instabilities** of meta-stable AdS false vacua and **dual RG flows**. In this picture, nucleation of vacuum bubbles in the bulk ought to trigger corresponding relevant deformations in the dual CFT, and the expansion of bubbles ought to drive the RG flow toward the IR. In order to support this proposal, we have computed the **entanglement entropy in three-dimensional thin-wall settings**, and we have built a number of c-functions with holographic methods: one from the Cardy-Calabrese relation [143, 144], one from the **null-energy condition** and one from the **trace anomaly**. In addition, we have applied the framework of holographic **integral geometry** [33] to address off-centered bubbles. Finally, we have outlined a **concrete scenario** in which our proposal could potentially be studied quantitatively, placing the D1-branes of the orientifold models in a weakly-coupled region of the static Dudas-Mourad geometry, resulting in a non-supersymmetric gauge theory in flat space-time. This theory ought to flow to a strongly fixed point coupled in the IR, and a **one-loop computation appears consistent** with this picture, which we would like to investigate making use of large-N techniques.

In Chapter 8 we turned to dS cosmology, generalizing the no-go result that

we have described in Chapter 3 to more general warped flux compactifications. We have derived an **expression for the space-time cosmological constant** in these settings, which underlies an extended **no-go result** that we have connected to recent conjectures about dS solutions and the swampland [17]. Furthermore, we have added **localized sources** in the effective theories at stake, deriving their contributions to the cosmological constant and, therefore, to the no-go result, which takes a more complicated form in this case. Finally, we have focused on **brane-world constructions**, applying the proposal recently revisited in [35–37] to the non-supersymmetric string models discussed in Chapter 2. Extending the results valid for near-extremal branes to our settings, where the effective charge-to-tension ratio is enhanced by an $\mathcal{O}(1)$ factor, we have built an **effective dS geometry** on the world-volume of fundamental branes which appears to be parametrically under control. Taking into account back-reactions ought to lead to the Einstein equations on the world-volume [36, 37] at low energies, and thus the complete effective field theory would involve gravity coupled to (non-)Abelian gauge fields and matter. Moreover, models of this type appear to accomodate massive particles of arbitrarily small, if unlikely, masses via open strings stretching between expanding branes. We would like to further explore these enticing constructions, and the two-dimensional case, which pertains to D1-branes in the orientifold models, appears to provide a simpler toy model in this respect. On the other hand, a detailed description the six-dimensional case, which pertains to NS5-branes in the heterotic model, appears more puzzling in the absence of a deeper understanding of non-supersymmetric dualities.

OUTLOOK

The results that we have discussed in this thesis suggest a tantalizing, if still elusive, picture of the rich dynamics that underpins supersymmetry breaking in string theory. Even on a fundamental level, the back-reaction of the gravitational degrees of freedom intrinsic to string theory appears dramatic to such an extent that *bona fide* vacua seem either completely absent or necessarily strongly coupled. As a result, any effective static space-times that we have investigated show a tendency to end in a

singularity at a finite distance, and their existence appear to rest on the presence of localized sources that act as a symmetry-breaking compass. Hence, the oft-fruitful paradigm of studying a system via its effect on probe sources has proven all the more necessary in this context, and in particular, as we have described, it holds some potentially intriguing lessons to be unveiled: from a theoretical perspective, the rich dynamics of non-supersymmetric branes hints at a deeper connection with the microscopic interactions of open strings, and thus with holography, that could lead to further quantitative progress on the ultimate fate of non-supersymmetric string "vacua". On the other hand, from a phenomenological perspective, the very same dynamics appear to be able to accomodate naturally interesting cosmological models with a number of desired features. Indeed, the simplest configurations lead to higher-dimensional cosmologies, modified power spectra and points to a tendency toward spontaneous compactification, while more elaborate constructions lead to lower-dimensional dS brane-world scenarios. All in all, it seems clear that, among the long-standing issues with supersymmetry breaking, instabilities often arise from an attempt to force naturally dynamical systems into static configurations, while the most coveted phenomenology reflects the accelerated expansion of our universe. Therefore, embracing instabilities as a starting point in this respect could help to shed some light on these issues, which are of primary interest both for applications to fundamental physics, but also of foundational value for a deeper understanding of string theory on a foundational level.

UNRELATED PROJECTS

During the course of my PhD studies, I have been part of a number of projects unrelated to the material presented in this thesis. In particular, I have been involved in a more detailed investigation of the back-reacted geometries sources by non-extremal branes in the presence of exponential dilaton potentials in collaboration with R. Antonelli. In addition, I have obtained some results in collaboration with A. Platania on all-order curvature corrections in string cosmology.

Specifically, within a mini-superspace framework applied to low-energy effective

actions of string theory in $d + 1$ dimensions, (perturbative) α'-corrections are deter-
mined by a single function of the Hubble parameter $\dot{\sigma}$ on T-duality grounds [228–231].
The resulting action can then be written as an asymptotic series of the form

$$
\Gamma_{\text{string}} \sim \frac{\text{Vol}_d}{16\pi G_{\text{N}}} \int dt \, \frac{1}{n} \, e^{-\Phi} \left(-\dot{\Phi}^2 + d \, n^2 \sum_{m=1}^{\infty} a_m \left(\frac{\dot{\sigma}}{n} \right)^{2m} \right) , \tag{9.1}
$$

up to integration by parts and terms that vanish on-shell. The coefficients a_m are
related to the coefficients c_m of [229–231] according to $a_m = 8 \, (-1)^m \, c_m$, in units where
$\alpha' = 1$. Since the above expression is expected to encode at least all perturbative
α'-corrections, we have applied functional RG techniques to extract flow equations for
their coefficients that are in principle correct to all orders. Then, within a leading-
order ϵ-expansion around two space-time dimensions, we have obtained an exact
solution to the flow equations that exhibits an interacting UV fixed point, two relevant
deformations and a consistent weakly-coupled IR regime, where the effective action
takes the form

$$
\Gamma_{\text{string}} = \frac{\text{Vol}_d}{16\pi G_{\text{IR}}} \int dt \, n \, e^{-\Phi} \left[\Lambda - \frac{\dot{\Phi}^2}{n^2} + \frac{\dot{\sigma}^2}{n^2} + \frac{8}{3\pi} G_{\text{IR}} \Lambda L \left(\frac{\dot{\sigma}^2}{n^2 \Lambda} \right) \right] , \tag{9.2}
$$

where Λ is one of the two relevant deformations, alongside the Newton constant, and

$$
\begin{aligned}
L(s) &\equiv -1 - \frac{23}{12} s + \left(\frac{3}{2} + s \right) \log \left(1 + \frac{s}{2} \right) \\
&\quad + (1 + s)^{\frac{3}{2}} \sqrt{\frac{2}{s}} \operatorname{arctanh} \left(\sqrt{\frac{s}{2 \, (1 + s)}} \right) .
\end{aligned} \tag{9.3}
$$

Starting from this action one can study the resulting effective cosmologies, which
for $\alpha' \Lambda = \mathcal{O}(1)$ is expected to modify qualitatively the initial singularity at the
string-scale.

Tensor spherical harmonics: a primer

In this appendix we review some results that were needed for our stability analysis in Chapter 4, starting from an ambient Euclidean space. In Section 1 we build scalar spherical harmonics, and in Section 2 we extend our considerations to tensors of higher rank. The results agree with the constructions presented in [232, 233][1].

1 SCALAR SPHERICAL HARMONICS

Let $Y^1, \dots Y^{n+1}$ be Cartesian coordinates of $\mathbb{R}^{n+1}$, so that the unit sphere $\mathbb{S}^n$ is described by the constraint

$$\delta_{IJ} Y^I Y^J = r^2 \tag{A.1}$$

on the radial coordinate r, solved by spherical coordinates y^i according to

$$Y^I = r\, \widehat{Y}^I(y)\,. \tag{A.2}$$

The scalar spherical harmonics on $\mathbb{S}^n$ can be conveniently constructed starting from harmonic polynomials of degree ℓ in the embedding Euclidean space $\mathbb{R}^{n+1}$. A harmonic polynomial of degree ℓ takes the form

$$H^{\ell}_{(n)}(Y) = \alpha_{I_1 \dots I_\ell} Y^{I_1} \dots Y^{I_\ell}\,, \tag{A.3}$$

and is therefore determined by a completely symmetric and trace-less tensor $\alpha_{I_1 \dots I_\ell}$ of rank ℓ, as can be clearly seen applying to it the Euclidean Laplacian

$$\nabla^2_{n+1} = \sum_{I=1}^{n+1} \frac{\partial^2}{\partial Y_I^2}\,. \tag{A.4}$$

---

[1] For a more recent analysis in the case of the five-sphere, see [234].

The scalar spherical harmonics $\mathcal{Y}_{(n)}^{I_1\ldots I_\ell}$ are then defined restricting the $H_{(n)}^\ell(Y)$ to the unit sphere S^n, or equivalently as

$$H_{(n)}^\ell(\widehat{Y}(y)) = r^\ell \, \alpha_{I_1\ldots I_\ell} \, \mathcal{Y}_{(n)}^{I_1\ldots I_\ell}(y) \,. \tag{A.5}$$

As a result, the Euclidean metric can be recast as

$$ds_{n+1}^2 = dr^2 + r^2 \, d\Omega_n^2 \,, \tag{A.6}$$

and the scalar Laplacian decomposes according to

$$0 = \nabla_{n+1}^2 H_{(n)}^\ell(Y) = \frac{1}{r^n} \frac{\partial}{\partial r}\left(r^n \frac{\partial H_{(n)}^\ell(Y)}{\partial r}\right) + \frac{1}{r^2} \, \nabla_{S^n}^2 \, H_{(n)}^\ell(Y) \,, \tag{A.7}$$

where

$$\frac{\partial H_{(n)}^\ell(Y)}{\partial r} = \frac{\ell}{r} \, H_{(n)}^\ell(Y) \tag{A.8}$$

for the homogeneous polynomials $H_{(n)}^\ell(Y)$. All in all

$$\nabla_{S^n}^2 \, \mathcal{Y}_{(n)}^{I_1\ldots I_\ell} = -\,\ell\,(\ell + n - 1)\, \mathcal{Y}_{(n)}^{I_1\ldots I_\ell} \,, \tag{A.9}$$

and the degeneracy of the scalar spherical harmonics for any given ℓ is the number of independent components of a corresponding completely symmetric and trace-less tensor, namely

$$\frac{(n + 2\ell - 1)\,(n + \ell - 2)!}{\ell!\,(n-1)!} \,. \tag{A.10}$$

2 SPHERICAL HARMONICS OF HIGHER RANK

In discussing more general tensor harmonics, it is convenient to notice that, in the coordinate system of eq. (A.6), the non-vanishing Christoffel symbols $\widetilde{\Gamma}_{IJ}^K$ for the

ambient Euclidean space read

$$\widetilde{\Gamma}^r_{ij} = -\, r\, g_{ij}\,, \qquad \widetilde{\Gamma}^i_{jr} = \frac{1}{r}\, \delta^j_i\,, \qquad \widetilde{\Gamma}^k_{ij} = \Gamma^k_{ij}\,, \tag{A.11}$$

where the labels i, j, k refer, as above, to the n-sphere, whose Christoffel symbols are denoted by Γ^k_{ij}.

The construction extends nicely to tensor spherical harmonics, which can be defined starting from generalized harmonic polynomials, with one proviso. The relation in eq. (A.2) and its differentials imply that the actual spherical components of tensors carry additional factors of r, one for each covariant tensor index, with respect to those naïvely inherited from the Cartesian coordinates of the Euclidean ambient space, as we shall now see in detail. To begin with, vector spherical harmonics arise from one-forms in ambient space, built from harmonic polynomials of the type

$$H^\ell_{(n)\,J}(Y) = \alpha_{I_1\dots I_\ell,\,J}\, Y^{I_1}\dots Y^{I_\ell}\,, \tag{A.12}$$

where the coefficients $\alpha_{I_1\dots I_\ell,\,J}$ are completely symmetric and trace-less in any pair of the first ℓ indices. They are also subject to the condition

$$Y^J\, H^\ell_{(n)\,J}(Y) = 0\,, \tag{A.13}$$

since the radial component, which does not pertain to the sphere S^n, ought to vanish. This implies that the complete symmetrization of the coefficients vanishes identically,

$$\alpha_{(I_1\dots I_\ell,\,J)} = 0\,, \tag{A.14}$$

and on account of the symmetry in the first ℓ indices. As a result, $H^\ell_{n,\,J}(Y)$ is thus transverse in the ambient space,

$$\partial^J H^\ell_{(n)\,J}(Y) = 0\,. \tag{A.15}$$

Moreover, any Euclidean vector V such that $V_I Y^I = 0$ couples with differentials according to the general rule inherited from eq. (A.2),

$$V_I \, dY^I = V_I \, r \, d\widehat{Y}^I \, , \tag{A.16}$$

so that the actual sphere components, which are associated to $d\widehat{Y}^I$, include an additional power of r, and the vector spherical harmonics $\mathcal{Y}^{I_1...I_\ell, J}_{(n)\,i}$ are thus obtained from

$$r^{\ell+1} \, \mathcal{Y}^{I_1...I_\ell, J}_{(n)\,i} \, \alpha_{I_1...I_\ell, J} \, dy^i = r \, H^\ell_{(n)\,J}(Y) \, d\widehat{Y}^J \, . \tag{A.17}$$

Therefore,

$$\nabla_r \nabla_r \left(r \, H^\ell_{(n)\,J}(Y) \right) = \left(\frac{\partial}{\partial r} - \frac{1}{r} \right)^2 \left(r \, H^\ell_{(n)\,J}(Y) \right) = \frac{\ell\,(\ell-1)}{r} \, H^\ell_{(n)\,J}(Y) \, , \tag{A.18}$$

while the remaining contributions to the Laplacian give

$$\frac{1}{r^2} \, \nabla^2_{\mathbb{S}^n} \left(r \, H^\ell_{(n)\,J}(Y) \right) + \frac{n\,(\ell+1) - n - 1}{r} \left(r \, H^\ell_{(n)\,J}(Y) \right) \, , \tag{A.19}$$

taking into account the Christoffel symbols in eq. (A.11). Since the total Euclidean Laplacian vanishes by construction, adding eqs. (A.18) and (A.19) finally results in

$$\nabla^2_{\mathbb{S}^n} \, \mathcal{Y}^{I_1...I_\ell, J}_{(n)\,i} = - \left(\ell\,(\ell+n-1) - 1 \right) \mathcal{Y}^{I_1...I_\ell, J}_{(n)\,i} \, , \tag{A.20}$$

with $\ell \geq 1$.

In a similar fashion, the spherical harmonics $\mathcal{Y}^{I_1...I_\ell, J_1...J_p}_{(n)\,i_1...i_p}$, corresponding to generic higher-rank transverse tensors which are also trace-less in any pair of symmetric I-indices, can be described starting from harmonic polynomials of the type $H^\ell_{(n)\,J_1...J_p}(Y)$, and satisfy

$$\nabla^2_{\mathbb{S}^n} \, \mathcal{Y}^{I_1...I_\ell, J_1...J_p}_{(n)\,i_1...i_p} = - \left(\ell\,(\ell+n-1) - p \right) \mathcal{Y}^{I_1...I_\ell, J_1...J_p}_{(n)\,i_1...i_p} \, , \tag{A.21}$$

with $\ell \geq p$.

In Young tableaux language, the scalar harmonics correspond to trace-less single-row diagrams of the type

$$
\boxed{I_1}\,\boxed{I_2}\,\ldots\,\boxed{I_l}\quad,\tag{A.22}
$$

while the independent vectors associated to vector harmonics correspond to two-row trace-less hooked diagrams of the type

$$
\begin{array}{l}
\boxed{I_1}\,\boxed{I_2}\,\ldots\,\boxed{I_l}\\[2pt]
\boxed{J}
\end{array}\quad,\tag{A.23}
$$

as we have explained. Similarly, the independent tensor perturbations of the metric in the internal space correspond to trace-less diagrams of the type

$$
\begin{array}{l}
\boxed{I_1}\,\boxed{I_2}\,\ldots\,\boxed{I_l}\\[2pt]
\boxed{J_1}\,\boxed{J_2}
\end{array}\quad,\tag{A.24}
$$

while the independent perturbations associated to a $(p+1)$-form gauge field in the internal space correspond, in general, to multi-row diagrams of the type

$$
\begin{array}{l}
\boxed{I_1}\,\boxed{I_2}\,\ldots\,\boxed{I_l}\\[2pt]
\boxed{J_1}\\[2pt]
\vdots\\[2pt]
\boxed{J_{p+1}}
\end{array}\quad.\tag{A.25}
$$

The degeneracies of these representations can be related to the corresponding Young tableaux, as in [235]. The structure of the various types of harmonics, which are genuinely different for large enough values of n, reflects nicely the generic absence of mixings between different classes of perturbations.

Breitenlohner-Freedman bounds

In this appendix we collect some Breitenlohner-Freedman (BF) bounds [236] that play a crucial rôle in the stability analysis of AdS flux compactifications that we have presented in Chapter 4. We shall begin deriving the BF bound for a free scalar field in AdS$_d$ in Section 1, and then we shall extend the results to form fields in Section 2. In Section 3 we derive the BF bound for a spin-2 field, and finally in Section 4 we conclude with an alternative derivation of the scalar BF bound based on energy considerations, which mirrors the treatment in [236].

1 THE BF BOUND FOR A SCALAR FIELD

Let us begin studying a free massive scalar field φ. To this end, it is convenient to work in conformally flat Poincaré coordinates, so that the AdS$_d$ metric takes the form

$$ds^2 = L^2 g_{MN} \, dx^M \, dx^N = \frac{L^2}{z^2} \left(dz^2 + dx_{1,d-2}^2 \right) , \tag{B.1}$$

where $(\mu, \nu = 0, \ldots, d-2)$. The non-vanishing Christoffel symbols are then

$$\Gamma_{zz}^z = -\frac{1}{z} \, , \qquad \Gamma_{\nu z}^\mu = -\frac{1}{z} \, \delta_\nu^\mu \, , \qquad \Gamma_{\mu\nu}^z = \frac{1}{z} \, \eta_{\mu\nu} \, . \tag{B.2}$$

In this coordinate system the scalar Klein-Gordon equation for field modes $\varphi_k(x,z) \equiv e^{ik \cdot x} \varphi_k(z)$ of mass m takes the form

$$\varphi_k'' + \frac{2-d}{z} \, \varphi_k' - \left(k^2 + \frac{m^2 L^2}{z^2} \right) \varphi_k = 0 \, , \tag{B.3}$$

where "primes" denote derivatives with respect to z. Letting now

$$\varphi_k(z) = z^{\frac{d}{2}-1} \Psi_k(z) \tag{B.4}$$

reduces the field equation to the Schrödinger-like form

$$\left(-\frac{d^2}{dz^2} + \frac{4\,m^2\,L^2 + d\,(d-2)}{4z^2} \right) \Psi_k = -\,k^2\,\Psi_k \,, \tag{B.5}$$

so that the operator acting on Ψ can be recast in the form $\mathcal{A}^\dagger \mathcal{A}$, where

$$\mathcal{A} = -\frac{d}{dz} + \frac{a}{z} \,, \qquad \mathcal{A}^\dagger = \frac{d}{dz} + \frac{a}{z} \tag{B.6}$$

and

$$\left(a + \frac{1}{2} \right)^2 = m^2\,L^2 + \frac{(d-1)^2}{4} \,. \tag{B.7}$$

Requiring that $-k^2 > 0$, *i.e.* the absence of tachyonic excitations, and thus of modes potentially growing in time, in the Minkowski sections at constant z, translates into the condition that a be real, and hence into the BF bound for a scalar field,

$$m^2\,L^2 \geq -\frac{(d-1)^2}{4} \,. \tag{B.8}$$

As a final remark, let is recall that eq. (B.3) is solved by

$$\varphi_k(z) = \text{const.} \times z^{\frac{d-1}{2}}\,K_\nu(kz) \,, \qquad \nu \equiv \sqrt{m^2\,L^2 + \frac{(d-1)^2}{4}} \,, \tag{B.9}$$

where we have imposed regularity in the bulk of AdS. We shall make use of this result in Section 4.

2   THE BF BOUND FOR FORM FIELDS

One can treat the case of a massive vector in a similar fashion, starting from the massive Proca equation, which implies the divergence-less condition

$$A_z' + \partial^\mu A_\mu + \frac{2-d}{z}\,A_z = 0 \tag{B.10}$$

in Poincaré coordinates, and the resulting equations of motion

$$L^2 \,\Box\, A_M + \left(d - 1 - m^2 \, L^2 \right) A_M = 0 \tag{B.11}$$

for Fourier modes translate into

$$
\begin{aligned}
A_z'' + \frac{2-d}{z} \, A_z' - \left(k^2 + \frac{2-d+m^2 \, L^2}{z^2} \right) A_z &= 0\,, \\
A_\mu'' + \frac{4-d}{z} \, A_\mu' - \left(k^2 + \frac{m^2 \, L^2}{z^2} \right) A_\mu - \frac{2}{z} \, \partial_\mu A_z &= 0\,.
\end{aligned}
\tag{B.12}
$$

Changing variable as we have done in the preceding section for a scalar field, one can see that the first equation of eq. (B.12) leads to the condition

$$\left(a + \frac{1}{2} \right)^2 = m^2 \, L^2 + \frac{(d-3)^2}{4}\,, \tag{B.13}$$

from which one can infer the BF bound for a vector field,

$$m^2 \, L^2 \geq -\frac{(d-3)^2}{4}\,. \tag{B.14}$$

Let us stress that this bound refers to the mass term in the Lagrangian, since we have subtracted the contribution arising from commutators of covariant derivatives, which is also present in the massless case. The second equation of eq. (B.12) is apparently more complicated, since it contains A_z as a source. However, one can simplify it separating the longitudinal and transverse portions of A_μ. The former can be related to A_z via eq. (B.10), and one is lead again to the first equation of eq. (B.12). The latter satisfies the same equation as the scalar field, up to the replacement $d \to d-2$. All in all, one is thus led again to the BF bound of eq. (B.14).

This result can be generalized in a straightforward fashion to the case of massive $(p+1)$-form fields B_{p+1}, starting from their equations of motion

$$\left(L^2 \,\Box\, + (p+1) \, (d-p-1) - m^2 \, L^2 \right) B_{M_1 \ldots M_{p+1}} = 0\,. \tag{B.15}$$

Extending the preceding discussion, one can thus conclude that the BF bounds for $(p+1)$-form fields are

$$m^2 L^2 \geq -\frac{(d-3-2p)^2}{4}, \tag{B.16}$$

a result that applies insofar as[1] $d > p + 2$. Notice that this relation, which refers again to the mass term in the Lagrangian, is invariant under the "massive duality" [237] between $(p+1)$-form fields and $(d-p-2)$-form fields.

3   THE BF BOUND FOR A SPIN-2 FIELD

As a final example, let us consider a spin-2 field h_{MN}. The corresponding equations of motion stem from the quadratic Einstein-Hilbert Lagrangian

$$
\begin{aligned}
\mathcal{L}_{\text{EH}}^{(2)} &= \left(\frac{1}{8} \left(h^A{}_A \right)^2 - \frac{1}{4} h \cdot h \right) R + h^{MA} h_A{}^N R_{MN} - \frac{1}{2} h^A{}_A h^{MN} R_{MN} \\
&\quad - \frac{1}{4} \nabla_M h_{AB} \nabla^M h^{AB} + \frac{1}{4} \nabla_M h^A{}_A \nabla^M h^B{}_B \\
&\quad - \frac{1}{2} (\nabla \cdot h)_M \nabla^M h^A{}_A + \frac{1}{2} \nabla_M h_{AB} \nabla^B h^{AM}
\end{aligned} \tag{B.17}
$$

supplemented by the Fierz-Pauli mass term, or equivalently from the Fierz-Pauli equations in curved space-time. These imply the transverse and trace-less conditions, leaving a massive wave equation of the form

$$\left(\Box - \left(M_{\text{AdS}}^{(s)} \right)^2 - m^2 \right) h_{MN} = 0, \tag{B.18}$$

where the effective "gravitational mass" for spin-s fields is given by [238]

$$\left(M_{\text{AdS}}^{(s)} \right)^2 \equiv \frac{(s-2)(d-1) + (s-1)(s-4)}{L^2}. \tag{B.19}$$

---

[1] At any rate, for $d \leq p + 2$ the form field would have no local degrees of freedom.

The action of the $\Box$ operator on h_{MN}, which we shall write in units of L for convenience, is given by

$$
\begin{aligned}
\Box\, h_{MN} = {}& z^2\, h''_{MN} + z^2\, \partial^\mu \partial_\mu h_{MN} + z\, (6 - d)\, h'_{MN} + 2\, (2 - d)\, h_{MN} \\
& - d\, \delta^z_{(M}\, h_{N)z} + 2\, \eta_{MN}\, h_{zz} + 2\, \delta^z_M\, \delta^z_N\, \eta^{AB}\, h_{AB}\,,
\end{aligned}
\tag{B.20}
$$

where we imposed the transverse and trace-less conditions, and from eq. (B.18) one can separate the equations for the components $h_{\mu\nu}$, $h_{\mu z}$, h_{zz} and obtain the corresponding bounds. The most stringent of these bounds is

$$
m^2\, L^2 \geq -\frac{(d-1)^2}{4}\,,
\tag{B.21}
$$

which reproduces the results in [238][2] and actually holds for higher-spin fields in general.

4   A DERIVATION BASED ON ENERGY

Let us conclude this appendix presenting a physical argument for the scalar BF bound based on energy considerations. In order to obtain a variational problem that admits solutions with finite, conserved energy, following [236] let us introduce the improved stress-energy tensor[3]

$$
\widehat{T}_{MN} \equiv T_{MN} + \frac{h}{2}\, (g_{MN}\, \Box - \nabla_M \nabla_N - R_{MN})\, \varphi^2\,,
\tag{B.22}
$$

which is divergence-less for every h and, for a particular choice of h, allows for finite-energy wave-packets and boundary conditions with vanishing flux at the AdS (conformal) boundary. Indeed, the associated improved Hamiltonian

$$
\widehat{H} = \int d^{d-2}x\, dz\, z^{2-d}\, \widehat{T}_{00}\,,
\tag{B.23}
$$

---

[2] The analysis of [238] extends to higher-spin fields as well.

[3] At first glance, this procedure may appear only adequate for the scalar case, due to issues related to gauge invariance. However, let us remark that in this context fields are massive. At any rate, the massless cases where this construction is invalid trivially satisfy the corresponding BF bounds.

when evaluated on shell, contains two contributions to the boundary term, since the improvement ΔT_{MN} gives the divergence of an anti-symmetric tensor[4] upon contraction with a Killing vector ξ^M. Specifically,

$$\xi^M \Delta T_{MN} = \frac{h}{2} \nabla^M \left(\xi_{[M} \nabla_{N]} \varphi^2 - \varphi^2 \nabla_M \xi_N \right) , \tag{B.24}$$

and the resulting boundary term, which we shall write in units of L for convenience, reads

$$\frac{1}{2} \int d^{d-2}x \, z^{2-d} \left[\varphi \, \varphi' - 2h \left(\varphi \, \varphi' + \frac{1}{z} \, \varphi^2 \right) \right]_{z=\epsilon} , \tag{B.25}$$

where $\{z = \epsilon\}$ denotes the regularized boundary. Evaluating this boundary term on the expression of eq. (B.9), the total divergence is proportional to

$$\left(\frac{d-1}{2} - (d+1) \, h \right) K_\nu^2(kz) + (1 - 2\,h) \, kz \, K_\nu(kz) \, K_\nu'(kz)$$
$$= \left(\frac{d-1}{2} - (d+1) \, h - \nu \, (1 - 2\,h) + \mathcal{O}\left(z^{2\nu}\right) \right) K_\nu^2(kz) , \tag{B.26}$$

and the leading term, which is the only singular one as $z \to 0$, vanishes for

$$h = \frac{d - 1 - 2\,\nu}{2 \, (d + 1 - 2\,\nu)} . \tag{B.27}$$

Let us now see how the flux is modified. Since we have shown that the on-shell improved Hamiltonian $\widehat{H}$ differs by the canonical one by the subtraction of its divergent boundary term and, at most, an additive constant, the flux across the boundary is given by

$$\frac{d\widehat{H}}{dt} = \frac{1}{2} \int d^{d-2}x \, z^{2-d} \left(\dot{\varphi} \, \varphi' - \varphi \, \dot{\varphi}' \right) \Big|_{z=\epsilon} , \tag{B.28}$$

which on-shell can satisfy the no-flux condition only when ν is imaginary, and it does so for a discrete set of imaginary frequencies $\omega = i \, \gamma$ with a limit point at $\gamma = 0$. More precisely, finite-energy wave packets, needed to prevent the infra-red divergence

---

[4]The anti-symmetric tensor on the right-hand side of eq. (B.24) arises from the Killing equation and its associated integrability condition.

typical of plane waves, are to contain frequencies $\omega_n = i\,\gamma_n$ with discrete ratios

$$\gamma_1 = e^{\frac{\pi n_{12}}{|\nu|}}\,\gamma_2\,, \qquad n_{12} \in \mathbb{Z}\,, \tag{B.29}$$

which have a limit point corresponding to $\gamma = 0$. On account of eq. (B.9), the condition that ν be imaginary yields indeed the BF bound for a scalar field. The same conclusion can be derived writing directly the equation that encodes global energy conservation, or studying the boundary conditions for which the Schrödinger operator of eq. (B.5) is Hermitian.

C

Geodesics for thin-wall bubbles

In this appendix we shall discuss in detail the computation of geodesic in (constant-time slices of) the bulk geometry that describes a thin-wall bubble expanding in AdS$_3$ after nucleation, presenting the results of [109]. We have made use of the results of this appendix in Chapter 7, where we have associated geodesics length with holographic entanglement entropies within the framework of (holographic) integral geometry. We begin in Section 1 recasting the "no-kink" condition that determines the angle θ_B, discussed in Chapter 7, in the language of hyperbolic geometry, and we derive an expression for the geodesic length as a function of θ_B in Section 2.

1   THE NO-KINK CONDITION

In order to provide a visual representation of the geometry of constant-time[1] AdS$_3$ slices in the presence of the bubble, which consists of two hyperbolic planes $\mathbb{H}^2_\pm$ of different curvature radii suitably glued along a circle, we employ a conformal model constructed from two superimposed and glued Poincaré disks, relatively scaled in such a way that the circles along which the gluing is performed have the same size, as depicted in fig. C.1. In the same figure, we have marked a candidate polygonal curve for the injection-phase geodesic, discussed in Chapter 7, between boundary points A and $\overline{A}$. To find an actual geodesic it is necessary to determine the point B such that the no-kink condition is satisfied and, since the model is conformal, the kink also disappears visually. Rotating the model such that there is symmetry about the vertical axis, let us define θ_A (resp. θ_B) as the angle that the segment OA (resp. OB), respectively, make with the vertical axis. Then, $2\theta_A$ is the (angular) size of the boundary interval, which we regard as a given parameter.

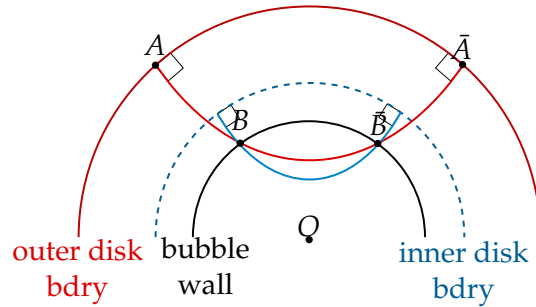[1] The relevant Penrose-like diagram is depicted in Chapter 7.

FIGURE C.1: the twofold Poincaré model with a candidate injection-
phase polygonal curve.

The no-kink condition is then equivalent to the statement that the angles that the hyperbolic line segments AB and $B\overline{B}$ make with the bubble radius through B, which we name α_{out}, α_{in} respectively, be equal.

Let us now consider the inner disk in fig. C.1. Let C be the intersection between $B\overline{B}$ and the radius that bisects the $\widehat{BO\overline{B}}$ angle or, equivalently, $\widehat{AO\overline{A}}$, as one can verify via a symmetry argument. Since $\theta_B = \widehat{BOC}$, noting that $\alpha_{\mathrm{in}} = \widehat{CBO}$ and that $\widehat{OCB}$ is right one finds, from the trigonometry of hyperbolic right triangles, that

$$\cosh \rho_- = \cot \alpha_{\mathrm{in}} \, \cot \theta_B \,, \tag{C.1}$$

where ρ_- is the geodesic radius of the bubble divided by L_-. Equivalently, the circumference of the bubble is $2\pi \, L_- \sinh \rho_-$.

For what concerns the outer disk, let us first show an identity for "omega triangles", namely hyperbolic triangles with exactly one ideal vertex. Let us consider an obtuse omega triangle with reference to fig. C.2. Then, the length of the segment PQ is given by

$$\frac{PQ}{L} = \cosh^{-1} \csc \gamma - \cosh^{-1} \csc \beta \,, \tag{C.2}$$

where L is the radius of the corresponding hyperbolic plane. This readily follows from dropping the perpendicular from Q to the opposite side and making use of the formula for the angle of parallelism.
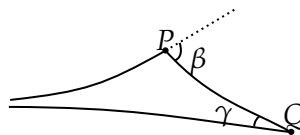

FIGURE C.2: an obtuse omega triangle, whose angles determine the
length of the segment PQ according to eq. (C.2).

Let us now turn to the entire outer $\mathbb{H}^2_+$, including the portion that has to be excised for the gluing in fig. C.1, and let us consider the obtuse omega triangle OBA in this plane. One may observe that the obtuse angle $\widehat{OBA}$ is supplementary to α_{out}, and that $\widehat{AOB} = \theta_A - \theta_B$. Therefore, using eq. (C.2) one finds

$$\rho_+ = \cosh^{-1}\csc(\theta_A - \theta_B) - \cosh^{-1}\csc\alpha_{\text{out}}\,,\tag{C.3}$$

where, as in the preceding case, $\rho_+ L_+$ is the geodesic radius of the bubble, now measured in the original $\mathbb{H}^2_+$ as if the interior $\mathbb{H}^2_-$ region were not present. More specifically, $\rho_\pm$ are related by the gluing condition that we have discussed in Chapter 7, and are therefore not independent. Indeed,

$$L_+ \sinh\rho_+ = L_- \sinh\rho_- = r\,.\tag{C.4}$$

Imposing the no-kink condition $\alpha_{\text{in}} = \alpha_{\text{out}}$ from eqs. (C.3) and (C.1) then yields the transcendental equation

$$\sqrt{1 + (\cosh\rho_- \tan\theta_B)^2} = \cosh\left(\cosh^{-1}\csc(\theta_A - \theta_B) - \rho_-\right)\tag{C.5}$$

for θ_B, which we have solved numerically alongside the constraint $|\alpha_{\text{in, out}}| < \frac{\pi}{2}$. We find that there is exactly one solution for θ_B in this range for all values of the parameters.

2 THE GEODESIC LENGTH

In order to compute the length of the geodesic, it is convenient to employ to an hyperboloid model in place of the disk model of fig. (C.1). Namely, let us embed $\mathbb{H}^2_\pm$ as the locus $\{X^\mu X_\mu = -1,\ X^0 > 0\}$ in $\mathbb{R}^{1,2}$, so that the geodesic distance between two points P and Q, in terms of their embedded images P^μ, Q^μ, is given by

$$d(P,Q) = L_\pm \cosh^{-1}\left(P^\mu Q_\mu\right)\,.\tag{C.6}$$

Since the length is divergent for points on the boundary, we regularize it placing A on a cutoff surface at a large, but finite, geodesic distance[2] Λ from the origin of $\mathbb{H}^2_-$. The length of the segments AB, $B\overline{B}$ and $\overline{B}\overline{A}$ can be computed using eq. (C.6), and the resulting total, which determines the entanglement entropy, is

$$
\begin{aligned}
\mathcal{L} - 2\,L_+\,\Lambda =\ & 2\,L_+ \log\left(\cosh\rho_+ -\ \sinh\rho_+ \cos\left(\theta_B - \theta_A\right)\right) \\
& + L_-\cosh^{-1}\left(\cosh^2\rho_- -\ \sinh^2\rho_- \cos\left(2\theta_B\right)\right) \qquad \text{(C.7)} \\
& + \mathcal{O}\left(\Lambda^{-1}\right).
\end{aligned}
$$

Once θ_B has been determined from the no-kink condition, one can insert it into eq. (C.7) to obtain a numerical estimate of the (finite part of the) length, and thus of the entanglement entropy according to the Ryu-Takayanagi formula.

---

[2]Let us observe that Λ is exponential in a cutoff on the global coordinate r, and this it can be identified with the usual UV cutoff employed in holography.

Bibliography

[1] A. M. Polyakov, "Quantum Geometry of Bosonic Strings", Phys. Lett. B **103**, edited by I. Khalatnikov and V. Mineev, 207–210 (1981).

[2] A. M. Polyakov, "Quantum Geometry of Fermionic Strings", Phys. Lett. B **103**, edited by I. Khalatnikov and V. Mineev, 211–213 (1981).

[3] J. Callan Curtis G., E. Martinec, M. Perry, and D. Friedan, "Strings in Background Fields", Nucl. Phys. B **262**, 593–609 (1985).

[4] J. M. Maldacena, "The Large N limit of superconformal field theories and supergravity", Int. J. Theor. Phys. **38**, [Adv. Theor. Math. Phys.2,231(1998)], 1113–1133 (1999), arXiv:hep-th/9711200 [hep-th].

[5] T. Banks, W. Fischler, S. Shenker, and L. Susskind, "M theory as a matrix model: A Conjecture", Phys. Rev. D **55**, 5112–5128 (1997), arXiv:hep-th/9610043.

[6] E. Witten, "String theory dynamics in various dimensions", Nucl. Phys. B **443**, 85–126 (1995), arXiv:hep-th/9503124.

[7] W. Fischler and L. Susskind, "Dilaton Tadpoles, String Condensates and Scale Invariance", Phys. Lett. **B171**, 383–389 (1986).

[8] E. Dudas, G. Pradisi, M. Nicolosi, and A. Sagnotti, "On tadpoles and vacuum redefinitions in string theory", Nucl. Phys. **B708**, 3–44 (2005), arXiv:hep-th/0410101 [hep-th].

[9] N. Kitazawa, "Tadpole Resummations in String Theory", Phys. Lett. **B660**, 415–421 (2008), arXiv:0801.1702 [hep-th].

[10] R. Pius, A. Rudra, and A. Sen, "String Perturbation Theory Around Dynamically Shifted Vacuum", JHEP **10**, 70 (2014), arXiv:1404.6254 [hep-th].

[11] S. Kachru, J. Pearson, and H. L. Verlinde, "Brane / flux annihilation and the string dual of a nonsupersymmetric field theory", JHEP **06**, 021 (2002), arXiv:hep-th/0112197 [hep-th].

[12]   S. Kachru, R. Kallosh, A. D. Linde, and S. P. Trivedi, "De Sitter vacua in string theory", Phys. Rev. D **68**, 046005 (2003), arXiv:hep-th/0301240.

[13]   F. Gautason, V. Van Hemelryck, and T. Van Riet, "The Tension between 10D Supergravity and dS Uplifts", Fortsch. Phys. **67**, 1800091 (2019), arXiv:1810. 08518 [hep-th].

[14]   Y. Hamada, A. Hebecker, G. Shiu, and P. Soler, "Understanding KKLT from a 10d perspective", JHEP **06**, 019 (2019), arXiv:1902.01410 [hep-th].

[15]   F. Gautason, V. Van Hemelryck, T. Van Riet, and G. Venken, "A 10d view on the KKLT AdS vacuum and uplifting", JHEP **06**, 074 (2020), arXiv:1902.01415 [hep-th].

[16]   H. Ooguri and C. Vafa, "Non-supersymmetric AdS and the Swampland", (2016), arXiv:1610.01533 [hep-th].

[17]   G. Obied, H. Ooguri, L. Spodyneiko, and C. Vafa, "De Sitter Space and the Swampland", (2018), arXiv:1806.08362 [hep-th].

[18]   N. Arkani-Hamed, L. Motl, A. Nicolis, and C. Vafa, "The String landscape, black holes and gravity as the weakest force", JHEP **06**, 060 (2007), arXiv:hep-th/0601001 [hep-th].

[19]   S. Sugimoto, "Anomaly cancellations in type I D-9 - anti-D-9 system and the USp(32) string theory", Prog. Theor. Phys. **102**, 685–699 (1999), arXiv:hep-th/9905159 [hep-th].

[20]   A. Sagnotti, "Some properties of open string theories", in Supersymmetry and unification of fundamental interactions. Proceedings, International Workshop, SUSY 95, Palaiseau, France, May 15-19 (1995), pp. 473–484, arXiv:hep-th/9509080 [hep-th].

[21]   A. Sagnotti, "Surprises in open string perturbation theory", Nucl. Phys. Proc. Suppl. **56B**, 332–343 (1997), arXiv:hep-th/9702093 [hep-th].

[22]   L. Alvarez-Gaume, P. H. Ginsparg, G. W. Moore, and C. Vafa, "An O(16) x O(16) Heterotic String", Phys. Lett. **B171**, 155–162 (1986).

[23]   L. J. Dixon and J. A. Harvey, "String Theories in Ten-Dimensions Without Space-Time Supersymmetry", Nucl. Phys. **B274**, [,93(1986)], 93–105 (1986).

[24] E. Dudas and J. Mourad, "Brane solutions in strings with broken supersymmetry and dilaton tadpoles", Phys. Lett. **B486**, 172–178 (2000), arXiv:hep-th/0004165 [hep-th].

[25] R. Antonelli and I. Basile, "Brane annihilation in non-supersymmetric strings", JHEP **11**, 021 (2019), arXiv:1908.04352 [hep-th].

[26] J. Mourad and A. Sagnotti, "*AdS* Vacua from Dilaton Tadpoles and Form Fluxes", Phys. Lett. **B768**, 92–96 (2017), arXiv:1612.08566 [hep-th].

[27] I. Basile, J. Mourad, and A. Sagnotti, "On Classical Stability with Broken Supersymmetry", JHEP **01**, 174 (2019), arXiv:1811.11448 [hep-th].

[28] E. A. Bergshoeff, M. de Roo, S. F. Kerstan, and F. Riccioni, "IIB supergravity revisited", JHEP **08**, 098 (2005), arXiv:hep-th/0506013 [hep-th].

[29] E. A. Bergshoeff, M. de Roo, S. F. Kerstan, T. Ortin, and F. Riccioni, "SL(2,R)-invariant IIB Brane Actions", JHEP **02**, 007 (2007), arXiv:hep-th/0611036 [hep-th].

[30] E. A. Bergshoeff and F. Riccioni, "String Solitons and T-duality", JHEP **05**, 131 (2011), arXiv:1102.0934 [hep-th].

[31] E. A. Bergshoeff and F. Riccioni, "Heterotic wrapping rules", JHEP **01**, 005 (2013), arXiv:1210.1422 [hep-th].

[32] E. A. Bergshoeff, V. A. Penas, F. Riccioni, and S. Risoli, "Non-geometric fluxes and mixed-symmetry potentials", JHEP **11**, 020 (2015), arXiv:1508.00780 [hep-th].

[33] B. Czech, L. Lamprou, S. McCandlish, and J. Sully, "Integral geometry and holography", Journal of High Energy Physics **2015**, 175 (2015).

[34] J. M. Maldacena and C. Nunez, "Supergravity description of field theories on curved manifolds and a no go theorem", Int. J. Mod. Phys. A **16**, edited by M. J. Duff, J. Liu, and J. Lu, 822–855 (2001), arXiv:hep-th/0007018.

[35] S. Banerjee, U. Danielsson, G. Dibitetto, S. Giri, and M. Schillo, "Emergent de Sitter Cosmology from Decaying Anti–de Sitter Space", Phys. Rev. Lett. **121**, 261301 (2018), arXiv:1807.01570 [hep-th].

[36] S. Banerjee, U. Danielsson, G. Dibitetto, S. Giri, and M. Schillo, "de Sitter Cosmology on an expanding bubble", JHEP **10**, 164 (2019), arXiv:`1907.04268` `[hep-th]`.

[37] S. Banerjee, U. Danielsson, and S. Giri, "Dark bubbles: decorating the wall", JHEP **20**, 085 (2020), arXiv:`2001.07433` `[hep-th]`.

[38] I. Antoniadis, E. Dudas, and A. Sagnotti, "Brane supersymmetry breaking", Phys. Lett. **B464**, 38–45 (1999), arXiv:`hep-th/9908023` `[hep-th]`.

[39] C. Angelantonj, "Comments on open string orbifolds with a nonvanishing B(ab)", Nucl. Phys. **B566**, 126–150 (2000), arXiv:`hep-th/9908064` `[hep-th]`.

[40] G. Aldazabal and A. M. Uranga, "Tachyon free nonsupersymmetric type IIB orientifolds via Brane - anti-brane systems", JHEP **10**, 024 (1999), arXiv:`hep-th/9908072` `[hep-th]`.

[41] C. Angelantonj, I. Antoniadis, G. D'Appollonio, E. Dudas, and A. Sagnotti, "Type I vacua with brane supersymmetry breaking", Nucl. Phys. **B572**, 36–70 (2000), arXiv:`hep-th/9911081` `[hep-th]`.

[42] C. Angelantonj and A. Sagnotti, "Open strings", Phys. Rept. **371**, [Erratum: Phys. Rept.376,no.6,407(2003)], 1–150 (2002), arXiv:`hep-th/0204089` `[hep-th]`.

[43] J. Mourad and A. Sagnotti, "An Update on Brane Supersymmetry Breaking", (2017), arXiv:`1711.11494` `[hep-th]`.

[44] E. Whittaker and G. Watson, *A course of modern analysis*, A Course of Modern Analysis: An Introduction to the General Theory of Infinite Processes and of Analytic Functions, with an Account of the Principal Transcendental Functions (Cambridge University Press, 1996).

[45] M. B. Green and J. H. Schwarz, "Anomaly Cancellation in Supersymmetric D=10 Gauge Theory and Superstring Theory", Phys. Lett. B **149**, 117–122 (1984).

[46] E. Dudas and J. Mourad, "Consistent gravitino couplings in nonsupersymmetric strings", Phys. Lett. **B514**, 173–182 (2001), arXiv:hep-th/0012071 [hep-th].

[47] A. Sagnotti, "Open Strings and their Symmetry Groups", in NATO Advanced Summer Institute on Nonperturbative Quantum Field Theory (Cargese Summer Institute) Cargese, France, July 16-30, 1987 (1987), pp. 521–528, arXiv:hep-th/0208020 [hep-th].

[48] G. Pradisi and A. Sagnotti, "Open String Orbifolds", Phys. Lett. **B216**, 59–67 (1989).

[49] P. Horava, "Strings on World Sheet Orbifolds", Nucl. Phys. **B327**, 461–484 (1989).

[50] P. Horava, "Background Duality of Open String Models", Phys. Lett. **B231**, 251–257 (1989).

[51] M. Bianchi and A. Sagnotti, "On the systematics of open string theories", Phys. Lett. **B247**, 517–524 (1990).

[52] M. Bianchi and A. Sagnotti, "Twist symmetry and open string Wilson lines", Nucl. Phys. **B361**, 519–538 (1991).

[53] M. Bianchi, G. Pradisi, and A. Sagnotti, "Toroidal compactification and symmetry breaking in open string theories", Nucl. Phys. **B376**, 365–386 (1992).

[54] A. Sagnotti, "A Note on the Green-Schwarz mechanism in open string theories", Phys. Lett. **B294**, 196–203 (1992), arXiv:hep-th/9210127 [hep-th].

[55] E. Dudas, "Theory and phenomenology of type I strings and M theory", Class. Quant. Grav. **17**, R41–R116 (2000), arXiv:hep-ph/0006190 [hep-ph].

[56] G. Pradisi and F. Riccioni, "Geometric couplings and brane supersymmetry breaking", Nucl. Phys. **B615**, 33–60 (2001), arXiv:hep-th/0107090 [hep-th].

[57] N. Kitazawa, "Brane SUSY Breaking and the Gravitino Mass", JHEP **04**, 081 (2018), arXiv:1802.03088 [hep-th].

[58] A. Sagnotti, "Low-ℓ CMB from string-scale SUSY breaking?", Mod. Phys. Lett. **A32**, [Subnucl. Ser.53,289(2017)], 1730001 (2016), arXiv:`1509.08204` `[astro-ph.CO]`.

[59] A. Gruppuso, N. Kitazawa, N. Mandolesi, P. Natoli, and A. Sagnotti, "Pre-Inflationary Relics in the CMB?", Phys. Dark Univ. **11**, 68–73 (2016), arXiv:`1508.00411 [astro-ph.CO]`.

[60] A. Gruppuso, N. Kitazawa, M. Lattanzi, N. Mandolesi, P. Natoli, and A. Sagnotti, "The Evens and Odds of CMB Anomalies", Phys. Dark Univ. **20**, 49–64 (2018), arXiv:`1712.03288 [astro-ph.CO]`.

[61] S. Kachru, J. Kumar, and E. Silverstein, "Vacuum energy cancellation in a nonsupersymmetric string", Phys. Rev. D **59**, 106004 (1999), arXiv:`hep-th/9807076`.

[62] C. Angelantonj and M. Cardella, "Vanishing perturbative vacuum energy in nonsupersymmetric orientifolds", Phys. Lett. B **595**, 505–512 (2004), arXiv:`hep-th/0403107`.

[63] S. Abel and R. J. Stewart, "Exponential suppression of the cosmological constant in nonsupersymmetric string vacua at two loops and beyond", Phys. Rev. D **96**, 106013 (2017), arXiv:`1701.06629 [hep-th]`.

[64] P. G. Freund and M. A. Rubin, "Dynamics of Dimensional Reduction", Phys. Lett. B **97**, edited by A. Salam and E. Sezgin, 233–235 (1980).

[65] E. Silverstein, "(A)dS backgrounds from asymmetric orientifolds", Clay Mat. Proc. **1**, 179 (2002), arXiv:`hep-th/0106209`.

[66] A. Maloney, E. Silverstein, and A. Strominger, "De Sitter space in noncritical string theory", in Workshop on Conference on the Future of Theoretical Physics and Cosmology in Honor of Steven Hawking's 60th Birthday (May 2002), pp. 570–591, arXiv:`hep-th/0205316`.

[67] J. M. Maldacena and H. Ooguri, "Strings in AdS(3) and SL(2,R) WZW model 1.: The Spectrum", J. Math. Phys. **42**, 2929–2960 (2001), arXiv:`hep-th/0001053`.

[68] R. Blumenhagen and A. Font, "Dilaton tadpoles, warped geometries and large extra dimensions for nonsupersymmetric strings", Nucl. Phys. B **599**, 241–254 (2001), arXiv:hep-th/0011269.

[69] E. Dudas, N. Kitazawa, and A. Sagnotti, "On Climbing Scalars in String Theory", Phys. Lett. B **694**, 80–88 (2011), arXiv:1009.0874 [hep-th].

[70] C. Condeescu and E. Dudas, "Kasner solutions, climbing scalars and big-bang singularity", JCAP **08**, 013 (2013), arXiv:1306.0911 [hep-th].

[71] C. Angelantonj and A. Armoni, "Nontachyonic type 0B orientifolds, non-supersymmetric gauge theories and cosmological RG flow", Nucl. Phys. **B578**, 239–258 (2000), arXiv:hep-th/9912257 [hep-th].

[72] C. Angelantonj and A. Armoni, "RG flow, Wilson loops and the dilaton tad-pole", Phys. Lett. **B482**, 329–336 (2000), arXiv:hep-th/0003050 [hep-th].

[73] E. Dudas and J. Mourad, "D-branes in nontachyonic 0B orientifolds", Nucl. Phys. **B598**, 189–224 (2001), arXiv:hep-th/0010179 [hep-th].

[74] I. R. Klebanov and A. A. Tseytlin, "D-branes and dual gauge theories in type 0 strings", Nucl. Phys. **B546**, 155–181 (1999), arXiv:hep-th/9811035 [hep-th].

[75] M. Montero, T. Van Riet, and G. Venken, "A dS obstruction and its phenomeno-logical consequences", JHEP **05**, 114 (2020), arXiv:2001.11023 [hep-th].

[76] E. Dudas, J. Mourad, and A. Sagnotti, "Charged and uncharged D-branes in various string theories", Nucl. Phys. **B620**, 109–151 (2002), arXiv:hep-th/0107081 [hep-th].

[77] J. D. Blum and K. R. Dienes, "Duality without supersymmetry: The Case of the SO(16) x SO(16) string", Phys. Lett. **B414**, 260–268 (1997), arXiv:hep-th/9707148 [hep-th].

[78] J. D. Blum and K. R. Dienes, "Strong / weak coupling duality relations for non-supersymmetric string theories", Nucl. Phys. **B516**, 83–159 (1998), arXiv:hep-th/9707160 [hep-th].

[79] D. Lüst and D. Tsimpis, "AdS$_2$ Type-IIA Solutions and Scale Separation", (2020), arXiv:2004.07582 [hep-th].

[80] F. Gautason, M. Schillo, T. Van Riet, and M. Williams, "Remarks on scale separation in flux vacua", JHEP **03**, 061 (2016), arXiv:1512.00457 [hep-th].

[81] D. Lüst, E. Palti, and C. Vafa, "AdS and the Swampland", Phys. Lett. B **797**, 134867 (2019), arXiv:1906.05225 [hep-th].

[82] F. Marchesano, E. Palti, J. Quirant, and A. Tomasiello, "On supersymmetric AdS$_4$ orientifold vacua", (2020), arXiv:2003.13578 [hep-th].

[83] A. R. Brown and A. Dahlen, "Small Steps and Giant Leaps in the Landscape", Phys. Rev. D **82**, 083519 (2010), arXiv:1004.3994 [hep-th].

[84] S. M. Carroll, M. C. Johnson, and L. Randall, "Dynamical compactification from de Sitter space", JHEP **11**, 094 (2009), arXiv:0904.3115 [hep-th].

[85] F. Apruzzi, M. Fazzi, D. Rosa, and A. Tomasiello, "All AdS_7 solutions of type II supergravity", JHEP **04**, 064 (2014), arXiv:1309.2949 [hep-th].

[86] F. Apruzzi, G. Bruno De Luca, A. Gnecchi, G. Lo Monaco, and A. Tomasiello, "On AdS$_7$ stability", (2019), arXiv:1912.13491 [hep-th].

[87] S.-W. Kim, J. Nishimura, and A. Tsuchiya, "Expanding (3+1)-dimensional universe from a Lorentzian matrix model for superstring theory in (9+1)-dimensions", Phys. Rev. Lett. **108**, 011601 (2012), arXiv:1108.1540 [hep-th].

[88] K. N. Anagnostopoulos, T. Azuma, Y. Ito, J. Nishimura, and S. K. Papadoudis, "Complex Langevin analysis of the spontaneous symmetry breaking in dimensionally reduced super Yang-Mills models", JHEP **02**, 151 (2018), arXiv:1712.07562 [hep-lat].

[89] N. Ishibashi, H. Kawai, Y. Kitazawa, and A. Tsuchiya, "A Large N reduced model as superstring", Nucl. Phys. B **498**, 467–491 (1997), arXiv:hep-th/9612115.

[90] S. S. Gubser and I. Mitra, "Some interesting violations of the Breitenlohner-Freedman bound", JHEP **07**, 044 (2002), arXiv:hep-th/0108239.

[91] O. DeWolfe, D. Z. Freedman, S. S. Gubser, G. T. Horowitz, and I. Mitra, "Stability of AdS(p) x M(q) compactifications without supersymmetry", Phys. Rev. D **65**, 064033 (2002), arXiv:hep-th/0105047.

[92] Y. P. Hong and I. Mitra, "Investigating the stability of a nonsupersymmetric landscape", Phys. Rev. D **72**, 126003 (2005), arXiv:hep-th/0508238.

[93] E. Malek, H. Nicolai, and H. Samtleben, "Tachyonic Kaluza-Klein modes and the AdS swampland conjecture", (2020), arXiv:2005.07713 [hep-th].

[94] I. R. Klebanov and E. Witten, "Superconformal field theory on three-branes at a Calabi-Yau singularity", Nucl. Phys. B **536**, 199–218 (1998), arXiv:hep-th/9807080.

[95] N. Itzhaki, J. M. Maldacena, J. Sonnenschein, and S. Yankielowicz, "Supergravity and the large N limit of theories with sixteen supercharges", Phys. Rev. D **58**, 046004 (1998), arXiv:hep-th/9802042.

[96] J. D. Brown and C. Teitelboim, "Dynamical Neutralization of the Cosmological Constant", Phys. Lett. **B195**, 177–182 (1987).

[97] J. D. Brown and C. Teitelboim, "Neutralization of the Cosmological Constant by Membrane Creation", Nucl. Phys. **B297**, 787–836 (1988).

[98] S. R. Coleman, "The Fate of the False Vacuum. 1. Semiclassical Theory", Phys. Rev. **D15**, [Erratum: Phys. Rev.D16,1248(1977)], 2929–2936 (1977).

[99] C. G. Callan Jr. and S. R. Coleman, "The Fate of the False Vacuum. 2. First Quantum Corrections", Phys. Rev. **D16**, 1762–1768 (1977).

[100] S. R. Coleman and F. De Luccia, "Gravitational Effects on and of Vacuum Decay", Phys. Rev. **D21**, 3305 (1980).

[101] J. J. Blanco-Pillado, D. Schwartz-Perlov, and A. Vilenkin, "Quantum Tunneling in Flux Compactifications", JCAP **0912**, 006 (2009), arXiv:0904.3106 [hep-th].

[102] A. R. Brown and A. Dahlen, "Bubbles of Nothing and the Fastest Decay in the Landscape", Phys. Rev. D **84**, 043518 (2011), arXiv:1010.5240 [hep-th].

[103] R. Bousso and J. Polchinski, "Quantization of four form fluxes and dynamical neutralization of the cosmological constant", JHEP **06**, 006 (2000), arXiv:hep-th/0004134.

[104] A. R. Brown and A. Dahlen, "Giant Leaps and Minimal Branes in Multi-Dimensional Flux Landscapes", Phys. Rev. D **84**, 023513 (2011), arXiv:1010.5241 [hep-th].

[105] E. Witten, "Instability of the Kaluza-Klein Vacuum", Nucl. Phys. **B195**, 481–492 (1982).

[106] G. Dibitetto, N. Petri, and M. Schillo, "Nothing really matters", (2020), arXiv:2002.01764 [hep-th].

[107] I. García Etxebarria, M. Montero, K. Sousa, and I. Valenzuela, "Nothing is certain in string compactifications", (2020), arXiv:2005.06494 [hep-th].

[108] A. R. Brown and A. Dahlen, "On 'nothing' as an infinitely negatively curved spacetime", Phys. Rev. D **85**, 104026 (2012), arXiv:1111.0301 [hep-th].

[109] R. Antonelli, I. Basile, and A. Bombini, "AdS Vacuum Bubbles, Holography and Dual RG Flows", Class. Quant. Grav. **36**, 045004 (2019), arXiv:1806.02289 [hep-th].

[110] J. M. Maldacena, J. Michelson, and A. Strominger, "Anti-de Sitter fragmentation", JHEP **02**, 011 (1999), arXiv:hep-th/9812073 [hep-th].

[111] N. Seiberg and E. Witten, "The D1 / D5 system and singular CFT", JHEP **04**, 017 (1999), arXiv:hep-th/9903224 [hep-th].

[112] M. Bianchi and A. Sagnotti, "The Partition Function of the SO(8192) Bosonic String", Phys. Lett. B **211**, 407–416 (1988).

[113] G. T. Horowitz and A. Strominger, "Black strings and P-branes", Nucl. Phys. **B360**, 197–209 (1991).

[114] A. Sagnotti, "Brane SUSY breaking and inflation: implications for scalar fields and CMB distortion", Phys. Part. Nucl. Lett. **11**, 836–843 (2014), arXiv:1303.6685 [hep-th].

[115] P. Fré, A. Sagnotti, and A. Sorin, "Integrable Scalar Cosmologies I. Foundations and links with String Theory", Nucl. Phys. B **877**, 1028–1106 (2013), arXiv:1307.1910 [hep-th].

[116] R. C. Myers, "Dielectric branes", JHEP **12**, 022 (1999), arXiv:hep-th/9910053 [hep-th].

[117] E. Witten, "Anti-de Sitter space and holography", Adv. Theor. Math. Phys. **2**, 253–291 (1998), arXiv:`hep-th/9802150 [hep-th]`.

[118] S. S. Gubser, I. R. Klebanov, and A. M. Polyakov, "Gauge theory correlators from noncritical string theory", Phys. Lett. **B428**, 105–114 (1998), arXiv:`hep-th/9802109 [hep-th]`.

[119] J. M. Bardeen, B. Carter, and S. W. Hawking, "The Four laws of black hole mechanics", Commun. Math. Phys. **31**, 161–170 (1973).

[120] A. Strominger and C. Vafa, "Microscopic origin of the Bekenstein-Hawking entropy", Phys. Lett. **B379**, 99–104 (1996), arXiv:`hep-th/9601029 [hep-th]`.

[121] A. Strominger, "Black hole entropy from near horizon microstates", JHEP **02**, 009 (1998), arXiv:`hep-th/9712251 [hep-th]`.

[122] J. R. David, G. Mandal, and S. R. Wadia, "Microscopic formulation of black holes in string theory", Phys. Rept. **369**, 549–686 (2002), arXiv:`hep-th/0203048 [hep-th]`.

[123] S. Ryu and T. Takayanagi, "Holographic derivation of entanglement entropy from AdS/CFT", Phys. Rev. Lett. **96**, 181602 (2006), arXiv:`hep-th/0603001 [hep-th]`.

[124] M. Rangamani and T. Takayanagi, "Holographic Entanglement Entropy", Lect. Notes Phys. **931**, pp.1–246 (2017), arXiv:`1609.01287 [hep-th]`.

[125] V. E. Hubeny, M. Rangamani, and T. Takayanagi, "A Covariant holographic entanglement entropy proposal", JHEP **07**, 062 (2007), arXiv:`0705.0016 [hep-th]`.

[126] S. Kanno and J. Soda, "Exact Coleman-de Luccia Instantons", Int. J. Mod. Phys. **D21**, 1250040 (2012), arXiv:`1111.0720 [hep-th]`.

[127] B. Freivogel and M. Kleban, "Vacua Morghulis", (2016), arXiv:`1610.04564 [hep-th]`.

[128] U. H. Danielsson, G. Dibitetto, and S. C. Vargas, "Universal isolation in the AdS landscape", Phys. Rev. **D94**, 126002 (2016), arXiv:`1605.09289 [hep-th]`.

[129] P. Burda, R. Gregory, and A. Jain, "Holographic Reconstruction of Bubbles", (2018), arXiv:`1804.05202 [hep-th]`.

[130] S. Hirano, "Brown-Teitelboim Instantons and the First Law of Thermodynamics of (Anti) de Sitter Space", (2018), arXiv:1804.09985 [hep-th].

[131] S. de Haro, I. Papadimitriou, and A. C. Petkou, "Conformally Coupled Scalars, Instantons and Vacuum Instability in AdS(4)", Phys. Rev. Lett. **98**, 231601 (2007), arXiv:hep-th/0611315 [hep-th].

[132] I. Papadimitriou, "Multi-Trace Deformations in AdS/CFT: Exploring the Vacuum Structure of the Deformed CFT", JHEP **05**, 075 (2007), arXiv:hep-th/0703152 [hep-th].

[133] A. Bhattacharyya, L.-Y. Hung, and C. M. Melby-Thompson, "Instantons and Entanglement Entropy", JHEP **10**, 081 (2017), arXiv:1703.01611 [hep-th].

[134] J. Maldacena, "Vacuum decay into Anti de Sitter space", (2010), arXiv:1012.0274 [hep-th].

[135] J. L. F. Barbon and E. Rabinovici, "Holography of AdS vacuum bubbles", JHEP **04**, 123 (2010), arXiv:1003.4966 [hep-th].

[136] D. Harlow, "Metastability in Anti de Sitter Space", (2010), arXiv:1003.5909 [hep-th].

[137] T. D. Brennan, F. Carta, and C. Vafa, "The String Landscape, the Swampland, and the Missing Corner", PoS **TASI2017**, 015 (2017), arXiv:1711.00864 [hep-th].

[138] J. D. Brown and M. Henneaux, "Central Charges in the Canonical Realization of Asymptotic Symmetries: An Example from Three-Dimensional Gravity", Commun. Math. Phys. **104**, 207–226 (1986).

[139] A. B. Zamolodchikov, "Irreversibility of the Flux of the Renormalization Group in a 2D Field Theory", JETP Lett. **43**, [Pisma Zh. Eksp. Teor. Fiz.43,565(1986)], 730–732 (1986).

[140] E. Witten, "(2+1)-Dimensional Gravity as an Exactly Soluble System", Nucl. Phys. **B311**, 46 (1988).

[141] S. Carlip, "(2+1)-dimensional Chern-Simons gravity as a Dirac square root", Phys. Rev. **D45**, [Erratum: Phys. Rev.D47,1729(1993)], 3584–3590 (1992), arXiv:hep-th/9109006 [hep-th].

[142] J. L. Cardy, "Operator Content of Two-Dimensional Conformally Invariant Theories", Nucl. Phys. **B270**, 186–204 (1986).

[143] P. Calabrese and J. L. Cardy, "Entanglement entropy and quantum field theory", J. Stat. Mech. **0406**, P06002 (2004), arXiv:hep-th/0405152 [hep-th].

[144] P. Calabrese and J. Cardy, "Entanglement entropy and conformal field theory", J. Phys. **A42**, 504005 (2009), arXiv:0905.4013 [cond-mat.stat-mech].

[145] W. Israel, "Singular hypersurfaces and thin shells in general relativity", Il Nuovo Cimento B (1965-1970) **44**, 1–14 (1966).

[146] C. Barrabes and W. Israel, "Thin shells in general relativity and cosmology: The Lightlike limit", Phys. Rev. **D43**, 1129–1142 (1991).

[147] E. Poisson, "A Reformulation of the Barrabes-Israel null shell formalism", (2002), arXiv:gr-qc/0207101 [gr-qc].

[148] L. F. Abbott and S. R. Coleman, "The Collapse of an Anti-de Sitter Bubble", Nucl. Phys. **B259**, 170–174 (1985).

[149] O. Aharony, S. S. Gubser, J. M. Maldacena, H. Ooguri, and Y. Oz, "Large N field theories, string theory and gravity", Phys. Rept. **323**, 183–386 (2000), arXiv:hep-th/9905111 [hep-th].

[150] H. Casini and M. Huerta, "A c-theorem for the entanglement entropy", J. Phys. **A40**, 7031–7036 (2007), arXiv:cond-mat/0610375 [cond-mat].

[151] R. C. Myers and A. Sinha, "Seeing a c-theorem with holography", Phys. Rev. **D82**, 046006 (2010), arXiv:1006.1263 [hep-th].

[152] R. C. Myers and A. Sinha, "Holographic c-theorems in arbitrary dimensions", JHEP **01**, 125 (2011), arXiv:1011.5819 [hep-th].

[153] R. C. Myers and A. Singh, "Comments on Holographic Entanglement Entropy and RG Flows", JHEP **04**, 122 (2012), arXiv:1202.2068 [hep-th].

[154] T. Albash and C. V. Johnson, "Holographic Entanglement Entropy and Renormalization Group Flow", JHEP **02**, 095 (2012), arXiv:1110.1074 [hep-th].

[155] H. Casini and M. Huerta, "On the RG running of the entanglement entropy of a circle", Phys. Rev. **D85**, 125016 (2012), arXiv:1202.5650 [hep-th].

[156] D. Anselmi, D. Z. Freedman, M. T. Grisaru, and A. A. Johansen, "Nonperturbative formulas for central functions of supersymmetric gauge theories", Nucl. Phys. **B526**, 543–571 (1998), arXiv:`hep-th/9708042 [hep-th]`.

[157] L. Girardello, M. Petrini, M. Porrati, and A. Zaffaroni, "Novel local CFT and exact results on perturbations of N=4 superYang Mills from AdS dynamics", JHEP **12**, 022 (1998), arXiv:`hep-th/9810126 [hep-th]`.

[158] M. Henningson and K. Skenderis, "The Holographic Weyl anomaly", JHEP **07**, 023 (1998), arXiv:`hep-th/9806087 [hep-th]`.

[159] D. Z. Freedman, S. S. Gubser, K. Pilch, and N. P. Warner, "Renormalization group flows from holography supersymmetry and a c theorem", Adv. Theor. Math. Phys. **3**, 363–417 (1999), arXiv:`hep-th/9904017 [hep-th]`.

[160] J. de Boer, E. P. Verlinde, and H. L. Verlinde, "On the holographic renormalization group", JHEP **08**, 003 (2000), arXiv:`hep-th/9912012 [hep-th]`.

[161] M. Bianchi, D. Z. Freedman, and K. Skenderis, "Holographic renormalization", Nucl. Phys. B **631**, 159–194 (2002), arXiv:`hep-th/0112119`.

[162] V. Balasubramanian and P. Kraus, "A Stress tensor for Anti-de Sitter gravity", Commun. Math. Phys. **208**, 413–428 (1999), arXiv:`hep-th/9902121 [hep-th]`.

[163] C. Fefferman and C. Graham, "Conformal invariants.", English, in *Élie Cartan et les mathématiques d'aujourd'hui. The mathematical heritage of Elie Cartan (Seminar), Lyon, June 25-29, 1984* (1985).

[164] C. Fefferman and C. R. Graham, "The ambient metric", Ann. Math. Stud. **178**, 1–128 (2011), arXiv:`0710.0919 [math.DG]`.

[165] S. Bhowmick, S. Das, and B. Ezhuthachan, "Entanglement entropy and kinematic space in BCFT", (2017), arXiv:`1703.01759 [hep-th]`.

[166] V. E. Hubeny, H. Maxfield, M. Rangamani, and E. Tonni, "Holographic entanglement plateaux", JHEP **08**, 092 (2013), arXiv:`1306.4004 [hep-th]`.

[167] B. Freivogel, R. Jefferson, L. Kabir, B. Mosk, and I.-S. Yang, "Casting Shadows on Holographic Reconstruction", Phys. Rev. **D91**, 086013 (2015), arXiv:`1412.5175 [hep-th]`.

[168] V. Balasubramanian and S. F. Ross, "The Dual of nothing", Phys. Rev. **D66**, 086002 (2002), arXiv:hep-th/0205290 [hep-th].

[169] V. Balasubramanian, K. Larjo, and J. Simon, "Much ado about nothing", Class. Quant. Grav. **22**, 4149–4170 (2005), arXiv:hep-th/0502111 [hep-th].

[170] J. He and M. Rozali, "On bubbles of nothing in AdS/CFT", JHEP **09**, 089 (2007), arXiv:hep-th/0703220 [HEP-TH].

[171] B. Freivogel, Y. Sekino, L. Susskind, and C.-P. Yeh, "A Holographic framework for eternal inflation", Phys. Rev. D **74**, 086003 (2006), arXiv:hep-th/0606204.

[172] A. B. Zamolodchikov, "Expectation value of composite field T anti-T in two-dimensional quantum field theory", (2004), arXiv:hep-th/0401146.

[173] A. Cavaglià, S. Negro, I. M. Szécsényi, and R. Tateo, "$T\bar{T}$-deformed 2D Quantum Field Theories", JHEP **10**, 112 (2016), arXiv:1608.05534 [hep-th].

[174] L. McGough, M. Mezei, and H. Verlinde, "Moving the CFT into the bulk with $T\bar{T}$", JHEP **04**, 010 (2018), arXiv:1611.03470 [hep-th].

[175] W. Donnelly and V. Shyam, "Entanglement entropy and $T\bar{T}$ deformation", Phys. Rev. Lett. **121**, 131602 (2018), arXiv:1806.07444 [hep-th].

[176] T. Hartman, J. Kruthoff, E. Shaghoulian, and A. Tajdini, "Holography at finite cutoff with a T^2 deformation", JHEP **03**, 004 (2019), arXiv:1807.11401 [hep-th].

[177] I. R. Klebanov, "Tachyon stabilization in the AdS / CFT correspondence", Phys. Lett. **B466**, 166–170 (1999), arXiv:hep-th/9906220 [hep-th].

[178] E. Witten, "Baryons and branes in anti-de Sitter space", JHEP **07**, 006 (1998), arXiv:hep-th/9805112 [hep-th].

[179] J. L. F. Barbon and E. Rabinovici, "Holography of AdS vacuum bubbles", Nucl. Phys. Proc. Suppl. **216**, 121–146 (2011).

[180] S. Kachru and E. Silverstein, "4-D conformal theories and strings on orbifolds", Phys. Rev. Lett. **80**, 4855–4858 (1998), arXiv:hep-th/9802183 [hep-th].

[181] A. E. Lawrence, N. Nekrasov, and C. Vafa, "On conformal field theories in four-dimensions", Nucl. Phys. **B533**, 199–209 (1998), arXiv:hep-th/9803015 [hep-th].

[182]   M. Bershadsky, Z. Kakushadze, and C. Vafa, "String expansion as large N expansion of gauge theories", Nucl. Phys. **B523**, 59–72 (1998), arXiv:hep-th/9803076 [hep-th].

[183]   M. Bershadsky and A. Johansen, "Large N limit of orbifold field theories", Nucl. Phys. **B536**, 141–148 (1998), arXiv:hep-th/9803249 [hep-th].

[184]   M. Schmaltz, "Duality of nonsupersymmetric large N gauge theories", Phys. Rev. **D59**, 105018 (1999), arXiv:hep-th/9805218 [hep-th].

[185]   J. Erlich and A. Naqvi, "Nonperturbative tests of the parent / orbifold correspondence in supersymmetric gauge theories", JHEP **12**, 047 (2002), arXiv:hep-th/9808026 [hep-th].

[186]   D. Tong, "Comments on condensates in nonsupersymmetric orbifold field theories", JHEP **03**, 022 (2003), arXiv:hep-th/0212235.

[187]   E. Gava, J. Morales, K. Narain, and G. Thompson, "Bound states of type I D strings", Nucl. Phys. B **528**, 95–108 (1998), arXiv:hep-th/9801128.

[188]   G. 't Hooft, "A Two-Dimensional Model for Mesons", Nucl. Phys. B **75**, 461–470 (1974).

[189]   D. Vassilevich, "Heat kernel expansion: User's manual", Phys. Rept. **388**, 279–360 (2003), arXiv:hep-th/0306138.

[190]   D. J. Gross and F. Wilczek, "Ultraviolet Behavior of Nonabelian Gauge Theories", Phys. Rev. Lett. **30**, edited by J. Taylor, 1343–1346 (1973).

[191]   N. Yamatsu, "Finite-Dimensional Lie Algebras and Their Representations for Unified Model Building", (2015), arXiv:1511.08771 [hep-ph].

[192]   Y. Frishman and J. Sonnenschein, "QCD in two-dimensions screening, confinement and novel nonAbelian solutions", Nucl. Phys. B **496**, 285–301 (1997), arXiv:hep-th/9701140.

[193]   S. Weinberg, "Effective field theories in the large N limit", Phys. Rev. D **56**, 2303–2316 (1997), arXiv:hep-th/9706042.

[194]   M. Moshe and J. Zinn-Justin, "Quantum field theory in the large N limit: A Review", Phys. Rept. **385**, 69–228 (2003), arXiv:hep-th/0306133.

[195] E. Witten, "Nonabelian Bosonization in Two-Dimensions", Commun. Math. Phys. **92**, 455–472 (1984).

[196] A. Cherman and D. Dorigoni, "Large N and Bosonization in Three Dimensions", JHEP **10**, 173 (2012), arXiv:`1208.1769 [hep-th]`.

[197] E. Silverstein and Y. S. Song, "On the critical behavior of D1-brane theories", JHEP **03**, 029 (2000), arXiv:`hep-th/9912244`.

[198] M. Cvetic, S. Griffies, and S.-J. Rey, "Nonperturbative stability of supergravity and superstring vacua", Nucl. Phys. **B389**, 3–24 (1993), arXiv:`hep-th/9206004 [hep-th]`.

[199] A. Ceresole, G. Dall'Agata, A. Giryavets, R. Kallosh, and A. D. Linde, "Domain walls, near-BPS bubbles, and probabilities in the landscape", Phys. Rev. **D74**, 086010 (2006), arXiv:`hep-th/0605266 [hep-th]`.

[200] M. Cvetic and H. H. Soleng, "Supergravity domain walls", Phys. Rept. **282**, 159–223 (1997), arXiv:`hep-th/9604090 [hep-th]`.

[201] I. Bandos, F. Farakos, S. Lanza, L. Martucci, and D. Sorokin, "Three-forms, dualities and membranes in four-dimensional supergravity", (2018), arXiv:`1803.01405 [hep-th]`.

[202] D. Friedan, Z.-a. Qiu, and S. H. Shenker, "Superconformal Invariance in Two-Dimensions and the Tricritical Ising Model", Phys. Lett. **151B**, 37–43 (1985).

[203] S.-S. Lee, "TASI Lectures on Emergence of Supersymmetry, Gauge Theory and String in Condensed Matter Systems", in Proceedings, Theoretical Advanced Study Institute in Elementary Particle Physics (TASI 2010). String Theory and Its Applications: From meV to the Planck Scale: Boulder, Colorado, USA, June 1-25, 2010 (2010), pp. 667–706, arXiv:`1009.5127 [hep-th]`.

[204] S. B. Giddings, S. Kachru, and J. Polchinski, "Hierarchies from fluxes in string compactifications", Phys. Rev. D **66**, 106006 (2002), arXiv:`hep-th/0105097`.

[205] P. Koerber and L. Martucci, "From ten to four and back again: How to generalize the geometry", JHEP **08**, 059 (2007), arXiv:`0707.1038 [hep-th]`.

[206] J. Moritz, A. Retolaza, and A. Westphal, "Toward de Sitter space from ten dimensions", Phys. Rev. D **97**, 046010 (2018), arXiv:`1707.08678 [hep-th]`.

[207] R. Kallosh and T. Wrase, "dS Supergravity from 10d", Fortsch. Phys. **67**, 1800071 (2019), arXiv:`1808.09427 [hep-th]`.

[208] C. Córdova, G. B. De Luca, and A. Tomasiello, "Classical de Sitter Solutions of 10-Dimensional Supergravity", Phys. Rev. Lett. **122**, 091601 (2019), arXiv:`1812.04147 [hep-th]`.

[209] J. Blåbäck, U. Danielsson, G. Dibitetto, and S. Giri, "Constructing stable de Sitter in M-theory from higher curvature corrections", JHEP **09**, 042 (2019), arXiv:`1902.04053 [hep-th]`.

[210] C. Córdova, G. B. De Luca, and A. Tomasiello, "New de Sitter Solutions in Ten Dimensions and Orientifold Singularities", (2019), arXiv:`1911.04498 [hep-th]`.

[211] U. H. Danielsson, S. S. Haque, G. Shiu, and T. Van Riet, "Towards Classical de Sitter Solutions in String Theory", JHEP **09**, 114 (2009), arXiv:`0907.2041 [hep-th]`.

[212] N. Kaloper, "Bent domain walls as brane worlds", Phys. Rev. D **60**, 123506 (1999), arXiv:`hep-th/9905210`.

[213] T. Shiromizu, K.-i. Maeda, and M. Sasaki, "The Einstein equation on the 3-brane world", Phys. Rev. D **62**, 024012 (2000), arXiv:`gr-qc/9910076`.

[214] D. N. Vollick, "Cosmology on a three-brane", Class. Quant. Grav. **18**, 1–10 (2001), arXiv:`hep-th/9911181`.

[215] S. S. Gubser, "AdS / CFT and gravity", Phys. Rev. D **63**, 084017 (2001), arXiv:`hep-th/9912001`.

[216] S. Hawking, T. Hertog, and H. Reall, "Brane new world", Phys. Rev. D **62**, 043501 (2000), arXiv:`hep-th/0003052`.

[217] L. Randall and R. Sundrum, "A Large mass hierarchy from a small extra dimension", Phys. Rev. Lett. **83**, 3370–3373 (1999), arXiv:`hep-ph/9905221`.

[218] L. Randall and R. Sundrum, "An Alternative to compactification", Phys. Rev. Lett. **83**, 4690–4693 (1999), arXiv:`hep-th/9906064`.

[219] S. B. Giddings, E. Katz, and L. Randall, "Linearized gravity in brane backgrounds", JHEP **03**, 023 (2000), arXiv:hep-th/0002091.

[220] G. Dvali, G. Gabadadze, and M. Porrati, "4-D gravity on a brane in 5-D Minkowski space", Phys. Lett. B **485**, 208–214 (2000), arXiv:hep-th/0005016.

[221] A. Karch and L. Randall, "Locally localized gravity", JHEP **05**, edited by M. J. Duff, J. Liu, and J. Lu, 008 (2001), arXiv:hep-th/0011156.

[222] H. Z. Chen, R. C. Myers, D. Neuenfeld, I. A. Reyes, and J. Sandor, "Quantum Extremal Islands Made Easy, Part I: Entanglement on the Brane", (2020), arXiv:2006.04851 [hep-th].

[223] S. Poletti, J. Twamley, and D. Wiltshire, "Charged dilaton black holes with a cosmological constant", Phys. Rev. D **51**, 5720–5724 (1995), arXiv:hep-th/9412076.

[224] D. L. Wiltshire, "Dilaton black holes with a cosmological term", J. Austral. Math. Soc. B **41**, edited by D. E. McClelland and S. M. Scott, 198–216 (1999), arXiv:gr-qc/9502038.

[225] K. C. Chan, J. H. Horne, and R. B. Mann, "Charged dilaton black holes with unusual asymptotics", Nucl. Phys. B **447**, 441–464 (1995), arXiv:gr-qc/9502042.

[226] G. T. Horowitz, J. Orgera, and J. Polchinski, "Nonperturbative Instability of AdS(5) x S**5/Z(k)", Phys. Rev. **D77**, 024004 (2008), arXiv:0709.4262 [hep-th].

[227] J. J. Blanco-Pillado and B. Shlaer, "Bubbles of Nothing in Flux Compactifications", Phys. Rev. D **82**, 086015 (2010), arXiv:1002.4408 [hep-th].

[228] K. A. Meissner, "Symmetries of higher order string gravity actions", Phys. Lett. B **392**, 298–304 (1997), arXiv:hep-th/9610131.

[229] O. Hohm and B. Zwiebach, "T-duality Constraints on Higher Derivatives Revisited", JHEP **04**, 101 (2016), arXiv:1510.00005 [hep-th].

[230] O. Hohm and B. Zwiebach, "Non-perturbative de Sitter vacua via α' corrections", Int. J. Mod. Phys. D **28**, 1943002 (2019), arXiv:1905.06583 [hep-th].

[231] O. Hohm and B. Zwiebach, "Duality invariant cosmology to all orders in α'", Phys. Rev. D **100**, 126011 (2019), arXiv:1905.06963 [hep-th].

[232] M. A. Rubin and C. R. Ordonez, "EIGENVALUES AND DEGENERACIES FOR n-DIMENSIONAL TENSOR SPHERICAL HARMONICS", (1983).

[233] M. A. Rubin and C. R. Ordonez, "Symmetric Tensor Eigen Spectrum of the Laplacian on n Spheres", J. Math. Phys. **26**, 65 (1985).

[234] P. van Nieuwenhuizen, "The compactification of IIB supergravity on S_5 revisted", in *Strings, gauge fields, and the geometry behind: The legacy of Maximilian Kreuzer*, edited by A. Rebhan, L. Katzarkov, J. Knapp, R. Rashkov, and E. Scheidegger (June 2012), pp. 133–157, arXiv:1206.2667 [hep-th].

[235] Z. Ma, *Group theory for physicists* (World Scientific, 2007).

[236] P. Breitenlohner and D. Z. Freedman, "Stability in Gauged Extended Supergravity", Annals Phys. **144**, 249 (1982).

[237] S. Ferrara and A. Sagnotti, "Massive Born–Infeld and Other Dual Pairs", JHEP **04**, 032 (2015), arXiv:1502.01650 [hep-th].

[238] H. Lu and K.-N. Shao, "Solutions of Free Higher Spins in AdS", Phys. Lett. B **706**, 106–109 (2011), arXiv:1110.1138 [hep-th].